Evolution of Two Periodic Meteoroid Streams: The Perseids and Leonids

by

PETER GORDON BROWN

Department of Physics and Astronomy
Graduate Program in Physics

Submitted in partial fulfillment
of the requirements for the degree of
Doctor of Philosophy

Faculty of Graduate Studies
The University of Western Ontario
London, Ontario
April 1999

Abstract

Observations and modelling of the Perseid and Leonid meteoroid streams are presented and discussed. The Perseid stream is found to consist of three components: a weak background component, a core component and an outburst component. The particle distribution is identical for the outburst and core populations.

Original visual accounts of the Leonid stream from 1832 – 1997 are analyzed to determine the time and magnitude of the peak for 32 Leonid returns in this interval. Leonid storms are shown to follow a gaussian flux profile, to occur after the perihelion passage of 55P/Tempel-Tuttle and to have a width/particle density relationship consistent with IRAS cometary trail results. Variations in the width of the 1966 Leonid storm as a function of meteoroid mass are as expected based on the Whipple ejection velocity formalism.

Four major models of cometary meteoroid ejection are developed and used to simulate plausible starting conditions for the formation of the Perseid and Leonid streams. Initial ejection velocities strongly influence Perseid stream development for the first ~five revolutions after ejection, at which point planetary perturbations and radiation effects become important for further development. The minimum distance between the osculating orbit of 109P/Swift-Tuttle and the Earth was found to be the principle determinant of any subsequent delivery of meteoroids to Earth. Systematic shifts in the location of the outburst component of the Perseids were shown to be due to the changing age of the primary meteoroid population making up the outbursts. The outburst component is due to distant, direct planetary perturbations from Jupiter and Saturn shifting nodal points inward relative to the comet. The age of the core population of the stream is found to be $(25\pm10)\times10^3$ years while the total age of the stream is in excess of 10^5 years. The primary sinks for the stream are hyperbolic ejection and attainment of sungrazing states due to perturbations from Jupiter and Saturn. Ejection velocities are found to be tens to of order a hundred m/s.

Modelling of the Leonid stream has demonstrated that storms from the shower are from meteoroids less than a century in age and are due to trails from Tempel-Tuttle coming within $(8\pm6)\times10^{-4}$ A.U of the Earth's orbit on average. Trails are perturbed to

Earth-intersection through distant, direct perturbations, primarily from Jupiter. The stream decreases in flux by two to three orders of magnitude in the first hundred years of development. Ejection velocities are found to be <20 m/s and average ~5 m/s for storm meteoroids. Jupiter controls evolution of the stream after a century; radiation pressure and initial ejection velocities are significant factors only on shorter time-scales. The age of the annual component of the stream is ~1000 years.

To my parents, Bob and Kathy

Co-Authorship

This thesis contains material from previously published manuscripts and manuscripts accepted for publication co-authored by: J. Jones and J. Rendtel. Copyright releases, declarations of co-author consent and detailed descriptions of co-author contributions are given in Appendices A. Herein I describe my personal contribution to individual chapters which are based on co-authored material:

Chapter 3. Observations of the Perseid Meteor Shower

I performed the final analyses, computations and wrote the manuscript.
I did not collect the original information or develop the procedure for the initial data reductions.

Chapter 4. Development and Application of a Numerical Model of the Formation and Evolution of the Perseid Meteoroid stream

I performed all the simulations and analysis, added planetary tables and other refinements to the numerical integrator, included other ejection routines to the cometary ejection program and wrote the manuscript.
I did not write the original integrator and cometary ejection programs.

Acknowledgements

Great credit goes to my supervisor, Jim Jones. He has been a continual source of inspiration, encouragement and most importantly patience. His expert advice and understanding made this work both possible and thoroughly enjoyable.

Thanks are due to colleagues who have each helped in their own way; in particular Rainer Arlt, Martin Beech, Margaret Campbell, Kerry Ellis, Bob Hawkes, Wayne Hocking, Juergen Rendtel, Milos Simek and Alan Webster.

A special thanks to Janice Gray for her patience, understanding and support throughout the period this work was carried out. Also, her editing assistance is acknowledged.

Lastly, thanks go to Aquarid, Leonid, Lyrid, Orionid, Meteors, and Perseid for doing all the work over the last five years.

Table of Contents

List of Tables

List of Figures

Chapter 1: Introduction

Frontispiece:

"*From the beginning of time, shooting stars have caught the attention of man and have been recorded sometimes with vivid expressions of admiration. It might then seem astonishing that this phenomenon has only recently occupied scientists' attention.*"

- translated from Chapter IV: Des Etoiles Filantes in Sur La Physique Du Globe by L.A.J. Quetelet (1861)

1.1 Periodic Meteor Streams

The study of meteors as an established scientific discipline originated with the great Leonid meteor storm of 1833. It was the sudden and unexpected appearance of the storm over North America, which prompted scholars of the time to begin studying meteors as an astronomical (as opposed to upper atmospheric) phenomenon.

That the Leonids were so obviously visible in 1833 and yet much weaker in 1834 reflects a fundamental characteristic of the stream; namely that it can be a storm (very strong meteor shower) in one year and a weak shower the next. That the Leonid storms come in cycles of 33 years reflects the strongly periodic nature of the activity associated with them and hence leads to their classification as a periodic stream.

Of the dozen or so meteor showers which occur throughout the year, the majority show consistent levels of activity from year to year at nearly the same location along the Earth's orbit. The showers which show no noticeable changes in activity from one year to the next are referred to as annual showers, while those with a periodic component in their levels of activity are referred to as periodic streams. Table 1.1 lists the most recognized showers visible throughout the year and their classification as periodic or annual.

Table 1.1. List of showers visible throughout the year (after Rendtel et al., 1995 and Hawkes, 1997). ZHR refers to the Zenithal Hourly Rate and gives an approximate measure of the number of meteors visible to a ground-based observer under good conditions at the maximum of the shower. A = Annual Stream, P = Periodic Stream, R = Visible for Radar observations only. V in ZHR column refers to variable.

Name	Date of Max	Velocity (km/s)	ZHR	Type of Shower
Quadrantids	Jan 3	41	120	A
Lyrids	Apr 22	49	15(V)	P
π Puppids	Apr 24	18	5(V)	P
η Aquarids	May 6	66	60	A
Arietids	Jun 7	39	60	A,R
ζ Perseids	Jun 9	29	40	A,R
β Taurids	Jun 30	30	25	A,R
Phoenicids	Jul 14	47	(V)	P
S. δ Aquarids	Jul 28	41	20	A
α Capricornids	Jul 30	23	4	A
N. δ Aquarids	Aug 9	41	4	A
Perseids	Aug 12	60	80 (V)	P
κ Cygnids	Aug 18	25	3	A
α Aurigids	Sep 1	60	10(V)	P
Orionids	Oct 21	66	20	A
S. Taurids	Nov 6	27	5	A
N. Taurids	Nov 13	29	5	A
Leonids	Nov 17	71	10(V)	P
α Monocerotids	Nov 20	60	5(V)	P
Geminids	Dec 13	35	110	A
Ursids	Dec 22	33	10(V)	P

Periodic meteor showers occur when the Earth intersects an uneven distribution of meteoroids from one year to the next. As a result, the levels of activity change dramatically when the Earth encounters this "clump" of material. This sometimes happens when the parent comet is near its time of perihelion and close to the Earth's orbit or it may be due to cyclical planetary perturbations moving parts of the stream into intersection with the Earth. As these "clumps" tend to disperse under the action of differential perturbations and differing orbital periods of the constituent particles, they are generally young in terms of orbital periods of the parent comet relative to the other components in the stream. It is the young age of the material associated with periodic streams that make the associated meteoroids of great scientific value. All other meteoroids associated with annual meteor streams are produced through a long process of decay of the parent comet; hence the age of any one meteoroid observed in the stream can only be guessed at in a broad statistical manner. As a result, the study of an annual stream and its evolution is complicated by the unknown age of the material making up the stream and thus features associated with the shower (such as its duration and dispersion) cannot be uniquely ascribed to initial ejection conditions from the comet or subsequent evolutionary effects.

Periodic streams allow us to separate to some degree the effects of perturbations (which affect the stream over time) from the initial conditions of ejection from the comet. In this sense the data concerning periodic streams can be interpreted as a direct probe of the comet-meteoroid birthing process. By comparing observations of periodic meteor showers with theoretical models of the formation and evolution of the associated meteoroid streams, we can formulate a more complete understanding of the factors which affect their evolution and set them on an Earth-crossing path, as well as how and when meteoroids from a given year's shower on Earth are released from their parent comets. It is a study of these matters that is the primary objective of this thesis.

1.2 Case Studies : The Perseids and Leonids.

A complete understanding of all aspects of periodic streams is possible only through exhaustive investigation of the major periodic streams listed in Table 1.1. Such investigation is beyond the scope of the current work. Instead, we will attempt to define some of the probable central mechanisms at work in the formation and evolution of periodic streams through studying two of the best documented periodic streams: the Perseids of August and the Leonids of November. In particular, it is our aim to develop a generic numerical model of the formation and subsequent evolution of these streams and to compare the resulting stream behaviour with observations. In this regard, we concentrate on those model outputs, which can be compared to observations, whether existing or future.

The Leonids is the archetype of the periodic streams as well as the first shower clearly documented to recur on an annual basis (Olmsted, 1834). The Perseids have long been categorized as an annual stream (cf. Lovell, 1954), but detailed observations over the last decade have revealed a periodic component as well (Brown and Rendtel, 1996). It is the wealth of recent observations of these two periodic streams, which has led to our adopting them as case studies.

Since the early 19th century, studies of meteor streams have proceeded along two principal lines: observational and theoretical. The former have included visual observations and more recently photographic, video and radar observations of meteor showers (cf. Steel, 1994 for a review) while the latter has only recently been developed in detail through the use of computer simulation of the formation and evolution of meteoroid streams (cf. Williams, 1992).

In this thesis we will examine the present observational summaries of the activity of the Leonids and the Perseids. To interpret these data in a theoretical framework, a numerical model for the formation and subsequent evolution of both streams will be developed and its "reality" measured via comparisons with the available observations. As well, we make predictions of the future times and magnitudes of activity based on these modelling results.

1.3 Thesis Outline and Focus

We will begin with a description of the basic physical and kinematic processes of meteoroid stream formation and the forces affecting its subsequent evolution in Chapter 2. In Chapter 3, a detailed summary of recent observations of the Perseids will be presented. In Chapter 4, a numerical model for the formation of the Perseid stream is developed and the evolution of the stream is compared to the observational results from Chapter 3. Similarly, Chapter 5 presents and summarizes our available observational information concerning the Leonid stream while in Chapter 6 the model is applied to the Leonid stream and compared to the observations enumerated in Chapter 5. Finally, Chapter 6 compares and contrasts the two streams, provides a brief synopsis of the major conclusions resulting from this study and suggests avenues for further work.

We wish to focus on some basic questions pertaining to these two streams, among them:

- What are the probable ages of the "young" periodic portions of these streams, as well as the older "annual" components?
- What are the model-inferred ejection velocities from the parent comets based on observations of the associated meteor showers?
- What is the root cause of the periodic component in each stream? Is material moved to Earth intersection primarily by planetary perturbations, radiation pressure, or other effects? Does the Earth intersect a dense cometary "trail" or are we simply skirting the outside of a much broader distribution of meteoroids?
- Why are the periodic components unstable in position from year to year and also in some cases from cometary passage to cometary passage?
- How does the stream "diffuse" over time, both in terms of removal of meteoroids (sinks) as well as quantitative changes in density within the stream? What does this imply about the variations in activity from year-to-year?

References

Brown, P., and J. Rendtel 1996. The Perseid Meteoroid Stream: Characterization of recent activity from Visual Observations. *Icarus* **124**, 414-428.

Hawkes, R.L. 1997. Meteor Shower Data - 1997, in *Observer's Handbook 1997*, ed R.L. Bishop, Royal Astronomical Society of Canada, Toronto.

Lovell, A. C. B. 1954. *Meteor Astronomy*. Oxford Univ. Press, London.

Olmsted, D. 1834. Observations of the Meteors of November 13, 1833. *Am. J. Sci.* **25**, 54-411, **6**, 132-174.

Rendtel, J., R. Arlt and A. McBeath 1995. *Handbook for Visual Meteor Observers*. International Meteor Organization, Potsdam.

Steel, D. 1994. Meteoroid Streams, in *Asteroids, Comets, Meteors 1993*, (eds. A. Milani et al.), p. 111-126, IAU.

Williams, I.P. 1992. The Dynamics of Meteoroid Streams, in *Chaos, Resonance and Collective Dynamical Phenomena in the Solar System*, (eds. S. Ferraz-Mello), p. 299-313, IAU.

Chapter 2

Evolution of Meteoroids and the Formation of Meteoroid Streams

2.1 Introduction

The process of a meteoroid's release from a parent body and its subsequent evolution is a central component of this work. While we still simulate these general processes through numerical models and study in detail two specific meteoroid streams (the Perseids and Leonids), the general physical concepts involved deserve attention and review. In what follows we describe the basic evolution of a given meteoroid from its "birth" through to its existence as an independent solar system body. For specific examples we shall confine our attention to the Perseid and Leonid stream orbits, but emphasize that these are not representative of the numerous, low-inclination meteoroid streams which constitute the bulk mass of the meteoroid complex. More extensive reviews of the entire subject of meteoroid stream formation and evolution can be found elsewhere (cf. Williams, 1993; Ceplecha et al., 1998; Steel, 1994).

The basic processes involved are: (1) The cometary ejection of meteoroids; followed by (2) the change in the osculating orbit of the ejected meteoroid from the parent body; and (3) the meteoroid's evolution under the gravitational and radiation forces acting upon it after release.

2.2 Cometary Ejection of Meteoroids

The origin of meteoroids as solid bodies begins in the outer atmosphere of cooling giant stars (Red Giants) when silicate material condenses to form grains (Greenberg and Haige 1989). These grains form the seeds for interstellar dust particles, which populate the plane of our galaxy. Later, condensation of volatiles from gas in the interstellar medium on the silicate core produces small grains with an organic-refractory matrix as well as an icy outer layer. Due to gravitational instability in some portions of these dust "clouds", stars (and planets) may grow over time. Such star-forming regions are heavily populated with gas and dust from the earlier decay of other stars.

The formation of our solar system out of just such a cloud (the initial solar nebula) some 4.5 billion years ago consisted of a central condensation (the future sun) and a disk of solid material (from interstellar dust) of varying size interspersed with gas (cf. Weidenshilling, 1988 and references therein for a more detailed review). Out of this disk of planetesmals, the planets were formed as smaller material coagulated through the process of gravitational accretion and collisional sticking. However, not all of the planetesmals were utilized in the formation of the planets. A large number ($\sim 10^{15}$) of kilometre-sized (and larger) chunks of unprocessed material, essentially frozen interstellar gas and dust stuck together, remained as separate, independent bodies in the outer solar system.

These bodies were initially confined to the plane of the solar system (i.e. the ecliptic plane). Through subsequent interaction with the planets and stars passing by, some of these bodies were isotropically ejected from the interior (i.e. beyond the orbit of Saturn) parts of the solar system, while others beyond Neptune continued to orbit in the ecliptic plane in an extended disk out thousands of A.U. from the sun. Many were lost forever into interstellar space, but a large fraction of those which were scattered remained loosely bound to the solar system in a distant (<100 000 A.U.) spherical cloud.

Some of these icy bodies have remained bound to the Sun since its formation and are still present in the form of the Oort cloud (named after J. van Oort who first brought widespread attention to the probable existence of such a cloud). The icy bodies making up

the Oort cloud are composed mainly of water ice (along with a small fraction of more volatile ices, like CO and CH_4) and dust - the same interstellar dust which began the whole process. Never heated more than 100 K above absolute zero since their formation, these objects have been in "cold" storage for the last 4.5 billion years.

When perturbations from a passing star or galactic tides alter the large orbits of these icy bodies, some may be moved into smaller orbits, which bring them within the reach of planetary perturbations from the major planets, or into close contact with the terrestrial planets. Once this happens, many will be permanently ejected from the solar system but a fraction will also be more tightly captured and potentially driven closer to the sun through repeated, complex interactions with the planets.

Once these icy bodies get closer than ~3 A.U. to the sun, the radiation from the sun will sublimate water ice (and at a much further distance more volatile ices like CO). This process leads to the formation of an envelope of gas about the icy central body and expels, through gas drag, the interstitial dust grains near the nucleus. The smallest of these grains (~micron sized) are driven directly away from the sun by solar radiation pressure (see 2.3) to form a "tail". As viewed from Earth at this point, the object looks like a fuzzy star with a tail which moves against the background stars - in literal translation "cometa" (Latin) meaning long-haired star - in its modern form, comet.

The majority of meteoroids are the products of cometary decay, both gradual and (occasionally) catastrophic. Whipple (1951) was the first to propose the modern model of a cometary nucleus - namely a homogenous collection of sand and ice - as a dirty snowball. Whipple also developed the equations dictating the velocity of ejection for a meteoroid of a given mass from a cometary nucleus. It is this initial ejection velocity which determines the starting orbit for the daughter meteoroids. While the details of meteoroid release from a cometary nucleus have been refined since Whipple's time (cf. Finson and Probstein, 1968; Crifo and Rodinov, 1999), the basic physical picture remains intact.

As the nucleus approaches the Sun, the mass loss per unit time, Γ, is given by

$$\Gamma = \frac{\pi R_c^{\,2} S}{n r^2 H} \qquad (2.1)$$

where R_c is the radius of the comet, S the solar constant, r the heliocentric distance of the nucleus, H the mean heat of sublimation for the ice and $1/n$ is the fraction of incoming solar energy used for sublimation. At some distance l from the nucleus surface the pressure on a grain due to free molecular collisions is

$$P = \frac{\Gamma \bar{v}}{2\pi l^2} \tag{2.2}$$

where v is the mean molecule velocity and the sublimation is assumed to be confined to the sunward hemisphere and $l >> R_c$.

The outward drag force experienced by a meteoroid grain due to coma gas is given by

$$F_{drag} = \frac{C_d}{2} PA \tag{2.3}$$

where C_d is the drag coefficient (=26/9 for a sphere which re-emits impacting molecules with thermal speeds) and A is the cross-sectional area of the meteoroid. Thus the acceleration relative to the nucleus is given by

$$a = \frac{F_{drag}}{m_p} - \frac{GM_c}{l^2} \tag{2.4}$$

where m_p is the mass of the meteoroid particle, M_c the mass of the nucleus and G the universal gravitational constant. Thus the velocity at infinity relative to the nucleus is

$$\int_{v_s}^{v_\infty} V dV = \left(\frac{\Gamma \bar{v} A C_d}{4\pi m_p} - m_p G M_c \right) \int_{R_c}^{\infty} \frac{dl}{l^2} \tag{2.5}$$

or (assuming the initial velocity is zero):

$$v_\infty^2 = 2R \left[\frac{39\bar{v}S}{72 r 2HSr} - \frac{R}{3} \frac{4\pi r G}{} \right] \tag{2.6}$$

where ρ_c is the bulk density of the cometary nucleus, σ is the radius of the meteoroid and ρ_m the bulk density of the meteoroid. The 2nd term in Eq 2.6 is typically a few percent of the first term.

Jones (1995) and others (cf. Gustafson, 1989) have re-examined this problem and found very similar equations, producing ejection velocities from physically identical starting conditions within a few tens of percent of the Whipple value.

That this is only an approximation is made clear by cometary observations showing the presence of isolated jets, nucleus rotation, complex coma behaviour etc. In particular, Steel (1994) has noted the existence of distributed production (i.e. the concept that sublimation is not confined just to the surface of the nucleus, but rather each of the initial meteoroids contribute to sublimation immediately after release), inferred from the observations of Halley's comet, and has suggested that this may produce radically different ejection velocities than those traditionally used in the Whipple approach. This is indeed the case and is developed in more detail in Chapter 4.

To this point we have been concerned with defining the probable ejection speeds, location of ejections and the most likely direction of ejection for meteoroids. The preceding physical model provides an estimate of the ejection speed likely for a given mass, while cometary observations (see Chapter 4) suggest ejection of meteoroids is unlikely beyond ~4 A.U.. We can only surmise that ejection of meteoroids is most probable on the sunward hemisphere of the comet at any instant. Rotation of the nucleus, thermal lag and the existence of isolated active regions will modify this last statement, but information on individual cometary nuclei is insufficient in most cases to warrant making a more precise choice for ejection directions which would deviate from a simple sunward ejection location (chosen at random).

Once we define the ejection location and velocity relative to the nucleus, the initial unperturbed orbit of the individual meteoroid can be defined. It is the ensemble of these initial orbits, which form the initial meteoroid stream.

2.3 Initial orbit upon Ejection

From the previous section we anticipate ejection velocities <~100 m/s for meteoroids of the size range of interest (>10^{-5} g) (cf. Jones, 1995 for detailed examples).

For ejections within 4 A.U. of the Sun, typical cometary velocities are of order V ~ 30-40 km/s for highly eccentric orbits (such as the Leonids and Perseids - see Fig 2.1). Thus the ejection velocity of the meteoroid relative to the comet, v, is such that $v<<V$ and

we denote the component of the velocity perpendicular to the cometary orbital plane and positive in the direction of the north cometary orbital "pole" as v_n, the component in the direction of the Sun as v_r and the component opposite the direction of the comet's instantaneous velocity vector as v_t. Fig 2.2 shows this right-handed coordinate system relative to the cometary orbit.

The total orbital energy per unit mass is given by (eg. Plavec, 1957):

$$\begin{aligned} E = T + U &= \frac{v^2}{2} - \frac{\mu}{r} \\ &= -\frac{\mu}{2a} \end{aligned} \tag{2.7}$$

where a is the osculating value of the semi-major axis, v is the heliocentric velocity, T is the kinetic energy, U is the potential energy and r is the heliocentric distance. μ represents GM_s where G is the universal gravitational constant and M_s the mass of the sun. For a particle ejected from the comet at r, its velocity relative to the comet causes a change in semi-major axis of

$$a_p = -\frac{2a^2}{\mu} V v_t + a \tag{2.8}$$

where a_p is the particle's semi-major axis immediately after ejection and we have assumed that $2Vv_t/\mu << 1$. The difference in semi-major axis (and thus energy) due to the velocity of ejection effectively depends on the magnitude of the meteoroid's ejection velocity parallel to the comet's velocity vector. The maximum change in semi-major axis is made when V is largest (i.e. at perihelion).

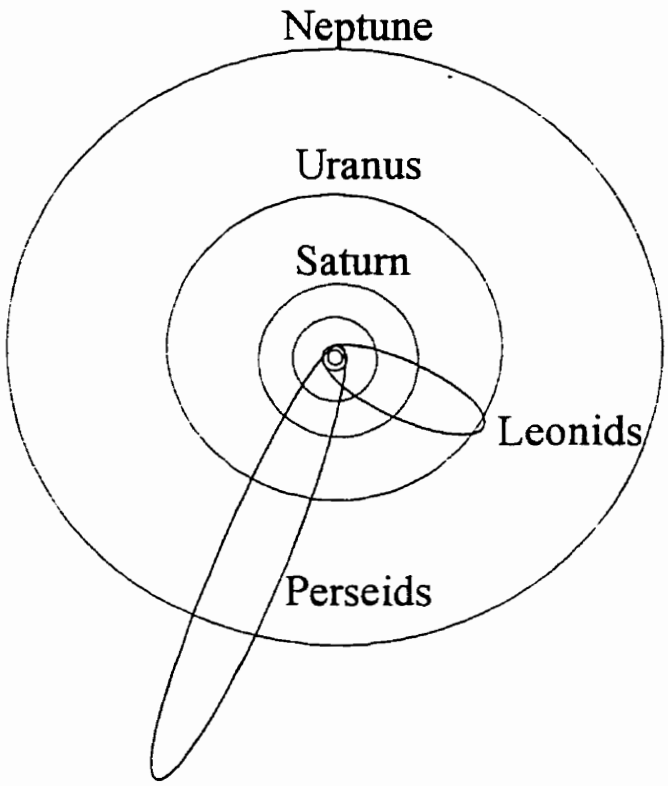

Fig 2.1: The orbits of the Leonid and Perseid meteoroid streams as seen from above the ecliptic plane of the solar system.

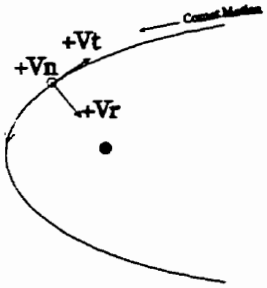

Fig 2.2: Cometocentric coordinate system for ejection of meteoroids. The normal component of the ejection velocity, v_n, is directed out of the page; v_r is positive in the direction of the sun, and v_t is positive in the direction opposite the comet's instantaneous velocity vector and is perpendicular to v_r.

It is possible to cast Eq 2.8 in a different form by making use of Kepler's third law and defining the fractional change in the period per revolution from ejection velocity as

$$\frac{dP}{P} = \frac{3a}{\mu} V v_t \tag{2.9}$$

In Fig 2.3 we show the expected fractional change in period resulting solely from ejection velocity for the Leonids and Perseids.

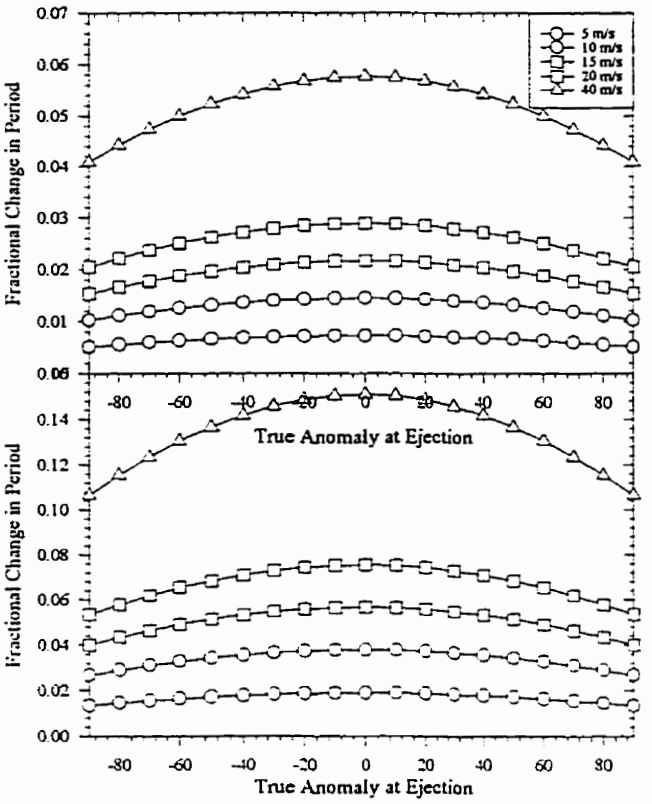

Fig 2.3: The fractional change in the orbital period for the Leonids (top) and Perseids (bottom) for ejection velocities from 5-40 m/s (see legend) for ejection at the given value of true anomaly. The change in period is calculated in steps of 10° of true anomaly.

Each of the orbital elements is similarly affected by the ejection velocity, but in a more complex fashion in a different manner and depending on the magnitude of each component. Pecina and Simek (1997) summarize these in detail but we note a few of physical interest here. The keplerian system of orbital elements is defined in Appendix A.

The change in the longitude of the ascending node Ω (which is a direct measure of when a given meteoroid is encountered during Earth's intersection with a stream) due to ejection velocity is given by

$$\Delta\Omega = \frac{\sqrt{a(1-e^2)}\sin(\theta+\omega)}{\mu^{\frac{1}{2}}(1+e\cos\theta)\sin i}\, v_n \qquad (2.10)$$

where θ is the true anomaly, ω is the argument of perihelion and i is the inclination of the initial orbit. Fig 2.4 shows the change in the longitude of the ascending node as a function of the normal component of the ejection velocity for various values of true anomaly for the Leonids. It is evident a larger change in Ω is accomplished the further from perihelion for any given value of v_n. Ejections near perihelion (and for Tempel-Tuttle slightly thereafter) have the least affect on the nodal longitude of the final orbit as the descending node is near perihelion.

For any meteoroid to actually intersect the Earth, its nodal radius (the point where it intersects the ecliptic) must be at the same distance from the sun as the Earth when the Earth is at the meteoroid's nodal longitude. This condition is

$$\frac{a(1-e^2)}{1\pm e\cos\omega} = Re \qquad (2.11)$$

where Re is the radius of the Earth's orbit at $\lambda(\Omega,\ \Omega+180°)$, the negative sign in the denominator of Eq. 2.11 is for the descending node and the positive sign is for the ascending node (where $\lambda=\Omega+180°$). By taking the differential of Eq. 2.10 (see Chapter 4) and using values for the osculating elements appropriate for the Perseids and Leonids we show directly the change in the descending node due to ejection velocity alone in Fig 2.5 a and b respectively. Typical ejection velocities of order 10-20 m/s in the orbital plane produce changes in the descending nodal radius of less than 10^{-3} A.U. for the Leonids near perihelion, while only slightly higher ejection velocities near 40 m/s produce an order of magnitude greater change (0.01 A.U.) for the less bound Perseid meteoroids. For identical

ejection velocities, Perseid meteoroid nodal radius differences are three to five times larger on average than those of Leonid meteoroids (depending on location of ejection).

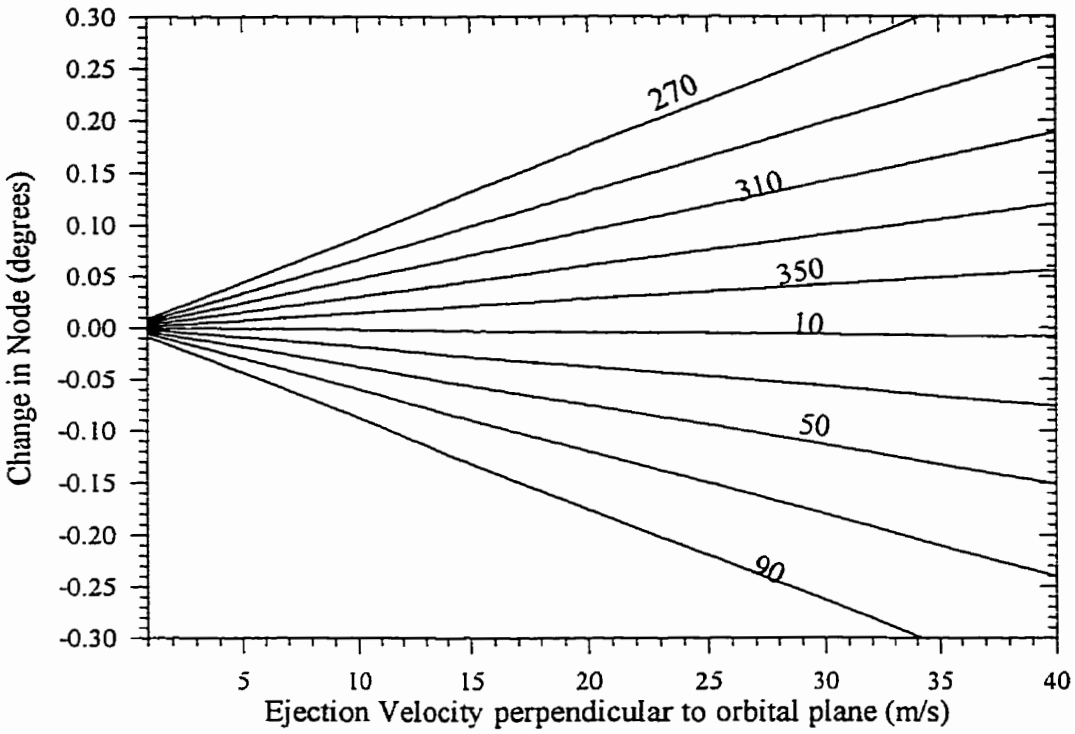

Fig 2.4: Change in the osculating value of the ascending node (Ω) for ejection from 55P/Tempel-Tuttle as a function of the normal component of the velocity (V_n) at different values of true anomaly from 270°-90° in 20° steps.

For comparison, the change in the nodal radius due to radiation pressure affects alone for the Leonids and Perseids (see next section) is shown in Fig 2.6. For both orbits, the effect is much smaller than that of ejection velocities, even for very small particles.

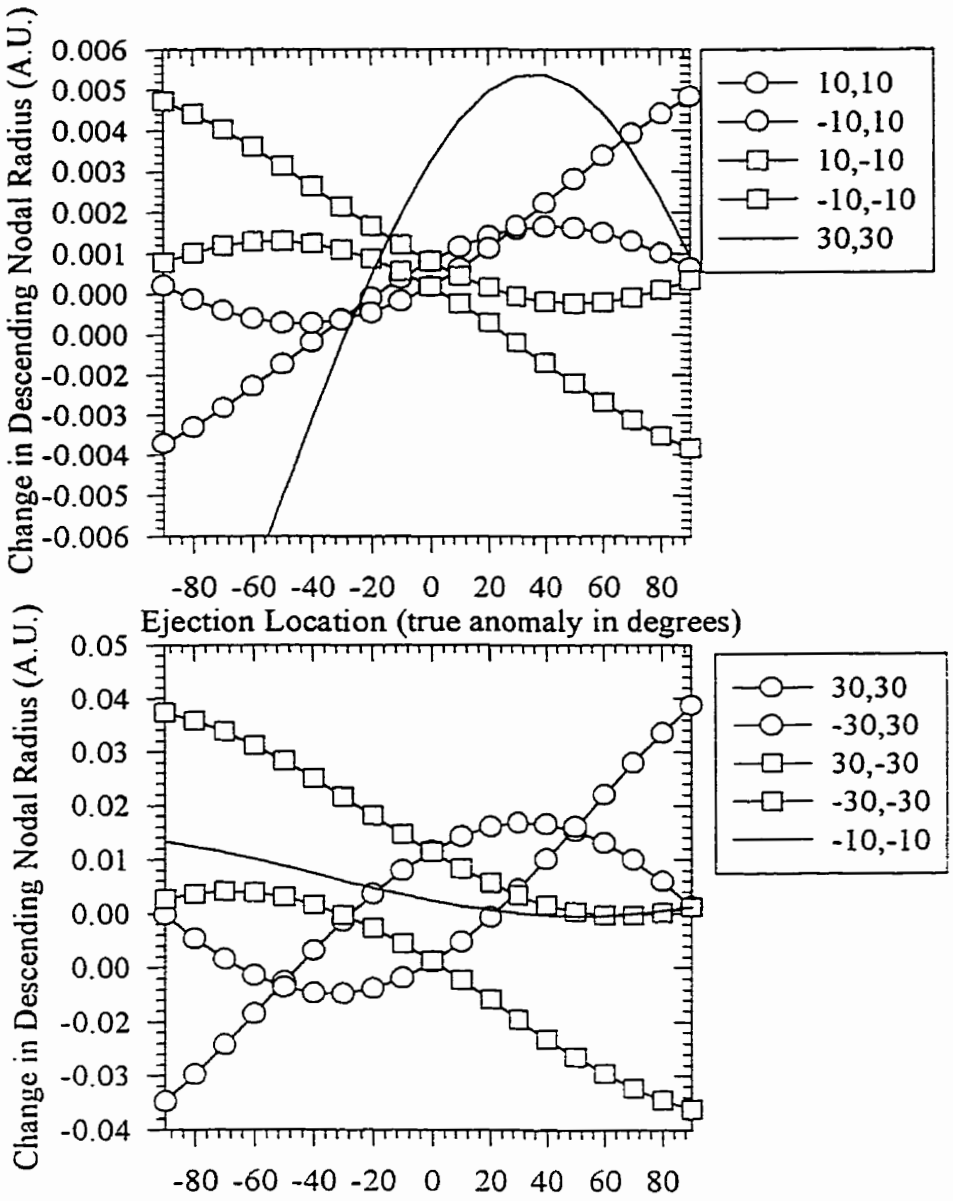

Fig 2.5: Change in the magnitude of the descending nodal radius as a function of ejection velocity and true anomaly of ejection for the Leonids (top) and Perseids (bottom). The legend shows the radial, transverse ejection velocity component pairs in units of m/s. Note that the ejections are assumed to be confined to the orbital plane (i.e. V_n=0).

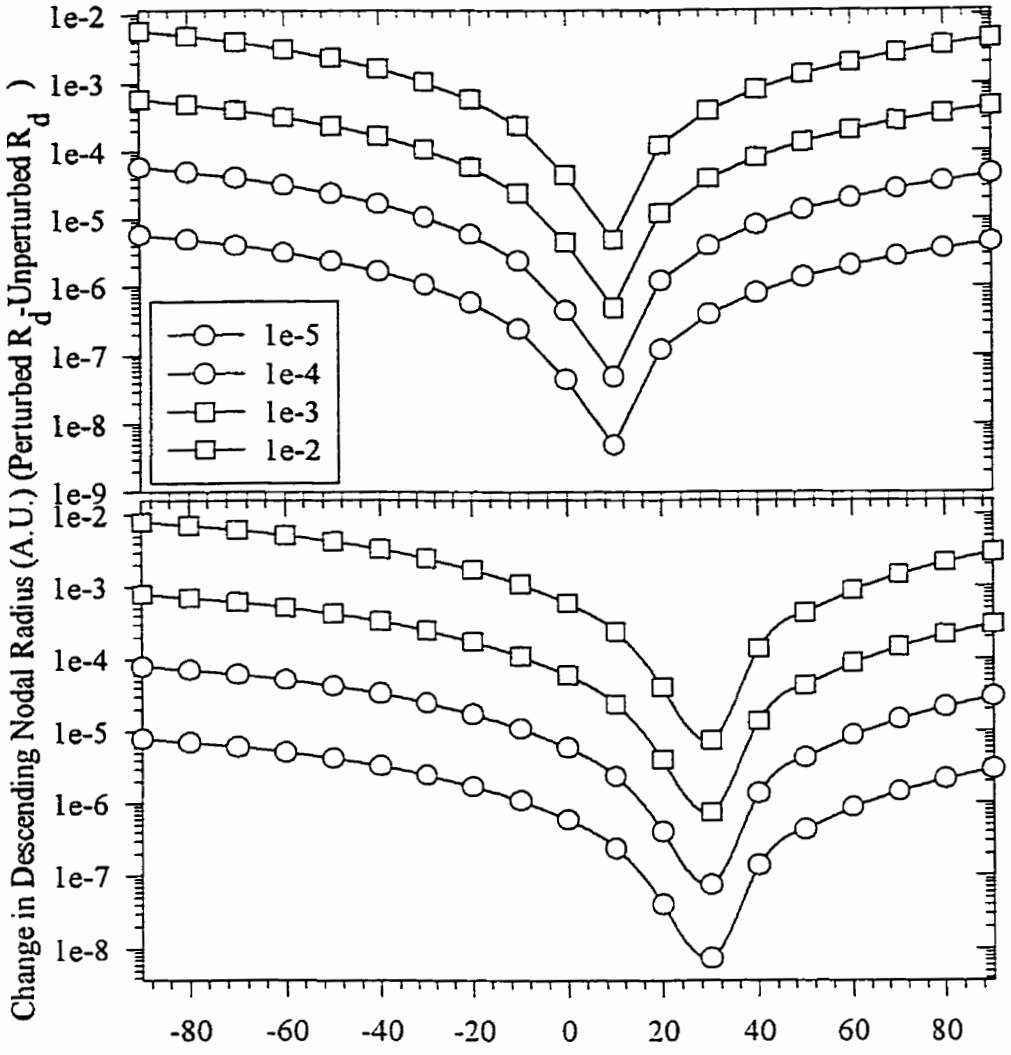

Fig 2.6: Change in the magnitude of the heliocentric radius of the descending node for the Leonids (top) and Perseids (bottom) resulting from radiation pressure as a function of position (in true anomaly) of release. The change is shown assuming a zero net ejection velocity. The legend gives values for β (defined in Chapter 3) associated with each curve. Note that the nodal radius affected by radiation pressure is always larger than the original nodal radius. Values are computed in steps of 10°.

2.4 Forces acting on the meteoroid after ejection

Immediately after ejection, the initial orbit established in Sect. 2.3 is modified by numerous forces (cf. Burns et al., 1979). In total, the relevant forces acting on a meteoroid of order 10^{-5} g and larger after ejection are given by

$$\ddot{\bar{r}} = -\frac{GM}{r^2}\hat{r} + \sum_{i=1}^{9} Gm_i\left[\frac{\bar{r}_i - \bar{r}}{|\bar{r}_i - \bar{r}|^3} - \frac{\bar{r}_i}{r_i^3}\right] + \frac{S}{c}\frac{A}{m}\left(\frac{M_s}{r^2}\right)\hat{r} - \frac{S}{c}\frac{A}{m}\left(\frac{M_s}{r^2}\right)\left(\frac{V_r}{c} - \zeta\cos\zeta\right) + \frac{8\pi}{3}\frac{s^2\sigma\varepsilon T^4}{mc}\frac{\Delta T}{T}\cos\zeta \qquad (2.12)$$

where the summation is over all planets from Mercury to Pluto; r is the radius vector from the sun to the meteoroids, r_i and m_i are the radius vector and mass of planet i; M_s is the mass of the sun, m the mass of the meteoroid; S is the solar flux at distance r (in A.U.) from the sun ($S=1.37/r^2$ in units of kW m^{-2}); A is the cross-sectional area of the meteoroid relative to the solar direction; c is the speed of light; V_r and V_t are the radial and transverse heliocentric velocities of the meteoroid respectively; s is the physical radius of the meteoroid; σ is the Stefan-Boltzmann constant; T is the mean temperature of the meteoroid; ΔT is the temperature differential across the meteoroid surface and ζ is the obliquity of the spin axis of the meteoroid relative to the orbital normal direction.

Eq. 2.12 is composed of six terms, each representing a separate physical force acting on the meteoroid, with the approximate relative importance of the forces decreasing approximately from left to right.

The first term represents the radial attraction of the sun and is by far the strongest of the forces acting on the meteoroid (the central force). The meteoroid's motion is defined in heliocentric terms, as this motion is an excellent approximation of a two-body system (sun-meteoroid).

The second term consists of the summation of the direct gravitational attraction of each of the planets. The specific terms of importance here depend to a great extent on the meteoroid's orbit, but typically Jupiter and/or Saturn dominate (see discussions in Chapters 4 and 6 relative to the Perseids and Leonids).

The third term is often referred to as indirect planetary perturbations or the barycentric correction term. This force is analogous to the (fictitious) centrifugal force in uniform circular motion and is purely a result of the choice of a non-inertial coordinate system. Physically, the meteoroid does not move about the sun (though we reference it to the center of the sun) but rather about the center of mass of the solar system. This point (called the barycenter) is slightly offset from the center of the sun, due primarily to the attraction of Jupiter and (to a lesser degree) Saturn. It also moves relative to the solar center depending on the position of the major planets. As a result, the heliocentric orbital elements appear to "wobble" in direct relation to the acceleration of the barycenter relative to the solar center. This force becomes more significant for objects with very eccentric orbits near aphelion, since the force is independent of the distance of the meteoroid from the sun and hence has greatest effect when the object is least bound to the sun (i.e. has the highest potential energy). The relative importance of the effect decreases as the object moves inward, becoming insignificant once the object is interior to Jupiter. The indirect perturbations are also typically smaller than the effects of distant (1-2 A.U.) direct perturbations from the major planets (see Chapter 6). Chambers (1995) has discussed the role of indirect perturbations in maintaining resonance behaviour in Halley-type comets and provides an excellent discussion of the role of the force for such highly eccentric orbits.

The fourth term in Eq. 2.12 is due to solar radiation pressure. Photons from the Sun carry momentum with them. When the meteoroid absorbs incident solar photons it removes momentum from the particle beam. This rate of change of momentum (a force) in the beam, as seen from the meteoroid, acts on the meteoroid in direct proportion to the exposed geometric surface area and its scattering efficiency. For a perfectly absorbing particle, the scattering efficiency is unity and we adopt this throughout. The force acts radially away from the Sun as the momentum of the incident photons is virtually all in this direction.

As this force is radial and falls off as $1/r^2$, like the central gravitational attraction of the Sun, it is often included with the central force term. More specifically, it is common to refer to the (constant) ratio of radiation force to gravitational force as $\beta=F_r/F_g$ or

$\beta=5.7\times10^{-6}/\rho s$, where ρ is the bulk density of the meteoroid and s the radius in MKS units. In this manner it is possible to recast the radiation force and gravitational force as

$$\bar{F} = GM(1-\beta)\frac{\bar{r}}{|\bar{r}|^3} \tag{2.13}$$

which makes it clear that the effect of radiation pressure is equivalent to a decrease in the central force (i.e. an effective decrease in the sun's mass). As the radiation pressure (which is typically the dominant radiation force for meteoroids of the size we are considering) acts immediately upon ejection (that is, it immediately begins moving under the new, effectively reduced central potential), while retaining its pre-release orbital velocity, it is straightforward to show that from energy considerations, a pre-ejection bound orbit can become unbound for ejection at true anomaly θ if the condition

$$\beta \geq \frac{1-e^2}{2(1+e\cos\theta)} \tag{2.14}$$

is met. Thus, the value of β that is required for very eccentric orbits ($e\rightarrow 1$) to become unbound is quite low (much less than 1). For ejection at perihelion (when the meteoroid and parent body are moving at their highest speeds relative to the Sun and the energy in the body is partitioned primarily into kinetic energy), a Leonid meteoroid with a value of $\beta > 0.05$ is unbound while for a Perseid the value is only 0.02.

The fifth term is due to radiation emission by the meteoroid. As radiation falls on the meteoroid it is re-emitted isotropically in the meteoroid's rest frame at the sizes we are concerned with. However, since the meteoroid is moving with non-zero velocity about the sun, the radiation emitted from its leading edge is doppler-shifted (towards the blue) relative to the radiation from its trailing edge. As a result, the force imparted to the particle from the blue-shifted light (which has higher momentum than red-shifted light) acts in the direction opposite to the leading edge (away from the instantaneous velocity vector) and works to "brake" the particle. This force is called the Poynting-Robertson (PR) effect (cf. Burns et al, 1979 for both a classical and relativistic treatment of this force).

From Eq. 2.12 it is clear that the PR effect is of order v/c (typically $\sim 10^{-4}$) relative to radiation pressure and is thus negligible for particle dynamics over the short time

periods or the larger meteoroids we investigate. The PR effect becomes significant only over long time intervals, cumulatively removing momentum and energy from a small meteoroid (of order μm in size) such that the orbit circularizes and the semi-major axis decreases, allowing the particle to move into regimes where other dynamics (such as planetary resonances) can affect it (cf. Liou and Zook, 1997).

The last term in Eq. 2.12 is the most difficult to measure physically and its relative importance has been debated for some time (eg. Olsson-Steel, 1987). It arises from the non-isotropic re-emission of radiation for a spinning non-isothermal body. In this scenario, extra radiation and energy (as well as momentum) are emitted in the "evening" hemisphere relative to the "morning" hemisphere due to the temperature difference between the two. Depending on the orientation of the rotation axis and the sense of the spin, this radiation emission imbalance can lead to forces, which act, on the meteoroid in any direction. As a result, unlike radiation pressure or the PR effect, this force (called the Yarkovsky-Radzievskii effect) is diffusive in nature and leads to a random-walk in the perturbed meteoroid motion. The direction in which the force acts depends on the orientation of the rotation axis. None of these quantities is known with high degrees of confidence for typical meteoroids. As a result, it is possible that in the extreme case of slow rotating objects, the Yarkovsky force may be 10^3-10^4 times that of the PR force, though the random direction of the force mitigates its role compared to the smaller but consistent drag from the PR effect. Even in this extreme case, however, the Yarkovsky effect is still only a fraction of a percent (and usually much less) of radiation pressure for meteoroids of the size range studied here. The real importance of the effect may be felt over long time periods and for very large bodies (cf. Bottke et al., 1998). As a result we do not include the Yarkovsky force in any of our numerical calculations, noting that over a few centuries (where most of our integrations are concerned) it is unlikely to be of significance.

References

Bottke, W. D.L.Rubincam and J.A. Burns, 1998. Dynamical Evolution of Meteoroids via the Yarkovsky Effect, American Astronomical Society, DPS meeting #30.

Burns, J.A. P.L. Lamy and S. Soter, 1979. Radiation forces on small particles in the solar system, *Icarus*, **40**, 1.

Ceplecha, Z., J. Borovicka, W.G. Elford, D.O. Revelle, R.L. Hawkes, V. Porubcan, and M Simek, 1998. Meteor Phenomena and Bodies, *Sp.Sci. Rev.*, 84, 327-471.

Chambers, J.E. 1995. The long term dynamical evolution of comet Swift-Tuttle. *Icarus* **114**, 372-386.

Crifo, J.F. and A.V. Rodionov, 1999, Modelling the circumnuclear Coma of Comets: Objectives, Methods and Recent Results, in press.

Finson, M.L. and R.F. Probstein, 1968. A theory of dust comets. I. Model and equations, *ApJ.*, **153**, 353.

Greenberg, J.M. and J.I. Hage. 1990. From Interstellar Dust to Comets:A Unification of Observational Constraints, *ApJ*, 361, 260-274.

Gustafson, B.A.S. 1989. Comet Ejection and Dynamics of Nonspherical dust Particles and meteoroids. *Ap.J.* **337**, 945-949.

Jones, J. 1995. The ejection of meteoroids from comets. *Mon. Not. R. Astron. Soc.* **275**, 773-780.

Liou, J-C. and H. Zook. 1997. Evolution of Interplanetary Dust Particles in Mean Motion Resonances with Planets, *Icarus*, **128**, 354.

Olsson-Steel, D. 1987. The dispersal of meteoroid streams by radiative effects, in *10th European Regional Astronomy Meeting of the IA.U.*, Prague, Czechoslovakia, Aug. 24-29, 1987, p. 157-161

Pecina, P. and M. Simek. 1997. The orbital elements of a meteoroid after its ejection from a comet, *A&A*, **317**, 594-600.

Plavec, M. 1957. *On the Origin and Early Stages of the Meteor Streams*, Czechoslovak Academy of Sciences, Publication No. 30., Prague.

Steel, D. 1994. Meteoroid Streams, in *Asteroids, Comets, Meteors 1993*, (eds. A. Milani et al.), p. 111-126, IA.U..

Weidenschilling, S.J. 1988. Formation processes and time scales for meteorite parent bodies, in *Meteorites and the Early Solar System*, (eds. J.F. Kerridge and M.S. Matthews), p.348-375, University of Arizona.

Whipple, F.L. 1951. A comet model II. Physical relations for comets and meteors. *AJ* **113**, 464-474.

Williams, I.P. 1993, The dynamics of Meteoroid Streams, In *Meteoroids and Their Parent Bodies* (J. Štohl and I. P. Williams, Eds.), p. 31-40. Astronomical Inst., Slovak Acad. Sci., Bratislava.

Chapter 3

Observations of the Perseid Meteor Shower[1]

3.1 Introduction

The Perseid meteor shower, which recurs annually near August 12, is among the most studied meteor showers of the present era. Hasegawa (1993) has noted that based on ancient records of its activity, the Perseids are among the oldest of all recorded showers,

During the Perseid returns of the 1860's, the first crude orbit determination of the stream was made by Schiaparelli (1867) who noted the stream's orbital similarity to the recently discovered comet 109P/Swift-Tuttle (1862 III), which has a period of just over 130 years. This was the first direct evidence connecting comets and meteor showers. Kronk (1988) has given a detailed historical review of the shower.

Many groups for the remainder of the 19th century and well into the 20th century carried out visual observations of the shower. These data provide our only direct measure of the activity from the shower until the middle of the 20th century and the advent of radar. These early observations were very inconsistent, as the methods used by individuals and sometimes groups of observers differed radically and were employed under widely varying sky conditions. As a result, determining the level of Perseid activity during most of the 19th and 20th century is problematic.

Interest in the Perseids increased during the late 1970's in anticipation of the return of 109P/Swift-Tuttle, which was expected to reach perihelion circa 1980 (Marsden, 1973). Meteor observations carried out during the late 1970's suggested activity was increasing toward a peak in the early 1980s, heralding 109P/Swift-Tuttle's return (Kronk, 1988). The comet, however, was not recovered within this time period.

---

[1] A version of this chapter has been published : P. Brown and J. Rendtel (1996) The Perseid Meteoroid Stream: Characterization of Recent Activity from Visual Observations. *Icarus*. **124**, 414-428.

In 1988 and more notably in 1989, a new "peak" was identified approximately 12 hours before the long-recognized "normal" stream maximum (located at 140.1° (J2000.0)) which was of similar strength to the regular maximum (Roggemans, 1989; Koschack and Roggemans, 1991). This new peak was widely interpreted as representing the early detection of newer meteoroids associated with the impending return of 109P/Swift-Tuttle. The position of the new peak in these years was very close to the nodal longitude of the comet (Ω=139.44°), which was ultimately recovered in September 1992 (Yau et al., 1994). Beginning in 1991, the Perseids have displayed strong outbursts in activity associated with the return of the parent comet 109P/Swift-Tuttle, which has continued through, to the late 1990's.

The best set of data recording these outbursts has been visual observations of the Perseids made by amateur astronomers. The quantity and uniformity of the observations permit precise reconstruction of the activity and flux profile of the stream at an unprecedented level. In what follows, we analyse the detailed visual activity of the Perseid meteor shower near its time of maximum for the years 1988-1994. In total, the visual meteor data consist of some 14,552 counting intervals, collected by 1,115 meteor observers from 38 countries who reported 243,227 Perseid meteors during 14,237 hours of effective observational time over these seven years. From these data we have selected subsets which met all our criteria for inclusion in this work (see Sect. 6.2) and summarized the final dataset in Table 3.1. The activity of the shower is characterized by both the Zenithal Hourly Rate (ZHR) and flux, Φ, along with their associated errors. Particle characteristics within the stream are represented through the population index (r) of the shower at specific points along the Earth's orbit. These are the basic quantities defining the stream, which could be derived from these observations.

3.2 Collection of Observations and Methods of data Reduction.

The methods used to observe meteors and reduce these data follows from the development of the visual techniques summarized by Kresakova (1966). Here we give an abbreviated qualitative discussion; for more detailed discussions; readers should refer to Koschack and Hawkes (1995) and Koschack (1995). Of importance is the fact that these techniques are applicable to single observers only; group observations, where data are pooled, cannot be used in this method.

In the most basic form, an individual observer uses only the naked eye to count the number of meteors seen during a specified time interval and then either associates each with a certain shower or records it as a sporadic meteor while noting the magnitude of each meteor. During this time, the observer also notes the faintest star visible in his/her field of view (denoted the limiting magnitude (LM)) and records the total effective time that the sky was actually monitored (T_{eff}). The LM is typically the result of a weighted mean of several such measurements taken during the observation at intervals determined by changing sky conditions and reported as averages to 0.01 M_v.

From each observation interval a quantity called the Zenithal Hourly Rate (ZHR) is calculated. The ZHR is the number of meteors from the shower a standard observer would see under unobstructed skies with the radiant point overhead and the LM=6.5. This definition forms the basis for "standardization"; the goal of all reductions is to correct an imperfect observation to this standard. To characterize the particle population, we define the population index (r) as:

$$r = \frac{N(M_v + 1)}{N(M_v)} \tag{3.1}$$

where $N(M_v)$ is the cumulative number of meteors of magnitude M_v or brighter. The population index characterizes the slope of the cumulative number of meteors vs their magnitude for the shower and can be related to the differential mass index s with appropriate connection between mass and magnitude via (McKinley, 1961):

$$s = 1 + 2.5\log(r) \qquad (3.2)$$

Using the population index along with the ZHR we are able to compute the flux in units of meteoroids km^{-2} $hour^{-1}$. Further details relating to the derivation of these quantities can be found in Koschack and Rendtel, 1988; Koschack and Rendtel, 1990a,b; Koschack, 1995 and Brown and Rendtel 1996.

3.3 Results of Perseid Observations 1988 - 1994

The ZHR activity, population index and corresponding flux profiles for the Perseid stream for each year from 1988-1994 are given in Figs. 3.1-3.7. Not shown in these figures are the sporadic hourly rates (HR) corrected for stellar limiting magnitude. These values are used during the initial selection cycle as indicators to aid in the detection of systematic errors in the shower ZHRs. Since observers contributing to the ZHR average at a given time are distributed over areas of order the size of a continent, the sporadic HR is not correctable in the same manner as the shower HR, a direct result of the fact that sporadic meteors do not have radiants which are uniformly over the celestial sphere (cf. Jones and Brown, 1993), but rather are concentrated in several diffuse sources. This implies that the sporadic HR varies as a function of geographic latitude and local time in a non-trivial manner and thus cannot be used accurately to correct relative shower rates from different locations.

Inspection of these curves shows that the level of flux appears to vary significantly throughout these years not only in the outburst component of the profile, but in the primary maximum as well. Some of this variation is due to lunar conditions as in 1990 and 1992. As a result, the corresponding profiles are uncertain, the effect being most evident in the large errors in the population index profiles in these years, caused by low limiting magnitudes and thus small numbers of faint meteors. The number of Perseid meteors, the total effective observing time and the number of contributing observers for each year are given in Table 3.1. The profiles also differ in some cases due to poor observer coverage, particularly in the Pacific region, and result in gaps during several years.

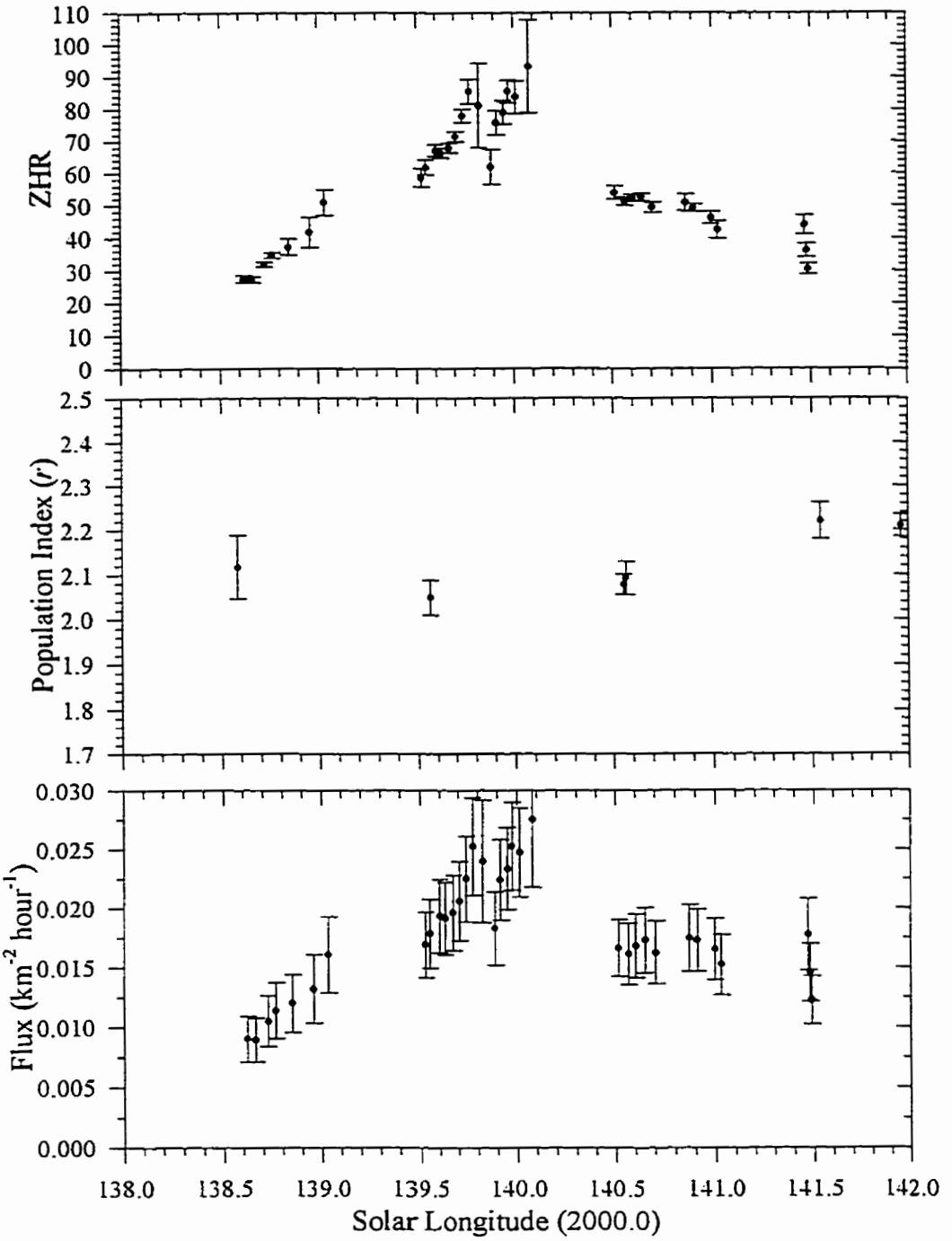

Figure 3.1: The ZHR (top), population index (middle) and flux (bottom) for the 1988 Perseid return.

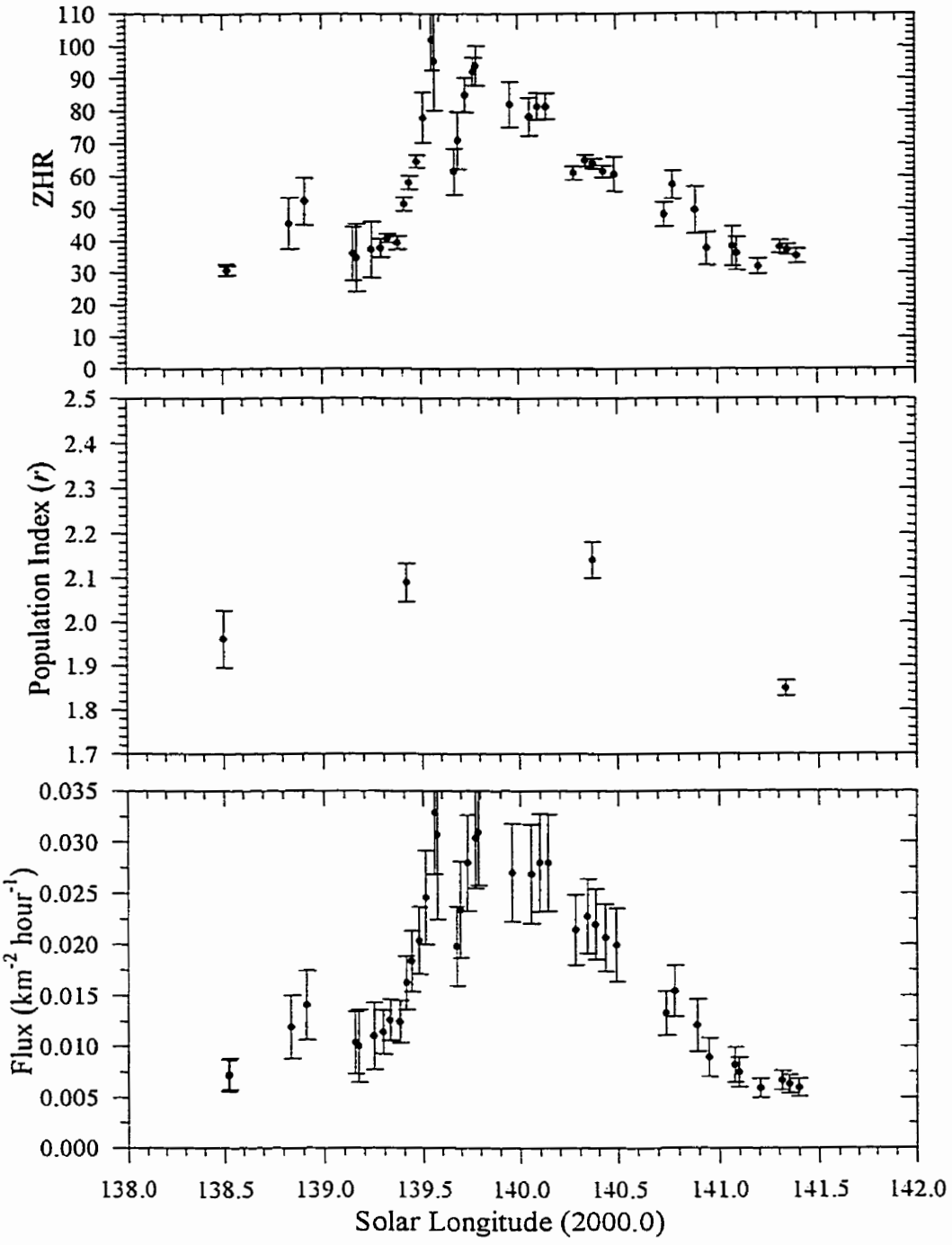

Figure 3.2: The ZHR (top), population index (middle) and flux (bottom) for the 1989 Perseid return.

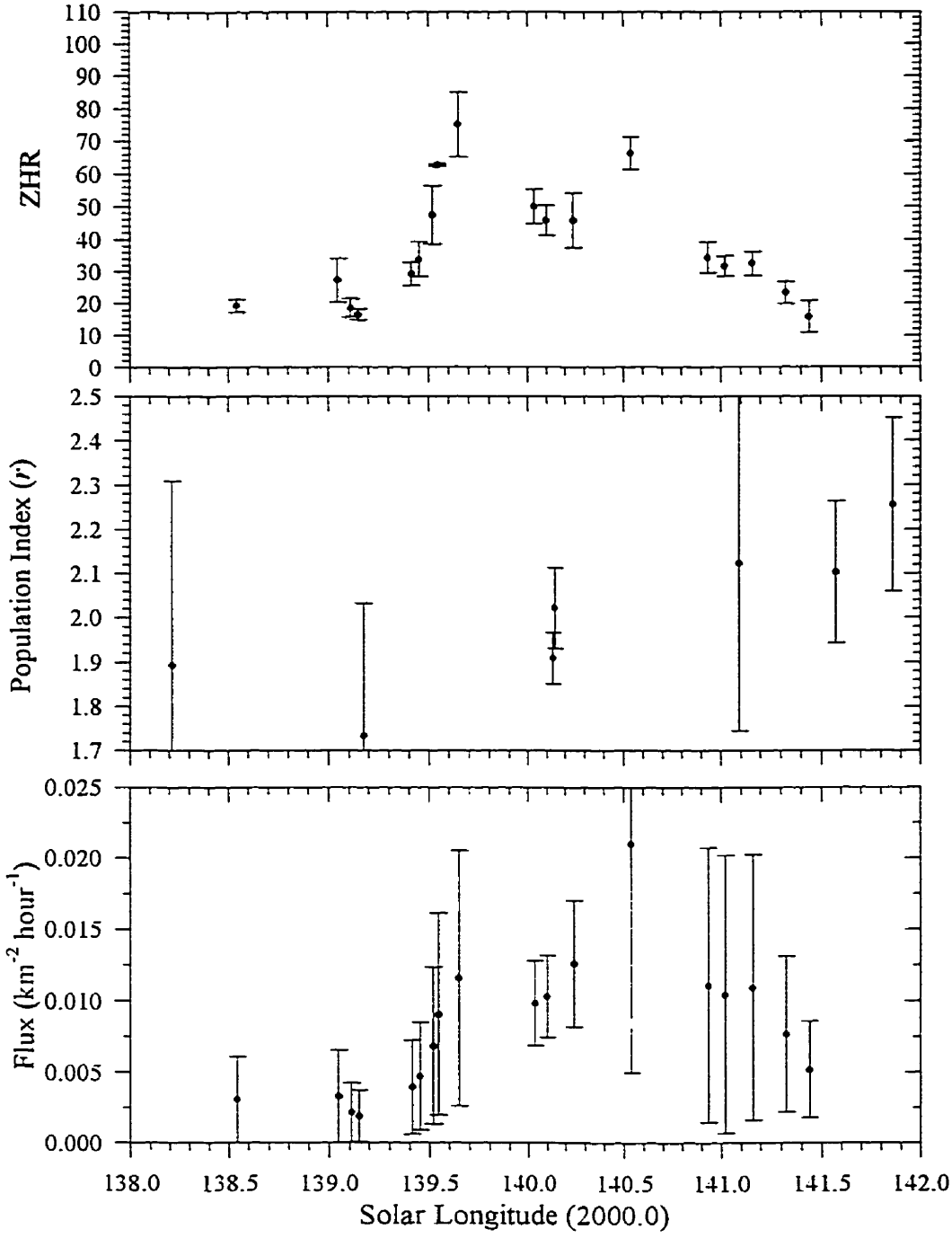

Figure 3.3: The ZHR (top), population index (middle) and flux (bottom) for the 1990 Perseid return.

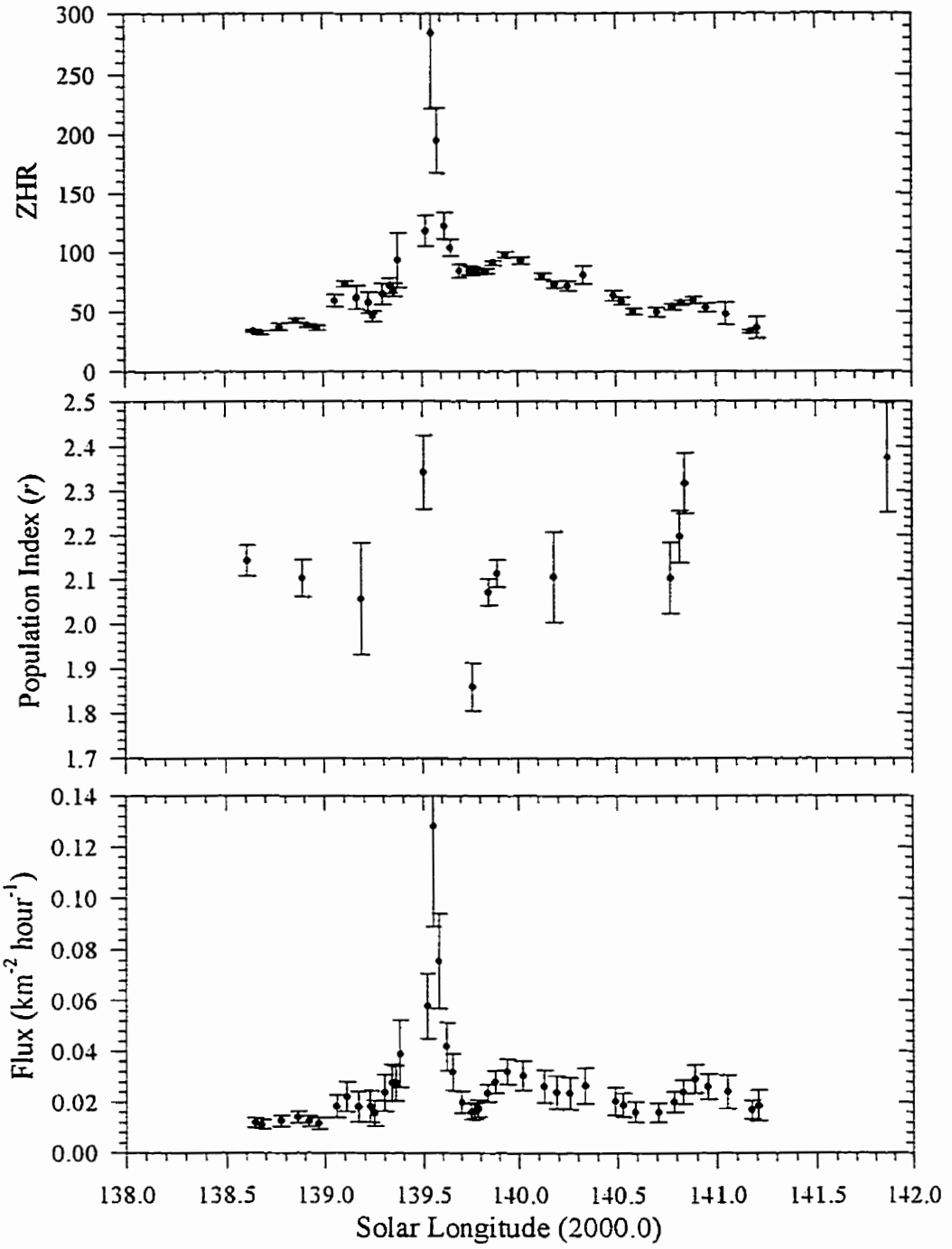

Figure 3.4: The ZHR (top), population index (middle) and flux (bottom) for the 1991 Perseid return.

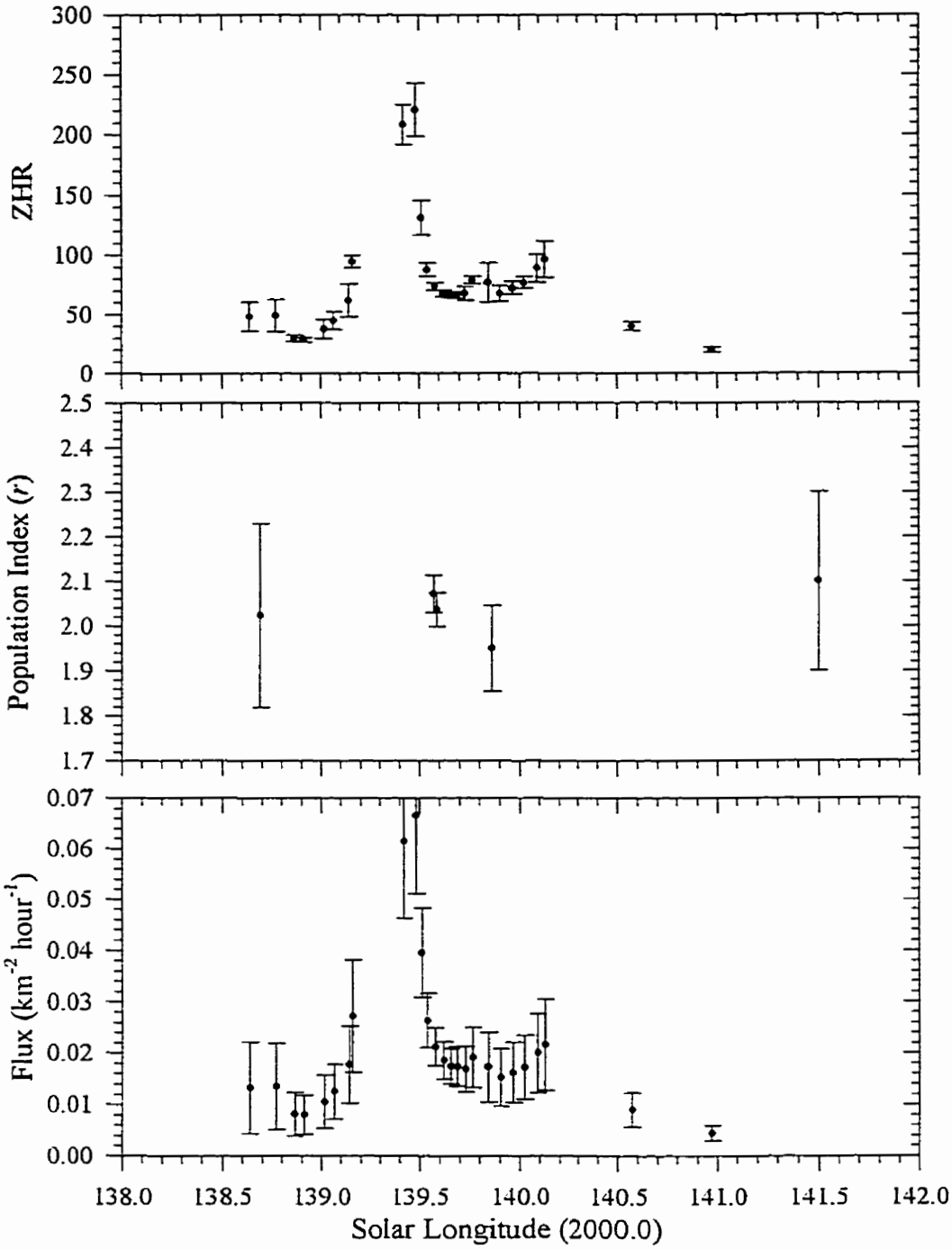

Figure 3.5: The ZHR (top), population index (middle) and flux (bottom) for the 1992 Perseid return.

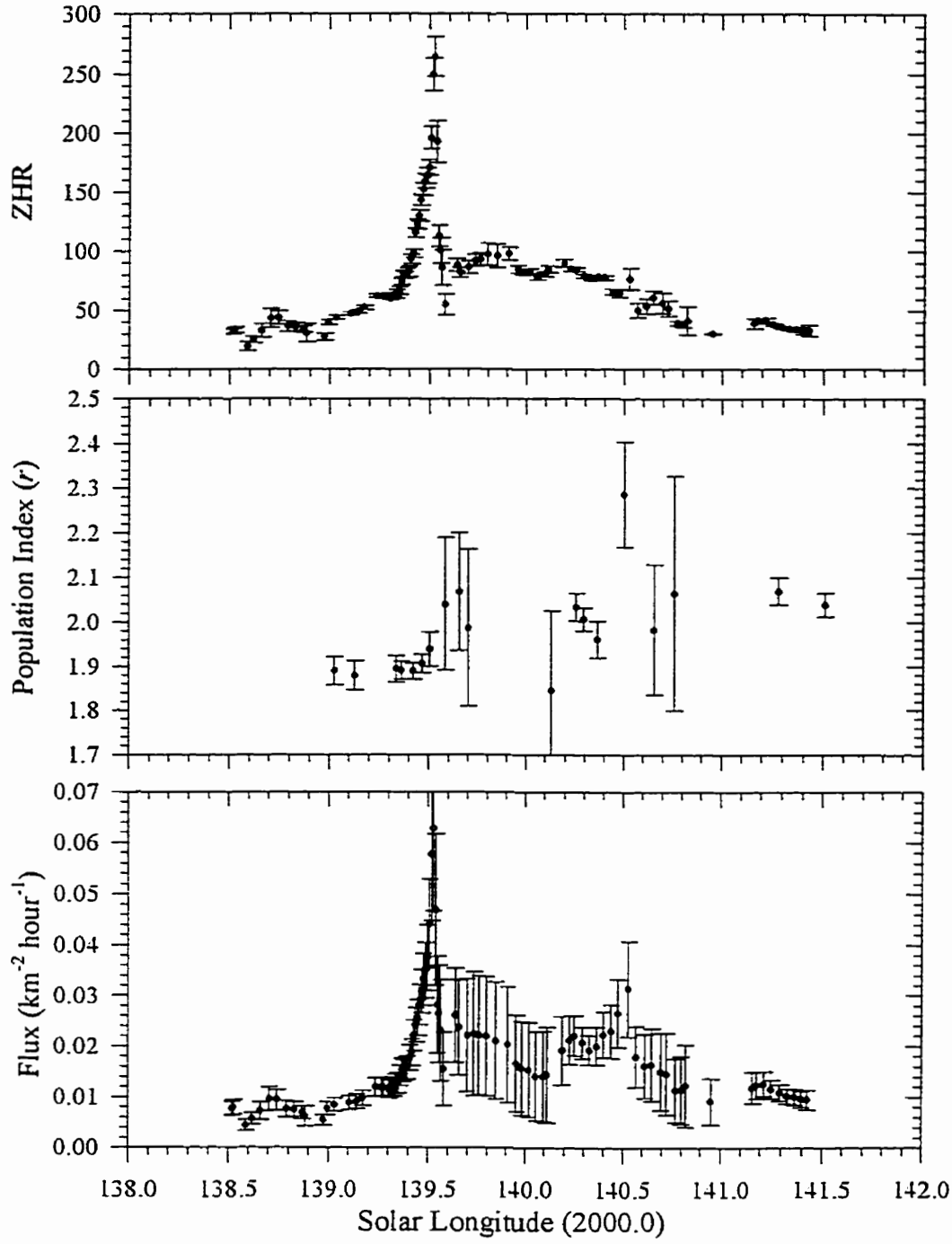

Figure 3.6: The ZHR (top), population index (middle) and flux (bottom) for the 1993 Perseid return.

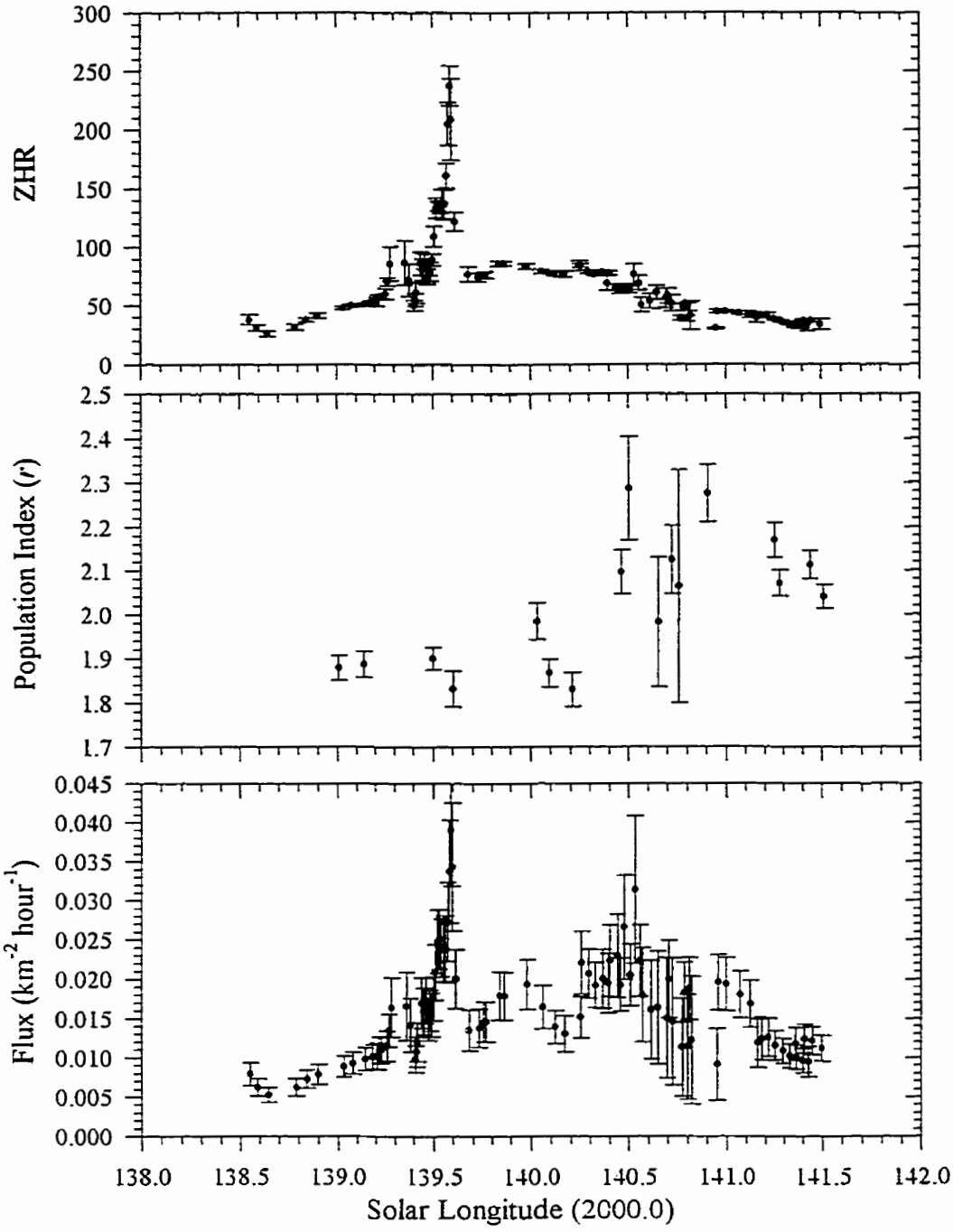

Figure 3.7: The ZHR (top), population index (middle) and flux (bottom) for the 1994 Perseid return.

Despite these difficulties, the large datasets clearly show that the level of Perseid activity varies from year to year. The shapes of the ZHR and flux profiles are generally similar, though significant variations in the population index, particularly after the main maximum, do tend to broaden the main peak of the latter. The flux curves shown here are for a limiting absolute magnitude of 6.5, or an equivalent limiting mass of 2×10^{-8} kg using the mass-magnitude-velocity correction of Verniani (1973). For the outburst portions of the profile, fainter meteors will tend to be under-represented as observers become overloaded recording shower meteors. This saturation effect has been documented in previous examinations of Perseid data (Koschack et al. 1993). The effect will be to make the flux values smaller than the true values; hence the values shown here for the new peaks are lower limits.

In 1988, the data are well distributed about both maxima. This was the first year that the "new" maximum was detected, in this case at λ=139.78°about 6 hours before the traditional peak which took place at 140.08° (Roggemans, 1989). The old and new

Table 3.1: The number of Perseid Meteors, the total effective observing time and the number of contributing observers for each year of the study. The numbers in parentheses represent the values for the average Perseid reference profile. The latter are not simple sums of the previous rows due to the exclusion of the time periods containing the outburst peak in the reference profile.

Year	Number of Perseids	Total Observing Time (hours)	Number of Observers
1988	22,526 (38,037)	1033 (2571)	194 (230)
1989	16,708 (25,227)	647 (1930)	187 (261)
1990	1,547 (3,877)	115 (863)	46 (137)
1991	36,073 (44,762)	1045 (2079)	219 (262)
1992	6,462 (10,870)	326 (1290)	105 (195)
1993	59,080 (81,538)	1768 (3211)	409 (454)
1994	33,210 (47,165)	1041 (2428)	268 (347)
1988-1994	206,872 (251,476)	13,538 (14,372)	1089

maxima were of very similar activity, but there are insufficient magnitude data to determine whether or not the particle composition differed between the peaks. The ascending branch of the early maximum is well defined and shows a half-width-to-half-maximum (HWHM) activity above the general profile of one hour. The descending branch is not well defined, but the few data here suggest a similar decline to a local minimum before activity again increases to the normal maximum. The descending branch of the main maximum is missing in these data and a higher maximum than shown here is possible, though the data do cover the interval during which the normal Perseid peak traditionally occurs and also where it is well defined in later data. The population index profile suggests a local dip of order a day in scale in the *r* value near the time of peak relative to the days before and after the maxima.

The 1989 profile in Fig 3.2 is similar to 1988 for times away from the maxima. The early maximum occurs at 139.56° while the normal maximum is at 139.8°. The magnitudes of the maxima are again very similar. The ascending branch of the early peak has a HWHM of two hours and is well defined. The descending branch from the early peak is absent in 1989 due to uneven observer coverage. The rising portion of the main profile shows a clear peak followed by several closely spaced points of decline, suggesting the maximum is better located than in 1988. Several features are notable in the falling portion of the main maxima, namely at 140.1° and 140.3°.

Data for 1990 are heavily contaminated by the moon, which was full on 6 August 1990 and thus affected all observations during the peak interval. Few observations made under good conditions were available. There appears to be a first peak near λ=139.6° with a maximum value of roughly 75, with the later peak occurring near λ=140.5° and having a ZHR value of 66. The extremely low ZHR values at peak are likely artifacts of the lunar conditions. Additional error is apparent from the shape of the sporadic activity curve, which closely mimics the Perseid curve, suggestive of numerous Perseids being counted as sporadic.

In 1991, the relative magnitudes of the two peaks become quite different, with the early peak dominating. The peak times for the maxima are clearly resolved as

λ=139.55° and λ=139.94° respectively. The ascending branch of the early peak has few data, but the HWHM can be roughly estimated as 0.5 hours. The descending portions have good coverage and reveal a HWHM of only one hour. The normal peak shows good coverage in 1991, displaying a HWHM value of 12 hours for the descending branch, but the ascending branch value is uncertain due to contamination from the earlier peak. Additional activity features after the main maximum are prominent in this profile, occurring at λ=140.34° and 140.9°. There is also an apparent difference in particle makeup across the broader profile, with a local minimum for *r* between the early and main maximum.

The lunar conditions near the shower peak were poor in 1992, with the full moon occurring on August 13. Nevertheless, good data coverage enables better determination of the time of the peak and its magnitude than in 1990. Information is obtainable about the descending portion of the early peak which was approximately one hour HWHM and occurred at λ=139.48°, while the main maximum appears at approximately λ=140.13° with a magnitude of 90.

The 1993 shower had the best coverage of all years in this study. The profile in the ascending branch of the early peak is the clearest of any of the profiles, displaying a HWHM of 1.5 hours. The descending branch is not well defined, but these data do suggest that the HWHM for the ascending branch was almost twice as wide as for the descending branch, with the early peak occurring at λ=139.53°. The main ZHR maximum was broad in extent, but occurred near λ=139.9°. A prominent secondary peak in both the ZHR and flux profiles after the main maximum is located at λ=140.2°; the flux profile also suggests that a secondary maximum in flux occurred at λ=140.5° accompanying a large increase in *r*.

In 1994 good observer coverage and excellent lunar conditions converged. The ascending portion of the profile is again well established with the early maximum having occurred at λ=139.59° and displaying a HWHM of only one hour. The magnitude data are particularly well defined in 1994 and show a decrease in *r* after the early peak. A strong asymmetry is present in the population index before and during maximum as compared to after both peaks when its value gets much larger. The main peak occurs at λ=139.9°.

These results are summarized below in Table 3.2.

Table 3.2: The locations and magnitudes of the Perseid maxima from 1988 to 1994. λ_1 is the position of the new (outburst) maximum and λ_2 is the position of the main or normal maximum. The peak fluxes associated with the first peak ($\Phi_{6.5\ outburst}$) and with the normal maximum ($\Phi_{6.5\ peak}$) are given in units of $\times 10^{-2}$ meteoroids km^{-2} hr^{-1} for Perseid meteors brighter than absolute magnitude +6.5.

Year	λ_1	$ZHR_{outburst}$	$\Phi_{6.5\ outburst}$	λ_2	ZHR_{peak}	$\Phi_{6.5\ peak}$
1988	139.78±0.03°	86±4	2.5±0.4	140.08±0.04°	106±22	2.4±0.4
1989	139.56±0.03°	102±10	2.6±0.3	139.80±0.09°	94±6	3.1±0.5
1990	139.55±0.05°	75±10	1.1±0.9	140.54±0.2°	81±61	1.7±0.1
1991	139.55±0.03°	284±63	13±4	139.94±0.04°	97±2	3.2±0.5
1992	139.48±0.02°	220±22	6.7±1.6	140.13±0.2°	84±34	2.5±0.4
1993	139.53±0.01°	264±17	6.3±1.6	139.91±0.04°	86±2	2.0±1.1
1994	139.59±0.01°	238±17	3.9±0.7	139.84±0.04°	86±2	1.8±0.3
1988-94	-	-	-	139.96±0.05°	86±1	2.5±0.4

3.4 High Temporal Resolution Profiles

To determine if any structure is present in the outburst component of the stream, the data for 1993 and 1994 near the locations of the outburst have been re-analyzed at higher temporal resolutions. Small-scale variations in flux-profiles near the time of outbursts have been reported in the past with the Draconids (Lovell 1954, p.330) and α-Monocerotids (Rendtel et al., 1996). Here all individual counting intervals greater than 0.5 hours were rejected to obtain a high resolution profile with steps as short as 0.004° in the solar longitude in the immediate region near the outburst peak. Strictly speaking, these averaging intervals would be too short if they consisted predominately of 0.5 hour (or longer) counting intervals, but fortunately most count intervals in this period are of the order of 5-15 min duration. The results are shown in Figs 3.8 and 3.9 where details of the averaging intervals and step lengths are given. Note that the 1993 data are more than an order of magnitude more plentiful than the 1994.

The buildup to the maximum in 1993 is extremely well-defined and shows two main components. The first is a gradually increasing branch which begins at λ=139.35° and continues to λ=139.49°. In this interval, the slope of the flux - solar longitude curve is 2×10^{-3} meteoroids km^{-2} $hour^{-1}$ per 0.01° of solar longitude brighter than +6.5 (hereafter $(M_v > 6.5)$ $0.01^{\circ-1}$). The second component is the interval from 139.49° - 139.53° where the slope changes dramatically to $\sim10^{-2}$ $(M_v > 6.5)$ $0.01^{\circ-1}$. These two sections suggest that the outburst may itself consist of several sub-components of differing ages with the steep increase being associated with the most recent ejecta and the broader increase just before it being due to material diffused somewhat from slightly older passages of Swift-Tuttle. Since the nodal longitude of Swift-Tuttle has been gradually increasing over time, one expects the oldest ejecta to be before the current nodal longitude of the comet.

This effect is further reflected in the descending component of the profile. Though less defined, it shows a steep decrease, having a mean slope of -2.6×10^{-2} $(M_v > 6.5)$ $0.01^{\circ-1}$ in the interval 139.53°-139.55°. The profiles in both the ascending and descending portions of the outburst in 1993 are relatively smooth. Only hints of slight variations near

139.45° and 139.39° are present. Similar structures are also visible in the 1994 profiles near 139.43° and 139.51°. Of interest is that the first of these is in a location similar to the structure present in 1993 and both are extremely close to the current nodal longitude of 109P/Swift-Tuttle. The latter fluctuation in 1994 corresponds closely to the location of maximum in 1993 and suggests that many of the meteoroids associated with the outburst maxima have a small spread in their semi-major axis, amounting to only a few tenths of an A.U. or are perturbed into Earth-intersecting orbits effectively for intervals of order a year.

In 1994, the buildup to the outburst peak is much slower than in 1993, first showing a plateau and then a jump in activity near 139.51°. The slope of the steeper ascending section of the outburst from 139.57° - 139.59° is 1.3×10^{-2} (M_v >6.5) $0.01^{\circ-1}$, very similar to the slope found in 1993. The descending branch of the profile has a slope of -1.4×10^{-2} (M_v >6.5) $0.01^{\circ-1}$ from 139.59° - 139.61° which is significantly less than in 1993, though the descending portions of both profiles are not well covered.

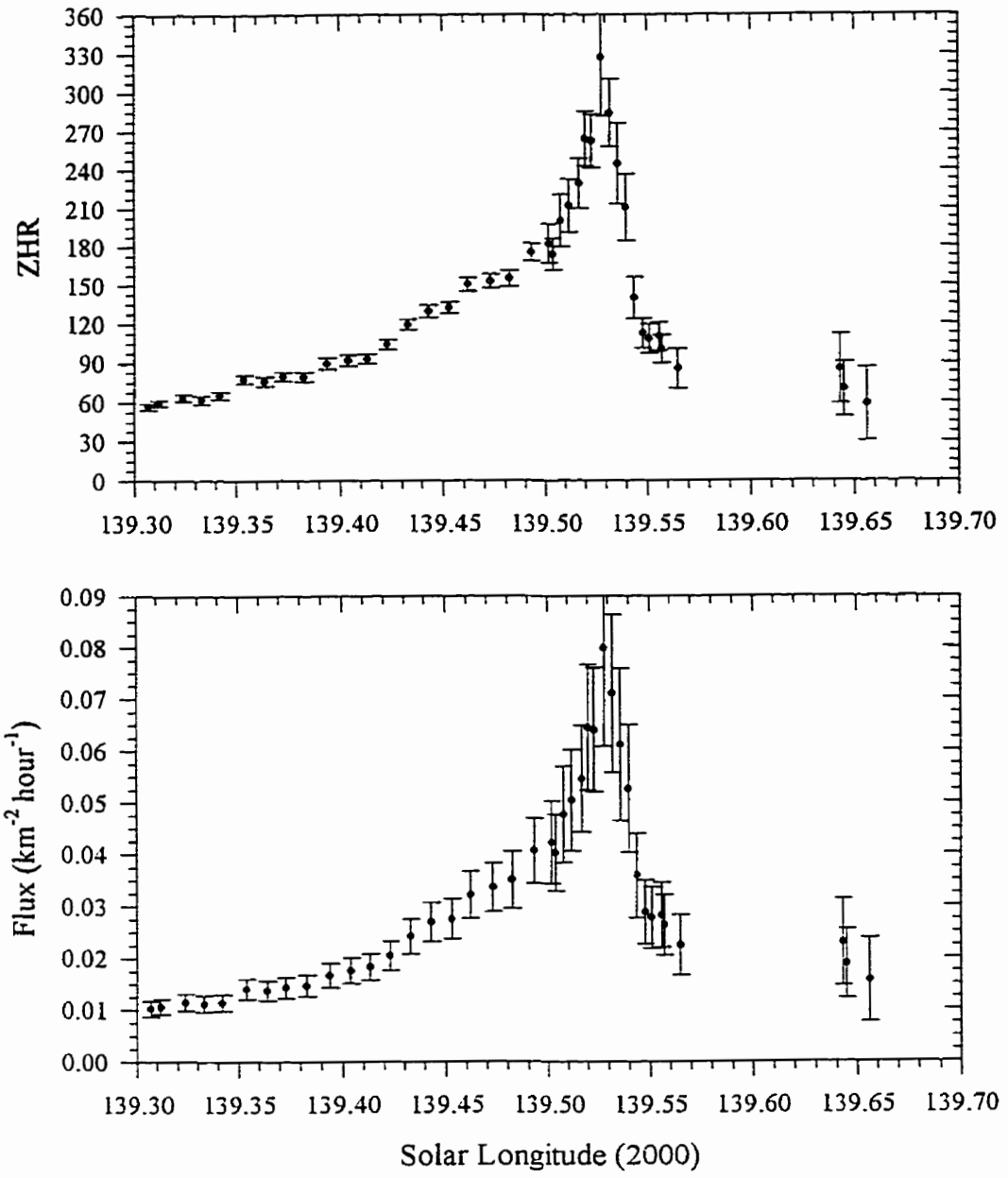

Figure 3.8: The ZHR (top) and flux (bottom) for the 1993 Perseid return. A total of 1260 count intervals, shorter than 0.3 hours in the central interval and less than 0.6 hours in the outer intervals, were used. Between λ=139.3° to 139.5° and 139.56° to 139.7°, the sampling interval was 0.02° shifted by 0.01°, while from 139.5°-139.56° the sampling window was reduced to 0.008° shifted by 0.004°.

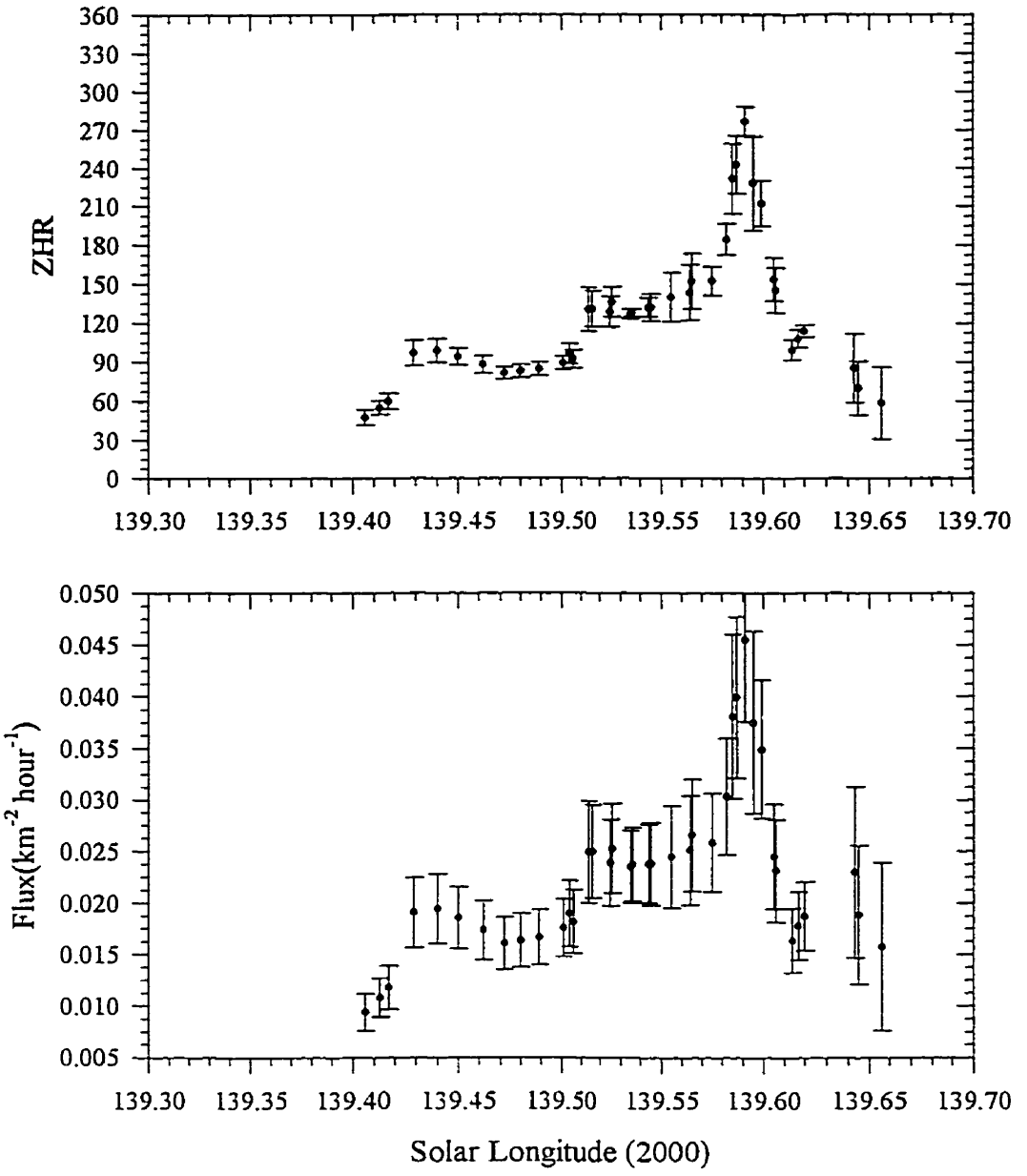

Figure 3.9: The ZHR (top) and flux (bottom) for the 1994 Perseid return. A total of 124 count intervals shorter than 0.3 hours in the central interval and less than 0.6 hours in the outer intervals were used. Between λ=139.3° and 139.5° and 139.62°-139.7° the sampling interval was 0.02° shifted by 0.01° while from 139.5°-139.62° the sampling window was reduced to 0.008° shifted by 0.004°.

3.5 Discussion

The Perseid stream, as described from the visual observations presented here, can be delineated broadly into three major components: a broad plateau displaying weak activity (background Perseids); a more concentrated component centred about the traditional Perseid peak (core Perseids); and a strongly time-varying component of short duration which appears in all profiles shortly after the nodal longitude of the parent comet (outburst Perseids). To see more clearly the first two components, which have only modest variations from year to year, we have synthesized a mean Perseid curve from all available visual observations from 1988-1994, but excluded those intervals showing the outburst component. The ZHR profile for this average curve, the associated sporadic rate, the mean population index profile and the flux profile are given in Fig 3.10 for the full period of Perseid activity. These same quantities are also shown for the ten day interval centred about the main Perseid peak in Fig. 3.11.

The background component is long-lived and shows weak activity extending from late July (~115°) until the end of August (~150°). This portion of the Perseid stream shows a very gradual increase in activity until ~ 138°, at which time the activity profile steepens as the core portion of the stream is encountered. The core component rises to a peak whose average position is λ=139.96°±0.05°. The steepest section of the peak associated with the core Perseids is very symmetrical, the ascending portion having a HWHM of 1.06°±0.07° compared to the descending profile with a HWHM of 1.04°±0.07°. A slight asymmetry in the overall shape of the ZHR curve is most evident at the 1/4-width points, located 2.58°±0.07° before maximum and 2.35°±0.07° after maximum. From these results, the Perseid shower is above the sporadic background from ~ 136°-143° or roughly one week.

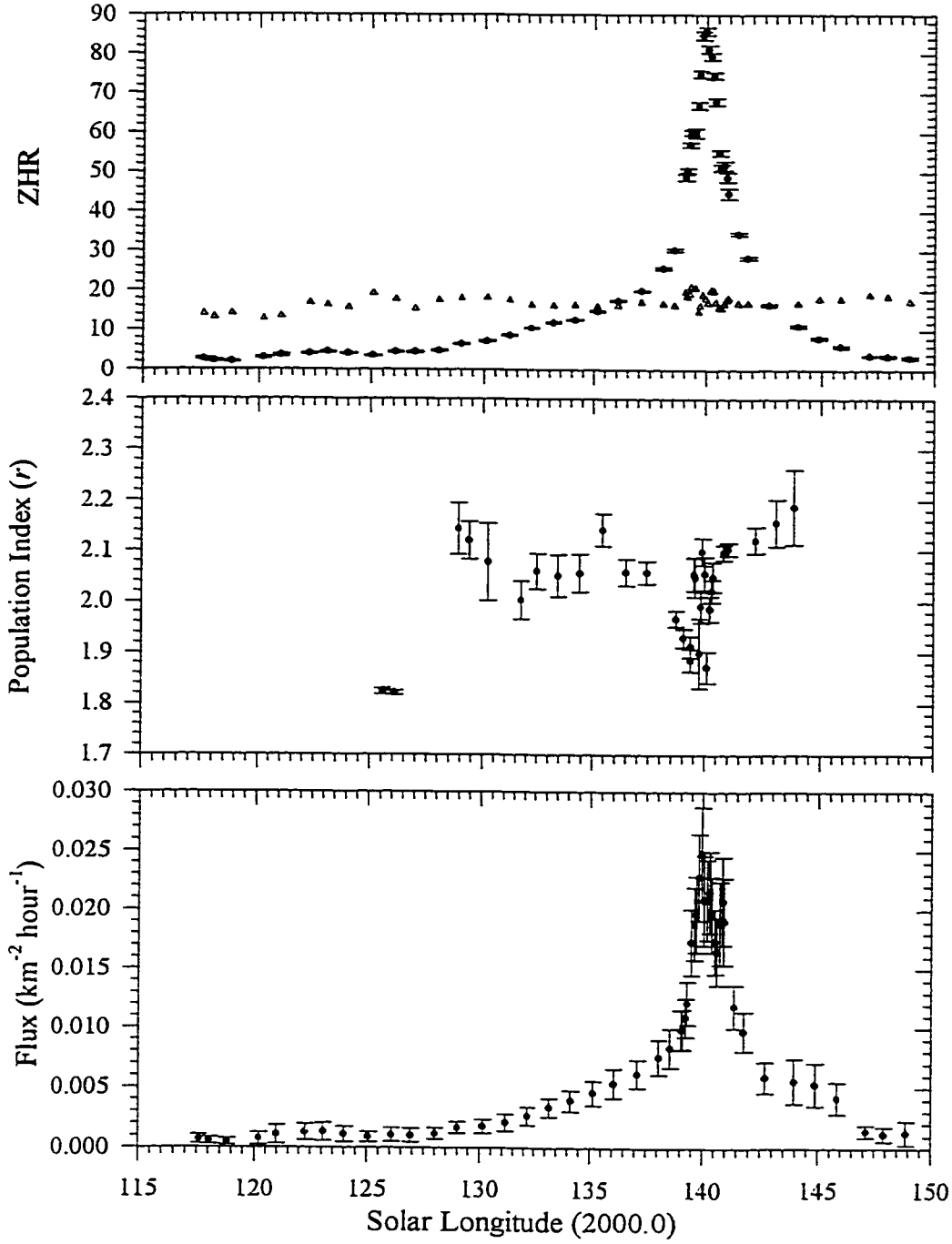

Figure 3.10: The ZHR (top), population index (middle) and flux (bottom) for the mean Perseid activity profile (1988-1994) along with the associated sporadic hourly rates denoted by Δ for the full period when visual Perseid activity is detectable visually.

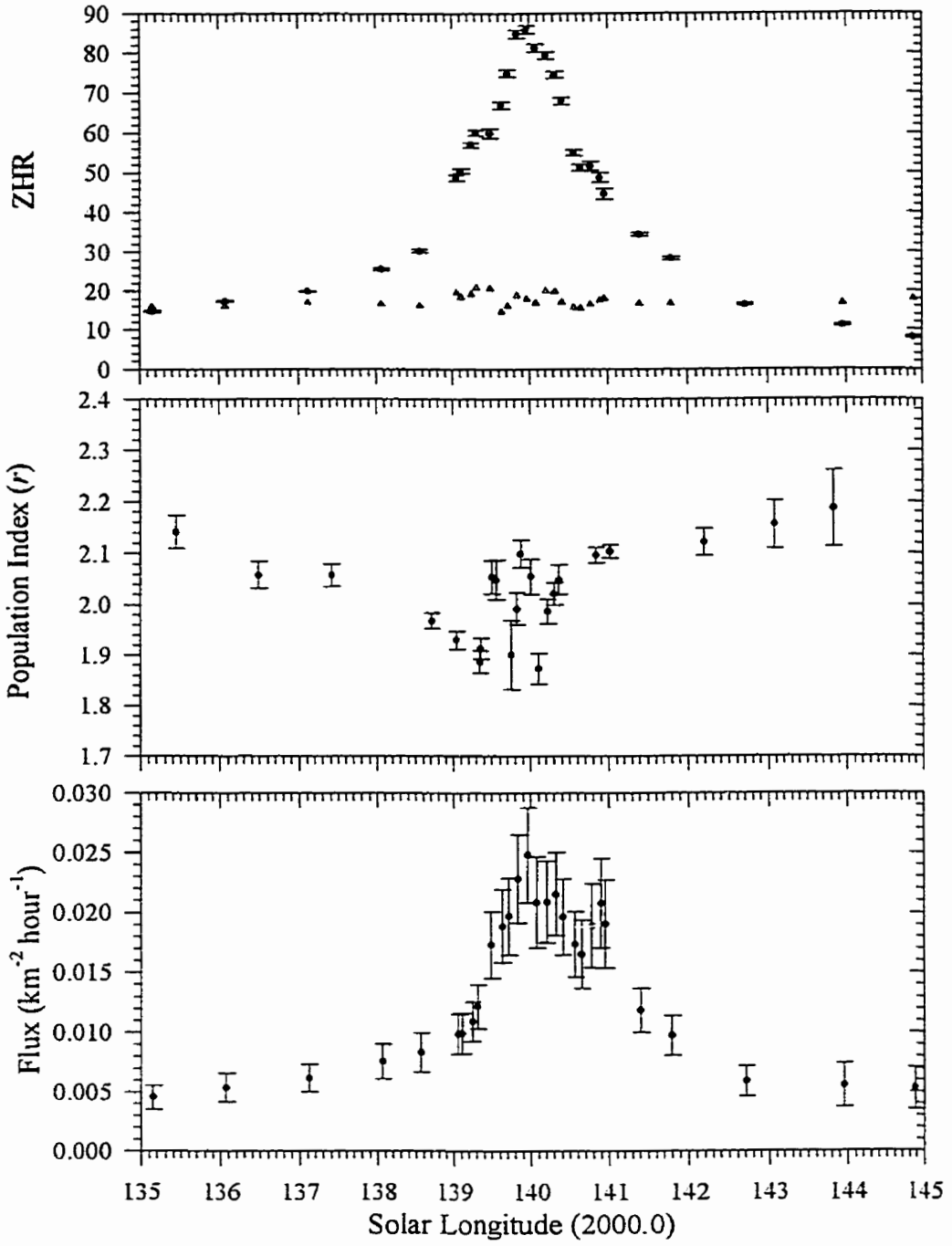

Figure 3.11: The ZHR (top), population index (middle) and flux (bottom) for the mean Perseid activity profile (1988-1994) along with the associated sporadic hourly rates denoted by Δ for the 10-day interval centred about the main Perseid peak.

That the average Perseid profile is a superposition of two components and is asymmetrical has been known for some time from visual observations (cf. Ahnert-Rohlfs 1952, Lindblad 1986, Mason and Sharp 1981, Zvolankova 1984) as well as radar data (Simek and McIntosh 1986, Lindblad and Simek 1986, Simek 1987). Harris et al. (1995) have modelled the overall activity of the stream through decay of 109P/Swift-Tuttle over a 160,000 year time period. Their model reproduces the asymmetry in the core portion of the stream and also predicts several strong secondary maxima before the main peak, most notably one lasting several days at λ=125°. Such secondary maxima are not present in the mean profile presented here. One possible explanation is that planetary perturbations on stream meteoroids are significant over long time scales, even for high-inclination streams such as the Perseids, while the Harris model ignored planetary perturbations.

Little structure is evident in the mean ZHR profile with the possible exception of a maximum near λ=140.9° and a slight maximum at λ=139.5°. The latter is undoubtedly related to the fact that the outburst component of the stream has not been entirely filtered from these data. In addition to these local features, a broad plateau is clearly visible in the flux profile immediately following the main maximum, a consequence of the increase in r after the main maximum.

The lack of strong sub-maxima is an expected result, as the smoothing procedures and addition of all data act as a filter to suppress any short period features from the mean profile, with sub-maxima being visible primarily in the yearly profiles. Stable sub-maxima in long-term Perseid data have been noted previously, particularly in radar data. Table 3.3 summarizes the reported locations of past sub-maxima detailed in the literature as well as the location of the main maximum. Previous visual and radar studies have suggested recurrent sub-maxima near λ=140.5°, but this is not supported by our mean profile. There are indications of a sub-maximum near this position in the 1993 and 1994 profiles; it is worth noting that these years had far better coverage after the main maximum than any of the other years. The most convincing candidates, however, for true sub-maxima in these years are located in the region λ=140.2°-140.3°. That sub-maxima are present in some years appears probable given the high statistical weight of the visual reports in the present

study, but the stability of such structures over many years is still questionable based on our results. Such structures may be linked with mean motion resonances operating in the Perseid stream as has been suggested by Wu and Williams (1995). Local maxima may simply be manifestations of groups of meteoroids with a common ejection origin sharing similar values of nodal longitude and semi-major axes and thus being more numerous in one year than in others. This sharp variation in the flux would be a direct result of a sharp peak in the distribution of semi-major axis within such a meteoroid sub-population.

In contrast, the main maximum shows a generally stable peak flux. Indeed, the peak flux from 1988-1994 associated with the main maximum varies from the average value $\Phi_{6.5\ peak} = (2.5\pm0.4)\times10^{-2}$ meteoroids km^{-2} $hour^{-1}$ for Perseids with $M_v>+6.5$ by less than 30%. This result contradicts past visual results, which suggest large variations in the flux. Zvolankova (1984) and Lindblad (1986) report variations of more than a factor of two in peak rates from visual observations made between the years 1944-1953 and 1953-1981 respectively. We suggest that these apparent variations are the result of biased sampling in past visual observations due to uneven observer coverage.

The changes in flux associated with the main maximum are given in Table 3.2 The average value for $\Phi_{6.5\ peak}$ of $(2.5\pm0.4)\times10^{-2}$ and of $(2.9\pm0.4)\times10^{-3}$ for $\Phi_{3.5\ peak}$, are in close agreement with the results of Kaiser et al. (1966) and Andreev et al. (1987) who derive an average $\Phi_{6.5\ peak}=(3.4\pm0.5)\times10^{-2}$ and $\Phi_{3.5\ peak}=3.7\times10^{-3}$, respectively from radar observations.

Table 3.3: Locations of the main maximum and literature reports of sub-maxima from recent radar and visual observations of the Perseids. λ is the reported position of the main maximum and λ_{sub} is the position of additional sub-maxima detected in the given year(s). Possible locations of sub-maxima from this analysis are also shown; values in parentheses are less certain.

Year(s)	λ	λ_{sub}	Source
1980	139.92±0.04°	-	Mason and Sharp (1981)
1958-1962, 1972	139.89±0.04°	139°;139.5°	Simek (1987)
1980-1985		140.5°;142°	
1958-1964	139.91±0.03°	140.5°	Simek and McIntosh (1986)
1953-1978	139.9±0.04°	140.46°	Lindblad and Simek (1986)
1953-1981	140.11°	140.45°	Lindblad (1986)
1964-1981	139.7±0.2°	-	Andreev et al. (1987)
1989	139.8±0.09°	140.1°;140.3° (140.9°)	This work
1991	139.94±0.04°	(140.34°); 140.9°	This work
1993	139.91±0.04°	140.2°; (140.5°)	This work
1994	139.84±0.04°	140.3°; (140.5°)	This work

Table 3.4: The population index, r, and the quantity of data that each r value is derived from for the average profile from 1988-1994.

λ	r	No. of Observers	No. of Perseids
139.045°	1.930±0.018	172	11,931
139.354°	1.886±0.022	101	10,257
139.362°	1.913±0.021	118	11,369
139.508°	2.054±0.032	43	2,806
139.562°	2.049±0.039	27	1,870
139.752°	1.900±0.068	13	1,140
139.828°	1.992±0.032	70	9,001
139.878°	2.099±0.027	83	11,641
140.011°	2.055±0.034	61	5,664
140.107°	1.873±0.031	76	5,389
140.224°	1.987±0.024	117	9.660
140.307°	2.022±0.022	162	15,257
140.370°	2.049±0.029	96	9,638

The variation in the population indexes of the stream shows several features (see Figs. 3.10b and 3.11b). The most obvious is the asymmetry in particle makeup in the day leading to the main maximum, when r is consistently low, compared to after the main maximum, when r shows a significant increase. The average value of r for the remainder of the profile, both before and after the maxima, is remarkably constant near 2.15. Two pronounced maxima in r are also evident near the time of the activity maxima. The first maxima in r occurs at λ=139.55°$\pm$ 0.07° and the second at λ=139°88$\pm$0.06°. That these features are statistically significant can be assessed from Table 3.4 where the amount of magnitude data used to derive each r value is given. These locations are potentially linked to the different evolutionary components of the stream. The first is probably related to the outburst component, which is still present despite our attempt to remove the central portions of the outburst activity in each year. The young meteoroidal material associated with the latest return of Swift-Tuttle is rich in smaller meteoroids as would be expected for recent ejecta. The main maximum is also rich in fainter meteors, indicating the presence of comparatively young material.

A single local minimum in the population of small meteoroids just before maximum has been previously noted by Mason and Sharp (1981). Andreev et al. (1987) found a local maximum in the proportion of small meteoroids at the time of maximum from radar data. It seems probable that the different ages of the outburst and core components of the stream are manifest not only in higher flux but also in differences in the average meteoroid population relative to the background population, and that recent ejections of fresher meteoroids have significantly different r values as shown by these visual data.

The outburst component of the stream has only been recognized in visual observations over the last few years (cf. Roggemans, 1989), though Lindblad and Porubcan (1994) have shown that photographic records of Perseid activity dating back to the 1950's had an earlier peak near the present nodal longitude for 109P/Swift-Tuttle. Simek and Pecina (1996) also detected the presence of the outburst peak as early as 1986 in the Ondrejov radar data and suggest that the sub-maxima reported at λ=139.5° by Simek (1987) in earlier radar data may also be a detection of the outburst component of

the stream. This component has been widely associated with the return of 109P/Swift-Tuttle to perihelion in 1992 and is generally associated with material from the last perihelion passage of Swift-Tuttle in 1862 (Wu and Williams 1993; Williams and Wu 1994; Jones and Brown 1996).

The position of the maximum of the outburst component of the stream given in Table 3.2 shows no clear variation as a function of the year. The relative magnitudes of the peaks are shown in Fig. 3.12a where the flux at the outburst peaks are given relative to $\Phi_{6.5\ peak}$. Here a clear demarcation occurs, with activity being weak before 1991 and strong thereafter. This sudden change in the outburst component, rather than a gradual increase in flux as predicted by model calculations assuming all new activity to result from 1862 ejecta (Williams and Wu 1994), suggests that meteoroids encountered before 1991 may have a different origin. On the basis of model calculations, Jones and Brown (1996) ascribe the material from 1988-1990 as being almost exclusively from the 1737 and 1610 passages of Swift-Tuttle, with meteoroids from the 1862 passage first encountered in significant quantities in 1991 (see Chapter 4).

The locations of the visual maxima in these years are very similar to those reported from overdense radar observations. Watanabe et al. (1992) analyzed the 1991 Perseid return with the Kyoto MU-radar and determined the time of peak for the outburst component to be λ=139.6, in good agreement with our results. They also found that the outburst peak flux was 3.4±0.8 times that of the main maximum.

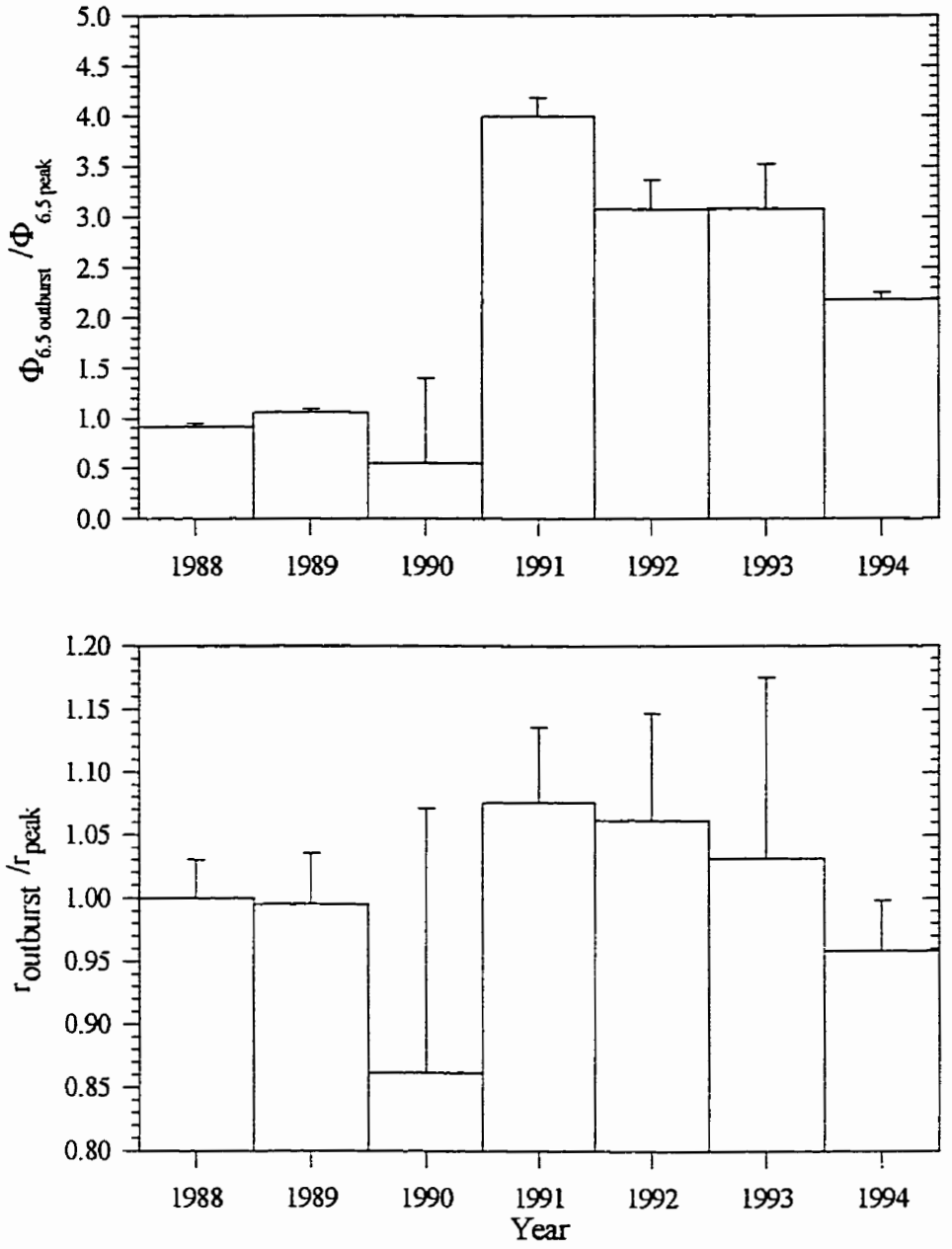

Fig 3.12: The relative magnitude of the peak flux (a - top) of the outburst component of the Perseid stream from 1988-1994 relative to the flux of the normal maximum. b - bottom, the change in the particle composition during the outbursts from 1988-1994 relative to the particle distribution at the time of the normal peak.

This result applies to meteors in the magnitude range $0>M_v>+3$ and is similar to the ratio of peak fluxes we find between the outburst peak and the core maximum in 1991 of 3.2 over the same magnitude range. For comparison, Simek and Pecina (1996) used the Ondrejov radar data and found the maximum to be located at an average position of $\lambda=139.58°\pm0.04°$ in the interval 1986-1994.

The particle composition of the outburst component of the stream relative to the main peak is shown in Fig.3.12b, where the ratio of the respective population indices has been plotted. Watanabe et al. (1992) report an increase in the proportion of large meteoroids during the outburst in 1991 and this notion has been variously supported by qualitative reports from observers during other Perseid outbursts (cf. Pin-xin, 1992). There is little question that the number of bright Perseids increases during the outbursts. Fig 3.12b, however, shows that the proportion of bright meteors during the outbursts does not differ substantially from the main peak. Thus the mass distribution of the outburst in all years, as measured by *r*, does not differ, within error, from the population associated with the core component of the stream. This contradicts the conclusions of Watanabe et al. (1992) and is consistent with the earlier observation of a maximum in the *r* values near the time of both maxima.

3.6 Summary and Conclusions

From the flux data and particle population presented here, it is evident that several outstanding features of the Perseid stream need to be addressed when attempting to model it. These include:

- The asymmetry in the background Perseids and the symmetry in the core population as defined by the locations of the 1/4-width (2.58°±0.07° before the main maximum and 2.35°±0.07° after maximum) and the 1/2-width (1.06°±0.07° before maximum and 1.04°±0.07° after maximum) positions.

- The location and magnitude of the outburst maxima for each year given in Table 3.2.

- The location and magnitude of the mean activity maximum associated with the core population at λ=139.96°±0.05° and with $\Phi_{6.5\ peak}=(2.5\pm0.4)\times10^{-2}$ meteoroids $km^{-2}\ hour^{-1}$.

- The change in particle composition across the stream, particularly in the region near the maxima in *r* at λ=139.55°±0.07° and at λ=139.88°±0.06°.

- The apparent similarity between the meteoroid populations associated with the outburst and core population.

- The broad shoulder in flux after the core maximum.

- The differing slopes in the branches of the outburst profile and the asymmetry in these profiles.

- The origins of the background, outburst and core populations.

Other characteristics not clearly discernable in these data, such as the possible presence of a sub-maximum near λ=140.2°-140.3° or at λ=140.5° and the existence of ephemeral sub-maxima at various locations after the core maximum in different years, need further observational confirmation.

Similarly, the location and the size of the mean radiant for the shower and its likely variation during the course of activity of the shower are important diagnostics for use in modelling.

From these data it is apparent that the Perseid meteoroid stream is highly dynamic and rich in structure. The complexities of the Perseids can only be understood in the context of a complete numerical model of the stream, which can explain features detected through observations, such as those described here.

References

Ahnert-Rohlfs, E. 1952. On the structure and the origin of the Perseid meteoroid stream. *Veröffentlichungen der Sternwarte Sonneberg* **2**, 5-38.

Andreev, G. V., L. N. Rubtsov, and N. V. Tarasova. 1987. On the spatial structure of the Perseids meteor stream. In *First GLOBMET Symposium* (R. G. Roper, Ed.), p. 39. ICSU-SCOSTEP, Urbana, Illinois.

P. Brown and J. Rendtel (1996) The Perseid Meteoroid Stream: Characterization of Recent Activity from Visual Observations, *Icarus*, **124**, 414-428.

Harris, N. W., K. C. C. Yau, and D. W. Hughes. 1995. The true extent of the nodal distribution of the Perseid meteoroid stream. *Mon. Not. R. Astron. Soc.* **273**, 999-1015.

Hasegawa, I. 1993. Historical records of meteor showers. In *Meteoroids and Their Parent Bodies* (J. Štohl and I. P. Williams, Eds.), p. 209. Astronomical Inst., Slovak Acad. Sci., Bratislava.

Jones, J. and P. Brown. 1993. Sporadic meteor radiant distributions: orbital survey results. *Mon. Not. R. Astron. Soc.* **265**, 524-532.

Jones, J. and P. Brown. 1996. Modelling the orbital evolution of the Perseid meteoroids. In *Physics, Chemistry and Dynamics of Interplanetary Dust* (B. Å. S. Gustafson and M. S. Hanner, Eds.), p. 105. Astronomical Society of the Pacific.

Kaiser, T. R., L. M. G. Poole, and A. R. Webster. 1966. Radio-echo observations of the major night-time streams. I. Perseids. *Mon. Not. R. Astron. Soc.* **132**, 224-237.

Koschack, R., R. Arlt and J. Rendtel. 1993. Global analysis of the 1991 and 1992 Perseids. *WGN J. IMO* **21(4)**, 152-168.

Koschack, R. 1995. Analyses and Calculations. In *Handbook for Visual Meteor Observers* (J. Rendtel, R. Arlt and A. McBeath, Eds.), pp. 280-289. IMO, Potsdam.

Koschack, R., and R. L. Hawkes. 1995. Observing instructions for major meteor showers. In *Handbook for Visual Meteor Observers* (J. Rendtel, R. Arlt and A. McBeath, Eds.), pp. 42-74. IMO, Potsdam.

Koschack, R., and J. Rendtel. 1988. Number density in meteor streams. *WGN J. IMO* **16**, 149-157.

Koschack, R., and Rendtel, J. 1990a. Determination of spatial number density and mass index from visual meteor observations. *WGN J. IMO* **18**, 44-59.

Koschack, R., and J. Rendtel, J. 1990b. Determination of spatial number density and mass index from visual meteor observations (II). *WGN J. IMO* **18**, 119-141.

Koschack, R., and P. Roggemans. 1991. The 1989 Perseid meteor stream. *WGN J. IMO* **19**, 87-99.

Kresáková, M. 1966. The magnitude distribution of meteors in meteor streams. *Contr. Skalnaté. Pleso* **3**, 75-109.

Kronk, G. W. 1988. *Meteor Showers: A Descriptive Catalog*. Enslow, New Jersey.

Lindblad, B. A. 1986. Structure and activity of the Perseid meteor stream from visual observations 1953-1981. In *Asteroids, Comets, Meteors II* (C.-I. Lagerkvist, B. A. Lindblad, H. Lundstedt, and H. Rickman, Eds.), p.531. Reprocentralen, Uppsala.

Lindblad, B.A. and V. Porubcan 1994. The activity and orbit of the Perseid meteor stream. *Planet. Sp. Sci.* **42**, 117-123.

Lindblad, B. A. and M. Šimek. 1986. The activity curve of the Perseid meteor stream from Onsala radar observations 1953-78. In *Asteroids, Comets, Meteors II* (C.-I. Lagerkvist, B. A. Lindblad, H. Lundstedt, and H. Rickman, Eds.), p.537. Reprocentralen, Uppsala.

Lovell, A.C.B. 1954. *Meteor Astronomy*. Pergamon, London.

Marsden, B. G. 1973. The next return of the comet of the Perseid meteors. *Astron. J.* **78**, 654-662.

Mason, J. W., and I. Sharp. 1981. The Perseid meteor stream in 1980. *JBAA* **91**, 368-390.

McKinley, D. W. R. 1961. *Meteor Science and Engineering*. McGraw-Hill, Toronto.

Olson, D. W., and R. L. Doescher. 1993. Meteor observations on August 10-11, 1863. *WGN J. IMO* **21**, 175-181.

Pin-Xin, X. 1992. The 1992 Perseid outburst in China. *WGN J. IMO* **20**, 198.

Rendtel, J., P. Brown, and S. Molau. 1996. The 1995 outburst and possible origin of the α- Monocerotid meteoroid stream. *Mon. Not. R. Astron. Soc.* **279**, L31-L36.

Roggemans, P. 1989. The Perseid Meteor Stream in 1988: A Double Maximum! *WGN J. IMO* **17**, 127-137.

Schiaparelli, G. V. 1867. Sur les Étoiles Filantes, et spécialement sur l'identification der Orbites des Essaims d'Août et de Novembre avec celles des Comètes de 1862 et de 1866. *Comptes Rendus* **64**, 598-599.

Šimek, M. 1987. Perseid meteor stream mean profile from radar observations in Czecheslovakia. *BAC* **38**, 1-6.

Šimek, M., and B. A. McIntosh. 1986. Perseid meteor stream: mean flux curve from radar observations. *BAC* **37**, 146-155.

Šimek, M., and P. Pecina. 1996. Activity of the new filament of the Perseid meteor stream. In *Physics, Chemistry and Dynamics of Interplanetary Dust* (B. Å. S. Gustafson and M. S.Hanner, Eds.), p. 109. Astronomical Society of the Pacific.

Verniani, F. 1973. An analysis of the physical parameters of 5759 faint radio meteors. *J. Geophys. Res.* **78**, 8429-8462.

Watanabe, J-I., T. Nakamura, M. Tsutsumi, and T. Tsuda. 1992. Radar Observations of the strong activity of a Perseid meteor shower in 1991. *PASJ* **44**, 677-685.

Williams, I. P., and Z. Wu. 1994. The current Perseid meteor shower. *Mon. Not. R. Astron. Soc.* **269**, 524-528.

Wu, Z., and I. P. Williams. 1993. The Perseid meteor shower at the current time. *Mon. Not. R. Astron. Soc.* **264**, 980-990.

Wu, Z., and I. P. Williams. 1995. Gaps in the semimajor axes of the Perseid meteors. *Mon. Not. R. Astron. Soc.* **276**, 1017-1023.

Yau, K., D. Yeomans, and P. Weissman. 1994. The past and future motion of comet P/Swift-Tuttle. *Mon. Not. R. Astron. Soc.* **266**, 303-316.

Zvolánková, V. 1984. Changes in the activity of the Perseid meteor shower 1944-1953. *Contr. Obs. Skalnaté Pleso* **12**, 45-75.

Chapter 4:
Development and Application of a Numerical Model of the Formation and Evolution of the Perseid Meteoroid stream[2]

4.1 Introduction

The recovery of comet 109P/Swift-Tuttle in 1992 marked the beginning of an intensive effort to characterize one of the largest known Earth-crossing bodies. Much has been learned of Swift-Tuttle in the intervening years (cf. Yau *et al.*, 1994), but the comet's equally famous trail of meteoroidal debris remains mysterious. The return of the comet was presaged by a strong increase in activity from the Perseids beginning most notably in 1991 (Brown and Rendtel, 1996). This marked the first occasion when a large change in the flux of the shower was unambiguously recorded. Indeed, Olivier (1925) comments that "...the Perseids appear with no remarkable variations in numbers practically every August".

The Perseid shower has been recognized in the sky almost as long as records of such phenomena have been kept. Hasegawa (1993) has traced ancient records of the

[2] A version of this chapter has been published : P. Brown and J. Jones (1998) Simulation of the Formation and Evolution of the Perseid Meteoroid Stream. *Icarus*, **133**, 36-68.

stream back 2000 years and it seems probable that the stream is older still. Detailed observational histories of the stream have been given by Kronk (1988) and Rendtel *et al.* (1995). The shower is also notable as the first instance in which a comet was definitively linked to a meteor shower, this connection having been made by Schiaparelli (1867).

The first attempts to understand the stream in an analytical form were those of Twining (1862), who investigated the perturbing effects of the Earth on Perseid meteoroids and found no sensible perturbations from this mechanism. Further research through the late 19th and early 20th century concentrated on interpreting visual observations of the shower. Throughout this period, there was general understanding that comets and meteoroid streams were linked, the weight of opinion being that the latter originated from the former, but contrary views were not uncommon. Whether meteoroids were continually discharged or periodically released from comets remained unclear.

That progress in understanding the stream relied heavily on the untangling of the cometary - meteoroid decay process is highlighted by Guigay (1947) who postulated that the stream was formed entirely by a collision between a proto-Swift-Tuttle and another body. The resulting spall accounted for the Perseids and at least five other comets noted by Guigay to have relatively close orbital intersections. Kresak (1957) pointed out the numerous difficulties in this interpretation and its contradiction to the mounting photographic meteor data then available for the stream.

Hamid (1951) was the first to model the ejection of the meteoroids from Swift-Tuttle using Whipple's (1951) "icy-snowball" cometary model and to analytically follow the resulting orbits under the effects of secular planetary perturbations. He noted that the formation and subsequent evolution of the stream is intimately linked with the past history of the comet, which he determined through secular perturbations of the then best available orbit for Swift-Tuttle. The variation in orbital elements for Perseid meteoroids was found to be in general agreement with photographic data, assuming ejection velocities of order 10 m/s, and the age of the stream was determined to be 40 000 years.

Southworth (1963) performed a more detailed analysis of the evolution of the stream by computing numerically the gravitational perturbations on individual stream meteoroids instead of mean perturbations from secular theory. He found that the variation

observed in the radiant position and velocities of meteoroids in the stream implied scattering much stronger than planetary perturbations alone could explain. Using similar ejection velocities as Hamid, he concluded that either strong non-gravitational effects out of the orbital plane were at work or the stream was formed not through gradual disintegration of the parent comet but rather by way of a single, large cometary explosion (citing Guigay's (1947) hypothesis) approximately 1000 years ago. His work implied an upper limit of 6000 years for the age of the stream.

Sekanina (1974) investigated the dynamics of the Perseid stream based on a detailed consideration of the likely ejection conditions from the parent comet and the effects that variations in these conditions, such as location and direction of ejection, might make on the final meteoroid distributions. By examining ancient records of recorded appearances of the Perseids, he concluded that a systematic variation in the time of recorded Perseid returns relative to the perihelion passage of the comet suggested that the meteoroid emission lasted for several months, probably beginning shortly before perihelion process and implicitly assumed to be nearly continuous during this time. In particular, he suggested that the comet may vary its dust output dramatically from apparition to apparition, resulting in preferential locations for strong Perseid returns relative to the comet's perihelion passage and the initial emission epoch.

The concept that the Perseid stream was formed by emission of meteoroids at a single location along the orbit of Swift-Tuttle was further developed by Katasev and Kulikova (1975). Using a variety of ejection locations and velocities, they determined that the best agreement between computed orbits from an isotropically emitting Swift-Tuttle and the observed stream was found using velocities of 100 m/s and an ejection centered at 30° true anomaly. No account of subsequent planetary perturbations or the past history of the comet was employed and the fit relied entirely on the veracity of the orbital elements for the stream presented by Southworth (1963).

The failure of Swift-Tuttle to return in 1981, as predicted based on the 1862 orbital solution alone (cf. Marsden, 1973), was the most significant development in the understanding of the stream to that time. It became clear that our ideas about Swift-Tuttle based on these observations of the comet alone were in error and along with them

previous attempts to understand the stream. The recovery of 109P/Swift-Tuttle early in 1992, and its subsequent perihelion in December of that year, provided hope that serious attempts to understand the stream might be successful as the complete history of Swift-Tuttle's orbital evolution over the last two thousand years was then possible.

Wu and Williams (1993) have used Whipple's ejection model in conjunction with a Monte Cario approach to model the behavior of 500 test meteoroids of the same mass ejected during the 1862 passage of Swift-Tuttle. They conclude that gravitational perturbations from the planets move the original non-Earth intersecting orbits into Earth crossing paths and suggest that much of the recent intense activity from the Perseids is from 1862 ejecta, with 1994 being the culmination of this activity. The use of small numbers of test particles of only one mass and an older orbit for Swift-Tuttle limit the generality of their results. To improve on this early model Williams and Wu (1994) used a better orbit for the comet and a distribution of masses to make quantitative predictions concerning activity for the Perseids in the early 1990's as well as locations for the maximum of the shower in each year from 1988-1995. The results still suggested that peak activity would occur in 1994, but the predicted times for maximum were consistently two hours earlier than observed.

Harris and Hughes (1995) have investigated the distribution of semi-major axes of photographic Perseid meteoroids. They find no variation as a function of mass and conclude that the final ejection velocities for Perseid meteoroids are independent of mass and all of relatively high velocity. This result will be discussed in detail in Sect. 4.2. Harris *et al.* (1995) expanded upon this result by modelling the ejection of Perseids using a Maxwellian velocity distribution centered about 0.6 km/s. Through integration of 109P/Swift-Tuttle backward for 0.16 Ma, they also simulated formation of the stream as a whole, taking ejections from the comet every 5000 years without accounting for planetary perturbations or radiation forces. They conclude that the stream is roughly 160 000 years old.

Here we develop a detailed numerical model for the formation and subsequent evolution of the Perseid stream. From our analysis we will attempt to gain some understanding of several key questions, such as:

1. How do the initial ejection conditions assumed affect the final observed distributions and over what time scales are the initial ejection conditions "erased" due to radiation forces and planetary perturbations? In particular, are the final distributions sensitive to the assumed cone angle over which ejections take place, the largest distance from the sun the meteoroids are ejected and the assumed density of the meteoroids? What changes in the final distributions is a function of mass? What is the best model representation of the ejection process? What is the range of initial ejection velocities?

2. Why has the position of the outburst peak of the Perseids observed over the last decade changed position in the stream? Why has the outburst portion of the stream also varied in intensity so much in this time interval? Why did this recent outburst activity "turn-on" so quickly in 1991? What are the underlying causes of the outbursts - intrinsic changes in the dust output of the comet in the past, the recent passage of Swift-Tuttle or some other effect?

3. What ejection(s) contribute most to the outburst activity we have seen in the stream over the last decade? Are most of these meteoroids from the 1862 passage of the comet as has been widely assumed?

4. What is the age of the main core of the Perseid stream? What is the ultimate age of the stream?

5. What is the current progression rate of the node of the stream?

6. What effect does the Earth have on the longer-term development of the stream?

7. What are the mechanisms, which remove meteoroids from the stream and over what time-scales do they act?

8. What controls the delivery of Perseid meteoroids to Earth?

4.2 Initial Conditions: The Cometary Decay Process

4.2.1 Physical models

Stream meteoroids are ejected from comets. As comets approach the sun, the number of meteoroids ejected from a comet tends to increase, as does the magnitude of the ejection velocity. The ejection velocity is a small fraction of the orbital velocity of the comet and hence the daughter meteoroids move along similar orbits to the parent comet. Sublimating volatiles (primarily water-ice) are responsible for release of the particles through momentum exchange with the meteoroid grains.

The preceding paragraph summarizes those general aspects of the meteoroid ejection process for which there is near unanimous agreement by workers in the field. Adding additional details to the preceding picture, particularly quantitative ones, requires interpretation of often contradictory observational and theoretical aspects of the cometary ejection process. Remarkable as it seems, this picture is almost identical to the one first presented by Whipple (1951). The only major change from that early model which might be widely accepted today is the observational fact that the active regions of comets (and hence the areas where meteoroids might be ejected) are small fractions of the total surface area of the comet and thus dust is initially confined to collimated jets immediately after leaving the nucleus surface (cf. McDonnell *et al.* 1987). At great distances from the nucleus, however, the meteoroids in such jets tend to spread out into larger cones and the final physical picture may not be very different from Whipple's (cf. Jones, 1995).

To try to model the evolution of a meteoroid stream, the process by which the stream initially formed is of considerable interest. Whether the formation process is the dominant evolutionary process (in comparison to planetary perturbations or radiation forces) is not clear and may vary from stream to stream. Since uncertainty exists about the formation process, we choose to use several different models of formation along with wide variations for those parameters, which we feel, are particularly poorly known in order to determine just how strongly the initial conditions affect the final results. In the end, each model and set of parameter choices lead to a range of possible values for one

crucial number; namely the final ejection velocity of the meteoroid relative to the comet. Knowing this value along with the location of ejection, comet orbit and meteoroid shape permits forward integration of the equations of motion for the stream meteoroid and some approximate estimate of its future location.

As it is impossible to make a rigorous determination of the precise location of ejection for a meteoroid, a Monte Carlo approach must be employed. Here we assume that meteoroids are ejected at random values of true anomaly over the arc of the 109P/Swift-Tuttle's orbit inside 4 A.U. in numbers proportional to the amount of solar energy received by the nucleus. That meteoroids would be ejected with equal probability for all values of true anomaly (for 109P, between $233°<\nu<127°$) under these assumptions was first noted by Kresak (1976). This result is due to the r^{-2} variation of solar flux and the r^2 $d\nu/dt$ constant of motion from Kepler's second law removing the effects of changes in ν on the meteoroid production function. That ejection occurs inside 4 A.U. for 109P/Swift-Tuttle has been constrained partially by the observations of Boehnhardt *et al.* (1996) and O' Ceallaigh (1995) who observed little or no coma in Swift-Tuttle at 5 A.U. during its 1992 apparition. While water production is usually taken to cease near 3 A.U. (cf Festou *et al.* (1993)), some more distant production is commonly observed in many comets and we choose 4 A.U. as a compromise, acknowledging that much of this distant production is due to compounds more volatile than water, with the dust-gas interaction dynamics likely to be quite different. We will investigate the effects on the observed stream of choosing still smaller cut-offs in solar distance for meteoroid production in section 4.

The orbit of 109P/Swift-Tuttle has been determined with accuracy backward nearly 2000 years. Marsden *et al.* (1993) and Yau *et al.* (1994) have used observations from the 1992 perihelion passage along with older observations extending back to 69 BC to reverse integrate the equations of motion of the comet. Their independently derived results have a high level of agreement. We use these orbits as the initial seed orbits for all models, noting that the slight difference between the ephemera is much smaller than other uncertainties in our adopted models.

The shape (more precisely the cross-sectional area to mass ratio) of the meteoroids comes into play not only during the ejection process but also in the particles' subsequent

evolution under radiation forces. Gustafson (1989) has noted the large variation in ejection velocity predicted solely on the basis of modest variations in the shape factor for meteoroids. Similar work by Nakamura *et al.* (1994) supports the notion that shapes other than the idealized sphere would tend to have higher ejection velocities. We discuss our attempts to account for this effect in Sect. 4.3. The effect of shape on radiation pressure is significant only for the smallest of meteoroids considered here and is discussed further in section 3.

Past attempts to model meteoroid streams (cf. Williams, 1993 for a review) have relied almost entirely on the Whipple model and the numerical relation he determined assuming gas drag lifts a spherical meteoroid away from the sunward side of the nucleus, namely

$$V_{eject} = 8.03 r^{-1.125} \rho^{-\frac{1}{3}} R_c^{\frac{1}{2}} m^{-\frac{1}{6}} \qquad (4.1)$$

where R_c is the radius of the cometary nucleus in km, ρ the bulk density of the meteoroid in g/cm^3, m the mass of the meteoroid in grams, n the fraction of incident solar radiation used in sublimation, r is heliocentric distance in A.U. and V_{eject} is the final grain ejection velocity relative to the nucleus in m/s. A typical value of these parameters (R_c=5 km, ρ=0.800 g cm^{-3}, n=1, and m=0.1g) results in a V_{eject} of 36 ms^{-1} at 1 A.U. Note that we have explicitly ignored the gravitational attraction of the nucleus in Eqn 4.1.

Indeed, the Whipple ejection formula provides the starting point for much of the modelling we perform. The shortcomings of the Whipple model, namely the assumption of blackbody limited nucleus temperature (instead of sublimation temperature limited) and the neglect of the adiabatic expansion of the gas have been corrected by (among others) Jones (1995) and we use his revised Whipple formula

$$V_{eject} = 10.2 r^{-1.038} \rho^{-\frac{1}{3}} R_c^{\frac{1}{2}} m^{-\frac{1}{6}} \qquad (4.2)$$

for our basic model. In particular, the Whipple formulation ignores the role of isolated jets of activity, which is taken into account in the Jones' model. Despite the modifications, the Jones' equation is very close to that of the original Whipple model. We examine the

effects of changes in ejection cone angle (the angle between the solar-direction and velocity vector) to the final results in Sect. 4.4. .

Of the parameters in the Jones' formula, the radius of the nucleus is most certain in the case of 109P/Swift-Tuttle. From visible observations of the bare nucleus, Boehnhardt *et al.* (1996) conclude that the nucleus has a radius of 11.2±0.3 km, while O'Ceallaigh *et al.* (1995) have found that the nuclear radius is 11.8±0.2 km using similar observations. Fomenkova *et al.* (1995) derived a radius of 15±3 km from observations in the IR. These extremely large radius estimates are consistent with the apparent lack of non-gravitational forces needed to explain Swift-Tuttle's motion over the last two millennia (Yau *et al.*, 1994). We adopt a radius of 10 km throughout and note that this is almost twice the mean nuclear radius of Halley.

Theoretical models are no better than the assumptions on which they are based and if we ignore for the moment the details of the models we see that they agree on many of the parameters which govern the speed of ejection of the meteoroids. Of particular interest to us is the variation of the ejection speed with the Sun-comet distance. Both the Whipple-derived theories and most other models predict that the variation should be of the form

$$V \propto r^n \tag{4.3}$$

For the Whipple-like theories n is close to -1 while from observations of coma ejections/halo expansions (cf. Whipple, 1980; Combi, 1989), n is close to -0.5. While there can be much discussion on theoretical grounds as to what is the most appropriate value to adopt in practice, at this stage of the process we choose to investigate both possibilities and to make the final choice on the basis of which better describe the observed activity of the stream.

Another shortcoming of the Whipple approach is its assumption that all sublimation is confined to the nucleus surface and is the sole source for gas in the coma. Data gathered during the Halley fly-bys in particular have suggested that sublimation occurs throughout the coma as active grains continue evaporating and releasing H_2O. This contention is supported by the observation that cometary coma gas distributions tend to be spherical despite the presence of jets of activity, that the near-nucleus brightness of the coma drops off slower than l^{-1} (where l is the distance from the surface of the nucleus) as

expected for surface production away from the surface and that the terminal dust grain velocity inferred from cometary tail observations shows a weak mass dependence, suggesting that fragmentation of large grains far from the nucleus might be the source for many of the smaller grains. This concept of "distributed" production in the coma is not new but Crifo (1995) has recently incorporated the concept of distributed production into a general physicochemical model of the inner coma along with detailed numerical results of the resulting effects on the terminal dust velocity as a function of mass. He finds that dust ejection velocities for a given mass are broad distributions which tend to have velocity peaks lower than the "classic" surface production models as compared to the single valued velocities derived from the Whipple model. Steel (1994) has emphasized the need to incorporate this effect in the cometary coma into meteor stream modelling, but to date this has not been done.

4.2.2 Constraints from meteor data

Recently, Harris and Hughes (1995) examined photographic meteor data in an attempt to use such information to constrain the cometary ejection process for the Perseids. In particular, their work (as well as that of Williams (1996)) has concentrated on the distribution of semi-major axes of stream meteoroids. These authors suggest that, if no substantial planetary perturbations affect a meteoroid, it is possible to use the true semi-major axis of the particle along with assumed distributions of ejection directions and locations along the cometary orbit to constrain the ejection velocity of the meteoroids. Indeed, Harris and Hughes (1995) suggest that there is no sensible variation in the semi-major axis distribution with meteoroid mass and conclude that all meteoroids reach essentially the same final velocity independent of mass. By comparing the observed distributions of semi-major axes to trial distributions, they suggest that this velocity is close to the final mean gas velocity, about 0.6 km/s for Swift-Tuttle at perihelion.

In using the photographic data of the stream compiled from more than a half dozen different surveys, the effects of measurement errors have not been discussed in detail by either Harris and Hughes (1995) or Williams (1996).

These data consist of Perseid orbits derived from the photographic databases of the 1 A.U. Meteor Data Centre (Lindblad, 1991). To find a value for a (semi-major axis) from photographic observations the original heliocentric velocity must be determined. In measuring the atmospheric velocity, however, a number of possible errors may be encountered, among them:

- The measured velocity in the atmosphere must be corrected for deceleration of the meteoroid over the course of the length of the trail, but this can only be done in an approximate manner. Older observations have used the classic $dv/dt=a+bt+ce^{kt}$ empirical velocity correction (Jacchia and Whipple, 1961) whose validity is questionable and which yields results different from modern applications of methods to account for deceleration such as the gross-fragmentation model of Ceplecha *et al.* (1993).
- For short trails, the number of measured points may be limited and the resulting velocity uncertain. This is particularly a problem with Perseids, which tend to have very short-lived trails in the atmosphere.
- Wake, fragmentation and flares along the trajectory may make measurement of the trail breaks difficult.
- Instrumental effects, particularly related to the frequency of the shutter, can lead to systematic errors. Such effects have recently been found (and removed) from the photographic observations of the Lost City fireball (Ceplecha, 1996)

The same photographic databases used by the previous authors have been examined in detail by Kresakova (1974) and Porubcan (1977) in relation to the Perseids. They have shown that among the dozen major photographic surveys, intersurvey deviations of the rms intrasurvey variation in the measured heliocentric velocity for Perseid meteoroids (which is approximately 41 km/s at 1 A.U.) vary from 0.3 km/s to more than 2.0 km/s, with the majority of surveys greater than 1 km/s. At 1 A.U. the measured heliocentric velocity is related to the semi-major axis via

$$V_h^2 = GM(2 - \frac{1}{a}) \tag{4.4}$$

where G is the universal gravitational constant, M the mass of the sun and V_h is the heliocentric velocity in terms of the circular velocity at 1 A.U. Fractional errors in velocity translate into very large errors in a, especially for large values of a (such as the Perseid stream orbit). More precisely if a >>1 then from

$$\frac{da}{a} = 4a\left[\frac{dV_h}{V_h}\right] \tag{4.5}$$

which implies that the smallest rms intrasurvey deviations in V_h for the Perseids corresponds to error dispersions in a of nearly 100%. The bulk of the data have much higher errors, which would be expected to push a beyond the hyperbolic limit. In fact, nearly 1/3 of all available Perseid orbits are at or beyond the parabolic limit, though none of these are seriously considered hyperbolic.

The conclusion for the Perseids is that the distribution of semi-major axis observed by even the most sensitive techniques currently available still produces no useful information concerning the initial conditions of ejection of the stream meteoroids. Kresak (1992) has recently reached a similar conclusion.

While semi-major axis distributions are prone to large errors masking original ejection velocity information for the Perseids, geocentric radiant distributions and flux information for the stream do not suffer as greatly. Indeed, such information provides the basis for the interpretation and validation of the results of our modelling and help to discriminate the most probable initial conditions for the ejection of Perseid meteoroids. These data are presented in Sect. 4.4 along with a discussion of the model results.

4.3 The Initial Ejection Models

4.3.1 Overview

From the forgoing discussion, it is clear that an ejection model of the classic-Whipple type alone does not cover the many possible important variations in ejection conditions, which current observational data and theoretical modelling suggest are possible. As the differences in the final meteoroid distributions may be sensitive to the initial model choices, it is desirable to use several different ejection schemes and compare the final results. The resulting differences will determine which models are best able to fit the available Perseid observations assuming the intermodel differences are great enough to distinguish the outcomes.

After reviewing the available information on the cometary ejection process as summarized in Sect 4.2, we have decided to use four major models of ejection of meteoroids from 109P/Swift-Tuttle.

The first model uses the results of Crifo's (1995) coma modelling for distributed production in the coma. His result for the average terminal velocity of the dust (appropriate for grains from 10 cm > s > 10^{-4} cm) for olivine grains as a function of grain radius, *s*, can be expressed empirically as:

$$Log_{10}(V_{eject}) = -2.143 - 0.605 Log_{10} s \qquad (4.6)$$

and we assume the production varies with heliocentric distance as $r^{-0.5}$. The result is scaled from his simulation work (which was designed for Halley to compare the final results with Giotto measurements) to that appropriate for 109P/Swift-Tuttle assuming the same fractional area on both comets was active. This value for the average velocity (V_{eject}) from Eqn 4.6 is then used along with Crifo's velocity distribution for the differential flux as a function of velocity for a mass of 10^{-2} g, which has an empirical form of:

$$P(V - Veject) = \frac{1}{e^{3.7}} \exp\left[\frac{3.7 - 10.26(V - Veject) + 4.12(V - Veject)^2}{1 - 1.03(V - Veject) + 0.296(V - Veject)^2}\right] \qquad (4.7)$$

where *P(V-Veject)* is the relative probability of finding a grain with ejection velocity V. This is model 1.

The second model is the Jones modification to the original Whipple formula with the exception that the solar distance dependence on ejection velocity is taken to be $r^{-0.5}$. We call this variant model 2.

As the Whipple model has been used by almost all previous workers in modelling streams it seems appropriate for comparison of our final results to past results to include this model. The slight modification to the Whipple model by Jones is used and we call this model 3 throughout. It is similar to 2 except that the heliocentric velocity dependence is $r^{-1.038}$.

The fourth and final model uses the same ejection velocity formulation as model 3, with the exception that it is not a single-valued function for a given choice of input parameters. Instead, we use a parabolic distribution centred about the nominal Jones velocity in an attempt to account for the different ejection velocities for a given mass due to the differing shape factors. Since we have no numerical constraints a priori regarding grain shapes, we use this parabolic distribution in an attempt to account for this variation. This is model 4.

For each model, the absolute value for the grain ejection velocity will vary as a function of the chosen meteoroid density. Estimates for cometary nucleus densities vary widely, with evidence from Halley suggesting values in the ~100 kg m^{-3} range (Rickman, 1986) or lower, while Sagdeev *et al.* (1987) estimate this value to be closer to ~600 kg m^{-3}. However, the nucleus density may have little relationship to the density of smaller grains. Indeed, Ceplecha (1988) and Verniani (1973) have analyzed fireball and radio meteor sized bodies (10^{5}-10^{-4} g) and find bulk densities near 800 kg m^{-3}. In contrast, Babadzhanov (1993) finds densities closer to ~4000 kg m^{-3} from photographic meteor data and the application of a fragmentation model to the observed data. These wide ranges for the possible densities of Perseid meteoroids have led us to adopt three distinct densities we use for all models; namely 100 kgm^{-3}, 800 kgm^{-3}, and 4000 kgm^{-3}, which we enumerate as 1,2, and 3 model variants. Thus the distributed production model with meteoroids of density 100 kgm^{-3}, 800 kgm^{-3}, and 4000 kgm^{-3} are referred to as models 11, 12 and 13

respectively. The ejection velocity formula for each model is given in Table 4.1 and sample distributions for ejection velocities as a function of heliocentric distance are shown in Fig. 4.1 for Perseid meteoroids of mass 10^{-2} g.

We have taken the meteoroid mass to be the independent variable and plot all results in terms of initial ejection mass. In total we have 12 distinct model variants and for each we eject 10 000 test meteoroids at differing masses from 10^{-5}-10 g for each perihelion passage of 109P/Swift-Tuttle. We have used 61 mass categories over this mass range for the 1862 and 1737 passages of the comet for each model variant - each mass category is 0.1 greater in Log(M(g)) space than the previous category. This implies a total of 610 000 test meteoroids are ejected for each model variant, totalling 7.32×10^6 particles for each passage (1862 and 1737). For passages from 59-1610 A.D. only 7 mass categories are used over the full mass range due to computational limitations, each 10 times greater than the previous (1.0 in Log (M(g)) space)) totalling 8.4×10^5 meteoroids per perihelion passage. These choices for mass, coupled with the three chosen values for densities imply a range of β in our simulations of $10^{-5}<\beta<10^{-2}$.

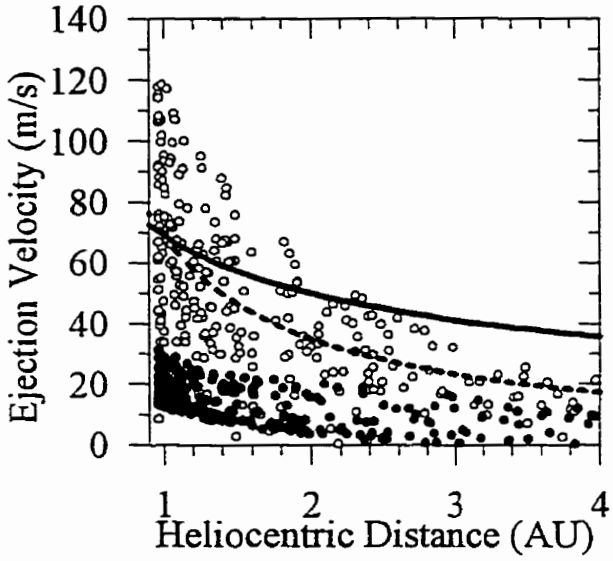

Fig 4.1: Sample ejection velocity distribution for Perseids ejected in 1862 of mass 0.01g and density 800 kg m^{-3} ($\beta=5\times10^{-4}$) as a function of heliocentric ejection distance. Model 1 meteoroids are shown as filled circles, model 2 as a solid line, model 3 as a dotted line and model 4 as open circles.

For each model variant, the same basic Monte Carlo approach is taken to determine the point of ejection and ejection velocity/direction. As described in Sect. 4.2, the point along the orbit of 109P/Swift-Tuttle where ejection occurs is chosen randomly from within the true anomaly range from $233°<\nu<127°$ or $r<4$ A.U. After this ejection point is determined, the appropriate ejection speed is then found, depending on the model variant, using one of the formulae given in Table 4.1. The direction of ejection is confined to the sunward side of the comet and randomly chosen while the final ejection magnitude is calculated according to each model formula. The resulting cometocentric velocity is added to the cometary velocity at the ejection location to derive the initial orbit. This process is repeated for all 10 000 meteoroids for a particular run and this file is then used as the input to the numerical integrator.

Table 4.1 : Formula for determining the Ejection velocity of a meteoroid of mass m from Swift-Tuttle for each model variant.

Model #	Name	Ejection Formula
1	Crifo Distributed Production	$Log_{10}(V_{eject}) = -2.143 - 0.605 Log_{10}(radius) - 0.5 Log_{10} r$ $P(V - Veject) = \frac{1}{e^{3.7}} \exp\left[\frac{3.7 - 10.26(V - Veject) + 4.12(V - Veject)^2}{1 - 1.03(V - Veject) + 0.296(V - Veject)^2}\right]$
2	Jones Ejection Distribution with Modified Heliocentric Velocity Dependence	$V_{eject} = 10.2 r^{-0.5} \rho^{-\frac{1}{3}} R_c^{\frac{1}{2}} m^{-\frac{1}{6}}$ P(V-Veject) = 1 for V=Veject and 0 if V≠ Veject
3	Jones Ejection Distribution	$V_{eject} = 10.2 r^{-1.038} \rho^{-\frac{1}{3}} R_c^{\frac{1}{2}} m^{-\frac{1}{6}}$ P(V-Veject) = 1 for V=Veject and 0 if V≠ Veject
4	Jones ejection distribution with parabolic probability distribution	$V_{eject} = 10.2 r^{-1.038} \rho^{-\frac{1}{3}} R_c^{\frac{1}{2}} m^{-\frac{1}{6}}$ $P(V - Veject) = 1 - (\frac{V}{Veject} - 1)^2$ for 0<V<2Veject and 0 outside

4.3.2 The Numerical Integrator

The basic form of the numerical integrator uses an RK4 architecture with variable step-size. Jones (1985) described an early version of this integrator where more details can be found. This integrator has been specifically designed for integrating large numbers of bodies as quickly as possible over (relatively) short solar system times. Whereas typical integrators used in solar system work such as RADAU (Everhart, 1985) or SWIFT (Levison and Duncan, 1994) are designed for high precision and long-periods of integration, we are concerned with maintaining only modest precision and concentrating instead on particle throughput.

To this end, the integrator uses a simple RK4 numerical integration scheme adapted from Press *et al.* (1986). The basic step-size was chosen initially based on numerical experiments offsetting speed and accuracy - a typical value being 0.01 years. For an orbit as eccentric as 109P/Swift-Tuttle, variable step-size routines we tested suggested that the large number of steps near perihelion did not increase the overall orbital accuracy (our primary interest) and that the resulting numerical round-off errors and loss of speed were significant. Jones (1985) found that an empirical formula of the form $h=h_0 r^p$ where r is the distance to the closest major body in the integration and p is chosen empirically provides an acceptable compromise between speed and numerical accuracy. For orbits as elliptical as 109P/Swift-Tuttle a value of $p=1.5$ is close to optimum in the product of integration time and final total accumulated error and we use this throughout. Other integration schemes are available which are superior in speed and produce somewhat more precise results. For our purposes, however, the RK4 integrator is entirely adequate and has been tested against output from SWIFT and RADAU and found to show no variations of significance within our range of adopted bin sizes in parameter space.

To further speed up integrations, the $(n-1)^2$ computations normally found in n-body calculations (and general features of other solar system integrators) were removed entirely by generating pre-defined planetary position tables in memory. These tables were derived from the DE404 JPL planetary ephemeris and are stored in computer memory

with planetary positions interpolated via cubic splines to accuracies (relative to the original DE404 ephemeris) no worse than 100 km for the positions of the major planets over the last 2000 years, with average errors nearly one order of magnitude better than this value.

All numerical computations are performed taking into account planetary perturbations, barycentric corrections, radiation pressure and the Poynting-Robertson effect (cf. Chapter 2 for a basic description and Burns *et al.*, (1979) for a detailed description of the latter two forces). The barycentric corrections are significant for orbits as large and elliptical as 109P/Swift-Tuttle (cf. Chambers, 1995) and necessitated an upper limit of between 0.2 - 0.4 years in the largest step-size, independent of distance to the nearest perturbing body.

The above integrations required approximately four months of continuous computation on five Pentium PC's.

4.4. Results

4.4.1 Previous Perihelion Passage (1862)

We begin by examining the meteoroid distribution at the present epoch due to Perseids ejected in 1862. Some general comments concerning the overall evolution of the modelled meteoroids from 1862 to the present are in order. It was found that models 2 and 3 show virtually identical outcomes both in terms of flux as a function of time and solar longitude of maximum in any given year, locations of radiants, stream dispersion etc. The choice of $r^{-0.5}$ or r^{-1} dependence on the ejection velocity was found to be the most insensitive variation among models from 1862 and always resulted in very similar final distributions. As the majority of the meteoroids are ejected near perihelion (as required by the condition of random distribution in true anomaly), the small number of more distant ($r>2$ A.U.) ejections do not make a strong contribution to the overall activity of the stream presently observed in the context of our modelling. The only noticeable difference between the more distantly ejected population ($2<r<4$ A.U.) and meteoroids ejected near perihelion is a larger spread in nodal longitudes for the former which becomes particularly evident at small masses.

Fig 4.2 shows a temporal plot of the distribution by mass of test meteoroids having nodes within 0.005 A.U. of the Earth's orbit from model 32. We use 0.005 A.U. as our sieving distance and hereafter refer to all such meteoroids as Earth intersecting. Smaller sieving distances were used, but found to be inconsequential for the Perseids in overall terms. There is an obvious periodicity in the figure apparent in all model variants of ejecta from 1862. Fig 4.3 shows a plot of nodal distance versus time for model 42 meteoroids of mass 10^{-2} g, demonstrating that the reason for the periodicity is an impulsive change in the mean nodal distance of shower meteoroids inwards every 12 and 30 years. This effect is the result of distant direct perturbations on the stream by Jupiter and Saturn and is developed in more detail in Sect 4.5.

In general, all models show that the most recent activity associated with the 1862 ejecta is concentrated from 1991-1994 with a peak in 1993. It is clear from Fig 4.3 that meteoroids not perturbed by planetary perturbations after ejection in 1862 have nodes outside Earth's orbit, a result that holds for all models and all masses. In rare cases, smaller meteoroids (generally of higher density) ejected with high velocities can reach within 0.005 A.U. outside of Earth's orbit and be "accepted" as visible at Earth in years well away from the inward nodal shifts due to planetary perturbations, but this number is very small. Some activity is also apparent near 1980 and near 2010 at lower levels.

For activity in any year from 1992-1994, the distribution of nodes for all models is strongly concentrated in the region from 139.3°-139.6°, with maximum in the region 139.42°-139.5°. This result changes with cone angle in such a way that smaller cone angles tend to concentrate the peak into a smaller range of solar longitude centred about the node of the comet (139.44°) as would be expected. The particle distribution in these years from the 1862 ejection is also heavily skewed toward the largest (lowest ejection velocity least radiation pressure affected) masses.

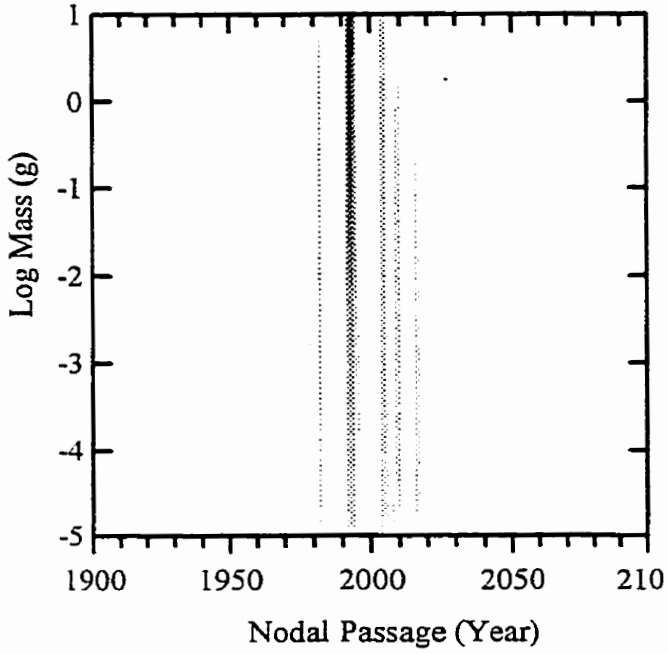

Fig 4.2: Activity at the present epoch from ejecta released in 1862 for model 32. The gridding is 1 year bins for the nodal passage time and 0.1 in log M. The greyscale has a dynamic range from 0 to 700 for this choice of binning intervals.

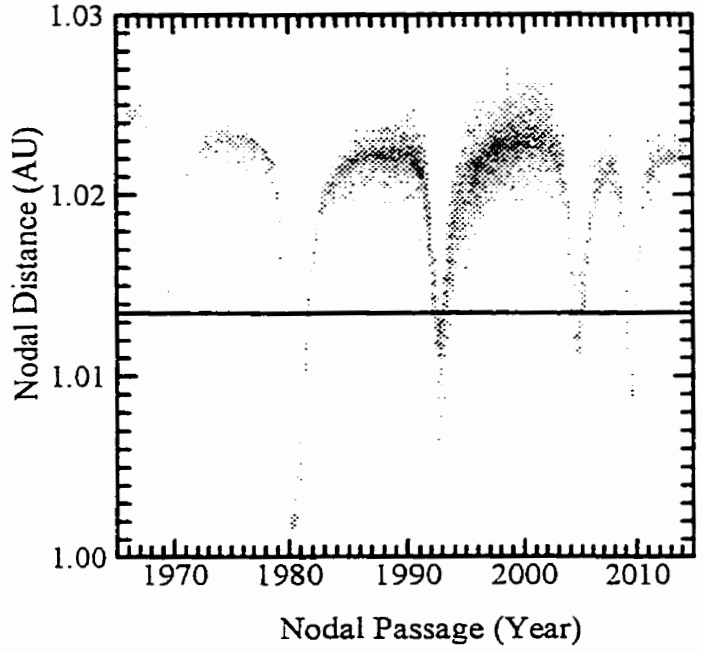

Fig 4.3: Nodal distance versus nodal passage time for meteoroids ejected in 1862 from model 42 of mass 0.01 g. The Earth's distance at the time of Perseid maximum is 1.01355 A.U. and is shown by the horizontal line. The greyscale has a dynamic range from 0 to 19 for this binning. The gridding is to a resolution of 0.0002 A.U.

The radiant size is determined entirely by the distribution of initial ejection velocities; for the models used here, the 1862 radiant rms diameter is ~0.1 degrees. The location of the radiant varies from year to year by a small amount (about 0.3 degrees in declination and 0.2 degrees in RA) due to differential planetary perturbations.

4.4.2 Recent Ejections (2000 years).

Results of ejections from 109P/Swift-Tuttle at each perihelion passage from 59 A.D. to 1610 A.D. were carried out at 7 discrete mass intervals separated by one order of magnitude in mass in the range 10 g-10^{-5} g. For completeness, the same mass categories were extracted from the more extensive runs from 1737 and 1862.

The final distributions of meteoroids at the present epoch reveal that the difference in closest approach between the comet and Earth at the epoch of ejection is a strong determinant of subsequent activity.

Fig 4.4 shows a plot of the minimum approach distance between the osculating orbit for 109P/Swift-Tuttle at the epoch of each perihelion passage (listed as years in the abscissa) and the Earth. The dashed line shows the total number of meteoroids from all models ejected from each passage, which still have nodes within 0.005 A.U. of Earth at the nodal passage closest to the 1992 perihelion date. There is no significant correlation between the age of ejection over this time interval and the fraction of all ejected meteoroids currently in earth-intersecting orbits. This finding suggests that the Earth-comet orbit distance at the time of ejection, rather than planetary perturbations, control the large scale delivery of Perseid meteoroids on this time scale. It is for this reason that material ejected in 1737 and 1610, though quite young, is expected to be less prolific on average at present than ejecta from 1479. Indeed, it is found that for the years from 1995-1997, for example, the material from 1479 is the dominant Perseid population observed at the Earth for the outburst portion of the stream. A similar trend is seen for each model, further indicating that neither the assumed particle density or ejection velocity plays a dominant role in the subsequent encounter conditions with the Earth.

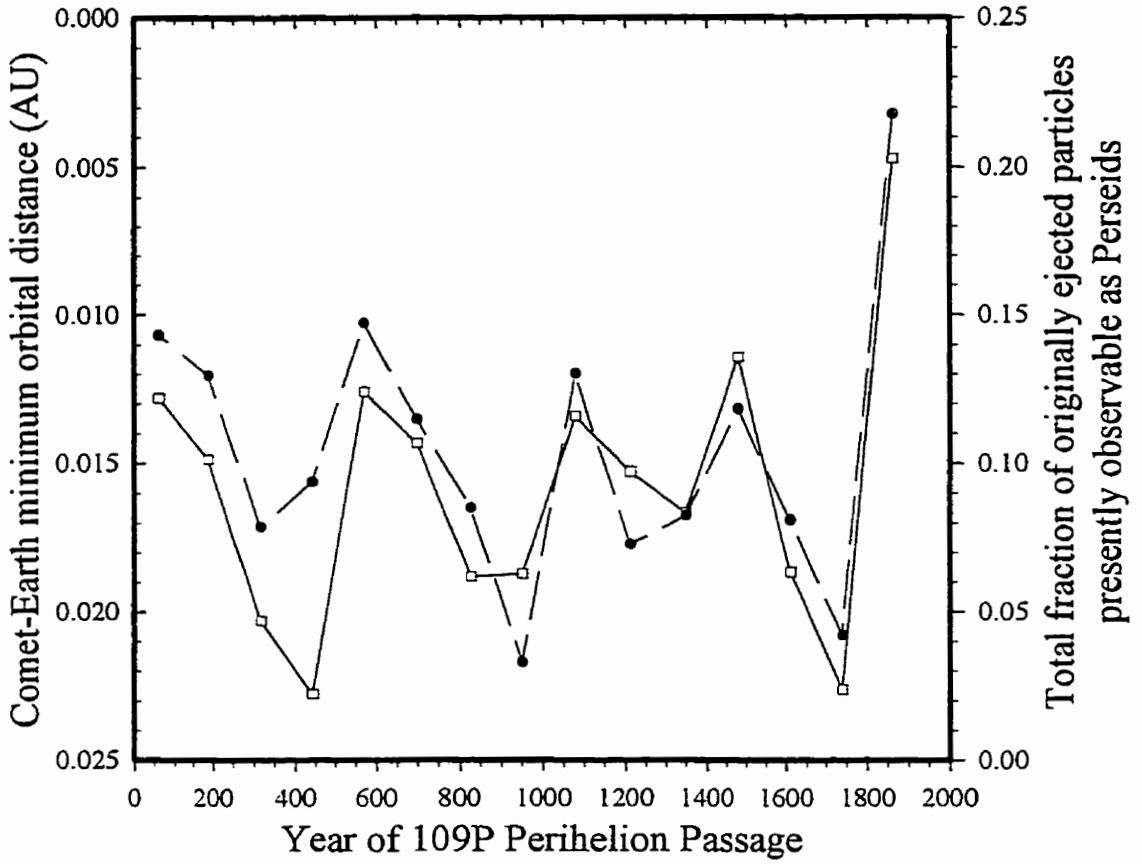

Fig 4.4: The minimum comet-Earth distance for 109P/Swift-Tuttle (open squares) and the fraction of Perseid meteoroids summed over all models and all masses which currently have descending nodal points within 0.005 A.U. of the earth from each perihelion ejection (solid circles).

The total number of Earth intersecting Perseids as a function of time at the present epoch summed over all ejecta for meteoroids capable of producing visual meteors ($>10^{-3}$ g and larger) over the last 2000 years is shown in Fig. 4.5 for three representative models. The general form of the activity is similar for all 12 model variants - namely a 12 and 30 year periodicity reaching peak strength near 1992-1993. For each ejection model, higher meteoroid densities (smaller β's) yield more Earth intersecting meteoroids, a result of the general trend toward larger nodal distances as radiation pressure increases at larger β (see Sect. 4.5). The year of ejection associated with the most numerous population of meteoroids varies significantly from year to year in the current epoch; as a result we expect that the position of peak activity in the stream for the outburst component will similarly vary.

The rms angular width of the radiant as a function of time is shown in Fig. 4.6. Here we have plotted the rms spread in the distribution of individual geocentric radiant points calculated from each Earth-intersecting visual-sized Perseid and added the distributions in a cumulative manner. Hence, the value at 2000 years is the angular spread in the total radiant area from all 15 perihelion ejections from 59 A.D.-1862. Note that the positions of the radiants from any one ejection vary in RA and DEC due to planetary perturbations; thus the rms spread in this cumulative plot is greater than the individual radiant spreads from each individual ejection. The initial size of the radiants and early evolution of the size of the radiant area are controlled by the ejection velocity, with higher average velocities having larger initial dispersions, but within 500 years (roughly four passages) the absolute levels of spread vary inversely with the density of the meteoroids for all models. This suggests that in the longer term, the absolute level of rms spread is controlled (either directly or indirectly) by radiation pressure and to a lesser degree by the initial ejection velocity. However, the slope of the radiant dispersion is constant and similar for all models, showing that planetary perturbations and initial ejection comet-Earth geometry are the "drivers" of the actual shape of the radiant.

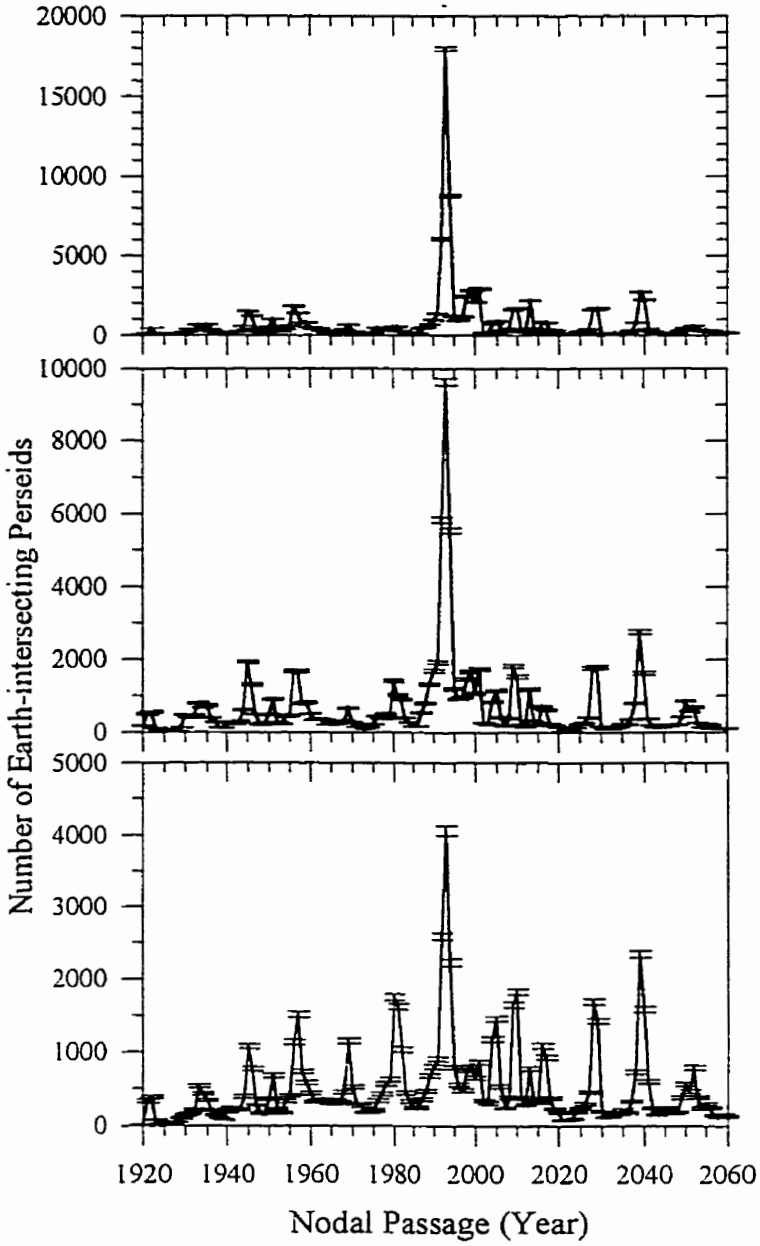

Fig 4.5 : The total number of visual class (>10^{-3} g) Earth intersecting Perseid meteoroids versus their nodal passage time summed from all ejections from 59-1862 A.D. for models 12 (top), 33 (middle) and 41 (bottom). Activity is summed into yearly bins and the error bars represent the poisson error margins ($n^{1/2}$).

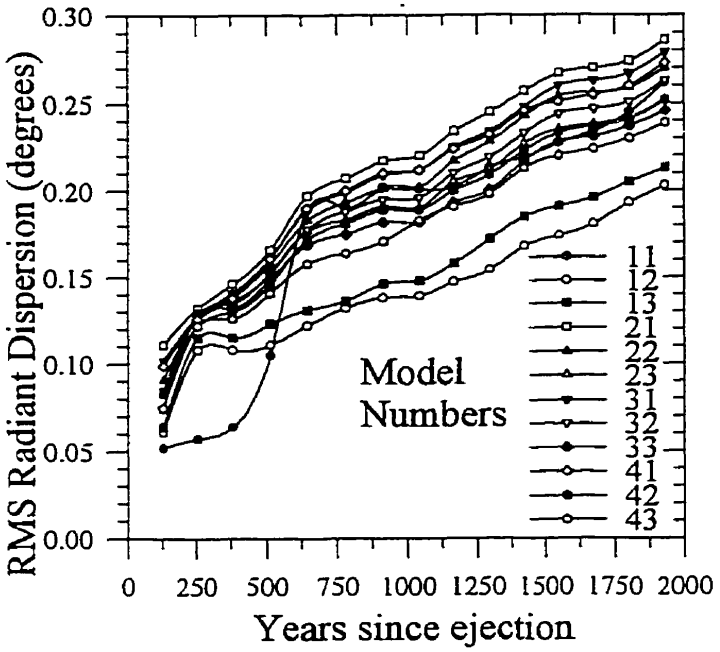

Fig 4.6: Root-mean squared (rms) spread in radiant size for all models as cumulative distributions observed at present from ejections between 59-1962 A.D. The time in years (abscissa) refers to years before present (i.e. year 0 is 2000 A.D.).

A regression fit to the radiant spread from 500-2000 years yields an annual change of 6.5×10^{-5} degrees/annum. The particularly small values for model 1 are a direct consequence of the extremely low ejection velocities associated with the extended production model. The correctness of the above conclusions can be evaluated through consideration of the very low initial dispersion for this model due to the extremely low ejection velocities for larger particles in model 11 (or equivalently for lower density particles of the same mass - the opposite to the dependence from the other models - see Eqn 4.6) and its sudden increase relative to models 12 and 13 after four to five revolutions as the full effects of radiation pressure expand the radiant.

The scatter in the rms spread at any one time between all models is of order 0.1 degrees over this 2000 year period. The location of the radiant after the full 2000 years of accumulated ejections (i.e. now) over the mass range 0.1-10 g (photographic) is α=46.09±0.02 and δ=57.66±0.02 (J2000.0). The variation in α throughout this time is

very linear and well represented by $\alpha=45.88+1.128145\times10^{-4}Y$ where Y is the year of the last included ejection figured backwards in time in the summation, referenced to an origin at 2000 A.D.. The declination shows much more scatter during the last 2000 years as it depends more on planetary perturbations than α (which is more closely linked to the progression of the node). The variation is approximately represented by $\delta=57.67+10^{-5}Y$. All radiant measures are referenced to J2000 and $\lambda_O=139.7°$ (139.0° in B1950.0).

The locations and strength of the observed visual peak associated with the outburst component of the stream derived from Chapter 3 and from Rendtel and Arlt (1996) are shown in Fig 4.7, together with the model predictions for the same quantities. The locations of the visual peaks in outburst activity and their shape were found by taking the average Perseid ZHR profile from Chapter 3 over the period 1988-1994 and subtracting this profile from each year's activity after scaling for differences in peak activity between the average profile and each yearly profile's main (or normal) maximum ZHR value. It was found that the mean curve of Perseid ZHR activity from 1988-1994 in the interval from $139°<\lambda_O<140.1°$ is approximated by:

$$ZHR = 1.84110984\times10^{8} - 3.95803796\times10^{6}\lambda_O + 28363{\lambda_O}^{2} - 67.67{\lambda_O}^{3} \quad (4.8)$$

From Fig 4.7, it is clear that the predicted and model times of peak are generally in good agreement, with the exceptions of the 1993 and 1994 peak locations, where model values are 1-2 hours earlier than observed. The overall trend of observed changes in peak location and the model locations are consistent, reflecting the dominance of older ejecta before 1992 and after 1994 (see Table 4.2). Note that the ZHR of the outburst peak in 1988 was found to be of negligible magnitude after subtraction of the mean scaled background, drawing into doubt the reality of the feature in 1988. We thus omit it from further analysis. The move in the time of the peak away from the current nodal longitude (139.44°) of Swift-Tuttle reflects the fact that 109P's nodal longitude has been higher than its present value for most passages over the last 1000 years and hence older ejecta are now well ahead of the comet's nodal longitude. This ejection geometry implies that ejecta from as recently as 1348 can be found as late at nearly 139.8° at the present epoch, all other ejections over the last 2000 years peaking earlier.

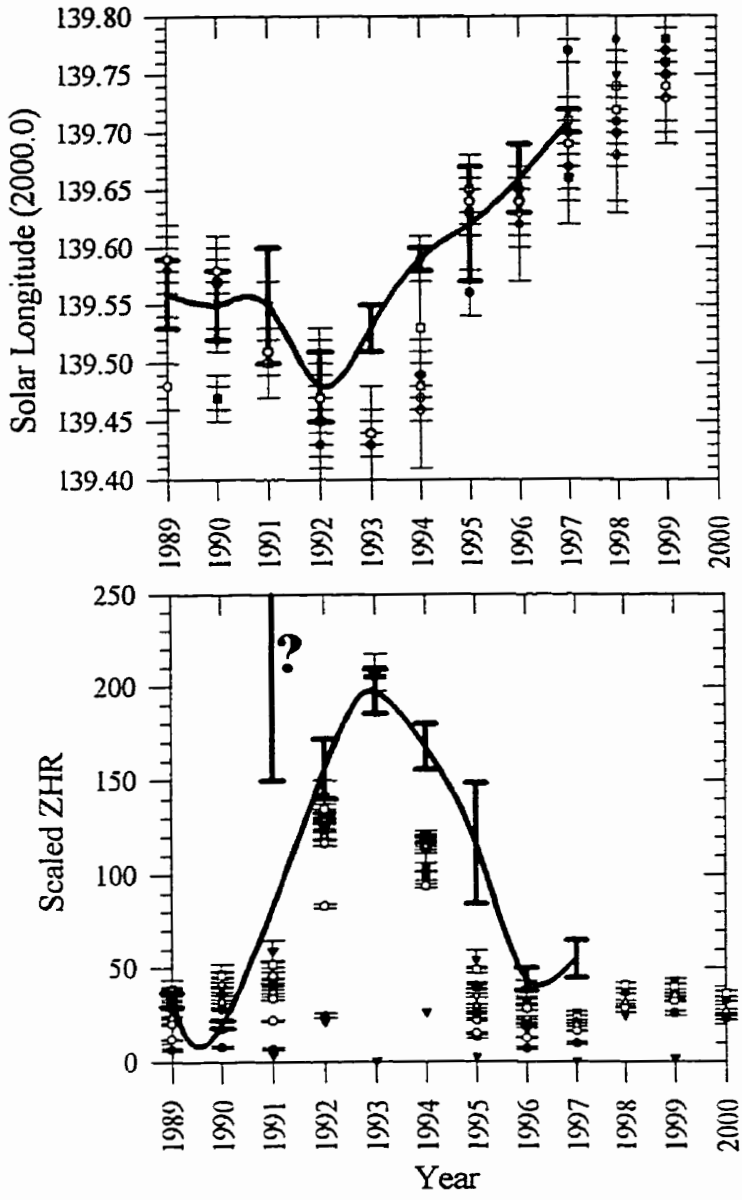

Fig 4.7: Observed locations (J2000) of the outburst peak for the Perseids (bold solid line) together with model predictions of peak locations (top). The scaled ZHR for the observed outburst peaks from 1989 to 1997 and individual model predictions are also given (bottom). Symbols for each model variant for both plots are the same as used in Fig 4.6. Observational data are from Chapter 3. The question mark next to the 1991 observed ZHR value reflects the high uncertainty of this datum (see discussion of this point in the previous chapter). The solid curve for the bottom graph is formed without using 1991.

The cumulative activity for visual-sized meteoroids is shown in Fig 4.8 for two representative models as a function of solar longitude. All meteoroids ejected over the last 2000 years currently have nodal longitudes greater than 139° and the profile from just these 15 ejections already shows remarkable similarity to the shape of the core Perseid activity found from visual observations, the asymmetry of both being particularly notable.

The relative change in the strength of the peaks is reproduced, though the peak observed ZHR in 1991 (which has large error margins) does not fit the trend well, the model underestimating its strength. A similar, though less substantial effect, is also seen in 1994 and 1995 suggesting that for the strongest years the model tends to underestimate peak ZHR activity.

Table 4.2 summarizes the age breakdown of the recent Perseid activity (all of the outburst peak and part of the core activity of the stream) in terms of the summation of all ejections (59A.D. - 2000) for each of the years 1988-1996 for visual class meteoroids. The total number of Earth intersecting test meteoroids as well as the fraction of this total contributed by the three most significant ejections is also shown. It can be seen that the activity for all models peaks in 1992-1993 and that the makeup of the ejecta observed as the outburst component of the Perseids changes dramatically from year to year. In 1988-1990, ejections from 1610 and 1737 are predominant and account for the majority of the activity, while in 1991 material from 1862 and 1610 is found in roughly equal proportions. The 1991-1994 outburst maxima are composed primarily of material from 1862 and to a lesser degree 1610. Note that even in these years, the fraction of all meteoroids of recent origin (last 2000 years) is still greater from all earlier passages than from 1862 alone. In 1995 and 1996 the origin of the outburst material changes again, with 1479 dominant and 1079 and 1862 making contributions. These age breakdowns and total numbers of accepted particles refer to the integrated flux (fluence) of meteoroids over the full activity interval of the shower while the higher fluxes are most likely to be associated with younger material more concentrated in solar longitude.

	11		12		13		21		22		23	
1988	95		472		748		589		688		716	
	441	0.24	1737	0.71	1737	0.56	1610	0.26	1610	0.39	1610	0.48
	698	0.24	1610	0.15	1610	0.32	1862	0.16	1737	0.20	1737	0.31
	59	0.13	441	0.04	826	0.03	1479	0.15	1479	0.10	826	0.05
1989	122 (1.73)		691 (1.14)		1178(.93)		659 (.45)		961(.31)		1277(.27)	
	698	0.21	1737	0.52	1610	0.49	1610	0.32	1610	0.49	1610	0.55
	188	0.19	1610	0.37	1737	0.40	1862	0.17	1737	0.18	1737	0.22
	59	0.17	59	0.04	59	0.03	1479	0.15	1479	0.12	1479	0.08
1990	144(.36)		965(.97)		1681(.95)		827(.46)		1168(.51)		1585(.79)	
	1348	0.31	1610	0.48	1610	0.54	1610	0.39	1610	0.50	1610	0.58
	698	0.14	1737	0.45	1737	0.37	1862	0.20	1737	0.18	1737	0.23
	188	0.14	59	0.02	1479	0.03	1737	0.10	1479	0.10	1479	0.07
1991	124(1.51)		1351(.97)		2127(.88)		927(.76)		1282(.54)		1689(.66)	
	59	0.20	1862	0.37	1610	0.38	1862	0.31	1610	0.34	1610	0.39
	569	0.20	1610	0.36	1862	0.36	1610	0.25	1862	0.33	1862	0.33
	698	0.11	1737	0.23	1737	0.20	1737	0.10	1737	0.12	1737	0.14
1992	448(.82)		6071(.24)		8063(.2)		2100(.75)		3240(.56)		4586(.31)	
	1862	0.44	1862	0.47	1862	0.43	1862	0.29	1862	0.37	1862	0.41
	826	0.18	1610	0.15	1610	0.19	1610	0.15	1610	0.15	1610	0.16
	1079	0.11	1737	0.07	1479	0.08	1479	0.10	1479	0.10	1479	0.08
1993	3780(4.96)		17971(4.16)		20120(3.86)		2971(5.56)		5142(3.61)		7714(3.94)	
	1862	0.70	1862	0.49	1862	0.42	1862	0.32	1862	0.37	1862	0.39
	826	0.04	1610	0.12	1610	0.15	1610	0.17	1610	0.16	1610	0.19
	1079	0.03	1079	0.06	1079	0.07	1079	0.09	1079	0.09	1079	0.11
1994	1804(2.86)		8773(4.01)		9094(5.06)		1542(3.54)		2578(4.48)		4213(5.24)	
	1079	0.18	1079	0.18	1862	0.21	1862	0.34	1862	0.34	1862	0.28
	569	0.16	1862	0.15	1079	0.12	1479	0.19	1479	0.15	1610	0.16
	826	0.16	826	0.14	826	0.12	1079	0.09	1610	0.10	1479	0.14
1995	241(0.38)		1189(0.16)		1482(0.04)		779(0.05)		983(0.30)		1183(0.22)	
	1079	0.29	1479	0.32	1479	0.49	1479	0.40	1479	0.49	1479	0.56
	569	0.14	1079	0.24	1079	0.15	1862	0.27	1862	0.19	1079	0.12
	950	0.14	569	0.10	698	0.09	1079	0.07	1079	0.09	1862	0.08
1996	132(3.51)		926(1.35)		1231(1.19)		592(0.82)		795(1.20)		934(0.90)	
	1079	0.20	1479	0.44	1479	0.53	1479	0.48	1479	0.65	1479	0.69
	569	0.19	1079	0.20	1079	0.13	1862	0.24	1862	0.10	1079	0.09
	950	0.14	569	0.09	698	0.08	1079	0.05	1079	0.05	698	0.04
Totals	6890 (16.13)		38409 (13.0)		45724 (13.11)		10986 (12.39)		16837 (11.51)		23897 (12.33)	

Table 4.2 : The number of Earth intersecting Perseids by year (from 1988-1994) and by model at the present epoch. Each column title represents the model number. Each row is the model results for the given year. The rows list the total number of particles from a particular model accepted in the given year, followed by a breakdown of the three most numerous ejection epochs represented, with the year of ejection in the left half-column and the fraction of the total number of particles contributed by this ejection in the right.

	31		32		33		41		42		43	
1988	471		655		800		474		626		724	
	1610	0.36	1610	0.41	1610	0.42	1610	0.31	1610	0.38	1737	0.46
	1737	0.23	1737	0.34	1737	0.42	1737	0.26	1737	0.37	1610	0.37
	826	0.08	826	0.05	826	0.04	1862	0.10	826	0.04	826	0.04
1989	678(.14)		948(.45)		1327(.39)		680(.42)		871(.37)		1171(.47)	
	1610	0.44	1610	0.52	1610	0.57	1610	0.40	1610	0.52	1610	0.55
	1737	0.17	1737	0.24	1737	0.29	1737	0.19	1737	0.28	1737	0.31
	1479	0.11	1479	0.08	1479	0.04	1479	0.09	1479	0.07	1479	0.04
1990	831(.48)		1272(.57)		1696(.81)		802(.70)		1185(.72)		1628(.88)	
	1610	0.47	1610	0.54	1610	0.60	1610	0.43	1610	0.54	1610	0.58
	1737	0.18	1737	0.22	1737	0.29	1737	0.19	1737	0.25	1737	0.31
	1862	0.08	1479	0.09	1479	0.06	1862	0.11	1479	0.07	1479	0.05
1991	940(.41)		1308(.77)		1916(.77)		909(.47)		1372(.68)		1955(.89)	
	1862	0.35	1862	0.36	1862	0.39	1862	0.36	1862	0.37	1862	0.39
	1610	0.29	1610	0.34	1610	0.35	1610	0.28	1610	0.33	1610	0.35
	1737	0.11	1737	0.15	1737	0.17	1737	0.11	1737	0.16	1737	0.18
1992	2428(.51)		3926(.32)		5827(.22)		2588(.32)		4410(.18)		6692(.21)	
	1862	0.37	1862	0.40	1862	0.43	1862	0.38	1862	0.43	1862	0.44
	1610	0.12	1610	0.14	1610	0.15	1610	0.13	1610	0.14	1610	0.16
	1479	0.09	1479	0.09	1737	0.09	1479	0.08	1737	0.08	1737	0.09
1993	3741(5.46)		6334(3.93)		9623(3.89)		4064(3.88)		7586(3.97)		11896(3.75)	
	1862	0.38	1862	0.38	1862	0.39	1862	0.37	1862	0.39	1862	0.40
	1610	0.14	1610	0.16	1610	0.17	1610	0.14	1610	0.16	1610	0.15
	1079	0.09	1079	0.10	1079	0.10	1079	0.09	1079	0.10	1079	0.09
1994	2112(5.44)		3693(4.82)		5539(4.68)		2222(5.24)		4196(5.45)		6661(5.21)	
	1862	0.36	1862	0.35	1862	0.32	1862	0.31	1862	0.34	1862	0.32
	1610	0.17	1610	0.18	1610	0.16	1479	0.12	1610	0.14	1610	0.12
	1479	0.10	1479	0.09	1079	0.12	1610	0.12	1079	0.10	1079	0.12
1995	881(0.23)		1071(0.23)		1199(0.16)		795(0.25)		1072(0.03)		1283(1.23)	
	1479	0.36	1479	0.46	1479	0.59	1479	0.41	1479	0.50	1479	0.55
	1862	0.27	1862	0.15	1079	0.12	1862	0.20	1862	0.12	1079	0.14
	1079	0.07	1079	0.07	950	0.05	1079	0.06	1079	0.09	826	0.07
1996	513(1.71)		698(1.20)		921(0.87)		559(1.50)		791(0.94)		1072(5.54)	
	1479	0.50	1479	0.66	1479	0.71	1479	0.51	1479	0.62	1479	0.66
	1862	0.14	1079	0.06	1079	0.08	1862	0.14	1079	0.08	1079	0.10
	1079	0.09	1862	0.06	826	0.04	1079	0.08	826	0.06	826	0.06
Totals	12595 (14.38)		19905 (12.29)		28848 (11.79)		13093 (12.78)		22109 (12.34)		33082 (18.18)	

Table 4.2 (continued): Same as previous page, but covering results from models 31-43. Note that the numbers in parentheses at the bottom represent the difference between the modelled activity profiles and the observed ZHR profiles summed for all years from 1989 - 1994 (see text for more explanation). Additionally, the rms fit for each year is given in parentheses immediately after the total number of test particles for each model.

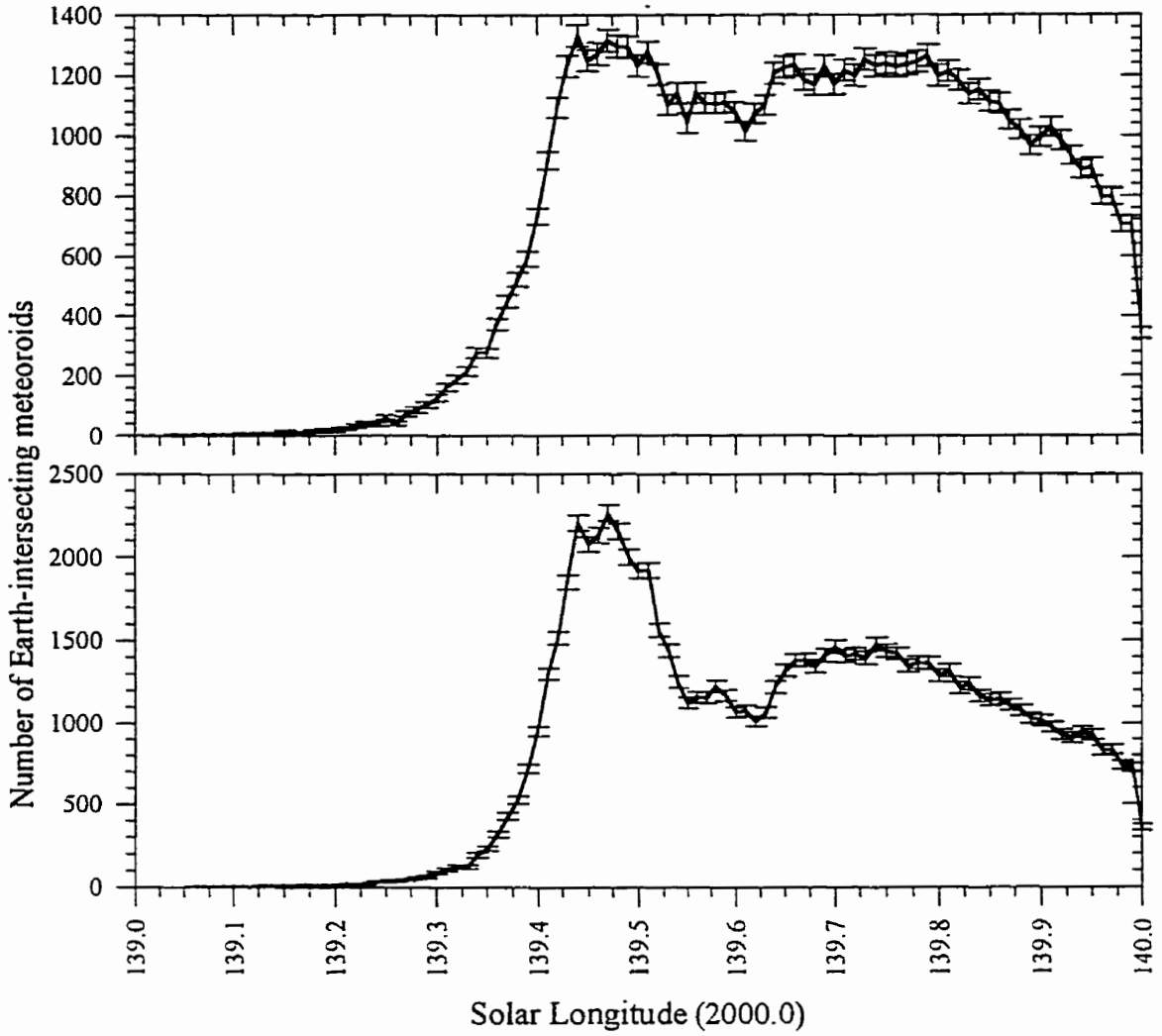

Fig 4.8: Cumulative activity as a function of solar longitude for model 22 (top) and model 33 (bottom) from the past 2000 years of ejections from Swift-Tuttle at the present epoch.

The model peaks generally follow closely to one another. A glaring exception here is model 11, which shows marked deviation from the other models and the observed peak locations. This anomaly may in part be explained by the relatively small number of meteoroids from this model in several of the examined years. As well, the ejection conditions for this model (low density meteoroids, with low ejection velocities) may be unrealistic. The distribution of variances of fit between the predicted and the observed

times of maximum are quite small for all models (except 11), with the best overall fit being due to model 21. Indeed, model 21 is the only model which agrees with the observed times of peak within error for all eight years, except 1993.

The coefficient of relative fit for the activity profile at Earth each year and for each model is also given in Table 4.2 in parentheses after the total number of test meteoroids encountered in a given year. This value is found from subtraction of the observed outburst profile for each year from the normalized number of test meteoroids found in every equivalent solar longitude bin (to a resolution of 0.01°) from 139°-140° and summation of the squares of the difference between the observed and theoretical profile in this interval. Note that the difference in fit between years is not generally significant owing to differing numbers of observational intervals from year to year with only intermodel comparisons having meaning for one particular year.

The totals in the last row suggest that the ZHR profiles in these years can best be represented by model 22 (Jones ejection velocity with $r^{-0.5}$ heliocentric velocity dependence), though the difference between many models is not large. The exceptions here are model 43 and 11 which have unusually large variances in fit between the observed and theoretical profiles.

4.4.3 Long-Term Evolution (100 000 years)

To study the behaviour of the Perseids over a significant fraction of the lifetime of the stream (variously estimated to be as much as 250 000 years of age (cf. Hughes, 1995), one must first know the orbit of the comet. Unfortunately, one cannot, as 109P/Swift-Tuttle has been observed only since 69 BC (Yau *et al.*, 1994). The chaotic effects of random errors in initial conditions imply that the position and ultimately the orbital elements of the comet quickly diverge during backward integrations.

Chambers (1995) investigated the long-term motion of Swift-Tuttle both forwards and backwards. He found that the comet's past behaviour implied a Lyapunov exponent of approximately 180 years in the immediate past and its current and future motion to be influenced by the 1:11 libration Swift-Tuttle currently experiences with Jupiter.

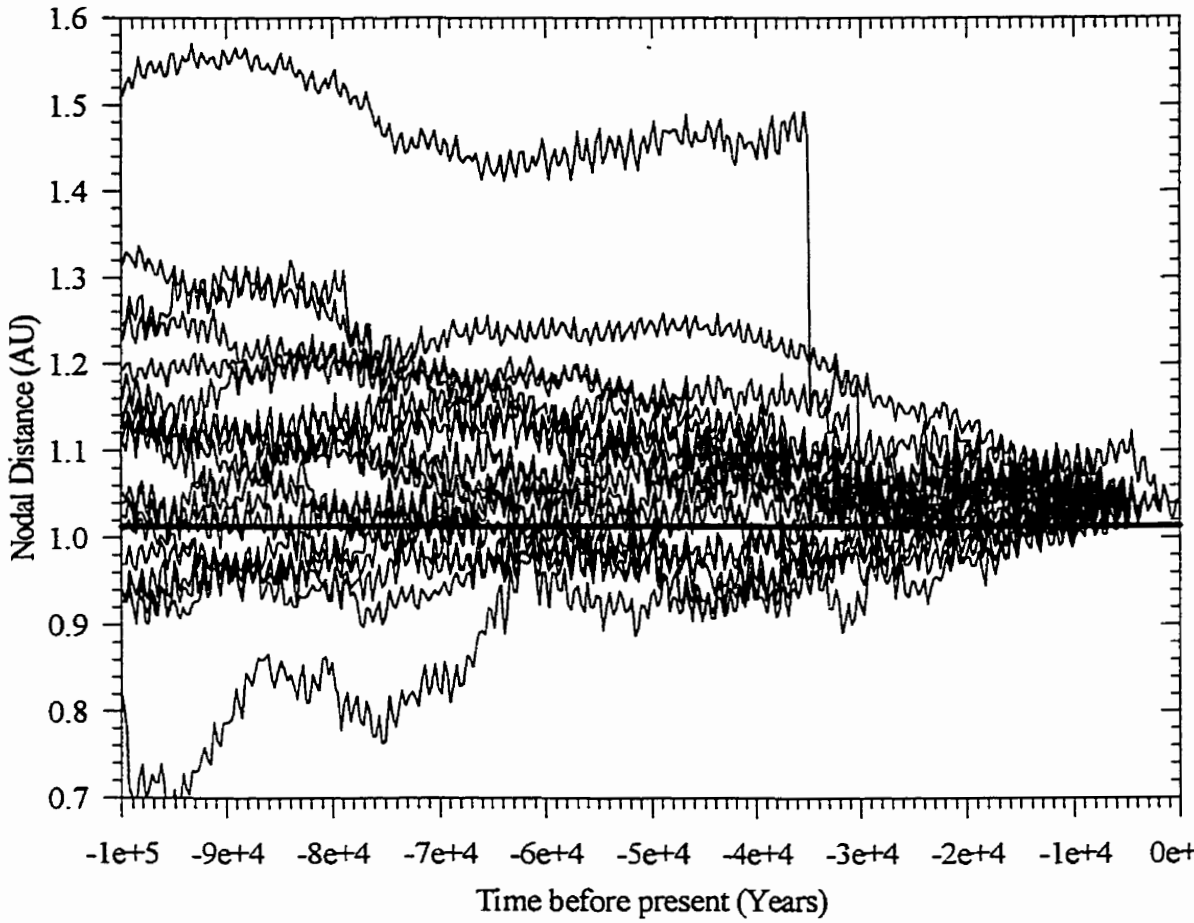

Fig 4.9: Nodal distances of 20 cloned variations of 109P/Swift-Tuttle integrated backwards starting from the present 100 000 years (see text for more details).

To attempt to model the stream, we generated plausible past orbital elements for the comet by taking the six-vector of the comet at perihelion in 1862 and "cloning" 20 different seed orbits about the nominal position of the comet within a sphere of radius 10 km (comparable to the size of the nucleus of the comet). Each seed orbit was then integrated backward in time using the SWIFT symplectic integrator (cf. Levison and Duncan (1994)) with a timestep of 0.25 days for 100 000 years using the JPL DE404 ephemeris to generate all initial planetary positions and velocities. Of greatest importance to the visibility of the Perseid stream on Earth present is the distance of the descending node of the comet from the Earth's orbit (based on our earlier results from Fig 4.4). This is shown at 300 year increments for all 20 cloned orbits for the full integration time in Fig.

4.9. The general position of the node over this time is remarkably close to the Earth, a result also found by Chambers (1995). Indeed, for the last 20 000 years no nodes are found outside $0.9<R_d<1.15$, a similar finding to Chambers (1995). From the ensemble of 20 cloned orbits, two orbits were chosen at intervals of approximately 5000, 10 000, 20 000, 50 000, 75 000 and 100 000 years. The two orbits were selected to be the most "extreme" from the set in the sense of having the largest or smallest semi-major axis. The orbital elements used for each of these two seed orbits (1 for the lower values and 2 for the larger values of a) are given in Table 4.3. Using these input orbits, a full set of test Perseid starting orbits was generated using a model 42 variant (which was felt at the outset to be most representative) for ejection velocities as with the shorter-term integrations. By comparing the final results of these simulation runs, we hope that some indication of the importance of the cometary starting orbit and thus the probable error in the simulation can be inferred, given that the true orbit from this long ago is not known a posteriori.

The final distributions of meteoroids at the present time show much less temporal variation than did the test particles from integrations over the last 2000 years as might be expected. Even ejections only 5000 years of age show a surprisingly constant annual level of activity with an average of roughly 30 earth-intersecting meteoroids encountered per year. Some small periodic variations in the annual influx from orbit #1 for ejection 5000 years ago is evident and is possibly attributable to the accumulated effects of Jovian impulses (see Sect. 4.5.). The number of Earth-intersecting test meteoroids drops off nearly linearly in time for orbit #2, but much more slowly for orbit #1 particles. This effect might be attributable to the node of orbit #1 being inside the Earth's orbit for more recent cometary starting orbits resulting in easier delivery of meteoroids to Earth as radiation pressure preferentially moves the nodes (on average) further outward.

The distribution in solar longitude of meteoroids for older ejections is given in Table 4.4. The locations of the maximum for long-term ejecta at the present epoch, found by fitting a gaussian to the present distribution of modelled meteoroid nodal longitudes, shows a slight decrease in position with age, the maximum position following $\lambda_O=(141.05 \pm 0.08) - (3.23 \pm 1.23) \times 10^{-5}$ Y.

Ejection	a	e	i	ω	Ω	T
5000	25.21880	0.9605500	114.755	151.850	137.475	-6990.0
	28.14470	0.9656100	113.121	152.250	138.321	-6990.0
10000	24.59700	0.9617600	114.866	152.909	136.251	-11989.0
	30.34540	0.9685600	112.882	153.146	136.833	-11989.0
20000	22.97440	0.9567600	116.881	150.168	132.322	-21990.0
	31.78580	0.9691800	113.291	156.677	133.632	-21990.0
50000	22.06170	0.9574700	118.929	156.287	114.114	-51990.0
	37.59280	0.9714600	111.332	154.537	128.582	-51990.0
75000	21.40130	0.9495200	123.386	150.150	108.858	-76990.0
	39.68530	0.9728500	111.641	156.933	124.972	-76990.0
100000	20.72780	0.9357000	120.977	175.776	83.694	-101980.0
	49.09810	0.9808400	113.213	163.645	119.646	-101980.0

Table 4.3: Initial seed orbits (1 and 2) for Perseid integrations from 100 000 years to the present at the intervals (before present) shown in the first column. All angular elements are J2000.0; the final column is the epoch of perihelion in units of years before the present.

This relation would imply that the rate of nodal progression is very similar for all ejecta and the parent comet up to 5000 years ago. This relation also explains the asymmetry in the broad rate profile of the shower, namely that past ejections accumulate in the region 139°-141° with the older ejections occurring predominantly in the earlier portions of this interval. Note that this relation does not take into account the position of current ejecta maximum (more recent than ~6000 years ago) which is located closer to the comet's current nodal longitude than the much older ejecta and peaks roughly 1.5 degrees earlier than the above relation would suggest.

The gaussian half-width of the nodal distribution profiles of earth-intersecting meteoroids at the present epoch follows the relation

$$W = (0.774 \pm 0.550) + (9.183 \pm 0.830) \times 10^{-5}\ Y \qquad (4.9)$$

Time since Ejection	λ_{peak}	Width
6990.0	140.56°±0.02°	1.70°±0.02°
	140.85°±0.03°	1.90°±0.03°
11989.0	140.04°±0.04°	1.67°±0.04°
	139.81°±0.08°	2.46°±0.08°
21990.0	141.55°±0.09°	2.30°±0.1°
	139.62°±0.14°	2.80°±0.16°
51990.0	133.31°±0.11°	4.59°±0.11°
	140.13°±0.32°	7.36°±0.32°
76990.0	146.99°±0.26°	8.00°±0.26°
	139.39°±0.42°	8.95°±0.42°
101980.0	122.99°±0.86°	15.31°±0.95°
	136.00°±0.78°	11.07°±0.78°

Table 4.4: Solar longitude locations and widths of maxima for each ejection for Earth intersecting Perseid meteoroids at the present epoch for seed orbits 1 and 2.

This demonstrates how the stream can be so long-lived at the current epoch given even a modestly long age, with ejections 100 000 years ago currently having full widths of nearly 25 degrees in solar longitude.

The development of the stream over the last 100 000 years is summarized in Fig. 4.10 where nodal positions of test meteoroids at the present epoch are presented. The

central portion of the meteoroid nodal footprint of the stream always remains very close to the Earth for both orbits and all masses. The nodal distribution formed from orbit #2 shows considerably more elongation than orbit #1, reflecting the higher eccentricity and semi-major axis of the latter orbit and the large number of test meteoroids which move into sungrazing and near-sungrazing orbits.

4.5 Discussion

The above results suggest the models used are not unreasonable representations of the actual ejection process of 109P/Swift-Tuttle one that is undoubtedly more complicated than our very simplified ejection schemes. In general, the three most reliably measured stream parameters, namely the activity as a function of solar longitude per year and variations in peak activity from year to year as well as geocentric radiant distributions of shower meteors, are consistent with the modelling results within the limitations of both.

The investigation of the change in the final distribution of Perseid activity seen at Earth with variations in cone angle has revealed simply that the narrower cone angles tend to concentrate the resulting meteoroids more closely to the original comet nodal locations for recent ejections. Over periods of order five revolutions, the effects of narrower cone angles become masked as planetary perturbations begin to dominate the dispersion of the stream.

The one major remaining discrepancy between the modelled results and the actual observations which remains is the one to two hour difference in peak time for the 1993 and 1994 Perseid outburst maxima. There are two possible explanations for the differences. One would be that material associated with the outburst in 1993 and 1994 is richer in older ejections, implying that the comet was particularly active in 1610 or 1479, the two passages other than 1862 which our simulations suggest should contribute significantly to the outburst portion of the stream in these years. The ejecta from both of these passages would place the nodal longitude of the peak roughly 0.1° later than what is currently given by the models and could explain the discrepancy.

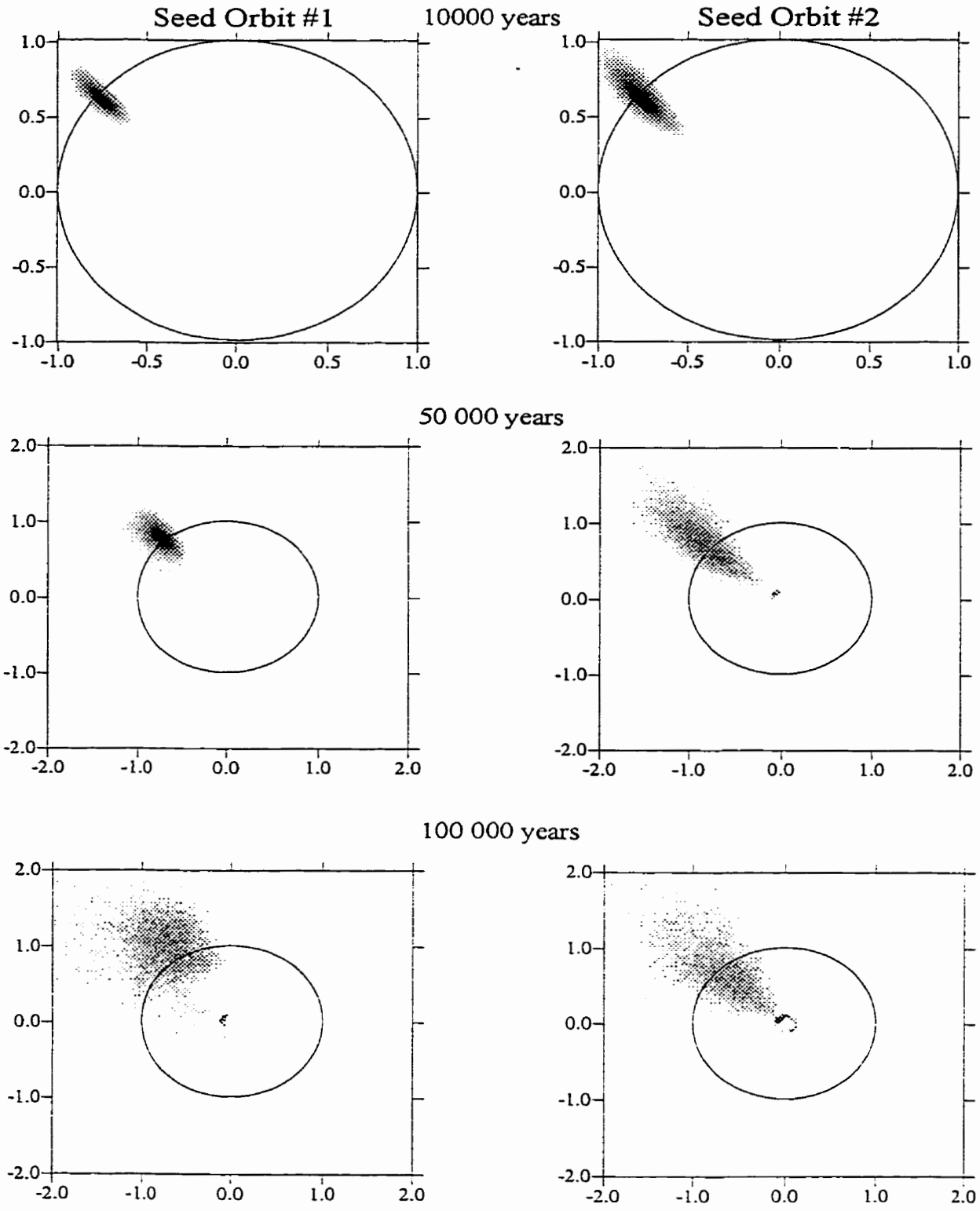

Fig 4.10: Descending nodal distribution of all Perseid meteoroids of mass 0.1g (for model 42 this means $\beta=2\times10^{-4}$) with the ages shown for both initial seed orbits. The circular outline is the orbit of the Earth and all measurements are in A.U.

The geometry of the comet's passage in 1610 and 1479 placed it well below the likely detection threshold for visual observations (Yau et al, 1994) and the fact that no observations exist for either of these returns suggests that the comet was not intrinsically brighter than its long-term average. Alternatively, the ejection geometry in 1862 might have been much more collimated than the rather broad, hemispherical ejection geometry adopted. In particular, for ejections with a substantial velocity component normal to the cometary plane, it is possible to change the mean nodal longitude as much as 0.1-0.2° with normal "Whipple"-sized ejection velocities. More precisely, the change in nodal longitude can be described by (Roy, 1978):

$$\Delta\Omega = \frac{r\sin(\theta+\omega)}{na^2\sqrt{1-e^2}\sin i}\Delta V_n \qquad (4.10)$$

where n is the mean angular velocity (2π/T), θ the true anomaly and ΔV_n is the component of the velocity normal to the orbital plane such that the object is seen to orbit in the counterclockwise direction as seen from this pole. Thus to increase the nodal longitude from the initial ejection velocity alone requires a positive value for ΔV_n. Fortunately, detailed observations from the 1862 passage of Swift-Tuttle exist and these have been examined in detail by Sekanina (1981). In particular, he reconstructed the velocity vectors of the major jets near perihelion based on observations of fans and other structures visible to Earth-based observers during that passage. Over the two month period nearest perihelion, it was found that some 70% of all observed ejections had a velocity component with positive ΔV_n.

Fig 4.11 shows the change in the osculating node for the Perseids as a function of the normal component of the ejection velocity (V_n) and the ejection position along the orbit. For ejection pre-perihelion at a modest distance from the sun (r>1.5 A.U.), a velocity of less than 50 m/s is needed in the normal direction to produce a positive shift of 0.1° in the nodal longitude. This is well within the allowable range of ejection velocities for visual-sized meteoroids using the normal Jones/Whipple ejection model for a comet the size of Swift-Tuttle and suggests that the activity from 1993 and 1994 might best be

explained by pre-perihelion ejection from isolated sites residing at latitudes significantly different from the sub-solar point. Indeed, Sekanina (1981) noted that "..the net momenta exerted on the nucleus by ejecta from the active areas in 1862 were virtually all directed to the south of the orbital plane.", implying that almost all ejections had a strong northward (positive V_n) component.

Perseid photographic data, representing roughly 600 orbits according to Lindblad and Porubcan (1994), also contains detailed distributions of all

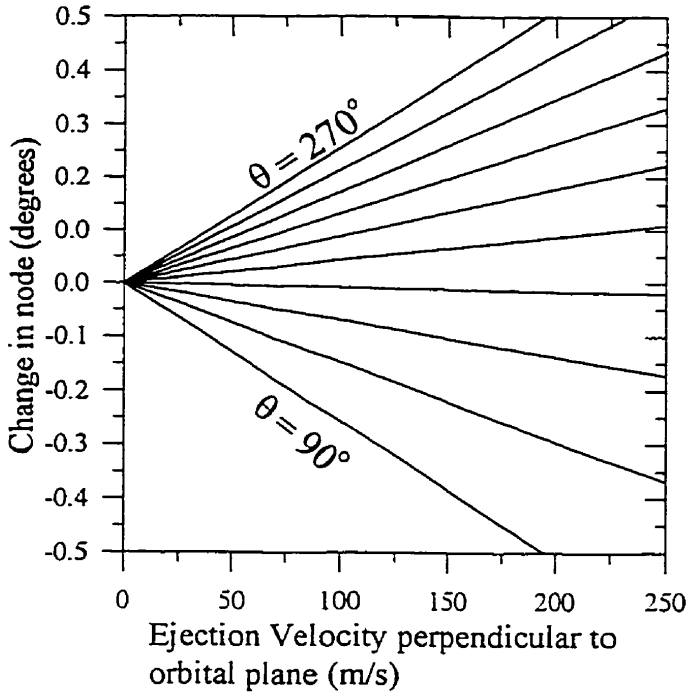

Fig 4.11: The change in the osculating nodal longitude at ejection for meteoroid test particles as a function of the normal component (V_n) (relative to the cometary orbital plane) of the initial ejection velocity and true anomaly (θ) at ejection. Each line represents values for the true anomaly from 270°-90° in steps of 20°.

orbital elements. However, the previous discussion concerning large errors in semi-major axis, for example, applies to lesser degrees to the errors for many other orbital elements and renders their usefulness questionable. The original data sources from whence these orbits are extracted often do not list estimates of the errors in other elements for individual

orbits. An examination of the dispersion in mean elements from the simulation output yields standard deviations less than 0.003 A.U. in q, 0.5° in inclination, and 0.6° in the argument of perihelion for the combined ejections over the last 2000 years. For comparison, Spurny (1995) lists detailed data (and errors) for 27 Perseids photographed with fish-eye cameras during the 1993 Perseids. His distributions show average errors of 0.005 A.U. in q, 1.1° in inclination and 2.4° in the argument of perihelion. In all cases the average errors are 2-4 times the maximum dispersion in the cumulative theoretical distributions for the same elements. Porubcan (1977) examined most of the presently available Perseid orbits and showed that there are significant intersurvey differences in dispersion among various photographic datasets. He concluded that the observed dispersions are greater than the true dispersion in the stream, a conclusion we also have reached. Of the several hundred Perseid orbits available, there is a small number of very precise orbits with errors smaller than our expected dispersions; in this case, however, the number of usable orbits drops to a one to two dozen and thus no statistically meaningful comparisons can be made. We do not treat photographic orbital elements further and discuss only geocentric radiant distributions in the remainder of this work.

The considerable evolution experienced by some Perseid particles, particularly the changes in the argument of perihelion over time periods of order 50 000 years, resulted in movement of the ascending node of some test meteoroids to Earth-intersection. The result was a shower of duration two to three weeks which occurs in mid-March from the southern hemisphere. Table 4.5 provides orbital details of this theoretical twin shower of the Perseids, along with drift of the radiant point and spread in the radiant. A search for showers possibly associated with this theoretical radiant yielded two with close similarities: the Gamma Normids and the Theta Centarids (Jenniskens, 1994). Both have radiant positions very close to our expected location and peak at very nearly the same nodal longitudes expected for the Perseid southern shower. The lack of velocity information for these streams means that the values for a, e and q are uncertain; within uncertainties the showers might be linked to the southern Perseid radiant. The Theta Centarids, in particular, show similarity to the theoretical stream and it would be most

interesting to get accurate velocity information for these streams to test for any association.

Stream	a	e	i	ω	Ω	q	α	δ
Theoretical Southern Perseid Twin	21±3	0.99±0.01	121±21	76±24	165±22	0.61± 0.19	220	-43
γ Normids	∞	1.0	133	41	172	0.89	249	-51
θ Centarids	∞	1.0	128	27	153	0.90	210	-41

Table 4.5: Orbital elements and radiant location for the theoretical Perseid southern twin (at ascending node) and the same for two observed showers with comparable elements and radiant locations in mid-March (from Jenniskens (1994)).

4.5.1. Planetary Impulses on the Perseid Stream.

The planets Jupiter and Saturn pass within 1.6 and 0.9 A.U. respectively of the orbit of 109P/Swift-Tuttle. The comet's high inclination is usually invoked to suggest direct planetary perturbations on the stream to be minimal and the stream quite stable. Over long time periods this is certainly true as most stream meteoroids have moved in essentially the same general orbit as Swift-Tuttle for many thousands of years, a result confirmed by our direct integrations and others (cf. Hamid 1951).

However, as the Perseid stream is a continuous ring of meteoroids, some meteoroids always experience the maximum direct perturbations from either Jupiter or Saturn. Since at the present epoch the descending node of the parent comet is only very slightly outside the Earth's orbit (0.004 A.U. outside for the 1862 passage), even small perturbations can move Perseid meteoroids from non-intersecting to Earth-crossing orbits.

In general, a Perseid meteoroid passing some distance from a planet will experience an impulse that changes its orbit by a small amount. This small perturbation

results in a significant change in a and e since the orbit of 109P is nearly unbound. As the stream orbit does not pass close to any of the outermost planets (minimum distances from Uranus and Neptune are 2 and 6.5 A.U. respectively), only Saturn and Jupiter are important in this regard. Fig 4.12 shows the envelope of closest possible distances between Jupiter and Saturn and the mean orbit of Swift-Tuttle. Any actual encounter between a Perseid meteoroid and one of these planets will have a planet-meteoroid distance curve inside these envelopes and with larger curvature. A typical encounter between Jupiter and a Perseid meteoroid is also shown in Fig. 4.12 (thin line).

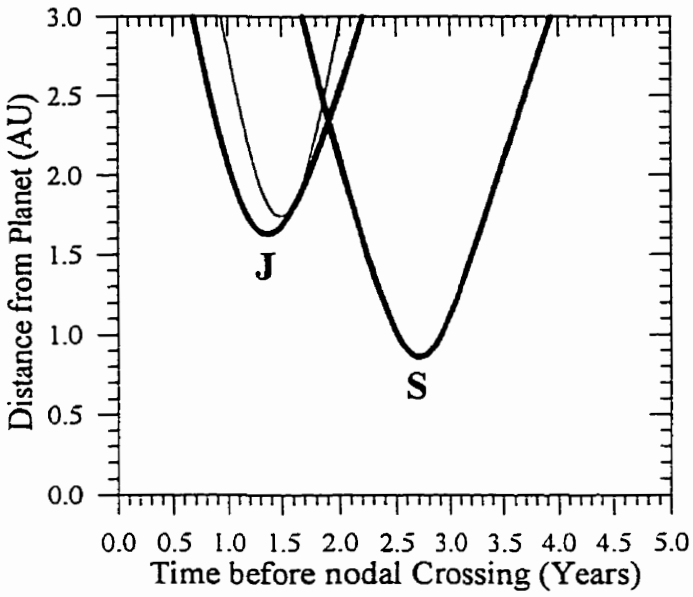

Fig 4.12: Closest approach distances between the mean Perseid orbit (taken as the osculating orbit of 109P at its 1862 perihelion passage) and the planets Jupiter and Saturn (shown as bold lines) as a function of the time before nodal passage. The change in distance between Jupiter and a typical Perseid meteoroid is also shown (thin line).

For Earth-encounter, the radius of the descending node must equal the Earth's orbital distance from the sun. In general the descending nodal radius in A.U. (R_d) is given by

$$R_d = \frac{a(1-e^2)}{1-e\cos\omega} \tag{4.11}$$

where ω is the argument of perihelion. The change in the nodal radius due to variations in the individual osculating elements is given by

$$dR_d = R_d \frac{da}{a} + \frac{e}{1-e\cos\omega}\left[a(1-2e) + R_d\cos\omega\right]\frac{de}{e} + \frac{R_d e \sin\omega\, d\omega}{1-e\cos\omega} \qquad (4.12)$$

In an encounter between a planet (in this case Jupiter or Saturn) and a Perseid meteoroid on a retrograde orbit crossing the planet's orbit above the ecliptic plane with dominant motion perpendicular to the planet's orbit and inward, the net impulse is always a positive one and increases the energy of the associated meteoroid. The result of this effect is that the impulse delivered by Jupiter and Saturn produces a net inward shift in the node of perturbed Perseids. This shift results from the fact that the perturbation decreases the effective perihelion distance of the orbit. Physically, the effect can be understood once it is seen that the encounter with either of Jupiter or Saturn will rotate the velocity vector toward the ecliptic plane. It is precisely this effect which causes the inward shift of the node of meteoroids visible in Fig. 4.3 by a maximum amount of approximately 0.01 A.U. It is not possible to use an Opik-like (or two-body) formalism to describe this encounter with Jupiter as the closest approach distance is almost 5 Hill Sphere radii from Jupiter and the impulse occurs over an extended region where the meteoroids' heliocentric velocity changes appreciably (cf. Greenberg *et al.*, 1988 for a discussion of two-body encounters).

We have investigated this effect through numerical simulation and find that virtually all of the impulse causing this change occurs during the short interval of approximately ~1 year on either side of the closest approach to the planet. To verify that this encounter causes the observed nodal shift, we used 5000 test Perseid meteoroids ejected in 1862 and stopped the integration in 1986, mid-way between Jovian perturbations (1979 and 1991). We then used these new elements as starting orbits where each particle was followed with the direct perturbation term for Jupiter present and with it absent. All particles were followed to their descending nodes and the results of the perturbed and unperturbed final orbits compared. In all cases we found the perturbed meteoroids arrived at the node after the unperturbed meteoroids and with smaller nodal radii in the intervals nearest the Jovian closest approaches. The energy difference between

perturbed and unperturbed meteoroids in this simulation was greatest for particles having the largest Jovian perturbations, with particles passing closest to Jupiter always found to have larger energies than the equivalent unperturbed trajectories. Fig 4.13 shows the relative energy difference between meteoroids experiencing close approaches to Jupiter relative to those which do not. Note that the local maximum near 2008 is an artifact owing to the inclusion of the perturbations from Saturn during its 2006 close approach to the stream.

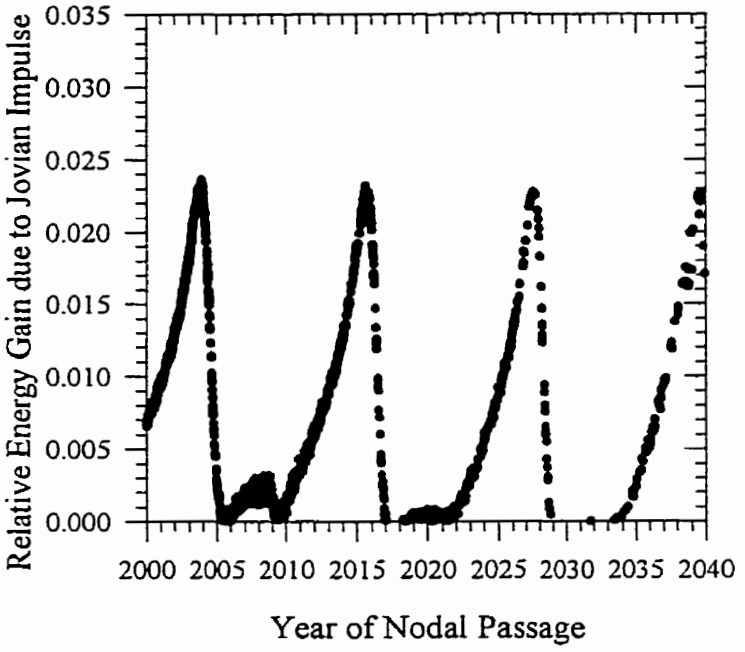

Fig 4.13: Change in the energy of Jovian perturbed meteoroids relative to unperturbed Perseid meteoroids as a function of the time of their nodal passage.

The magnitude of the perturbation in nodal radius is almost exactly the same for Jupiter as for Saturn, the net gravitational impulses for closest approach Perseids being identical owing to the closer distance of approach to Saturn (1.77 times) and slightly longer impulse time (for Saturn perturbations) precisely compensating the factor of 3 lower mass for Saturn.

Since 109P/Swift-Tuttle has had a nodal point outside the Earth's orbit for the last several thousand years, most meteoroids from these recent ejections are not accessible to Earth. On average, we have found that for our simulations the mean effect of radiation

pressure is to move the node slightly further outward, though this is not strictly the case for any one Perseid meteoroid, the final difference being a function of the initial ejection distance, velocity and particularly subsequent planetary perturbations for any given test particle. Only impulsive perturbations from Jupiter and Saturn can cause enough change in nodal distance for recently ejected meteoroids to make them visible at Earth.

This effect should produce noticeable changes which may persist for several years in the activity of the stream over restricted intervals in solar longitude every 12 and 30 years. This activity may be further heightened by the "focusing" effects of the perturbation, which concentrates the otherwise scattered nodal points of individual meteoroids, a direct result of the impulsive effects being larger than the smearing effects of initial ejection velocity and ejection geometry for recent ejecta. The close approaches by Jupiter and Saturn to the stream and an observed inward shift in the nodal positions of meteoroids show a lag of 1-3 years and a comparable duration (see Fig. 4.3). Table 4.6 lists the dates of close approach to the stream by Jupiter and Saturn over an interval of one century.

That the position of the planets might affect the observed shower activity on Earth is not a new idea. Guth (1947) suggested that some showers were prone to increases in activity when the stream's orbit was in conjunction with a major planet. More recently, Jenniskens (1997) has shown that many streams show outbursts preferentially when the positions of Jupiter and Saturn are near conjunction with the stream. We suggest that in these cases an impulse effect similar to the one found for the Perseids is also at work.

Table 4.6: Dates of closest approach between Jupiter and Saturn and the Perseid stream over the interval 1860-2050.

Jupiter Closest Approach Date (YY/MM/DD)	Saturn Closest Approach Date (YY/MM/DD)
1860/9/15	1889/1/1
1872/7/26	1918/6/13
1884/6/5	1947/11/21
1896/4/18	1977/5/4
1908/2/27	2006/10/8
1920/1/7	2036/3/24
1931/11/17	
1943/9/27	
1955/8/7	
1967/6/17	
1979/4/26	
1991/3/6	
2003/1/14	
2014/11/24	
2026/10/4	
2038/8/14	

4.5.2 Geocentric Radiant Distributions - Theoretical vs. Observed.

The distribution of the theoretical radiants for the full 2000 year and 100 000 year integrations are shown in Figs. 4.14 and 4.15 for photographic sized meteoroids ($10g<m<0.1g$). The temporal change in the rms width of the cumulative radiant distribution as a function of time for both orbit #1 and orbit #2 is shown in Fig. 4.16. The radiant dispersion for older ejections was approximated by weighting each geocentric radiant from an older ejection by the time between the next most recent and next oldest

ejection in the model divided by the mean period of the comet.

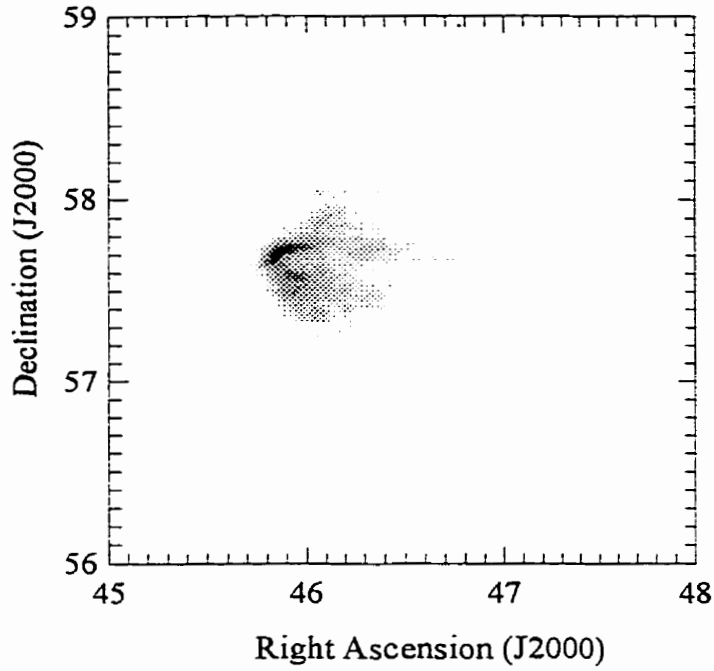

Fig 4.14: Geocentric radiant distribution for all Earth intersecting Perseids ejected 59 to 1862 A.D. at the present epoch for photographic-sized meteoroids (mass > 0.1 g) from model 42. Grid resolution is 0.02°. The dynamic greyscale range for this binning is from 0 to 320.

While some difference exists between the dispersions found from orbit #1 and #2, the most consistent relation for the dispersion of the Perseid radiant over the full 100 000 years using the average of both orbits is

$$W = (4.74 \pm 0.84) \times 10^{-3} Y^{0.55} \tag{4.13}$$

where W is in degrees and Y in years. The exponent in this power-law is very close to the 0.5 expected for the case of random-walk-type diffusion.

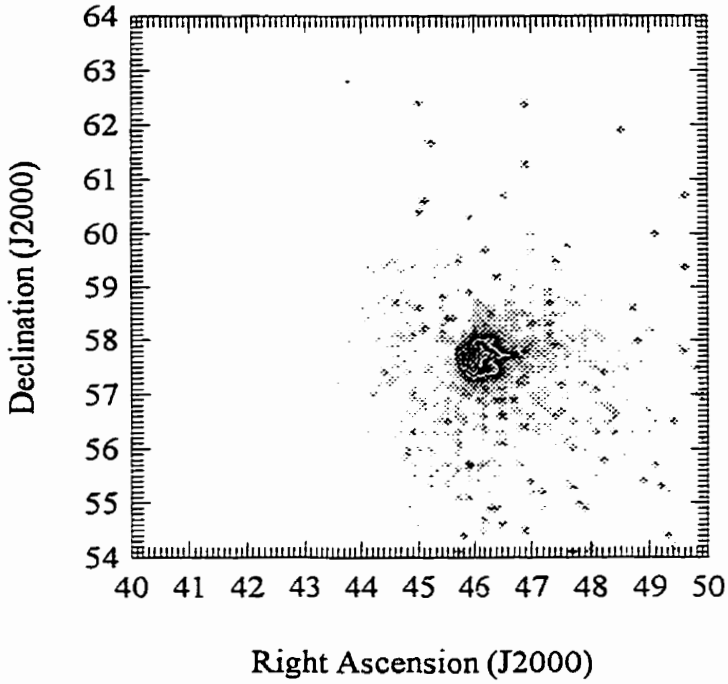

Fig 4.15: Geocentric radiant distribution for all Earth intersecting Perseids ejected over the past 100,000 years at the present epoch for photographic-sized meteoroids (mass>0.1 g) for model 42. The dynamic greyscale range for this binning is from 0 to 350.

The observed radiant dispersion for the Perseids changes as the Earth passes through the stream. Kresak and Porubcan (1970) investigated the radiant of the stream using 250 photographed Perseids. They found the radiant showed a significant change in size across the stream, with the average dispersion being 1.39° for λ_O<139°, 1.10° for 139°<λ_O<140.3° and 1.33° for λ_O>140.3°. A more recent examination of the same question by Lindblad and Porubcan (1995) revealed a similar trend. While this trend is often interpreted as suggestive of older material outside the core portion of the stream (an observation supported by our findings), it is also significant that material further from the core of the stream has been, by definition, more affected than Swift-Tuttle by planetary perturbations and is thus more dispersed. Fig 4.17 shows the dispersion at the present epoch for individual ejections in the intervals before, during and after the main maximum. It is clear there is a large increase in dispersion away from the core of the stream for ejections of the same age.

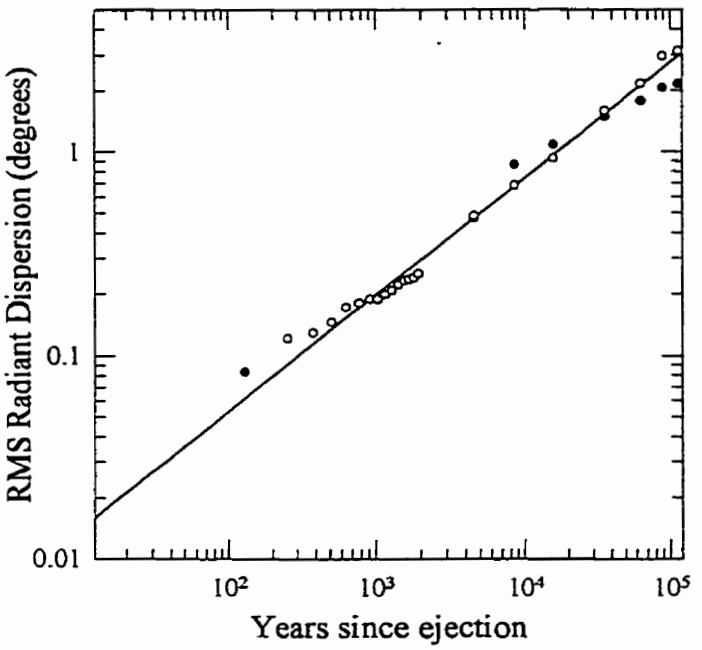

Fig 4.16: Change in the rms width of the Perseid radiant for cumulative ejections over the past 100 000 years for seed orbit #1 (filled circles) and seed orbit #2 (open circles).

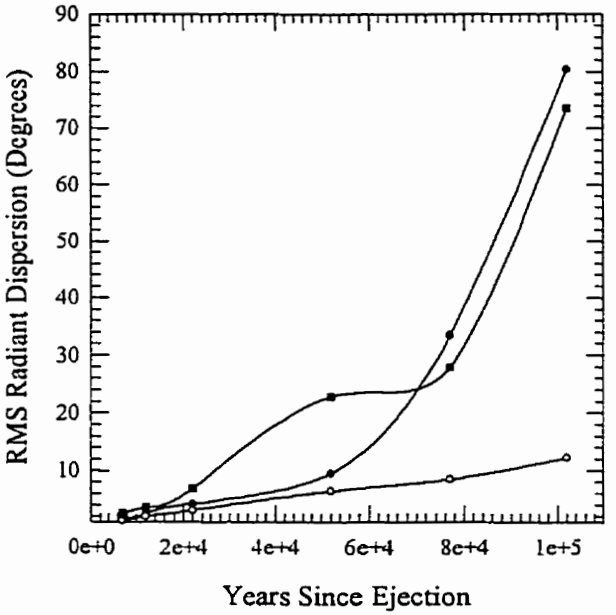

Fig 4.17: Radiant dispersions for individual ejections of photographic-sized meteoroids from 5000-100,000 years ago for Perseids in the pre-maximum period ($\lambda < 139°$)(solid circles), the maximum period ($139° < \lambda < 140.3°$) (open circles), and in the post-maximum region ($\lambda > 140.3°$) (solid circles).

Whipple and Wright (1954) noted a strong correlation between the nodal width of a stream and radiant dispersion. They also noted that the change in scatter as a function of mass should indicate whether physical forces such as initial ejection velocity and radiation effects are dominant over planetary perturbations. In Sect. 4.2 it was shown from an examination of visual-sized meteoroid radiant spreads from all models over the last 2000 years that the absolute rms size of the radiant is dominated for the first few revolutions by the initial ejection velocity and later affected by radiation pressure, whereas the rate of change of the radiant size is similar for all initial ejection conditions and densities of meteoroids and hence controlled by planetary perturbations (see Fig. 4.6). In Fig. 4.18 the radiant dispersion for faint visual and radar class meteoroids (10^{-3} g<m<10^{-5} g) is shown for comparison to the photographic class meteoroids from the same models for orbit #2. In general, the radiant dispersion at present from any past ejection over this period tends to be greater for the smaller meteoroids than for the larger ones, but the variation of the change between the two mass categories is similar for each period of activity of the stream. This supports the earlier conclusions of 4.2.

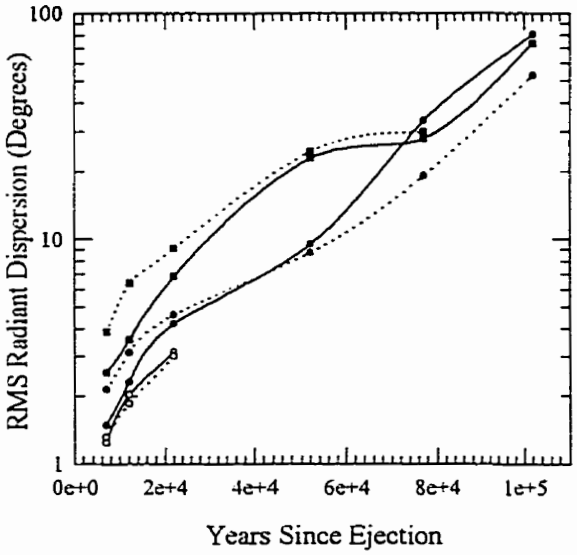

Fig 4.18: Radiant dispersion of faint visual and radar class meteoroids (dotted line) as compared to brighter photographic Perseids for ejections from 5000-100 000 years ago. Symbols have the same meaning as in Fig 4.17; only ejections with at least 20 representative Earth intersecting members at the present epoch are included.

Lindblad and Porubcan (1995) found that the radiant area increased as the magnitude of the photographic Perseid decreased. Porubcan (1973) noted the telescopic radiant spread of the shower to be significantly larger than the photographically determined width. All of these observations are consistent with our results showing the radiant spread to generally be larger at the present time for smaller meteoroids.

The average position of the geocentric radiant for photographic sized meteoroids from ejections over the last 2000 years is at α=46.1° ± 0.1° and δ=57.66° ± 0.05° referenced to J2000.0 and solar longitude 139.7°. This compares well to the location of the "new" component of the stream (outburst portion) found by Lindblad and Porubcan (1995) at α=46.85° ± 1.8° and δ=57.6° ± 0.99°.

4.5.3 Progression Rate of the Node.

The orbits of the Perseids and Swift-Tuttle are retrograde, hence the secular perturbations on the stream due to the planets result in a positive increase in the nodal longitude for the shower and the comet.

Hughes and Emerson (1982) have examined the change in position of the peak of the stream from ancient records. They find that since 36 A.D. the node of the stream has advanced at an average rate of $(3.8 \pm 2.7) \times 10^{-4}$ degrees/year on the basis of the reported times of observation of the shower.

To derive a theoretical value for this number, we determined the position of the maximum of ejecta for each mass category at the current epoch for all ejections over the last 2000 years for all models. The slope of this distribution through time is found to be remarkably independent of mass; all masses were found to have an annual nodal progression rate well represented by

$$\frac{d\lambda_{\odot}}{dt} = (2.2 \pm 0.2) \times 10^{-4} \quad ^{\circ}/\text{year} \tag{4.14}$$

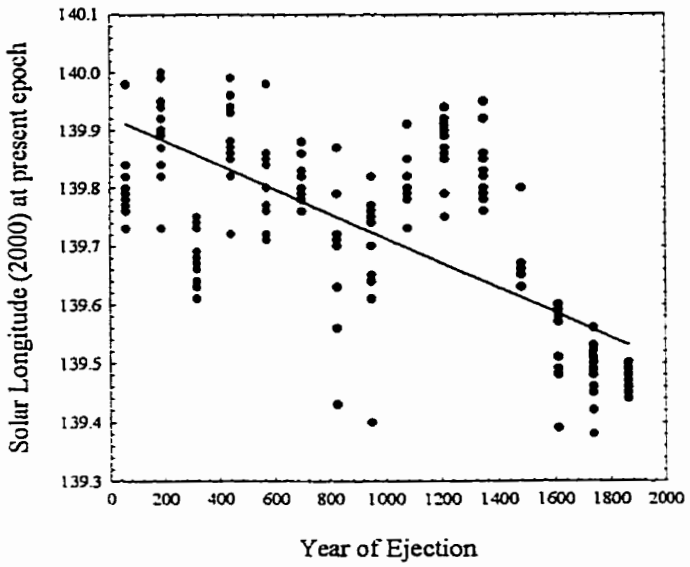

Fig 4.19: Location of the maximum in activity as a function of solar longitude at the present epoch for individual ejections of 0.01g Earth intersecting Perseids over the past 2000 years. The results from all models have been included and each determination of the location of the maximum for each ejection epoch is represented by a single solid circle. The line of best fit is also shown.

Fig 4.19 shows the distribution of maxima as a function of time for 0.01 g Perseids over the last 2000 years.

This nodal progression rate is an order of magnitude larger than the rate found over the interval from $5000<t<100000$ years ago (Sect 4.4.3). It is possible the actual progression rate was lower in the distant past as the progression rate would be expected to decrease as we move backward in time if Swift-Tuttle's inclination more closely approached 90°. We note, however, the value of the progression rate at present to be most affected by recent ejections shown to be far more concentrated than older ejections and also more efficient at transporting Perseids into Earth intersecting orbits as the comet's orbit probably passes closer to the Earth than it did in the past. The theoretical progression rate we find is consistent with Hughes and Emerson's (1982) value.

4.5.4 Age of the Stream.

The age of the Perseid stream has remained difficult to determine from past studies. From the nearly perpendicular orientation of the orbital plane, no major perturbations on the parent comet or stream are encountered. From the recent passage of the comet, we know Swift-Tuttle is among the most massive of the Halley-family of comets. Further observations supporting the stream's great antiquity include its very long period of activity and large mass (Hughes and McBride, 1989), estimated to be upwards of 10^{17} g.

That the shower is much older than typical meteoroid streams can be readily inferred simply from its long duration. Southworth (1963), for example, estimated the stream age to be less than 6000 years on the basis of the rate of change in observed elements of photographic Perseids. In the other direction, Katasev and Kulikova (1975) noted that the stream must be younger than the time it takes for Poynting-Robertson drag to cause the particles to collide with the sun, a time of order 10^6 - 10^7 years for visual - sized Perseids. Very few additional attempts to determine the age of the stream have been made.

From the modelling output there are several methods we can employ to estimate the age of the stream.

First, we may use the "average" radiant dispersion and Eq. 4.13. Kresak and Pourbcan (1970) found the mean width of the radiant throughout its period of activity to be 1.27°. This yields an age estimate of $(30 \pm 10) \times 10^3$ years. From a data set with nearly double the number of Perseids, Lindblad and Pourbcan (1970) derived a mean angular dispersion of 1.84° for the entire activity period of the shower which corresponds to an age estimate of $(55 \pm 20) \times 10^3$ years. We note that in both cases these ages represent upper limits as the effects of individual radiant errors are not taken into account in these analyses and thus the true radiant rms spread is smaller than these values.

For the central portion of the stream we attempted to make a direct age estimate on the basis of the current position of the main visual maximum (139.96 ± 0.04°). This

was done by summing the activity from each ejection; with each additional passage, the location of the secondary peak in activity (corresponding to the broad maximum as opposed to the outburst maximum) was found. Here we defined such a sub-maximum to be present if the peak in number of test meteoroids in any interval of 0.01° of solar longitude was above the number in all bins between 0.05° before and 0.05° after the position of the local maximum. By doing this for all 15 ejections from 59A.D.-1862 we noticed a slight shift in the position of this maximum as more ejections were added to the total. By assuming the geometry of encounter with Swift-Tuttle has remained reasonably similar to the average over the last 2000 years for the past ~10 000 years (a fact supported by our long term integration of the comet's orbit in Sect. 4.4.3), we can then use this rate of shift, averaged for all models, to extrapolate the number of total ejections needed to produce a peak at 139.96° at present. This procedure was done for all models and the position of the secondary maximum (found to move from approximately 139.7°-139.75° over the whole 2000 year period) as a function of number of ejections added to the total (or equivalently the time) was determined. We note that this produces a lower limit as older ejections add fewer meteoroids to the core portion of the present population (all other things being equal) and each new ejection causes less of a change in the peak position due to the large number of previously existing meteoroids. In this way we find that the shift in maxima would be such as to equal the present location of the observed maximum after $(11 \pm 3) \times 10^3$ years.

We can also use the width of the ZHR-profile at present and compare it to the width of the distributions found for each of the long-term ejections to derive a lower limit for the age of the central portion of the stream, since the width of the individual distributions at present will always be larger than the actual width from cumulative ejections. From Chapter 3, the observed FWHM of the Perseid profile is approximately $2.1 \pm 0.1°$. Using Eq. 4.9, the ejections attain this width after $(14 \pm 7) \times 10^3$ years, implying that the age of the central portion of the stream must be >7000 years.

The absolute location in (α,δ) of the new and old components of the stream can also be compared with the rate of change in these elements and with the weighted cumulative distribution location for the same elements in order to derive two approximate

estimates for the age. Lindblad and Porubcan (1995) have shown that the average radiant location (referenced to λ_O = 139.7° (J2000.0)) is located at α=47.52° and δ=57.96° (from their Eqs. (1) and (2)). From the cumulative distributions over the last 2000 years averaged over all models and referenced to the same solar longitude, the change in right ascension is well represented by

$$\alpha = (45.88 \pm 0.01) + (1.13 \pm 0.03) \times 10^{-4} Y \qquad (4.15)$$

This yields an estimate of $(15 \pm 1) \times 10^3$ Y years for the age of the central portion of the stream.

For the location of the "average" declination for the stream, there is considerably more scatter in the slope of best-fit to the theoretical distribution because the secular variation in the declination is small in comparison to amplitude variations caused by planetary perturbations.

An approximate expression averaged over all models is:

$$\delta = (57.66 \pm 0.01) + (9.3 \pm 3.8) \times 10^{-6} Y \qquad (4.16)$$

which yields a median estimate of ~$(38 \pm 16) \times 10^3$ years. Taken together these two determinations suggest an age of 15-20 000 years as most appropriate.

The above estimates represent the effective age of the majority of the photographic/visual-sized meteoroids in the Perseid stream. The age of the most ancient meteoroids in the stream is much older, the amount of material from older returns having been diffused and hence not contributing significantly to the bulk of the currently visible core population. Perhaps the most effective means of gauging the total age of the stream is by comparing the full nodal spread of the current stream to the theoretical spread. The duration of the visibly detectable stream extends from roughly λ_O = 115° - 150° (from the results of Chapter 3), corresponding to calendar dates from mid-July to late August each year. There are hints that some activity from the shower might be visible outside this boundary, but the levels are lower than can be distinguished using visual observation techniques and we adopt the above as the minimum length of time the shower is presently active.

From Sect. 4.4.2 and 4.4.3, the nodal dispersion from ejections at all visual-sized masses over the last 2000 years remains effectively contained within the region 139-140.5°. Taking Eq. 4.9, the Gaussian half-width from past ejections reaches this full width after nearly 180 000 years, though we caution that this is extrapolated well beyond the region where Eq. 4.9 was determined. If we take a "weak" level of observed activity to be possible even when the mean level of the theoretical activity is at a distance of 2σ from the peak, this would imply an overall age for the stream of ~90 000 years.

4.5.5 Long-Term effects of Terrestrial Perturbations.

Since the earliest recognition of the Perseids in the 19th century, the question of the role of the Earth in the development of the stream has been posed by a number of authors (cf. Twining (1862), Shajn (1923)). Previous works have examined the expected effects based on approximate analytic treatments of the average effect the Earth has on the stream, while ignoring the true physical character of the stream as a collection of many individual particles.

In an effort to address this question directly, we re-ran all long-term integrations using seed orbit #1 with every condition identical, except that the direct planetary perturbations from the Earth were removed. We expect, a priori, that the influence of the Earth will be detected through an increase in the scatter of the orbital elements, particularly, a, i, and Ω in the simulation set containing the Earth as compared to the set without the Earth. The results show that in overall terms the Earth does have a perceptible effect on the evolution of the stream but it is not more than a secondary influence in absolute terms.

That the Earth affects the stream is most evident in the width of the final nodal distributions as shown in Fig. 4.20. Here the difference between the gaussian fit-widths and the final ejections with Earth and without are presented. The influence of the Earth is to add ~10% to the total width of the stream for those points containing the largest number of test particles. Similarly, the radiant dispersion increases by ~10% for any given age of ejection with inclusion of the Earth.

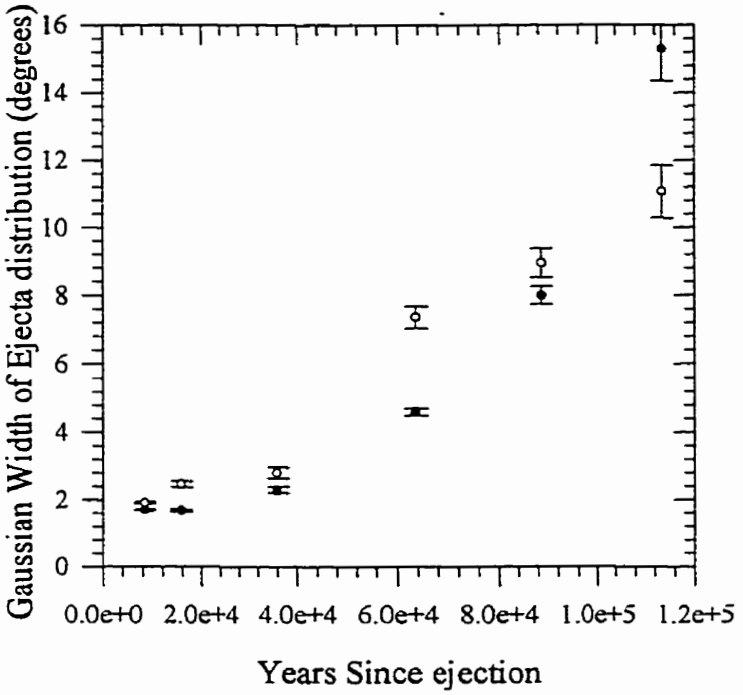

Fig 4.20: The width of the final nodal distribution for Earth intersecting Perseids for orbit #1 with the Earth perturbations (open circles) and without Terrestrial perturbations (solid circles).

The terrestrial effect on the orbital element dispersions is shown in Table 4.7. Here the difference in the rms dispersion in the distribution of a, i and ω for the Earth/No Earth simulations is given as well as the total number of meteoroids used in each distribution. There is a distinct tendency for the dispersions to be lower for the simulation where the Earth is removed (negative values), however the effect is far from universal. Particularly for the oldest ejections where fewer particles are involved, the small statistics overwhelm the relatively minor effect of the Earth's perturbations.

Ejection Time (Year)	Mass grams	# of Meteoroids Earth (No Earth)	Semi-Major Axis (a) (A.U.)	Inclination (i) (degrees)	Argument of Perihelion
5000	10	496 (466)	-0.01	-0.49	-0.11
	0.1	491 (471)	-0.14	-0.54	0.00
	0.001	444 (530	+0.02	-0.53	-0.05
10000	10	400 (383)	+0.1	-0.09	-0.27
	0.1	370 (430)	-0.04	-0.16	-0.26
	0.001	367 (390)	-0.25	-0.8	-0.06
20000	10	253 (303)	-0.09	-0.5	+0.07
	0.1	255 (270)	-0.47	-0.89	+0.29
	0.001	243 (246)	+0.05	+0.42	+0.02
50000	10	198 (212)	-0.7	-0.86	-0.17
	0.1	183 (200)	-1.3	-2.85	-0.83
	0.001	189 (188)	+1.06	-0.18	+0.81
75000	10	87 (88)	+2.15	-2.88	-6.69
	0.1	91 (89)	-1.17	-2.45	+2.32
	0.001	84 (96)	-2.79	-2.68	+0.75
100000	10	40 (49)	-0.17	-3.77	+2.93
	0.1	70 (60)	+0.21	+0.91	+3.98
	0.001	72 (85)	-0.36	+0.41	+2.34

Table 4.7: The difference in Keplerian element rms dispersion of the Perseid stream for seed orbit #1 meteoroids at their descending nodal passage at the current epoch with and without the direct planetary perturbations of the Earth present. The number of meteoroids in each sample is given for the simulations with Earth perturbations present (and without in brackets). The differences represent $\sigma_{\text{No Earth}} - \sigma_{\text{Earth}}$. Negative values imply that the presence of the Earth makes the dispersion larger.

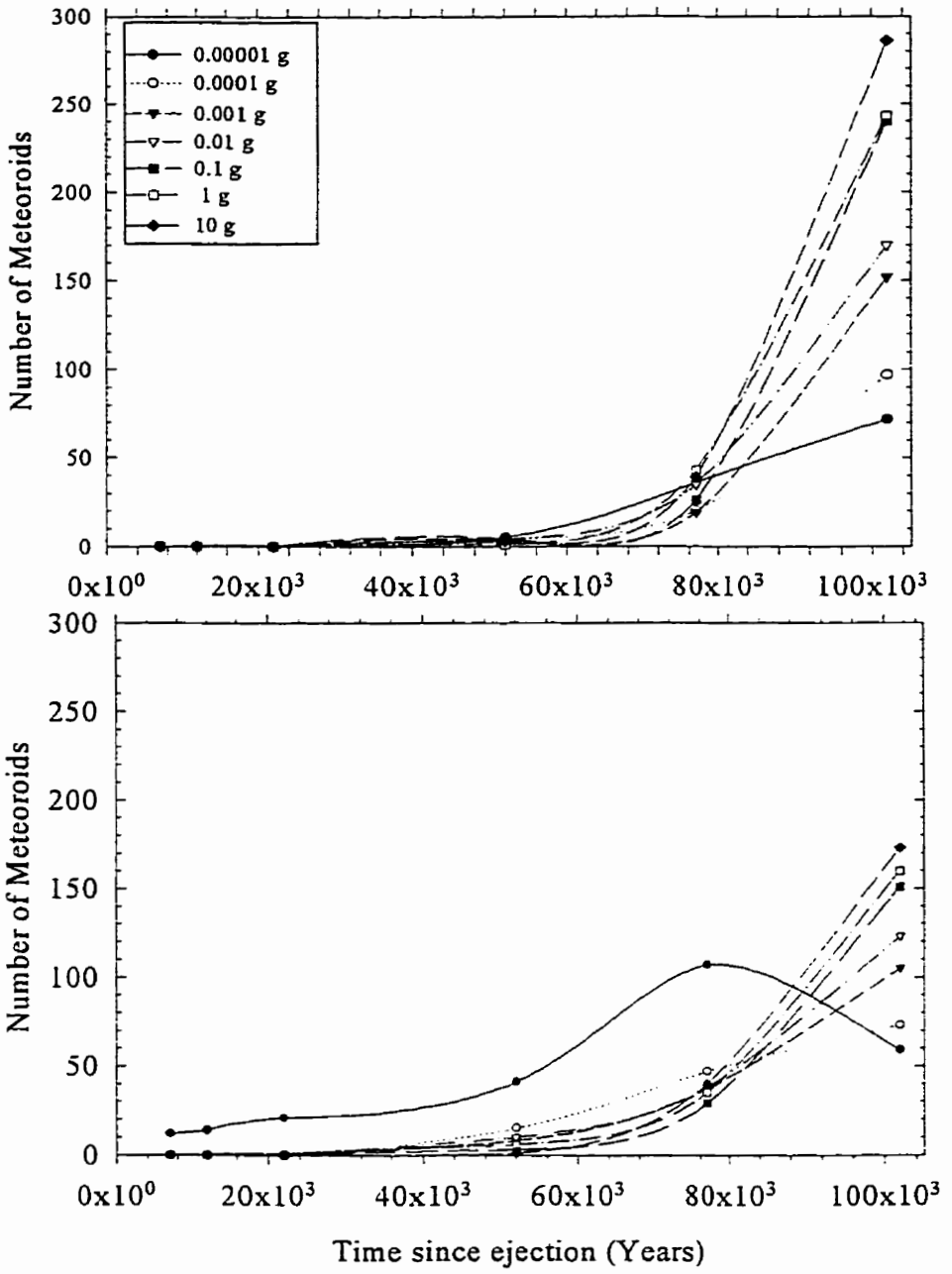

Fig 4.21: Number of Perseid meteoroids which reach a sungrazing state as a function of time since ejection for simulation with the Earth present (bottom) and with it removed (top graph) for all seven mass categories. The legend shows the symbol-mass correspondence. All meteoroids are from model 42 (see text for more details).

When the number of hyperbolically ejected Perseids is examined as a function of time (see Sect. 4.5.6 for more details) in comparison to the number lost without the Earth there is found to be no statistical difference between the two distributions at all masses. This attests to the dominance of Jupiter in ejecting Perseids from the solar system. Curiously, the same comparison of the number of Perseids lost due to attainment of a sungrazing state (when particle gets closer than 0.1 A.U. to the sun) does show a noticeable difference. With the Earth removed it is found that the number of sungrazing states reached is lower for the first 50 000-60 000 years after ejection. The difference is most striking for the smallest mass, where there is a much larger number of sungrazers for all times after ejection right up to 10^5 years. This effect is shown in Fig. 4.21 where the number of sungrazing Perseids is plotted against the year since ejection for simulations with and without the Earth. The Earth plays a more direct role in bringing Perseids to sungrazing states, possibly through the effects of close approaches.

4.5.6 Sinks for Stream Meteoroids: Sungrazers and Hyperbolic ejection

It is usually assumed that the major sink for the Perseid stream is hyperbolic ejection due to planetary perturbations. The effect of collisions in removing meteoroids from the stream has been investigated in detail by Steel and Elford (1986) and they find the survival lifetimes to be at least several million years for Perseid meteoroids, making this a negligible loss channel over the 100 000 year period of our study.

For the long-term integrations, particles were removed from further integration when either their semi-major axis exceeded 200 A.U. or their perihelia decreased below 0.1 A.U., corresponding to a sungrazing end-state. This latter removal condition is likely too strict as several annual meteoroid streams have perihelia inside this distance; the survivability of Perseids this close to the sun is not known, but the evidence from other streams suggests that our sungrazing (or near-sungrazing) conditions should be viewed as upper limits. For comparison, the cometary lexicon typically defines sungrazing states as orbits with perihelia of 0.01 A.U. or less (Bailey *et al.*, 1992).

The fraction of Perseids removed in either of these ways varied dramatically between the long-term orbits #1 and #2. In particular, orbit #2, with a much larger eccentricity and semi-major axis (and hence lower energy) showed an order of magnitude greater loss than orbit #1 for both loss channels.

The primary loss mechanism, especially for smaller meteoroids, was found to be hyperbolic ejection due mainly to direct perturbations from Jupiter with a minor contribution from Saturn. For both orbit #1 and #2 the hyperbolic loss tended to increase as the Perseid mass decreased (and hence β increased), this effect being the result of radiation pressure which increases the average energy of the meteoroid orbit and leads to more losses. However, for orbit #1 this trend was nearly reversed for ejections 10^5 years ago, attesting to the importance of the cometary orbit at time of ejection. After 10^5 years, the percentage hyperbolic loss for orbit #2 for radar-sized meteoroids (10^{-5} g) approached 35% of all ejected meteoroids. For comparison, only 1% of orbit #1 Perseids were lost in any given mass category due to hyperbolic ejection after 10^5 years. Fig 4.22 shows the number of ejected Perseids released at various ejections over the last 10^5 years for all masses for orbit #1 and #2 removed due to hyperbolic ejection before the present epoch.

Bailey *et al.* (1992) demonstrated that comets with orbits nearly perpendicular to the ecliptic plane and perihelion moderately close to the sun (0 - 2 A.U.) are susceptible to sungrazing states. We have found that for larger Perseids ($>10^{-3}$ g) and for both orbit variations used here, our near-sungrazing end state can be almost as efficient as hyperbolic ejection (and in some cases even more so) as a sink for the stream. Fig 4.23 shows the number of Perseids, which enter sungrazing states as a function of ejection time for orbit 1 and 2. The same mass dependence is found as for hyperbolic ejection, with the smallest Perseids being preferentially removed.

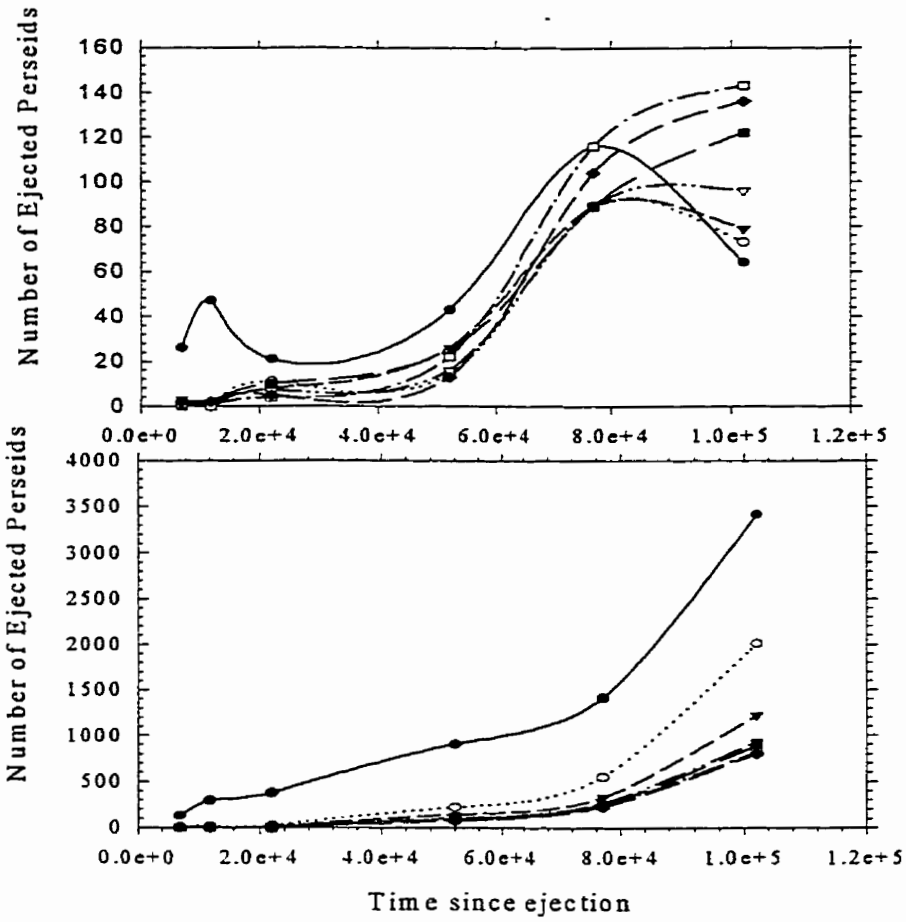

Fig 4.22: The number of hyperbolically ejected Perseid meteoroids as a function of ejection year for seed orbit #1 (top) and orbit #2 (bottom) meteoroids. The symbols are the same as in Fig 4.21.

The length of time needed for meteoroids to enter either of these states depends primarily on the comet orbit adopted (which changes significantly from one ejection epoch to another) for initial ejection from Swift-Tuttle and to a lesser extent on mass. For all but the smallest mass category, the average time taken before any significant number (>10) of Perseids are thrown onto hyperbolic orbits is 40 000 - 60 000 years for both seed orbits. For sungrazing orbits the time taken to reach this state falls in the range from 10 000 - 80 000 years, with an average near 60 000 years. The slope of the number of meteoroids lost

as a function of time for either loss channel varies between the two seed orbits, between masses, and times of ejection. In general, a linear or quadratic increase in the number of meteoroids lost is a good representation of the distribution after the initial loss time (as given above), with photographic-sized meteoroids being lost at a peak rate of one to five test particles for every revolution of the comet (corresponding to 0.01-0.05% of the number of total meteoroids initially ejected) after this time from any one mass category due to hyperbolic ejection. This implies a lower limit for the removal time of 50% of the largest particles due to attainment of hyperbolic orbits of ~200 000 years.

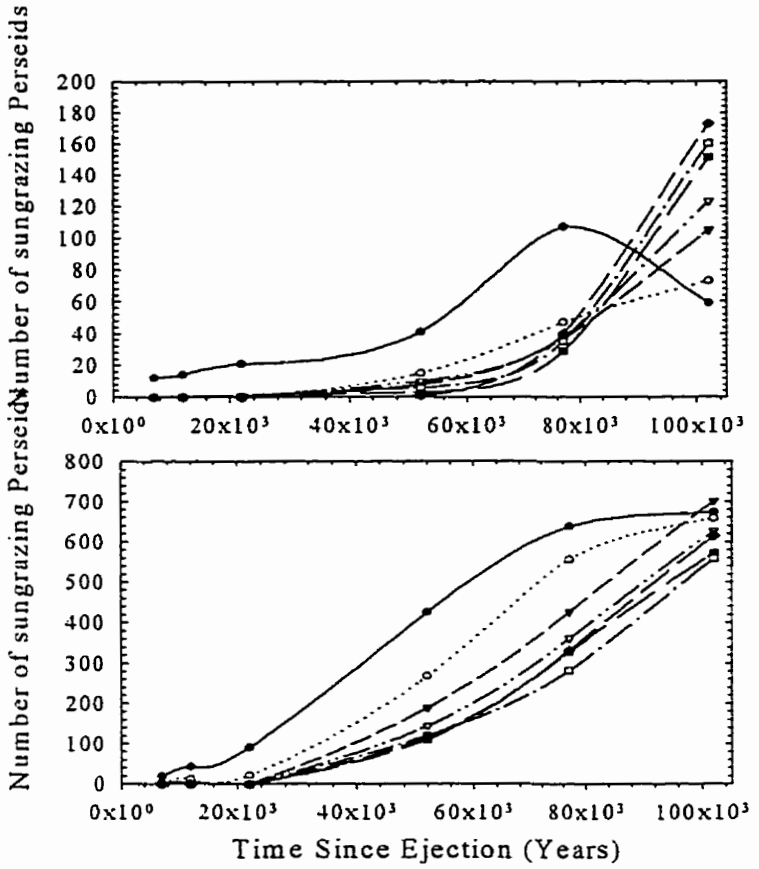

Fig 4.23: The number of Perseids that enter sungrazing states as a function of time since ejection for orbit #1 (top) and orbit #2 (bottom) for all seven mass categories. Symbols are the same as in Fig 4.21.

The removal rate resulting from entry into a sungrazing state is comparable to this value only for the largest meteoroids. The actual removal time is typically at least several times larger than this lower limit (depending on mass) based on our integrations, with some combinations of initial seed ejection orbit and masses showing loss rates which correspond to survival times almost two orders of magnitude longer than this lower limit.

From all of the above considerations, it is apparent that a Perseid meteoroid can, on average, survive for a minimum of several 10^5 years before being removed by one of these loss mechanisms, thus testifying to the possible great age of the stream, which we suspect is limited only by the capture time of Swift-Tuttle.

4.6 Future Activity of the Perseids

If the modelling results presented here are representative of the true Perseid stream, then some predictions of the time and strength of the activity of the stream for the next several years may serve to validate the model. In Table 4.8 is given the predictions of the peak time and strength for the outburst maximum for the Perseids from 1997-1999. The composition of each of these outburst maxima, in terms of the fraction of encountered meteoroids from the three most significant perihelion passages of Swift-Tuttle, summed over all models, is also presented. If the locations of maximum and levels of activity are found to be in good agreement with observations over the next few years, this will present the opportunity to record Perseid meteoroids whose ejection origin is somewhat constrained and for which precision observations would be most valuable as a result.

Over the longer term, Fig. 4.5 shows that the activity of the Perseids is expected to wax and wane and that the strength of the outburst maximum should be quite variable over the coming years. In particular, a minimum in annual activity from the outburst portion of the stream might be expected circa 2001-2 and a subsequent revival in 2004-2006. The latter increase in activity would be the direct result of the close approach to stream meteoroids by Jupiter early in 2003.

Year	Weighted Location of Maximum (J2000)	Contributing ejection epochs	Estimated ZHR of outburst maximum
1997	139.68 ° ± 0.04°	1479 (0.31) 1079 (0.17) 0826 (0.14)	95 ± 6
1998	139.73° ± 0.05°	1079 (0.20) 0826 (0.14) 1479 (0.11)	111 ± 6
1999	139.76 ° ± 0.05°	1079 (0.18) 0826 (0.16) 0698 (0.13)	115 ± 8

Table 4.8: The times of recent past and future theoretical locations for the peak times of the outburst portion of the Perseid stream and the approximate ZHRs (scaled to the mean average main peak ZHR of 86±1 found in Chapter 3).

4.7 Conclusions

From analyzing the results of the numerical modelling of the stream we may draw several conclusions pertinent to the opening questions presented in the introduction:

(1) The initial ejection conditions (which are typically of order several 10 - 100 m/s for visual-sized Perseids at perihelion for the models used here) play a central role in the final observed distribution of Perseid meteoroids at the Earth over time-scales of order ~5 cometary revolutions. After this interval, the effects of planetary perturbations and radiation forces begin to dominate the subsequent evolution of the stream, an effect manifested in the changing radiant size at present as a function of the time since ejection and by the lack of difference in the relative final activity as seen at Earth due to all the different ejection models from older ejections.

The choice of sun-centred cone angle makes only a marginal difference to the final activity outcomes. Different cone angles produce small changes to the total length of time over which activity occurs in any one year, particularly for recent ejections, with larger

cone angles associated with longer activity. Narrower cones also limit the range of masses of Perseids subsequently accessible to Earth for more recent ejections.

From the model outputs, dust ejected at larger distances from the sun has a very minor effect on the final activity of the stream observed at Earth. The primary reason for this is the assumption of uniform ejection over the allowable range of true anomalies, which automatically concentrates the majority of the ejections close to perihelion. The outlying dust tends to end up on the periphery of the overall nodal longitude distributions (see Fig. 4.11).

The density (and thus the range of β) assumed for the meteoroids have the largest effect on the final distributions. That the evolutionary path is so sensitive to the assumed density of the particles is apparent by the systematic and consistent change in the number of meteoroids observed at Earth within each model as density is changed (cf Table 4.2). In particular, the number of meteoroids encountered increases with increasing assumed density (larger β). The change in density is related to both the ejection velocity and radiation pressure (both values increasing as density decreases for a given mass meteoroid). However, since 109P/Swift-Tuttle's descending node has been outside Earth's orbit for the last 2000 years, all meteoroids destined to encounter the Earth must be perturbed inward. Higher ejection velocities allow some meteoroids to have osculating orbits at ejection with lower nodal radii than the parent comet. One possibility is that this is a result of radiation pressure and differential perturbations moving the meteoroidal nodal points further out from the sun and of these forces being greatest for the lower density particles, as confirmed directly in 4.1. In this case, the effect dominates over the inward nodal motion caused by the initial ejection velocity dispersion. This effect is most noticeable on those large-β meteoroids that are ejected with large velocities along the comet's orbital motion and hence are in even lower energy orbits than the parent comet. Alternatively, the higher ejection velocities may simply spread the nodal "footprint" of the high-β meteoroids over a wider region than for lower-β and lead to lower concentrations everywhere (including near the Earth).

In using observations to constrain the model output, radiant location and orbital element distributions were found to be subject to measurement errors substantially larger

than those intrinsic to the actual physical dispersions predicted by all models investigated. A quantitative assessment of the goodness of fit between the observed and predicted peak flux of the outburst portion of the stream and the location of the outbursts for the years 1989-1996 demonstrated that models 22 and 21 provided the best overall fit respectively. The lowest ejection velocity model (model 1 - distributed production) showed significantly poorer fits to the flux than did the other models for Swift-Tuttle. This suggests that very low ejection velocities of a few m/s to a maximum of a few tens of m/s are not representative of the decay process associated with Swift-Tuttle and that the density of meteoroids associated with the outburst portion of the stream is of the order 100-1000 kg m^{-3}.

At the other extreme, the very high ejection velocities recently proposed to explain the distribution in semi-major axes within the stream by Harris and Hughes (1995) and Williams (1996) are also not consistent with observation. In particular, by using such high ejection velocities (0.6 km/s near perihelion), it was found that the geocentric radiant dispersion from 1862 would be greater than 0.5 degrees. Our results (see Fig 4.6) suggest that "normal" ejection velocities from 1862 would produce radiant dispersions close to 0.1 degrees at present. From our simulations, the Perseid outbursts from 1991-1994 consist primarily of material ejected in 1862. Shiba *et al.* (1993) report photographic observations of the 1991 outburst showing a radiant dispersion of ~0.1 degrees from seven of nine photographed Perseids, while Spurny (1995) reports that the radiant dispersion for the 1993 outburst was 0.3 degrees for the concentrated portion (13 of 19 recorded Perseids) during that outburst. As individual radiant errors have not been incorporated into these measures, each of the observed dispersions represent upper limits with the true dispersions being smaller. As such, the ejection velocities we have employed appear to match the observed radiant sizes well and at the same time rule out the very high (~0.6 km/s at perihelion) ejection velocities proposed elsewhere. This is also consistent with our earlier remarks concerning the inadmissibility of orbital elements for the determination of original ejection velocities using current photographic techniques given the present size of their measurement errors.

(2 and 3) The location of the outburst portion of the Perseid stream has changed position over the last eight years due to a change in the age of the meteoroids found in this portion of the stream during that interval. From the simulation results, the outbursts from 1988-1990 were principally composed of meteoroids ejected in 1610 and 1737, while the 1991-1994 maxima consisted of material released in 1862 and 1610. The most recent outbursts (1995-1996) are from particles released in 1479 and 1079. The progressive relative increase in the solar longitude of the maxima in the years away from 1993 is due to the influence of the older ejections, released from the parent comet at larger nodal longitudes than the comet's current location and were further increased due to secular perturbations.

The high activity from the stream, particularly in the years 1991-1994, is due in part to the return of Swift-Tuttle and the numerous meteoroids in the Perseid stream with very similar periods to the parent comet. This, however, is a necessary but not sufficient condition for the occurrence of the outbursts. An impulsive change inwards of the nodal radius of the youngest portion of the stream due to a close approach to the stream orbit by Jupiter in 1991 was the additional condition sufficient to ensure that significantly enhanced activity from the shower occurred. This also explains the sudden onset in 1991; prior to this time meteoroids from 1862 were generally outside Earth's orbit and inaccessible to it as a result.

The discrepancy in the observed times of peak nearest Swift-Tuttle's perihelion passage (particularly in 1993 and 1994) could be due to a strong asymmetry in dust production during the 1862 passage of Swift-Tuttle. In particular, observations from that epoch indicate a strong tendency for ejections to have a large component of their total velocity in the positive normal direction relative to Swift-Tuttle's orbit. This tends to produce activity at Earth in the present epoch with larger nodal longitudes than the parent comet and may explain the difference between the (earlier) model predicted peak times and those observed nearest Swift-Tuttle's return when ejecta from 1862 predominated.

Our results also suggest that some smaller levels of "outburst" activity from the stream should have been visible well before the return of Swift-Tuttle as a result of the direct perturbations from Jupiter and Saturn. That no definitive visual observations of

prior outbursts of the stream exist may be due to the fact that the first global synthesis of large numbers of visual observations of the stream did not occur until 1988. Thus the appearance of an early maximum in that year may not be intrinsic to the stream but only to the scrutiny with which it was observed. Indeed, Lindblad and Porubcan (1994) investigated the solar longitude distribution of previous photographically observed Perseids and concluded that the present outburst maximum was detectable as early as 1950. It is interesting to note further that on the basis of the present simulations we expect that some enhanced activity associated with the outburst portion of the stream should have been most apparent in the years around 1921, 1933, 1945, 1951, 1957, 1969, and 1980 with the maxima in 1921, 1945, 1957 and 1980 most prominent. Kronk (1988) lists the years 1920, 1931, 1945 and 1976-1983 as unusual for their reportedly high activity. Given the vagaries of moonlight and sparse observer distributions in these periods, there appears to be a remarkable concordance between the two lists. It is particularly noteworthy that several other studies of the 1980 Perseid return, in particular, suggest enhanced activity, such as that of Russell (1990) who suggested on the basis of his photographic observations that the 1980 Perseids may have been particularly prone to fragmentation and therefore of recent origin. Simek (1987) summarized nearly 30 years of radar observations of the Perseids and found that the 1980 return was the strongest recorded from 1958-1985 (with all the years from 1962-1972 having no observations), while Bel'kovich *et al.* (1995) determined that the returns from 1980-1982 were the strongest as recorded visually over the interval 1972-1990 from the former Soviet Union.

(4) From comparison of the radiant size of the Perseid stream and our model estimates of the change in radiant dispersion with age, the photographic-sized meteoroids in the main core of the stream are approximately 40 000 years old. Using the rate of change in the apparent location of the maximum, a lower limit of 11 000 years is obtained for the core of the stream. Similarly, using the width of the ZHR profile of the stream compared to the theoretical estimates yields another lower limit estimate for the central portion of the stream of 14 000 years. The photographic radiant locations at maximum are reproduced in the modelling with ejections 15-20 000 years of age. These estimates, along

with their errors as given in Sect 4.4, are most consistent with a core population of Perseids having mean ages of order $(25 \pm 10) \times 10^3$ years. It is instructive to note that from the long-term integrations of the parent comet in Sect. 4.3, the most probable evolutionary paths for Swift-Tuttle all have nodal distances less than 0.1 A.U. from the Earth over the last 20 000 years; we would suggest that it is the dynamics of Swift-Tuttle's orbit over the last 20-30 millennia which control the highest activity portion of the stream presently visible at Earth.

The long duration of the Perseid shower indicates that the total age of the stream is much older. Our integrations show that some activity from the shower may be detectable at Earth for a significant portion of the entire year if the shower is as young as 10^5 years. The currently accepted duration of the shower of 40-45 days implies a lower limit for the age of the stream of order 10^5 years. It is not possible to be more precise given the uncertainties in the total length of time activity of the stream is visible at Earth and the precise evolutionary path followed by Swift-Tuttle.

A portion of our integrations suggests that, given enough time, some Perseid meteoroids may begin encountering the Earth at their ascending nodes in mid-March. Several candidate showers which are documented, but whose orbital elements are poorly known, have been identified. The existence of such a shower and positive association with Swift-Tuttle would imply a stream age of at least 50 000 - 75 000 years.

(5) We find that the current nodal progression rate of the stream (averaged over all models and masses for the last 2000 years) is $(2.2 \pm 0.2) \times 10^{-4}$ degrees/year. This is in good agreement with the observed rate of change of the location of the peak of the shower in historical times found by Hughes and Emerson (1982) of $(3.8 \pm 2.7) \times 10^{-4}$ degrees/annum.

(6) The Earth has a minor effect on the long-term evolution of the stream. In general terms we have found that the Earth contributes approximately ~10% to the total nodal dispersion of the stream and increases the radiant dispersion by a similar amount over time scales of order many thousands - tens of thousands of years. The Earth's scattering effect

on the stream is also visible in the rms spreads in the orbital elements (a,i,ω), with the rms scatter becoming smaller in these elements when the Earth is removed. The effect is apparent, but far from dominant, in these orbital element dispersions with small number statistics becoming increasingly important for the oldest ejections. The Earth plays no perceptible role in moving Perseids into hyperbolic orbits, but may play some role in shepherding Perseids into sungrazing states.

(7) Two dynamical effects remove Perseids from the stream: hyperbolic ejection due to Jupiter (and to a lesser degree Saturn) and entry into sungrazing states. The relative importance and absolute amount of loss due to these mechanisms depends on the precise evolutionary path assumed for Swift-Tuttle and also varies by mass. The smallest Perseids tend to be preferentially removed first due to their lower average orbital energies. The rate of removal varied dramatically between the two assumed seed orbits (and by mass) with as many as 35% of the initial Perseid population hyperbolically ejected after 10^5 years for small meteoroids using seed orbit #2 while seed orbit #1 produced a loss rate of 1% over the same interval. Typically it required 40 000-80 000 years before any significant number (>0.1% of the initial population) was removed due to either of these two effects, but the actual number varied significantly from case to case.

(8) The delivery of Perseid meteoroids into Earth-intersecting orbits is principally controlled by the evolutionary path of the parent comet. The closest approach distance between the osculating orbit of Swift-Tuttle at the time of release of the meteoroids and the number of Perseids visible at the present time is strongly correlated over the last 2000 years. Over the longer term, the assumed starting orbit for the initial ejections critically influences the subsequent development and activity of the shower as seen from Earth. In the short term, impulsive perturbations due to Jupiter and Saturn control the magnitude of the outburst component of the stream and thus the amount of relatively "fresh" Perseid material visible at the Earth.

References

Babadzhanov, P. 1993. Densities of Meteoroids. In *Meteoroids and their Parent Bodies*. (J. Stohl and I.P. Williams), pp. 295-302. Astronomical Inst. Slovak Acad. Sci., Bratislava.

Bailey, M.E., J.E. Chambers and G. Hahn 1992. Origin of sungrazers - A frequent cometary end-state. *A&A* **257**, 315-322.

Bel'kovich, O.I., A.I. Grishchenyuk, M.G. Ishmukhametova, S. Levin, A..S. Levina, V.V. Martynenko, N.I. Suleimanov, V. Yaremchuk 1995. The Structure of the Perseid Meteoric Stream from Visual Observations during 1972 - 1993. *Solar System Research* **29**, 473-477.

Boehnhardt, H., K. Birkle and M. Osterloh 1996. Nucleus and Tail studies of Comet P/Swift-Tuttle. *EMP* **73**, 51-70.

Burns, J.A., P.L. Lamy and S. Soter 1979. Radiation forces on small particles in the solar system, *Icarus* **40**, 1-48.

Brown, P., and J. Rendtel 1996. The Perseid Meteoroid Stream: Characterization of recent activity from Visual Observations. *Icarus* **124**, 414-428.

Ceplecha, Z. 1996. Luminous efficiency based on photographic observations of the Lost City fireball and implications for the influx of interplanetary bodies onto Earth. *A&A* **11**, 329-332.

Ceplecha, Z. 1988. Earth's influx of different populations of sporadic meteoroids from photographic and television data. *BAC* **39**, 221-236.

Ceplecha, Z., P. Spurny, J. Borovicka, and J. Keclikova 1993. Atmospheric fragmentation of meteoroids. *A&A* **279**, 615-626.

Chambers, J.E. 1995. The long term dynamical evolution of comet Swift-Tuttle. *Icarus* **114**, 372-386.

Combi, M.R 1989. The outflow speed of the coma of Halley's comet. *Icarus* **81**, 41-50.

Crifo, J.F 1995. A general physicochemical model of the inner coma of active comets. I: Implications of spatially distributed gas and dust production. *ApJ* **445**, 470-488.

Everhart, E 1985. An efficient integrator that uses Gauss-Radau spacing. In *Proceedings of IA.U. Colloquium No. 83: Dynamics of Comets: Their Origin and Evolution* (A. Carusi and G. Valsecchi, Eds.), pp.185. Reidel, Doredrecht.

Festou, M.C., H. Rickman and R.M. West 1993. Comets. 2: Models, evolution, origin and outlook. *A&ARev* **5**, 37-163.

Fomenkova, M.N., B. Jones, R. Pina, R. Puetter, J. Sarmecanic, R. Gehra and T. Jones 1995. Mid-Infrared Observations of the nucleus and dust of comet P/Swift-Tuttle. *AJ* **110**, 1866-1874.

Guigay, M. 1947. Reserches sur la constitution du courant d'etoiles filantes des Perseides, J. Observateurs. *Comptes Rendus* **30**, 33-48.

Guth, V. 1947. On the Periodicity of the Lyrids. *BAC* **1**, 1-4.

Gustafson, B.A.S. 1989. Comet Ejection and Dynamics of Nonspherical dust Particles and meteoroids. *Ap.J.* **337**, 945-949.

Greenberg R., A. Carusi and G.B. Valsecchi 1988. Outcomes of planetary close encounters: A systematic comparison of methodologies. *Icarus* **75**, 1-29.

Hamid, S.E. 1951. The formation and Evolution of the Perseid meteor stream. *AJ* **56**, 126-127.

Harris, N.W. and D.W. Hughes 1995. Perseid meteoroids - the relationship between mass and orbital semimajor axis. *Mon. Not. R. Astron. Soc.* **273**, 992-998.

Harris, N.W., K.C.C. Yau and D.W. Hughes. 1995. The true extent of the nodal distribution of the Perseid meteoroid stream. *Mon. Not. R. Astron. Soc.* **273**, 999-1015.

Hasegawa, I. 1993. Historical records of meteor showers. In *Meteoroids and their Parent Bodies*. (J. Stohl and I.P. Williams) pp. 209-227. Astronomical Inst. Slovak Acad. Sci., Bratislava.

Herrick, E.C. 1838. On the Shooting Stars of August 9th and 10th 1837 and on the Probability of the Annual Occurrence of a Meteoric Shower in August. *American Journal of Science* **33**, 176-180.

Hughes, D.W. and B. Emerson 1982. The stability of the node of the Perseid meteor stream. *The Obs.* **102**, 39-42.

Hughes, D.W. and N. McBride 1989. The mass of meteoroid streams. *Mon. Not. R. Astron. Soc.* **240**, 73-79.

Hughes, D.W. 1995. The Perseid meteor shower. *EMP* **68**, 31-70.

Jacchia, L. and F.L. Whipple, 1961. Precision orbits of 413 Photographic Meteors. *Smith. Contr. Astrophys.* **4**, 97-129.

Jenniskens, P. 1994. Meteor Stream Activity I: The annual streams. *A&A* **287**, 990-1013.

Jenniskens, P. 1997. Meteor Stream Activity IV: Meteor outbursts and the reflex motion of the sun. *A&A* **317**, 953-961.

Jones, J 1985. The structure of the Geminid meteor stream. I - The effect of planetary perturbations. *Mon. Not. R. Astron. Soc.* **217**, 523-532.

Jones, J. 1995. The ejection of meteoroids from comets. *Mon. Not. R. Astron. Soc.* **275**, 773-780.

Jones, J. and P. Brown 1996. Modelling the orbital evolution of the Perseid meteoroids. In *Proceedings of IA.U. Colloquium 150: Physics, Chemistry and Dynamics of Interplanetary Dust*. (B.A.S. Gustafson and M. Hanner, Eds.), pp. 105-108, Astronomical Society of the Pacific, San Francisco.

Katasev, L.A. and N.V. Kulikova 1975, Origin and Evolution of the Perseid meteor stream. *Solar System Research* **9**, 136-141.

Koschack, R., and R.L. Hawkes 1993. Observations during exceptionally high activity. *WGN J.IMO* **21**, 92-95.

Koschack, R., and R.L. Hawkes 1995. Observing instructions for Major Meteor Showers. In *Handbook for Visual Meteor Observers*. (J. Rendtel, R. Arlt, A. McBeath, Eds.)pp. 42-74, International Meteor Orgnanization, Potsdam.

Koschack, R., and P. Roggemans 1991a. The 1989 Perseid Meteor Stream. *WGN J. IMO* **19**, 87-99.

Kresak, L. 1957. On the collisional hypothesis of the origin of the Perseid meteor stream. *Contr. Skalnate. Pleso* **2**, 7-19.

Kresakova, M. 1974. On the accuracy of semimajor axes of meteor orbits, *BAC* **25**, 191-98.

Kresak, L. 1976. Orbital evolution of the dust streams released from comets, *BAC* **27**, 35-46.

Kresak, L. 1992. On the ejection and dispersion velocities of meteor particles. *Contr. Skalnate. Pleso* **22**, 123-130.

Kresak L. and V. Porubcan 1970. The dispersion of meteors in meteor streams I. The size of the radiant areas. *BAC* **21**, 153-170.

Kresakova, M. 1966. The Magnitude Distribution of Meteors in Meteor Streams. *Contr. Skalnate. Pleso* **3**, 75-109.

Kronk, G. W. 1988. *Meteor Showers: A descriptive Catalog*. Enslow Publishers Inc., New Jersey.

Lindblad, B.A. 1991. The IA.U. meteor data center in Lund. In *Origin and Evolution of Interplanetary Dust*, (A.C. Levasseur-Regourd and H. Hasegawa, Eds.), pp.311-315, Kluwer Academic Publishers, Dordrecht.

Lindblad, B.A. and V. Porubcan 1994. The activity and orbit of the Perseid meteor stream. *Planet. Sp. Sci.* **42**, 117-123.

Lindblad, B.A. and V. Porubcan 1995. Radiant Ephemeris and Radiant Area of the Perseid meteoroid stream. *EMP* **68**, 409-418.

Levison, H.F. and M.J. Duncan 1994. The Long-Term Dynamical Behavior of Short-Period comets. *Icarus* **108**, 18-36.

Marsden, B.G. 1973. The next return of the comet of the Perseid meteors. *AJ* **78**, 654-662.

Marsden, B.G., G.V. Williams, G.W. Kronk, and W.G. Waddington 1993. Update on Comet Swift-Tuttle. *Icarus* **105**, 420-426.

McDonnell, J.A.M. and 9 colleagues 1987. The dust distribution within the inner coma of comet P/Halley 1982i - Encounter by Giotto's impact detectors. *A&A*, **187**, 719-741.

McKinley, D.W.R. 1961. *Meteor Science and Engineering*, McGraw-Hill, Toronto.

Nakamura, R., Y. Kitada and T. Mukai 1994. Gas Drag forces on fractal aggregates. *PSS* **42**, 721-726.

O'Ceallaigh, D.P., A. Fitzsimmons and I.P. Williams 1995. CCD Photometry of comet 109P/Swift-Tuttle. *A&A* **297**, L17-L20.

Olivier, C.P. 1925. *Meteors*, Williams and Wilkens, Baltimore.

Porubcan, V 1973. The telescopic radiant areas of the Perseids and Orionids. *BAC* **24**, 1-8.

Porubcan, V 1977. Dispersion of orbital elements within the Perseid meteor stream. *BAC* **8**, 257-266.

Press, W.H., B.P. Flannery and S.A. Teukolsky 1986. *Numerical recipes. The art of scientific computing*, Cambridge University Press, Cambridge.

Rendtel, J. and R. Arlt 1996. Perseids 1995 and 1996 - An Analysis of Global Data. *WGN J IMO* **24**, 141-147.

Rendtel, J., R. Arlt and A. McBeath 1995. *Handbook for Visual Meteor Observers.* International Meteor Organization, Potsdam.

Rickman, H 1986. Masses and densities of comets Halley and Kopf. In *Proceedings ESA Workshop: Comet Nucleus Sample Return SP-249*, pp.195, ESA, Canterbury.

Roy, A.E 1978. *Orbital Motion*, Adam Hilger, Bristol.

Russell, J.A. 1990. Dissimilarities in Perseid meteoroids. *Meteoritics* **25**, 177-180.

Sagdeev, R.Z., J. Kissel, E.N. Evlanov, L.M. Mukhin, B.V. Zubkov, O.F. Prilutskii, and M.N. Fomenkova 1987. Elemental composition of the dust component of Halley's comet: Preliminary analysis. In *Proceedings 20th ESLAB Symposium on the exploration of Halleys comet ESA SP-250*(B. Battrick, E.J. Rolfe, and R. Reinhard, Eds.), pp.349-352., ESA, Heidelberg.

Schiaparelli, G.V. 1867. Sur les Etoiles Filantes, et specialement sur l'identification der Orbites des Essaims d'Aout et de Novembre avec celles des Cometes de 1862 et de 1866. *Comptes Rendus* **64**, 598-599.

Sekanina, Z. 1974. Meteoric Storms and the formation of meteor stream. In *Asteroids, Comets and Meteoric Matter* (C. Cristescu, W.J. Klepczynski and B. Milet, Eds.) pp. 239-267, Scholium International, New York.

Sekanina, Z 1981. Distribution and Activity of Discrete Emission Areas on the nucleus of Periodic Comet Swift-Tuttle. *AJ* **86**, 1741-1773.

Shajn, G 1923. The disturbing action of the Earth on Meteoric showers. *Mon. Not. R. Astron. Soc.* **83**, 341-344.

Shiba, Y., K. Ohtsuka, and J. Watanabe. 1993. Concentrated radiants of the Perseids outburst 1991. In *Meteoroids and their Parent Bodies*. (J. Stohl and I.P. Williams, Eds.), pp. 189-193. Astronomical Inst. Slovak Acad. Sci., Bratislava.

Simek, M 1987. Perseid meteor stream mean profile from radar observations in Czechoslovakia. *BAC* **38**, 1-6.

Southworth, R.B. 1963. Dynamical Evolution of the Perseids and Orionids. *Smith. Contr. Astrophys* 7, 299-303.

Spurny, P. 1995. EN Photographic Perseids. *EMP* **68**, 529-537.

Steel, D.I. 1994. Meteoroid Streams. In *Asteroids, Comets, Meteors 1993* (A. Milani, M. Di Martino and A. Cellino, Eds.), pp. 111-126, Kluwar Academic Publishers, Dordrecht.

Steel, D.I. and W.G. Elford 1986. Collisions in the solar system. III - Meteoroid survival times. *Mon. Not. R. Astron. Soc.* 218, 185-199.

Twining, A.C. 1862. On Meteoric Rings as affected by the Earth. *American Journal of Science* **32**, 244-258.

Verniani, F 1973. An analysis of the Physical Parameters of 5759 faint radio meteors. *JGR* **78**, 8429-8462.

Whipple, F.L. 1980. Rotation and Outburst of Comet P/Schwassman-Wachman 1. *AJ* **85**, 305-313.

Whipple, F.L. and F.W. Wright 1954. Meteor Stream-Widths and Radiant deviations. *Mon. Not. R. Astron. Soc.* **114**, 229-231.

Whipple, F.L. 1951. A comet model II. Physical relations for comets and meteors. *AJ* **113**, 464-474.

Williams, I.P. 1993. The dynamics of meteoroid streams. In *Meteoroids and their Parent Bodies* (J. Stohl and I.P. Williams, Eds.) pp. 31-41, Slovak Academy of Sciences, Bratislava.

Williams, I.P. 1996. What can meteoroid streams tell us about the Ejection velocities of Dust from Comets? *EMP* **72**, 321-326.

Williams, I.P. and Z. Wu 1994. The current Perseid meteor shower. *Mon. Not. R. Astron. Soc.* **269**, 524-528.

Wu, Z. and I.P. Williams 1993. The Perseid meteor shower at the current time. *Mon. Not. R. Astron. Soc.* **264**, 980-990.

Wu, Z. and I.P. Williams 1995. Gaps in the semimajor axes of the Perseid meteors. *Mon. Not. R. Astron. Soc.* **276**, 1017-1023.

Yau, K.C.C., D. Yeomans, and P.R. Weissman 1994. The past and future motion of Comet P/Swift-Tuttle. *Mon. Not. R. Astron. Soc.* **266**, 303-316.

Chapter 5:

Observational Record of the Leonid Meteor Shower[3]

5.1 Introduction

Meteor Science in its modern form was born on the morning of November 13, 1833. It was the great Leonid return of that year which provoked widespread interest in the subject after being observed extensively in North America (Olmsted, 1834). With its unique nature of producing strong showers every 33 years, the Leonid shower is probably the most extensively written-about meteoroid stream. This observational database permits useful constraints to be placed on modern theories of the stream's evolution.

Numerous past works have examined Leonid records both ancient (e.g. Hasegawa 1993) and more modern (e.g. Mason 1995). However, in virtually all of these secondary works, no examination of the original records was attempted and the actual activity profiles, locations of peak activity and other characteristics are ill-defined. Our motivation is to re-examine as many original accounts of the shower contains usable numerical information as possible and determine the characteristics of past showers, independent of the many secondary accounts which appear in the literature, in an effort to better understand the stream's past activity and interpret its basic physical properties. These data will also provide the basis for comparison with the numerical modelling of the stream, which is developed in Chapter 6.

We examine the available original records of the Leonids for modern returns of the shower (here defined to be post-1832). In doing so, we attempt to establish characteristics of the stream near its peak activity, as borne out by the original records, for the years near the passage of 55P/Tempel-Tuttle. We utilize firsthand and original records of the shower for each year to construct activity curves for the shower. Using these data we then estimate the solar

---

[3] A version of this chapter has been published: P. Brown (1999) The Leonid Meteor Shower: Historical Visual Observations, *Icarus*, **138**, 287-308.

longitudes for each return for which significant activity occurred and the approximate time of peak activity.

5.2 Observations of the Leonids

In what follows we present a detailed, though by no means complete, examination of the original accounts associated with the Leonids between 1832 - 1997. The original sources consulted to form the activity profile for each year are given in the figure captions. A brief discussion of shower activity in the years where it is highest is given and mention made of previous errors found in secondary sources. Years not discussed are specifically omitted due to lack of access to the original observational material.

Leonid activity reported in the historical literature is based on visual observations of the shower. From the hundreds of original accounts examined, it became obvious that any attempt to produce a precisely corrected activity curve of similar quality to those derived from modern amateur meteor observations would be entirely impossible and quite misleading. In an effort to quantify what hard data does exist in historical accounts, we performed only three main corrections to the raw reported numbers: a correction for the elevation of the radiant, a correction for the total effective observing time; and (where needed) a correction for the number of observers reporting as a group. The aim of such a minimalist approach to the corrections is to provide a lower limit to the estimate of the zenithal hourly rate (ZHR) of the shower, as well as reducing the propensity for subjective interpretation of the historical shower record. In those rare cases where it is explicitly stated, the fraction of the sky covered by clouds during observations is also included (see Chapter 3 for a detailed account of the methods of reduction for the ZHR).

Recall that the ZHR is the number of meteors from the shower that an average observer would see in one hour of net observing under unobstructed skies with the radiant overhead and the faintest visible naked eye star in the field of view equal to +6.5 (see Eqn. 3.1). The ZHR is not a direct measure of the flux from a shower. However, in those cases where the population index changes very little over the activity period of a shower, the variations in the

ZHR are a good measure of the relative changes in the flux to the effective limit of visual meteor observations (magnitude ~+3 - +4).

None of the historical accounts provides quantitative estimates of the darkness of the sky (LM or limiting magnitude) and very few provide any distinction between sporadic and shower meteors. We are interested in determining the time of peak activity, an estimate of the ZHR at the peak and some indication of intervals where no obvious observations have been made (hence a storm might have gone unnoticed). As well, less precise information, such as the duration of the shower noticeably above the sporadic background and (for storms) the width of the storm producing segment of the stream is useful.

To this end we completely ignore the correction for sky brightness, noting that this is a sensitive function of r and that modern observations almost always produce sky brightness corrections greater than one, i.e. the LM is rarely better than 6.5 for most observations. Making this approximation will generally result in an estimate of the ZHR, which is a lower limit to the true ZHR. In particular, in conditions where large numbers of shower meteors are present, we expect that our estimate for the activity will be a true lower limit, in part due to the omission of the sky brightness correction term and in part due to saturation effects (cf. Koschack et al. 1993). The presence of the moon will also further decrease the visibility of the shower. This is noted qualitatively in the description for each activity profile and developed more in the discussion section.

In addition to ignoring the sky brightness correction, we assume no significant perception corrections. From modern observations, observer perceptions may vary by as much as a factor of ~3 but typically the deviations are much smaller (cf. Koschack et al., 1993; Jenniskens, 1994). Given that we have no precise means to incorporate these effects in the archival data, we leave out perception corrections.

As many older observations are reported as group observations, the correction factors reported by Millman and McKinley (1963) for reducing group observations to that of a single observer are utilized.

By using either minimal or no assumptions in the corrections for historical observations (pre-1988) we are attempting to provide a picture of Leonid activity that is as unbiased as

possible. Note that for more recent observations (1988 - present) detailed estimations of sky brightness by observers are available and these data are incorporated to produce a more accurate ZHR profile.

To help further in interpretation we divide the historical observations into three quality categories: poor, medium and high quality. High quality observations are single observer reports with no cloud and with the radiant higher than 25° at the mid-point of the observation. For conditions where clouds are present but obscure less than 20% of the field of view, or radiant elevations are between 25° and 20°, or for group observations the records are considered medium quality. If two of the foregoing conditions are met for one observation, or for observations with the radiant below 20°, or for group observations which sum all meteors (i.e. multiple count single meteor events) the quality is automatically given as poor. Observations made with extremely small sections of the sky visible (i.e. through windows) or with radiant elevations below 15° are generally rejected outright.

The result of this process is activity curves (during years with little or modest Leonid activity) that are necessarily noisy but still contain enough information for us to conclude what lower limits may be reasonably placed on reported activity from past Leonid returns. Peak ZHRs, their locations (in terms of solar longitude - J2000.0 is used throughout) and other pertinent final information are given in Table 5.1 at the end. Note that we present here only an abbreviated form of the full discussion of each year's activity and concentrate instead on the final results and the most important Leonid returns (relative to the discussions in Chapter 6). A complete account can be found in Brown (1999).

5.3 Modern

The observing circumstances, comet-Earth geometry and details of the returns during each epoch from 1831-1997 are given in Table 5.1 (Section 5.5). For the strongest Leonid returns and those where enough observations of sufficient quality are available we have attempted to construct an activity profile for the stream based on these observations; elsewhere estimates of the peak time and associated rate only are given with appropriate references to the original material. All of this is summarized in Table 5.1.

5.3.1 The 1833 Epoch

The 1833 return has been described in detail by Olmsted (1834) and Twining (1834) where reports from throughout the Eastern and Southern US were collected together with reports from ships at sea. It is clear from the numerous accounts provided by Olmsted that the 1833 shower was quite broad, lasting for at least four and perhaps six hours. The time of maximum is stated by several independent observers to have occurred at approximately 13.4 Nov 1833. This time corresponds to more than an hour before astronomical twilight began over most observing locales in the Eastern US and fully two hours before the onset of civil twilight. Considering that at this time the radiant was still climbing in altitude, it seems likely that this represents the true time of maximum. The only precise numerical value for the 1833 display given by Olmsted (1834) refers to one observer from Boston who observed near 13.45 UT Nov 1833 and recorded 650 meteors in 15 minutes in heavy twilight. The observer further reports that his field of view was confined to less than 10% of the full horizon and that he missed at least 1/3 of the meteors. This yields an interpretation of the ZHR as >38 000 centred about this interval; the maximum rate slightly earlier must have been several times this number under darker skies. Olmsted also notes that this value probably underrepresented the true maximum strength of the storm. Henry (1833) observed the shower from Princeton, New Jersey close to sunrise and noted that, "When first seen by me they were so numerous that 20 might be counted almost at the same instant descending towards the horizon in vertical circles of every azimuth or point of the compass. While the exact meaning of "an instant" is not clear, it seems probable that this term reflects a meteor rate close to 20 per second. He also notes that

a student outside at 9.5 UT (13.4 UT) recorded 1500 meteors "...in the space of a few minutes...". Taken at face value, and assuming a minimum of two minutes for the observation, we have a maximum rate of ~750/minute or ~13 per second in general accord with Henry's own observation. These observations (probably the best numerically available for the peak of the 1833 display) imply peak ZHRs in the range of 50 000 - 70 000, a finding also consistent with interpretation of the observation of 38 000 reported by Olmsted (1834) from Boston almost an hour later, as a lower limit to the peak activity.

The first vestiges of the shower were recorded reliably near 13.3 Nov 1833, while the display continued into daylight over the Eastern US until at least 13.5 Nov 1833. The best estimate of maximum is 13.4 UT Nov 1833 with a peak rate of 60 000. Other sources quote 50 - 150 000 /hour for the peak (Kazimirchak-Polonaskaya et al., 1968; Yeomans, 1981; Kresak 1980) but the basis for these values is not discussed in these works.

In addition to the major storm of 1833, the preceding year also showed unusual Leonid activity. The storm produced in 1832 lasted many hours on the night of November 12/13, 1832 from at least Nov 12.8-Nov 13.3 and was chronicled in South America (Olmsted, 1837), the Middle East (Rada and Stephenson, 1992; Hasegawa, 1997), Western Europe (Olmsted, 1834) and Eastern Europe/Russia as far as 60°E (Sviatsky, 1930; Quetelet, 1839) as well as North America (Arago, 1857). This return is variously mentioned as rich in fireballs and may have been quite intense, taking into account the moon's position near the radiant on November 13, 1832. No Asian records of this storm were made. Several of the accounts mention that unusual numbers of meteors were visible the night before (12 Nov 1832), suggesting a very broad activity maximum of bright meteors. Gautier (1832) reports average hourly rates near 2000 from Switzerland at approximately 13.2 UT November, 1832, the only numerical data available for the 1832 storm.

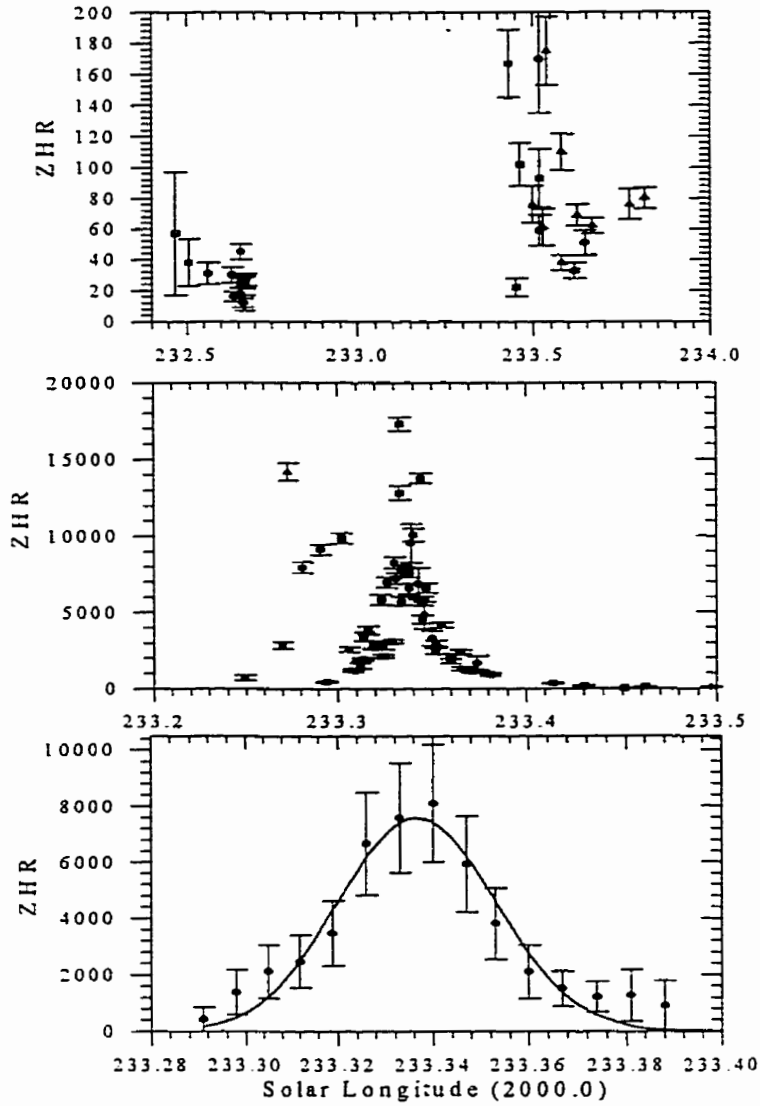

Fig 5.1: ZHR profile for the 1866 Leonid return. Data are taken from accounts given in Malta (Galea, 1994), Smyth (1867), Grant (1867), Main (1867), Newton (1867), De La Rue (1867), Dawes (1867), Hind (1867), and Cooke (1867). The top graph (a) shows the level of broader activity for a day on either side of the storm maximum (b) and (c) is a Gaussian fit (solid line) to the smoothed data in (b) using a smoothing window of 0.02° width shifted by 0.007° (10 minutes) in accordance with the shortest time counts.

5.3.2 The 1866 Epoch

The 1866 epoch was characterized by three strong Leonid returns, with storms occurring in at least 1866 and 1867 and a strong shower in 1868.

The 1866 return was extensively described by observers in England (cf. Herschel, 1867). Fig 5.1a and Fig 5.1b shows the complete activity curve for the 1866 return. The peak in activity occurred at 233.337°, when the ZHR reached a maximum of 8 000 ± 2 000, as computed from numerous 10 minute counts centred about this time interval from the UK. Note that the radiant from the UK was roughly 20° in elevation - hence the large correction factors. However, this possible overcorrection is balanced somewhat by the loss of shower meteors due to saturation effects as the visible rates were near a meteor per second from the UK. Sufficient observations exist near the maximum to perform a running average of the best observations; this is shown in Fig 5.1c. The curve fit is gaussian of the form

$$ZHR = A\left(\frac{1}{\sigma\sqrt{2\pi}}e^{-\frac{[\lambda_O-\lambda_{O\,max}]^2}{2\sigma^2}}\right) \qquad (5.1)$$

where A is a normalization constant, σ is the half-width of the distribution, λ_O is the solar longitude (independent variable) and $\lambda_{O\,max}$ is the location of the maximum. The curve is computed by performing a non-linear regression fit to the original smoothed data (shown as black dots). The result for 1866 is $\sigma = 0.017° \pm 0.002°$ and $\lambda_{O\,max} = 233.337° \pm 0.007°$ (J2000). This implies that to the Gaussian half-width points, the 1866 storm was 25 minutes in duration and peaked at 01:12 ± 0:10 UT on 14 Nov 1866. These results are comparable to those given by Kazimirchak-Polonaskaya et al., 1968 (maximum of 5 - 7 000 at 01:22 UT 14 Nov 1866) and somewhat lower than those found by Jenniskens (1995) (maximum of 17 000 ± 5 000 at 01:00 UT 14 Nov 1866). Yeomans (1981) lists a peak ZHR of ~2000 based on data from Kazimirchak-Polonaskaya et al., 1968 and Olivier (1925), but neither of these two specifically lists hourly rates of 2000 and Olivier lists only an hourly rate of 2800 for two people.

The 1867 shower was hampered by the nearly full moon. Nevertheless, large numbers of observations were made of the storm from Eastern North America. The ZHR profile for the

1867 Leonid storm is shown in Fig 5.2a. The raw observations show a considerable spread nearest the time of maximum, likely a product of the lunar interference. In Fig 5.2b the Gaussian fit to the activity is shown, which yields a maximum time of 233.423°±0.002° with a ZHR of 1200±300 and a half-width of the storm of 0.022°±0.002° or 32 minutes. Note that the ZHR here is a strong lower limit given the lunar interference. From modern observations, a correction of ~4 in the ZHR is typical under these full moon skies, so the true ZHR is most probably in the 4 000 - 5 000 range.

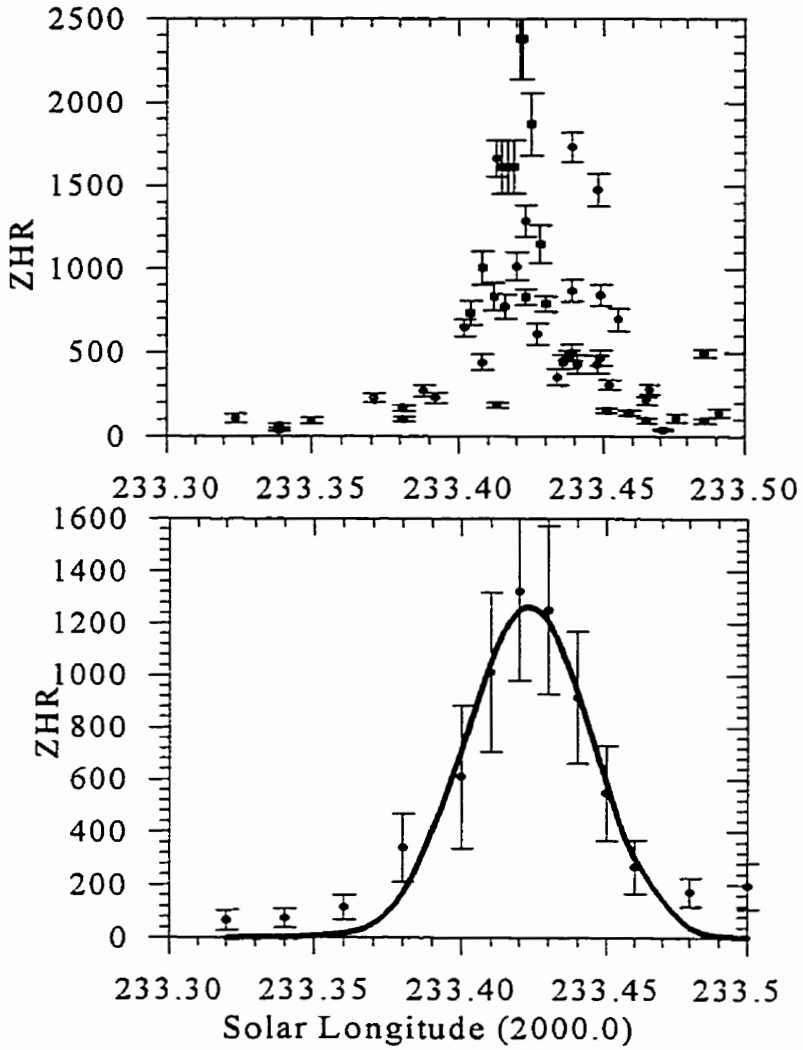

Fig 5.2: ZHR profile for the 1867 Leonid return. Data are from Annals of the Dudley Observatory (1871), Twining (1868), Anon (1871), Leonard (1936) and Stuart (1868). Fig 5.2a (top) shows the activity for the 5 hour period centred about the storm maximum.

Fig 5.2b (bottom) shows the Gaussian fit (solid line) to the smoothed data which are binned in a window of 0.05° shifted by 0.02° before 233.38° and after 233.46° and by 0.02° shifted by 0.01° inside this interval.

Jenniskens (1995) finds a very similar time of maximum at 233.713° (B1950) and a compatible (fully corrected) peak ZHR of 6 000 ± 2 000. Kazimirchak-Polonaskaya et al., (1968) list the peak hourly rate as 2184, based on values given in Olivier (1925), This in turn is derived from a report given in Twining (1868) of observations made in Chicago during the peak of the storm in 1867, where 1529 meteors were seen in 42 minutes. Olivier gives this number without further explanation and this value has subsequently been reported in other secondary sources (e.g. Roggemans, 1989). However, the value refers to the number of meteors seen by 8 - 30 observers (Twining, 1868), and is thus many times the single observer rate. Yeomans (1981) lists peak ZHRs as 5 000 based on data given in Kresak (1980), where a peak time 10 hours earlier than listed here is given, but that source reports no reference as to how either the time or strength is found.

The 1868 return occurred under new moon conditions and was widely reported from Europe and North America. Fig. 5.3 shows the activity profile covering the night of Nov 13 - 14, 1868. This display is unusual in that no clear peak is evident and activity remains significant for many hours. The solid line in Fig 5.3 shows the smoothed activity profile confirming little or no variation in the ZHR over a six hour period. Though considerable spread exists in the observations, it is clear that a very strong shower occurred and lasted for many hours. If any short-lived storm occurred, however, it appears to have been missed; the location of the 1866 and 1867 storms would have been over the Pacific in 1868. The peak ZHR in 1868 is approximately 400 ± 200 near 234.2° ± 0.1°. Jenniskens (1995) finds a ZHR of 700 near 233.122° (B1950) but this is based on only two sets of observations, one from Maclear (1869) and one from Grant (1869). Maclear's observations were made under a dense haze from South Africa with a low radiant and are not used here. The hourly rates reported by Kazimirchak-Polonaskaya et al. (1968) of <1200, Lovell (1954) of 1 000 and Yeomans (1981) of ~1 000 are based on Olivier's (1925) report of Kirkwood observing 900 in 45 minutes in the early morning hours of Nov 14 from Indiana. In fact, Kirkwood's original report (Kirkwood, 1869)

states that the 900 meteors were seen by "...a committee of the senior class", clearly demonstrating that the 900 in 45 minutes was a group observation and that the single observer ZHR number was much lower, consistent with our ZHR values.

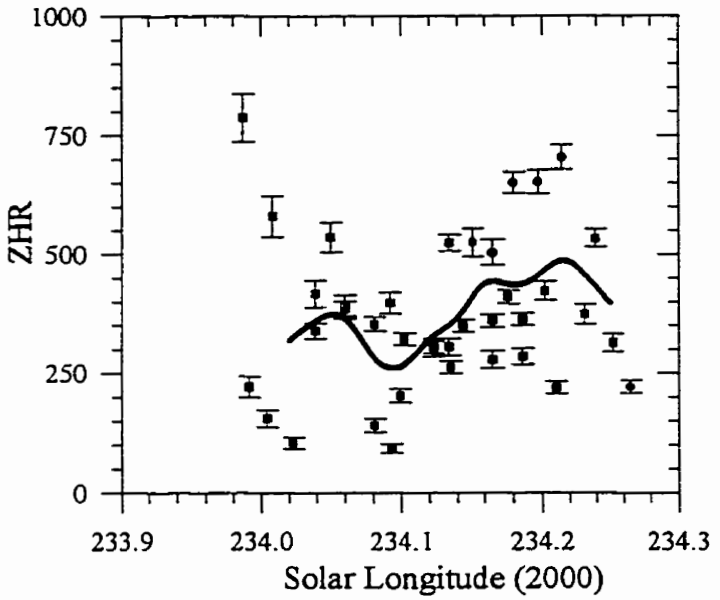

Fig 5.3: ZHR profile for the 1868 Leonid shower. Data are derived from reports in Newton (1869) and Grant (1869). The solid line is a smoothed average of the available observations smoothed over a window of 0.05° shifted by 0.02° from 234°-234.25°.

5.3.3 The 1899 Epoch

Of the showers from 1898-1903, only 1901 and 1903 details signficant activity, with 1898 being a strong shower.

The activity profile for the 1901 shower is shown in Fig. 5.4 and shows the activity profile derived from European and North American observations of the shower in that year. A very clear, consistent rise in activity was reported by observers across Western North America, culminating near dawn on the West coast when ZHRs approached 250. Accounting for sky conditions and saturation effects, which certainly would have been significant at this level of

activity, the peak ZHR in 1901 might well have approached 500 on the basis of these

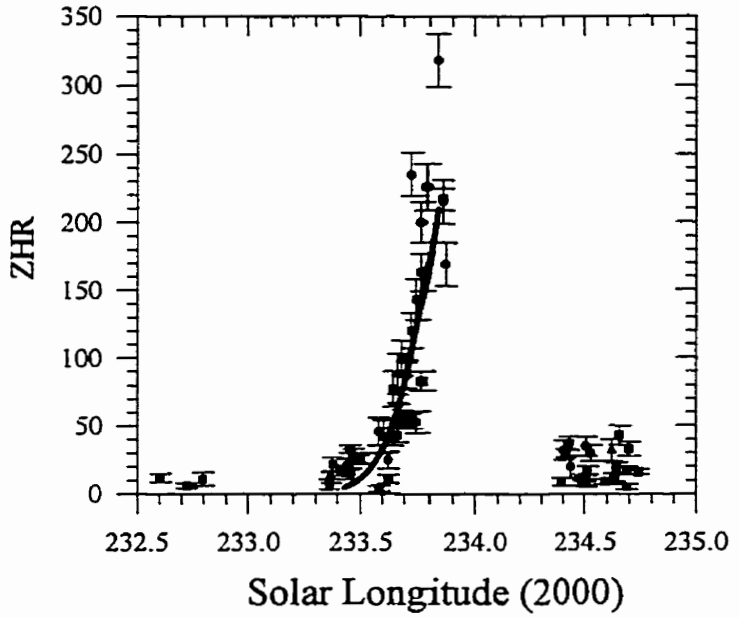

Fig 5.4: ZHR profile for the 1901 Leonid shower. Data are from Payne (1901), King (1902), Upton (1902), Salloms (1902), Dole (1902), Brenke (1902), Leavenworth (1902), Brackett (1902), Denning (1902), and Besley (1902). The solid line represents the ascending portion of the Gaussian fit to the data.

data. The solid line in Fig. 5.4 shows a Gaussian fit to the activity profile. Note that only the rise and (possibly) the peak were observed; the falling portion of the shower occurred unobserved over the Pacific. The location of the peak from available observations is 233.828° ± 0.014° and the half-width of the Gaussian profile is 0.095° ± 0.01°. This implies that the full-width of the strong outburst in 1901 lasted 5-6 hours (only 3 hours of which were actually observed) but never achieved storm levels. Notations in the literature often cite the 1901 Leonid return as a "storm", though no observational evidence for this exists. Kazimirchak-Polonaskaya et al. (1968) list rates of 144,000 per hour in 1901 as seen in the UK, clearly a typographical error which has been further reproduced in Yeomans (1981) and Roggemans (1989). Kazimirchak-Polonaskaya et al. (1968) further note hourly rates of 800 from California in 1901, but this value is derived from observations in Claremont, California which are given

second hand in Pickering (1902) and elsewhere, whereas the original report (Brackett, 1902) lists 717 seen by 4 observers in the final hour. of observation before twilight. The single observer hourly rate is less than 1/3 of this number, consistent with our ZHR values of 250. Jenniskens (1995) lists the 1901 shower as a "storm" with a peak ZHR of 7 000. There is no direct observational evidence for this and we further note that of the four observational sets used in his data, one has an improper time base, having been copied from Denning (1902) where the location for Echo Mountain observatory is mistakenly given as Virginia, when it is in fact in California. The value of 7 000 is calculated assuming a power law fit to the data extrapolated to the ZHR value of 7 000, whereas his individual measured values are no more than 500 as reported. His data are also not as complete as presented here and we suggest that the drop in rates occurring shortly after 233.84° is real. This suggestion is further supported by the reports in Taber (1902) which indicate that no unusual activity was seen in Hawaii, Guam or on steamships in the Pacific on the night of maximum.

The next year of strong activity was 1903 when the Leonid shower returned in full force. The outburst witnessed that year peaked at or slightly after morning twilight in the UK on the morning of Nov 16, where it was widely observed. Observations from North America several hours later show that the outburst had subsided by then and rates were at pre-outburst levels. Nautical twilight in the UK began near 234.05° on 16 November 1903 and this is precisely when rates appear to drop precipitously; clearly the shower ZHR was much higher than the 90 - 100 level calculated from the raw counts in this time period. However, the observations after 234.15° are from North America and represent only one observer (Olivier, 1903). The half-maximum time for the ascending portion of the activity profile is approximately two hours, while the descending portion is indeterminate due to the heavy interference from twilight in the UK (Fig. 5.5). The maximum ZHR is 200 - 250 and, given expected saturation effects and twilight conditions, might well have been as high as 300 - 400. Jenniskens (1995) lists the maximum ZHR in 1903 as 1 400 based solely on the observations from Denning (1904). His data are again extrapolated on the basis of an assumed power-law fit and no actual observational evidence for such high rates exists; to the contrary it appears very unlikely that

ZHRs ever exceeded the level of 400 in 1903 and more probable that they were close to 200 - 300 at maximum.

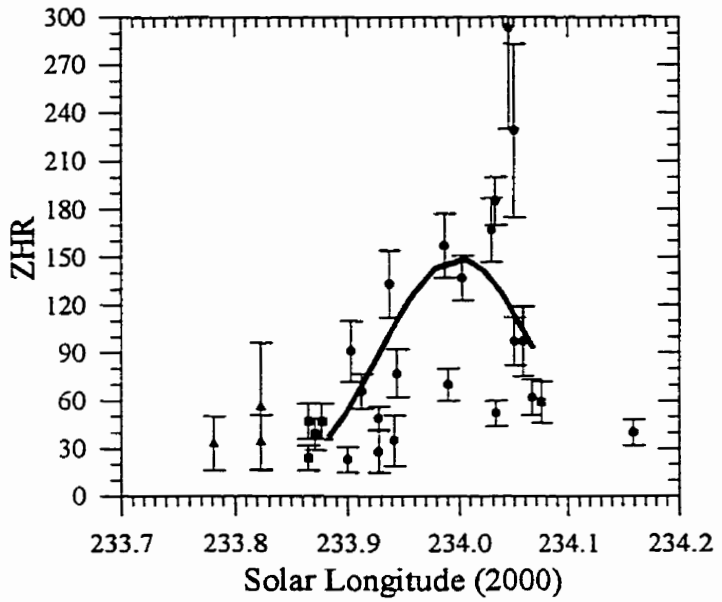

Fig 5.5: ZHR profile for the 1903 Leonid shower. Data are taken from reports contained in Henry (1903), King (1903), Rolston (1903), Young (1904), Rodriques (1904), Denning (1903), (1904), and Besley (1904). The solid line represents the best fit Gaussian to the raw data.

5.3.4 The 1933 Epoch

Clearly heightened activity from the Leonid shower next occurred in 1930. On Nov 17 of that year, observers across North America and the Caribbean reported Leonid rates close to 100/hr with only slight interference from a 26-day old moon. The 1931 Leonid return also produced another modest shower similar to that of 1930, with peak ZHRs at 110 ± 50 based on the average of all counts over the outburst interval, where the counts show nearly constant levels of activity.

The next year, 1932, was widely anticipated as the most probable for the Leonids to produce a meteor storm during the 1933 cycle (Olivier, 1929). Unfortunately, the presence of the moon only four days past full and less than 40° from the radiant, significantly denuded the

display. Strong activity, however, was noted from Europe and North America on 16 November 1932. The peak in activity occurred between 234.4° - 234.7° with an apparent ZHR of ~70 and fell to less than half this value on the days before and after the maximum. The true ZHR is probably 3-4 times this value and, given the typical corrections for lunar interference, is suggestive of an actual peak ZHR in the range of 200 - 300. Lovell (1954), Kazimirchak-Polonaskaya et al. (1968) and Yeomans (1981) list the 1932 return as having produced observed rates of 240/hr, implying true ZHRs in the 500 - 1000 range when the effects of lunar interference are factored in and is the apparent reason 1932 is often listed as a "storm" or "near-storm" of the Leonids. This value is based on secondhand reports in Wylie (1933) of counts made in Dubuque, Iowa. The original report (Theobald, 1933) also notes that the peak rate observed was 240/hr. Further reading, however, shows this to be for six observers; the single observer raw rate was 50 - 70, comparable with the apparent ZHRs we have found. We note that within the 2.5 hour window centred about the nodal crossing of Tempel-Tuttle in 1932 (235.06°) only a single hour of observation (from New Zealand) is available at a relatively low radiant elevation. This does leave open the very real possibility that much higher activity took place in 1932 but was missed over the Pacific.

Both 1933 and 1934 produced only modest Leonid displays (see Table 5.1).

5.3.5 The 1965 Epoch

By the 1965 epoch a general consensus existed that Leonids were no longer able to produce storms. Indeed, McKinley (1961) states that "it is highly improbable that we shall ever again witness the full fury of the Leonid storm". However, in 1966 the largest meteor storm ever recorded was witnessed over Western North America

Lunar conditions in 1966 were ideal, with a new moon occurring on November 12. Observations from 12 - 3 hours prior to the peak of the great 1966 Leonid storm indicate ZHRs of 10-20 (see Fig. 5.6a). Similarly, the ZHR had returned to a level near 20 by 235.5°. The rise toward the storm peak began at approximately 235.02° and ascended rapidly, surpassing the 100 level roughly one hour later at 235.07°. By the end of the next hour, at

235.11°, the ZHR was in excess of 500 and over the next 75 minutes climbed to a peak rate in the vicinity of 75 - 150 000 Leonids/hour (see Fig. 5.6b). The drop from this peak back to a level near 500 took another hour, at which time the final falling portion of the storm went unobserved over the Pacific ocean. It is interesting to note that the full extent of the storm was actually visible only to a few observers in the Central and Western USA and the Soviet arctic who saw the return under near ideal conditions. Observers further East in twilight saw a strong return, but it was only a fraction as intense as for those watching under dark skies: this highlights the high probability that many Leonid storms of the past were undocumented by virtue of poor weather, twilight, the moon and sparse concentrations of observers.

Fitting Eq 5.1 to the full observation set from 235.1° - 235.2° produces a Gaussian fit (shown in Fig. 5.6b) with a maximum at 235.160° ± 0.002°, a peak ZHR of ~115 000 and a FWHM of σ = 0.011° ± 0.001°, corresponding to a total duration of 30 minutes. For comparison, Brown et al. (1997) found from Canadian radar observations of the storm (to a limiting meteor magnitude of +6.8) a total duration using a Gaussian fit of 46 minutes. The longer duration of the shower from the radar data is consistent with the expectation that the storm is wider for smaller Leonid meteoroids which are expected to have a larger nodal spread purely on the basis of higher ejection velocities (cf. Jones, 1995).

The highest rates were reported by Milon (1967) from a group of observers under ideal skies at Kitt Peak in the USA. Other observers in less ideal conditions reported rates 2 - 4 times lower (Ashbrook, 1967). However, given the large numbers of Leonids visible, the very subjective methods of determining the rates at the peak, the wide variation in reported ZHRs (from 45 000 - 160 000) at the peak and the uncertain range of observing conditions from the few observers who reported usable information, it is worth stressing that the actual peak

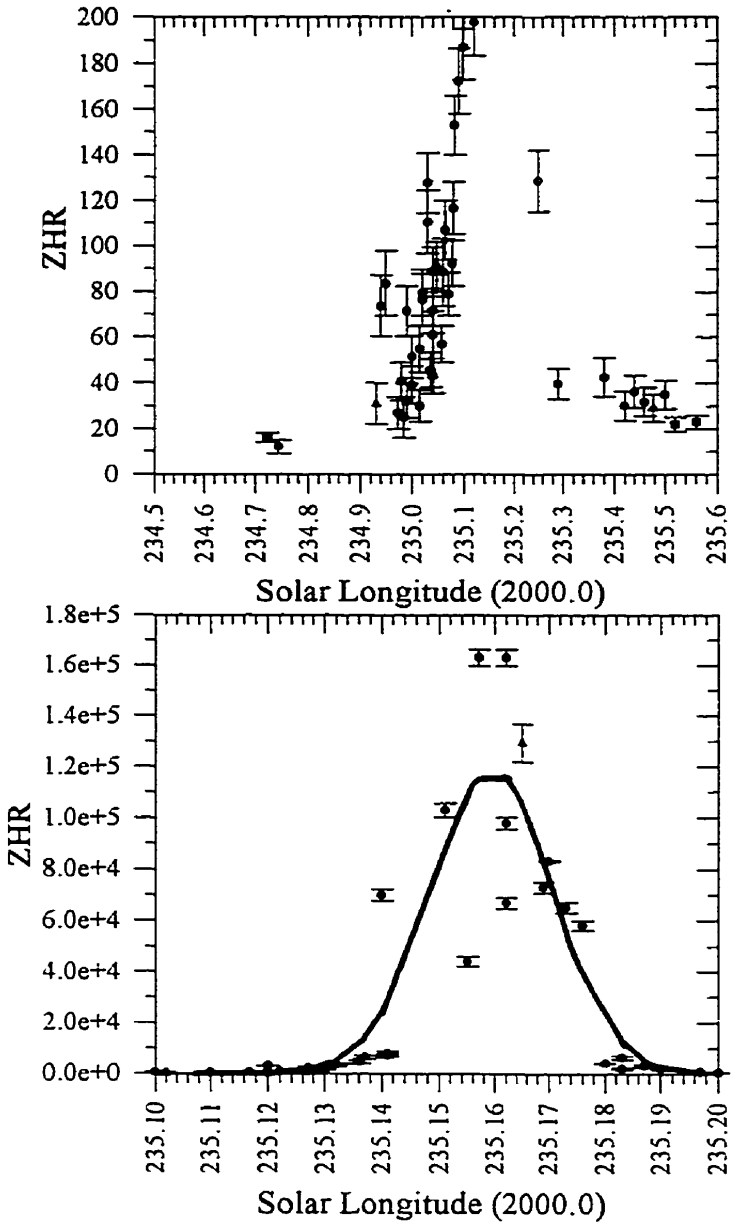

Fig 5.6: ZHR profiles for the 1966 Leonids. Data are from Milon (1966), Milon (1967), Bailey (1966), Ashbrook (1967), Rao et al. (1974), Gingerich (1966), Khotinok (1967), Divinskii (1968) and Terentjeva (1967) for the 24 hours around the storm peak (a - top) ZHR profile for the 1966 Leonids near the time of the peak of the storm (b -bottom) with a Gaussian fit to the raw data.

magnitude of the 1966 as inferred purely from visual data is uncertain to at least a factor of 2; a best guess from all available visual observations would place the peak ZHR of the storm between 75 000 - 100 000. It is instructive to note that the lower limit deduced for the peak flux from radar observations in 1966 by Brown et al. (1997) is equivalent to a minimum peak ZHR of 80 000. There are no visual observations from the peak to support the conclusion of Jenniskens (1995) that actual peak ZHRs never exceeded 15 000 during the storm. The widely quoted peak value of 144 000 (cf. Yeomans, 1981; Kazimirchak-Polonaskaya, 1968) is based largely on the account from Milon (1967) which, within error, is not unrealistic, although it is certainly the highest count made by any group of observers. The 1969 Leonid shower also occurred under good lunar conditions. North American observers reported a distinct, sharp peak in activity near 235.27°, with individual ZHRs as high as 300 (Fig. 5.7a). The Gaussian shape of the outburst is apparent when the data are smoothed as in Fig. 5.7b. The Gaussian shape permits a fit using Eqn 5.1 with a peak at 235.277° ± 0.003°, a maximum ZHR of 210 and a Gaussian width of 0.020° ± 0.003°, corresponding to approximately 1 hour FWHM, about twice as long as the 1966 storm. That the peak occurred so far from the location of the 1966 storm (at which time no enhanced activity was recorded) and the node of the comet suggests a different ejection origin for 1969.

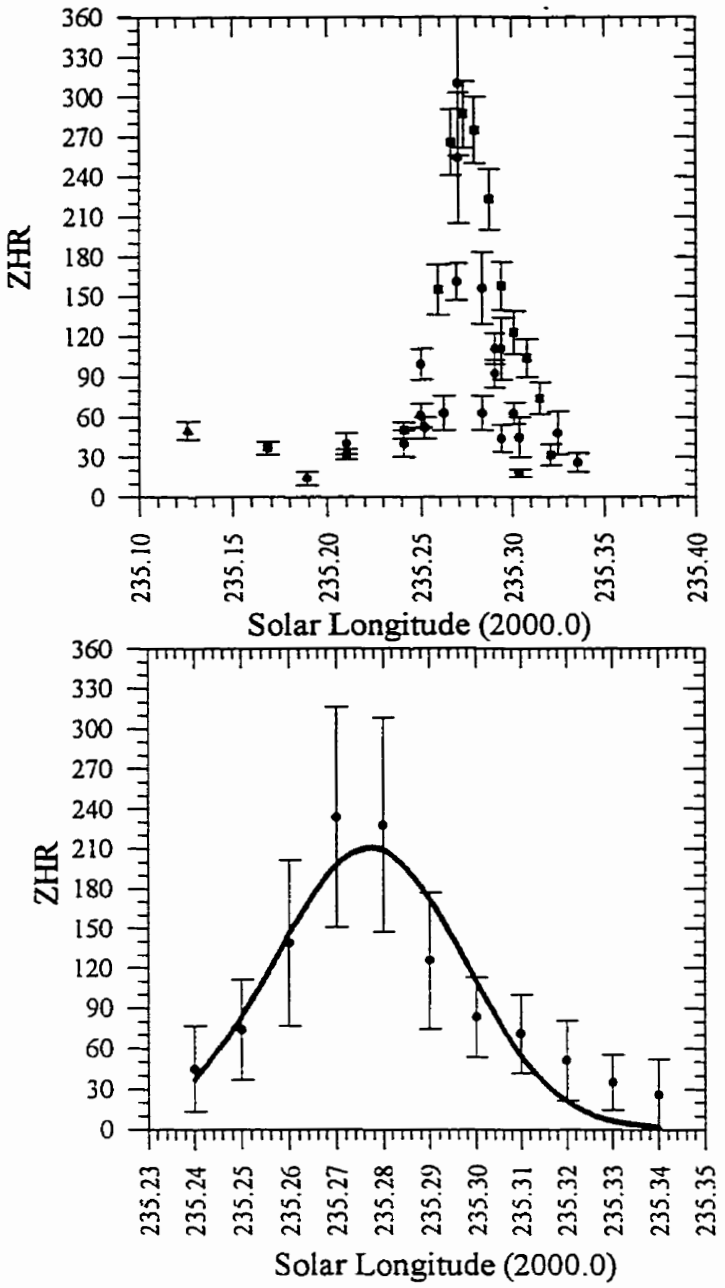

Fig 5.7: (a - top) ZHR profile for the 1969 Leonids. Data are from Robinson (1970) and Millman (1970). In (b - bottom) a gaussian fit to the original data smoothed in 0.02° bins shifted by 0.01° is shown.

5.4 Recent Activity from the Leonids

From 1969 to the present, numerous visual observations of the shower have been made. Unfortunately, most of these have been made with markedly different techniques and reduced in incompatible ways by various scattered amateur groups worldwide. Between 1988 and 1993 a compatible set of visual observations of the shower was obtained on a global scale using the standardized techniques and reduced in a homogeneous manner. As no single year produced more than a few hundred observed Leonids, and no indications of heightened activity were present in any one year, an average profile of the quiet (or clino-Leonids) part of the stream was generated based on six years of visual observations. The data from all years between 1988-1993 were amalgamated to produce the ZHR curve given in Fig. 5.8.

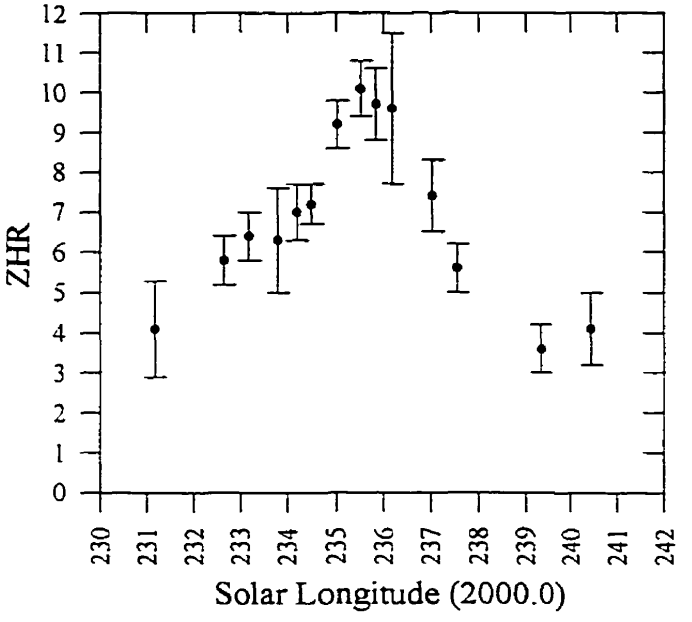

Fig 5.8: Mean ZHR profile for the annual-Leonids averaged from 1988-1994. Data are derived from Brown (1994).

A total of 182 observers contributed 2697 usable Leonid meteors in 1102 observing hours in this period to produce the ZHR-curve. Note that for this curve and for subsequent yearly curves given in Sect 5.4, a fully corrected ZHR is given, i.e. one that corrects for the

limiting stellar magnitude reported by observers (see Eq 3.1) and uses either a mean population index (r) or r-profile for computation of ZHRs. This differs from all previously presented ZHRs and implies that the ZHRs given in this section are more accurate.

As the statistical weight of the sample is still relatively low, we comment only on the apparent time of the maximum which is at 235.5° ± 0.3° (2000.0) with an apparent peak ZHR of ~10. Note that this value is sensitive to the value of r used, which in the present case is 2.0 (cf. Brown 1994). We also note that the background sporadic activity is at a level of about 10 - 15/hr in this figure; hence the annual Leonids reach the level of the sporadic background only for a few hours near the time of maximum.

The first enhanced activity of the current Leonid cycle took place in 1994 (Jenniskens, 1996). The full moon resulted in severe noisiness in the individually corrected ZHRs (cf. Brown, 1995 for the original results) with the peak in 1994 occurring near 235.8°. The overall profile is quite wide, having a full duration to half maximum in ZHR of more than one day. The peak ZHR is uncertain near 100.

In 1996 ideal lunar conditions and heightened observer awareness combined for another record number of visual Leonid observations. Fig. 5.9 shows the smoothed ZHR profile centred about the day of maximum (November 17, 1996). The activity features of note are the clear outburst maximum at 235.17°±0.05° and a smaller local maximum at 235.4°±0.1°. The former had a peak ZHR near 90±25 and the latter a value of 45±5. The early outburst maximum was witnessed primarily by a few European observers, but the coverage was sufficient to establish this as a genuine feature (Brown and Arlt, 1997). The outburst is also associated with an increase in the number of faint Leonids. In addition, the outburst was witnessed in radar observations of the shower (Brown et al., 1998) and to a lesser extent by TV observations. The peak flux from the visual observations corresponds to 0.012±0.004 meteoroids km^{-2} $hour^{-1}$ for Leonids of absolute magnitude +6.5 and brighter. The display showed heightened activity relative to the quiet-time profile for several days on either side of the maximum.

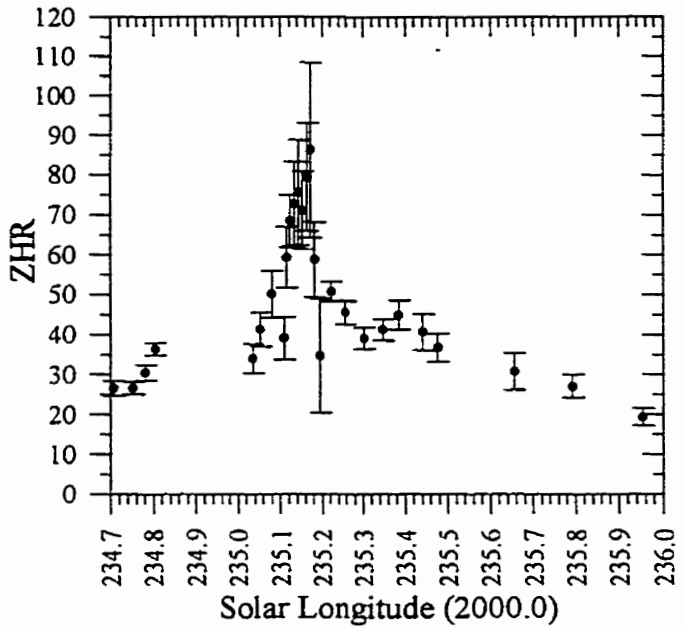

Fig 5.9: ZHR profile for the 1996 Leonids. Derived from Brown and Arlt (1997). Data were smoothed in windows of 0.1° shifted by 0.05° before 235.1° and from 235.2°-235.5° while bins of 0.02° shifted by 0.01° were used from 235.1°-235.2°. The region beyond 235.5° was smoothed in 0.5° intervals shifted by 0.25°

5.5 Discussion

While the results given in Table 5.1 have been computed without resorting to corrections for lunar biases, further examination of the dataset in order to elicit some useful information about the stream requires that some correction be adopted for this strong bias. That the moon significantly affects the observed strength of the stream is obvious from Fig. 5.10, where the Log (Peak ZHR) given in Table 5.1 is plotted versus the age of the moon at the time of the peak of the shower. It is clear that from about 9 - 24 days the trend is toward lower ZHRs, with the strongest displays for which numerical data exist all having been witnessed within a week of the new moon.

Table 5.1: Details of Leonid showers from 1832-present. The Comet Node-$\lambda_{O\,max}$ refers to the difference in time between the observed max and the node crossing. Age of the moon refers to the number of days since new moon at the time of maximum. Min Obs to Node is the closest recorded observation to the nodal passage. The 1998 Observations are preliminary from Arlt (1999). Values with ? are particularly uncertain.

Year	Time of Max (UT) (Nov)	$\lambda_{O\,max}$ J2000.0)	Comet Node - $\lambda_{O\,max}$ (degs.)	Peak ZHR	Activity Width(σ) (degrees) $\times 10^{-2}$	Dur. hours	Age of Moon (days)	Min Obs to Node hours
1832	13.2	233.2	-0.03	2000	-	days?	20	0
1833	13.4	233.15	0.02	60 000	-	~5	1	0
1834	13.25?	232.7	0.47	~60?	-	~7	12	-5
1835	14.8?	234.0	-0.83	~100?	-	-	23	+20
1836	13.3?	233.3	-0.13	100 - 150	-	-	5	+2
1865	13.25?	232.8	0.49	~150	-	-	25	-6
1866	14.05	233.34	-0.05	$8\pm 2\times10^{3}$	1.7±0.2	4	5	0
1867	14.40	233.423	-0.13	$>12\pm3\times10^{2}$	2.2±0.2	>5	17	+1.5
1868	14.40	234.2	-0.91	$4\pm2\times10^{2}$	-	>7	0	+18
1898	15.2	234.3	0.33	50-100	-	~day?	0	-1
1899	15.2	234.0	0.63	20-50	-	~12?	12	+5
1901	15.5	233.828	0.80	250	9.5±0.1	>7	3	0
1903	16.25	234.05	0.58	>200	7.0±0.2	~7	26	-10
1930	17.4	235.3	-0.22	100-140	-	>4?	26	+5
1931	17.35	235.0	0.08	~150	-	~8	7	0
1932	16.25	234.6	0.48	>70	-	>12	18	0
1933	16.4?	234.5	0.58	~50	-	~day	0	-1
1934	17.33	235.2	-0.12	50-60	-	~day	10	+2
1961	-	-	-	~70	-	-	10	-
1963	17.4	234.8	0.33	30	-	>5?	1	+2
1964	17.4	235.6	-0.47	~50	-	24	12	-3
1965	16.6	234.55	0.58	>120	-	~48	23	+1
1966	17.5	235.16	-0.03	$8\text{-}10\times10^{4}$	1.1±0.1	12	5	0
1967	17.5	234.9	0.23	40	-	-	15	0
1968	17.5	235.65	-0.52	~110	-	3	26	+7
1969	17.4	235.28	-0.15	300	2.0±0.3	3	8	0
1994	18.3	235.8	-0.54	~100	-	14	15	0
1995	18.3	235.5	-0.24	35	-	7	25	0
1996	17.2	235.17	0.09	90	-	2	8	0
1997	17.51	235.22	0.06	100	-	3	19	0
1998	17.05	234.5	0.78	250	-	20	28	0

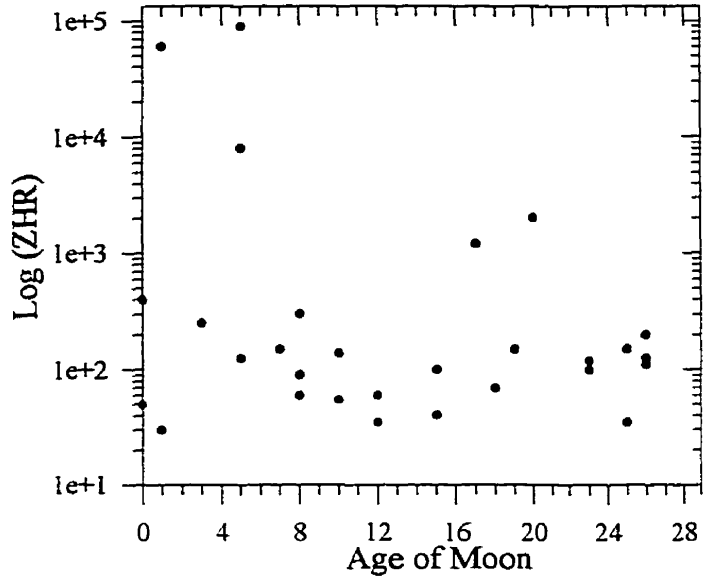

Fig. 5.10: Effect of the moon on activity of the Leonids (from Table 5.1).

From modern visual meteor observations, the difference between the apparent ZHR without sky brightness correction (as utilized here for historical accounts pre-1969) and actual ZHRs, taking into account lunar interference, amounts to approximately a factor of 2 for lunar ages of 9-10 and 24 days after the new moon; a factor of 3 for lunar ages of 11-12 and 22-23 days after new moon; and a factor of 4 for lunar ages at the time of a Leonid maximum from 13-21 days after new moon. In what follows, we have adopted these sets of corrections for pre-1969 observations to generate the most probable maximum ZHR (ZHR_{mp}), independent of the moon.

Of the returns listed in Table 5.1, six had sufficient observations to fit a smoothed profile with Eq 5.1. This allowed estimation of the gaussian width of the profile. This value is plotted against ZHR_{mp} in Fig. 5.11. The trend is toward wider profiles for lower ZHR_{mp}, a reflection of the expected older age of more widely dispersed material (McIntosh, 1973). We note that the fit for five of these six returns is very good; the lack of consistency for the sixth point arises from the 1969 shower which was well observed visually and had a similar profile

from radar records (Porubcan and Stohl, 1992); hence we must conclude that the relationship is only approximate for Leonid returns.

Using the five remaining points, however, a good least-squares fit is obtained such that the Gaussian width of the storm component of the stream and the peak ZHR are related via

$$Log(\sigma) = -0.29 - 0.35Log(ZHR_{pm}) \qquad (5.2)$$

where σ is given in units of degrees of solar longitude. As this dispersion relating to peak activity is likely associated only with the storm component of the stream, the relationship undoubtedly breaks down once ZHR_{pm} is below ~100 when the broader component of activity is dominant.

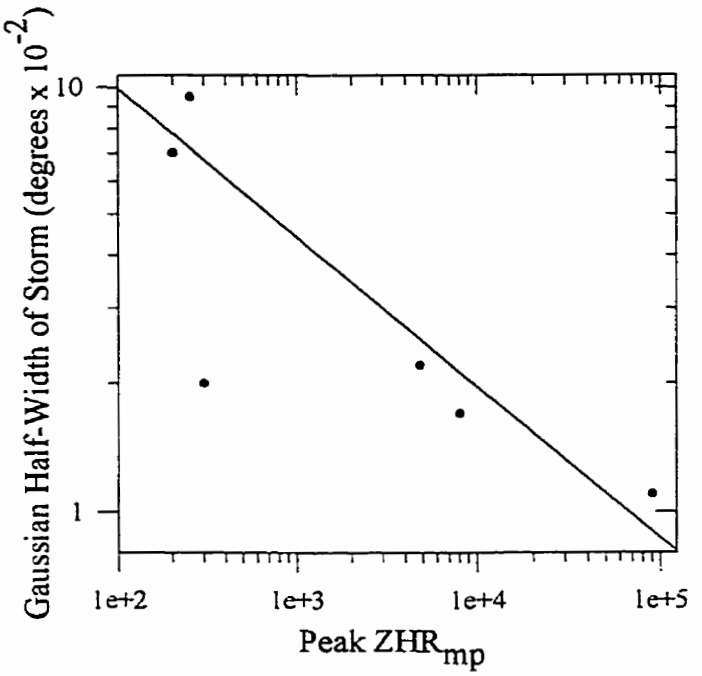

Fig 5.11: Gaussian width of Leonid storms versus most probable ZHR (ZHR_{mp}). Plotted data are from the Leonid returns of 1866, 1867, 1901, 1903, 1966 and 1969.

To determine if this is a reasonable result for the Leonids, we compare these results with those of the IRAS cometary dust trails (Sykes and Walker, 1992). Kresak (1993) has shown that such dust trails are precisely the same phenomenon that produces meteor storms at Earth and thus the width of the two should be similar. If we assume an average mass

distribution of s=2 within the central portion of the Leonid storms, (cf. Brown et al., 1997 for a discussion of this point in connection with the 1966 Leonid storm), and use the relation between ZHR and flux given in Chapter 3, we can translate Eq 5.2 into a relation between width along the Earth's orbit (σ in km) and spatial density (meteoroids per km^3) of Leonids (larger than mass m in kg) as:

$$S = \frac{6.604\ \sigma^{-2.85}}{m} \tag{5.3}$$

where S is the number of meteoroids per km^3 and σ is in km. We assume that the width of the dust trail for 55P/Tempel-Tuttle should be comparable to the average of the short-period comet trails observed by IRAS (found to be 30 000 km at r=1 A.U. (Kresak, 1993), and that the trail is composed primarily of meteoroids 1 mm and larger (10^{-6} kg Leonids) (Sykes et al., 1990). As noted by Kresak (1993), the strongest of the Leonid displays (ZHRs = 100 000) had spatial densities one order of magnitude below the IRAS detection limit. Assuming s=2 holds throughout, a Leonid ZHR of 10^6 (which would just be detectable as a trail in the IRAS survey) corresponds to spatial densities of S=10^{-5} meteoroids (>1 mm) per km^3. This corresponds to a σ of 1.5×10^4 km (using Eq 5.3) which is within a factor of two of the mean value found from the IRAS comet trail survey normalized to r=1 AU. Thus it appears Eq 5.2 and 5.3 are representative of the average relationship between the width and meteoroid spatial density within the dust trail of 55P/Tempel-Tuttle at 1 A.U. and are broadly consistent with the IRAS dust trail findings from similar short-period comets.

Similarly, the difference in the widths of the 1966 storm between radar and visual Leonids is a direct measure of the relative spread in ejection velocities for two different mass regimes within the stream. Using the Jacchia et al. (1967) mass-magnitude-velocity relationship, the limiting magnitude of the radar observations (+6.8) corresponds to Leonids with masses near 10^{-8} kg. The visual observations of the storm were effectively representative of Leonids with magnitudes between +3 and +4; these have masses of 10^{-7} kg. The storm width (in degrees of solar longitude) from radar (Brown et al., 1997) was 0.0156°±0.0008° for a gaussian fit, while a similar procedure applied to the visual observations presented here yields a value of 0.011°±0.001°. From the standard theoretical treatment of meteoroid ejection from

comets through gas-drag (cf. Jones, 1995), the final ejection velocity is expected to vary with particle mass as $v \propto m^{-1/6}$. Thus the average relative difference in the normal components of the ejection velocity for a decade difference in mass is expected to be 68%. That the visually determined width of the 1966 storm is 70% ± 10% of the radar determined value supports the standard gas-drag ejection treatments and is further evidence that the strongest Leonid storms are very young and have durations controlled by initial ejection velocities. That the locations of ejection of the responsible storm meteoroids along 55P/Tempel-Tuttle's orbit are unknown (if any single ejection location on the cometary orbit is actually entirely responsible for the 1966 storm) implies that this information alone is insufficient for a unique solution to the normal component of the ejection velocity question to be found.

Yeomans (1981) was the first to assume explicitly that the strongest shower peaks should occur close to the nodal longitude of the comet. As the closest distance between the comet and Earth increases, it would be expected that orbits of the dust encountered would be the most different from those of the parent comet and hence most likely to have a peak at a longitude different than the comet's nodal longitude.

In Fig. 5.12 we investigate this assertion by plotting the peak ZHR against the difference between the time of nodal passage and the time of observed maximum. There is nearly an even split with as many maxima occurring before the nodal passage as after.

It can be seen that as the peak ZHR_{mp} increases, there is a strong tendency for the shower maxima to occur closer to the nodal longitude of the comet. Intriguingly, most of the strongest showers peak 0.5 - 2 hours after the nodal point of Tempel-Tuttle. While this may be a simple statistical fluctuation related to the small number of points involved, it is worth noting that these five storms have among the best determined locations of peak activity. For returns where the Peak ZHR was at a sub-storm level (<500), there is no clear pattern. This suggests that the major storms are of distinct (probably very young) origin relative to all other Leonid returns. The observed negative lag for the major storms (i.e. peak activity reached after the nodal longitude of the comet), may indicate an asymmetry in dust ejection normal to the cometary orbital plane. The larger nodal longitudes for the storms could indicate that dust

ejection is in the positive normal direction to the cometary orbital plane and of order ten meters per second if ejected near perihelion.

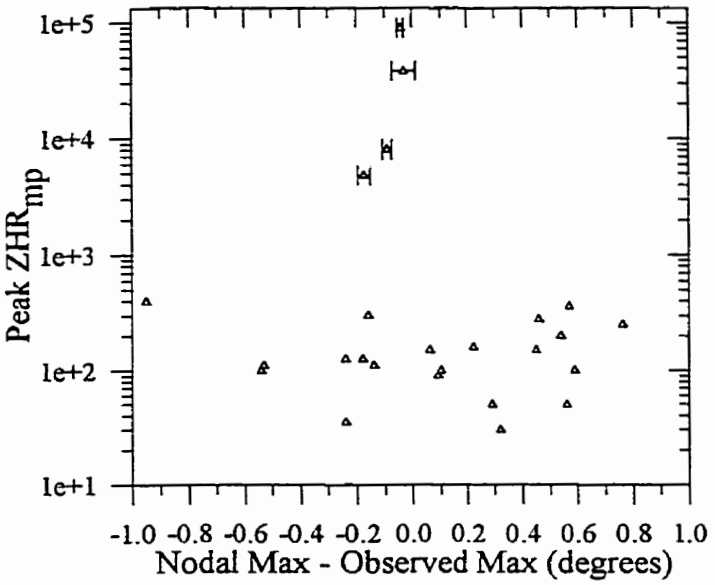

Fig 5.12: The most probable peak ZHR for all years given in Table 5.1 as a function of the difference in time between the observed peak activity and the nodal point of the comet (in degrees).

In an effort to determine the approximate relative distribution of dust about 55P/Tempel-Tuttle, the 30 independent ZHR determinations given in Table 5.1 have been combined with the orbital encounter geometry for each return in Fig. 5.13. Here Log (ZHR) is given in contour form. Note that these data include observations up to 1997. While this contour plot changes somewhat depending on the precise contouring technique applied, the overall shape of the distribution remains constant. As has been noted previously by numerous authors (cf. Yeomans, 1981; Wu and Williams, 1992), our results are consistent with the

greatest dust concentration being spatially outside the comet's orbit and temporally behind it. Note that in the data used here (post 1799) the Earth has only sampled dust from outside the comet's orbit, so from this alone we can say nothing about the concentration inside the comet's orbit (cf. Yeomans, 1981 or Mason, 1995 for a complete discussion of the dust distribution with reference to older showers encountered inside the comet's orbit).

Using these results to forecast activity over the next few years, it appears most probable that a Leonid storm of modest strength is most likely in the year 1999. Peak ZHRs of order 1000 during either of these two years are ostensibly predicted by examination of the overall distributions, but the paucity of datapoints in the region nearest these years suggests these values should be viewed with caution.

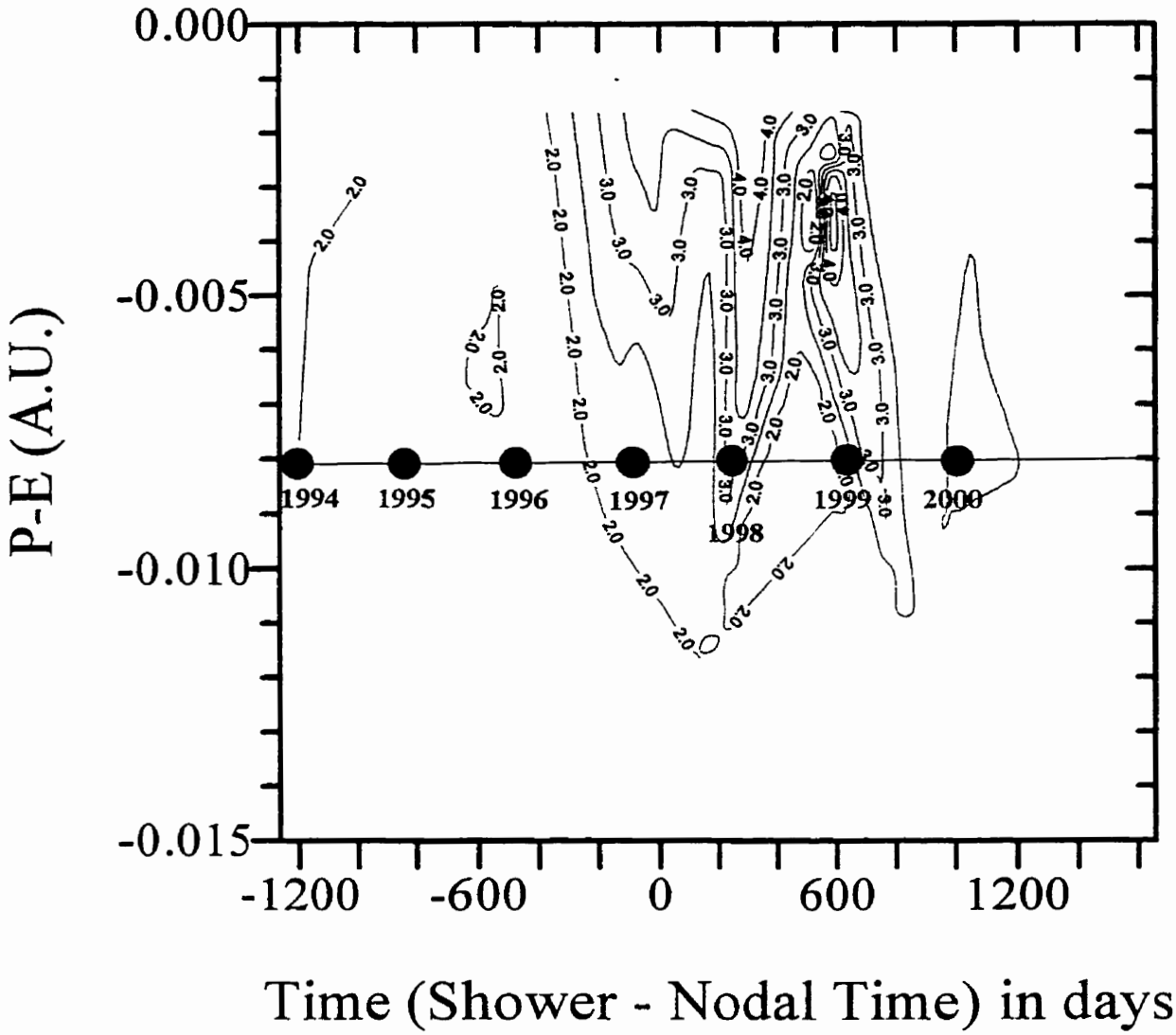

Fig 5.13: Contour distribution of dust density about 55P/Tempel-Tuttle. Contours are in units of Log (ZHR_{mp}). P-E (A.U.) is the closest distance between the cometary orbit (determined at perihelion for a given Leonid epoch) and the Earth's orbit in Astronomical Units. Time on x-axis is a measure of the observed time of the shower (in days) relative to the comet's nodal passage.

5.6 Conclusions

Examination of the original accounts of past Leonid storms has led to a revised list of times and strengths of past Leonid showers for the post-1832 era as summarized in Table 5.1. Based on the observational record alone it is concluded that:

- From the detailed yearly results, it is apparent that the activity of the shower in numerous years as quoted in many secondary sources is in error. The strongest of the Leonid storms show activity near the maximum which is well represented as Gaussian in shape.
- The profiles of the various Leonid returns suggests that there are three distinct components to the Leonid shower, some or all of which may be visible in any one year. A broad annual component which lasts for 3-4 days and barely reaches sporadic levels is almost certainly present every year and is the oldest section of the Leonid shower. In addition to this, a more moderate level of extended activity, often accompanied by brighter Leonids (an extended component), is visible in some (but not all) of the years near the time of Tempel-Tuttle's perihelion passage. This extended component may last up to two days (i.e. 1965) and may produce ZHRs as high as several hundred (i.e. 1868) for many hours. The extended component has been witnessed in every Leonid return from 1994-present. These two distinct components have been previously merged together and termed clino-Leonids.
- The last component is the storm component or ortho-Leonids. This part of the stream is undoubtedly the youngest, is characterized by short, intense activity and is generally present most often in the one or two years immediately following the passage of the comet. It represents the passage of the Earth in or near a dense structure associated with one of the last few returns of Tempel-Tuttle, analogous to IRAS dust trails (cf. Kresak 1993).
- Using the best available data for the duration and strength of five of the ortho-Leonid storms, a relationship between the width of the storm component and the peak spatial density is derived which is broadly consistent with the findings from the IRAS cometary trail survey of comparable short-period comets.
- Differences in the duration of the 1966 storm at two different limiting masses reveal the duration of the storms to be consistent with that expected, based on initial ejection velocities which follow standard gas-drag treatments.

- A possible systematic trend in the location of the peaks of storms after the nodal longitudes of the parent comet may represent an asymmetry in dust production normal to the cometary orbital plane.
- Interpolation of the dust density about 55P/Tempel-Tuttle for the years 1998 - 2000 suggests that a strong 1966-class storm is unlikely, but that ZHRs of order 1000 may be reached in 1999.

References

Arago, D.F.J. 1857. *Astronomie Populaire*, **4**, 181-322.

Ashbrook, J. 1967. Great Leonid Meteor Shower of 1966, *Sky and Telescope*, **33**, 4-10.

Astapovich, I.S. 1967. Observations of the Leonid Meteor Shower 1967 at Kiev, *Astron. Tsirk. No. 453.*

Bailey, D.K. 1966. Some observations from Colorado of the great Leonid Meteor display of 17 Nov. 1966, Millman Collection, NRC, Ottawa.

Barnard, E.E. 1903. The Leonid Meteors at Yerkes Observatory. *Pop. Astron.*, **11**, 580-581.

Besley, W.E. 1902. Meteoric Section, the Leonids 1901, *J.B.A.A.*, **12**, 163-167.

Besley, W.E. 1904. Meteoric Section, the Leonids 1903, *J.B.A.A.*, **14**, 91-95.

Brackett, F. P. 1902. Leonids at Pomona College, Claremont, California., *Pop. Astron.*, **10**, 165-67.

Brenke, W.C. 1902. The Leonids of 1901, *Pop. Astron.*, **10**, 105-106.

Brown, P. 1994. Bulletin 5 of the International Leonid Watch, *WGN J IMO*, **22**, 190-192.

Brown, P. 1995. Bulletin 6 of the International Leonid Watch, *WGN J IMO*, **23**, 178-179.

Brown, P. and Arlt, R. 1997. Bulletin 10 of the International Leonid Watch, *WGN J IMO*, **25**, 210-214.

Brown, P., M. Simek, and J. Jones. 1997. Radar Observations of the Leonids: 1964-1995, *A&A*, **322**, 687-695.

Brown, P. M. Simek, J. Jones, R., R. Arlt, W. K. Hocking and M. Beech, 1998. Observations of the 1996 Leonid meteor shower by radar, visual and video techniques, *Mon. Not. R. Astron. Soc.*, **300**, 244-250.

Cooke, J.P. 1867. November meteors in 1866 in the Sandwich Islands, *Am. J. Sci.*, **43**, 276.

Dawes, W.R. 1867. On the meteoric shower of 1866, November 13-14, *Mon. Not. R. Astron. Soc.*, **27**, 46-48.

De La Rue, W. 1867. Meteors observed at Cranford, November 13th-14th, 1866, *Mon. Not. R. Astron. Soc.*, **27**, 34-39.

Denning, W.F. 1902. Progress of Meteoric Astronomy in 1901. *Mon. Not. R. Astron. Soc.*, **62**, 296-303.

Denning, W.F. 1903. The Leonid shower of 1903. *Nature*, **69**, 57.

Denning, W.F. 1904. The shower of Leonids in 1903. *Mon. Not. R. Astron. Soc.*, **64**, 125-130.

Divinskii, M.L. 1968. Results of Observations on the Leonid Meteor Stream in 1966, *Sol. Sys. Res.* **2**, 51-52.

Dole, R.M. 1902. The Leonids, 1901., *Pop. Astron.*, **10**, 51-53.

Galea, A.J. 1994. Lions, storms and shooting stars, *The Malta Sunday Times*, 13 November, 1994, 54-55.

Gautier, A. 1832. Notice sur les meteores lumineux observes dans la nuit du 12 au 13 novembre, 1832, *Bibliotheque universalle des sciences, belles-lettres et arts*, **51**, 189-207.

Gingerich, O. 1966. Leonid Meteors 1966, *IAUC 1981.*

Grant, R. 1867. Observations of the Meteoric Shower of 1866, November 13-14, made at Glasgow Observatory, *Mon. Not. R. Astron. Soc.*, **27**, 29-31.

Grant, R. 1869. Observations of the Meteoric Shower of November 13-14, 1868 made at the Glasgow Observatory, *Mon. Not. R. Astron. Soc.*, **29**, 60-62.

Hasegawa, I. 1993. Historical records of meteor showers. In *Meteoroids and their Parent Bodies*. (J. Stohl and I.P. Williams) pp. 209-227. Astronomical Inst. Slovak Acad. Sci., Bratislava.

Hasegawa, I. 1997. Early Observations of the Leonids in East Asia, Transactions of the IAU Kyoto (in press).

Henry, J.R. 1903. Leonid meteor shower, 1903. *Nature*, **69**, 80.

Henry, J. 1833. Meteorological Phenomena, Notebook 7171, pages 75-78, Henry Papers, Smithsonian Archives.

Herschel, A.S. 1867. Radiant point of the November Meteors, 1866, *Mon. Not. R. Astron. Soc.*, **27**, 17-18.

Hind, J.R. 1867. The meteoric shower of November 13-14, as witnessed at Mr. Bishop's Observatory, Twickenham, *Mon. Not. R. Astron. Soc.*,**27**, 49-50.

Jacchia, L.G., Verniani, F., and Briggs, R.E. 1967. Analysis of the atmospheric trajectories of 413 precisely reduced photographic meteors, *Smith. Contr. Astro.*, **10**, 1-139.

Jenniskens, P. 1994. Meteor Stream Activity I: The annual streams. *A&A* **287**, 990-1013.

Jenniskens, P. 1995. Meteor Stream Activity II: Meteor Outbursts, *A&A* **295**, 206-235.

Jenniskens, P. 1996. Meteor Stream Activity III: Measurement of the first in a new series of Leonid outburst, *MPS*, **31**, 177-184.

Jones, J. 1995. The ejection of meteoroids from comets. *Mon. Not. R. Astron. Soc.* **275**, 773 - 780.

Kazimirchak-Polonskaja, E.I., Belijaev, N.A., Astapovic, I.S., and A.K. Terentjeva. 1968. Investigation of the perturbed motion of the Leonid meteor stream. In *Physics and Dynamics of Meteors Proceedings of IAU Symp No. 33*, (L. Kresak, and P.M. Millman, Eds.),pp. 449-475, D. Reidel, Dordrecht-Holland.

Khotinok, R.L. 1967. The Leonid Meteor shower of 1966, *Sol. Sys. Res.*, **1**, 62-63.

King, A. 1903. The Leonids of 1903, *Nature*, **69**, 105.

King, T.I. 1902. The November Leonids, 1901, *AJ*, **22**, 68.

Kirkwood, D. 1869. Meteors of November 13-14, 1868, *Mon. Not. R. Astron. Soc.*, **29**, 62-63.

Koschack, R., Arlt, R., and J. Rendtel. 1993. Global analysis of the 1991 and 1992 Perseids. *WGN J IMO*, **21**, 152-168.

Kresak, L. 1980. Sources of Interplanetary Dust. In *Solid Particles in the Solar System*, (I. Halliday and B.A. McIntosh Eds.), pp. 211-222, Reidel, Dordrecht.

Kresak, L. 1993. Cometary dust trails and meteor storms, *A&A*, **279**, 646-660.

Leonard, N.R. 1936. The 1867 Leonid Meteors, *Pop. Astron.*, **42**, 560-563.

Lovell, A.C.B. 1954. *Meteor Astronomy*, Oxford Univ. Press, Clarendon.

Maclear, G.W.H. 1869. On the Meteoric Shower of November, 1868 as seen at the Royal Observatory, Cape of Good Hope, *Mon. Not. R. Astron. Soc.*, **29**, 233-236.

Main, R. 1867. Observations of the Meteoric Shower of November 13-14, 1866, made at the Radcliffe Observatory, Oxford, *Mon. Not. R. Astron. Soc.*, **27**, 39-46

Mason, J.W. 1995. The Leonid meteors and comet 55P/Tempel-Tuttle, *J. Brit. astron. Soc.*, **105**, 219-235.

Millman, P.M. 1970. The Leonids-1969. *J.R.A.S.C.*, **64**, 55-57.

Millman, P.M. and D.W.R. McKinley. 1963. Meteors. *In The Moon, Meteorites and Comets*, (B.M. Middlehurst and G.P. Kuiper, Eds.), pp. 674-764. The University of Chicago Press Chicago.

Milon, D. 1966. Records of visual observation of Kitt Peak meteor team, Millman Collection, NRC, Ottawa.

Milon, D. 1967. Observing the 1966 Leonids, *J.B.A.A.*, **77**, 89-93.

McIntosh, B.A. 1973. Origin and Evolution of recent Leonid meteor shower, In *Evolutionary and Physical Properties of Meteoroids (NASA SP-319)*, (C.L. Hemenway, P.M. Millman and A.F. Cook, Eds.), pp. 193-199, NASA, Washington, D.C.

McKinley, D.W.R. 1961. *Meteor Science and Engineering*, McGraw-Hill, Toronto.

Newton, H.A. 1867. Shooting Stars in November, 1866, *Am. J. Sci.*, **43**, 79-88.

Newton, H.A. 1869. Meteors of November 14th, 1868, *Am. J. Sci.*, **45**, 118-126.

Olmsted, D. 1834. Observations of the Meteors of November 13, 1833. *Am. J. Sci.* **25**, 54-411, **6**, 132-174.

Olmsted, D. 1837. On the meteoric shower of November, 1836, *Am. J. Sci.*. **31**, 391.

Olivier, C.P. 1925. *Meteors*, Williams and Wilkins, Baltimore.

Olivier, C.P. 1903. Leonids at Leander McCormick Observatory, *Pop. Astron.*, **11**, 581.

Olivier, C.P. 1929. Meteor Notes, *Pop. Astron.*, **37**, 53-55.

Payne, W.W. 1901. The Leonids for 1901, *Pop. Astron.*, **9**, 559-563.

Pickering, W.H. 1902. The Leonids. *Pop. Astron.*, **10**, 400-403.

Porubcan, V. and J. Stohl. 1992. Burst of the 1969 Leonids and 1982 Lyrids, In *Asteroids, Comets, Meteors 1991*, (A.W. Harris and E. Bowell, Eds.), pp. 469-472, LPI, Houston.

Quetelet, L.A.J. 1839. Sur les Principles Apparitions d'Etoiles Filantes, *Memoirs de l'academie Royal des Sciences de Bruxelles*, **12**, 3-56.

Rada, W.S. and F.R. Stephenson, 1992. A Catalogue of Meteor Showers in Medieval Arab Chronicles, *Q.J. R. astr. Soc.*, **33**, 5-16.

Rao, M.S., P.V.S.Rama Rao and B. Lokanadham. 1974. The Leonid Meteor Shower Observed over Waltair during 1961-66, *Indian Journal of Radio and Space Physics*, **3**, 360-362.

Robinson, L.J. 1970. November Leonid Meteors Observed, *Sky and Telescope*, **39**, 62-63.

Rodriques, C. 1904. The Leonid shower of 1903, *Nature*, **69**, 521.

Roggemans, P. 1989. *The Handbook for Visual Meteor Observations*, Sky Publishing Corporation, Cambridge, Mass.

Rolston, W.E. 1903. The Late Leonid Meteor Shower, *Nature*, **69**, 127.

Salloms, J. 1902. Meteors at Dunmore, N. W. Territory, British America, *Pop. Astron.*, **10**, 51.

Smyth, P. 1867. On the meteor shower of 1866, November 13-14, *Mon. Not. R. Astron. Soc.*, **27**, 23-27.

Stuart, C. 1868. Meteoric Shower, November 1867, observed in Nassau, Bahamas, *Mon. Not. R. Astron. Soc.*, **28**, 54-56.

Sviatsky, D. 1930. Meteor Showers in Russian Chronicles, *Pop. Astron.*, **38**, 587 - 590.

Sykes, M.V., D.J. Lien and R.G. Walker. 1990. The Tempel 2 Dust Trail, *Icarus*, **86**, 236-247.

Sykes, M.V. and R.G. Walker. 1992. Cometary Dust Trails I. Survey, *Icarus*, **95**, 180-210.

Taber, R.B. 1902. The Leonids of Nov. 1901 from the reports, *Pop. Astron.*, **10**, 403-406.

Terentjeva, A.K. 1967. Observations of the Leonid Meteor Shower in 1967 carried out on board the plane, *Astron. Tsirk. No. 453.*

Theobald, J.A. 1933a. Dubuque Counts of the 1932 Leonids, *Pop. Astron.*, **41**, 56-59.

Twining, A.C. 1834. Investigations respecting the meteors of Nov. 13th, 1833, *Am. J. Sci.*, **26,** 320-352.

Twining, A.C., 1868. Shooting stars on the morning of November 14th, 1867, *Am. J. Sci.*. **45**, 78-92.

Upton, W. 1902. Observations of the Leonids, November, 1901, at Ladd Observatory, *Pop. Astron.*, **10**, 48-50.

Wu, Z. and I.P. Williams. 1992. Formation of the Leonid Meteor Shower and Storm, In *Asteroids, Comets, Meteors 1991*, (A.W. Harris and E. Bowell, Eds.), pp. 661-665, LPI, Houston.

Wylie, C.C. 1933. The Hour of the Leonid Maximum in 1932, *Pop. Astron.*, **41**, 170-171.

Yeomans, D. K. 1981, Comet Tempel-Tuttle and the Leonid Meteors, *Icarus*, **47**, 492-499.

Young, A.S. 1904. Leonid Meteors, *Pop. Astron.*, **12**, 683.

Chapter 6:
Simulation of the Formation and Evolution of the Leonid Meteoroid Stream

6.1. Introduction

The Leonid meteor shower has been visible on Earth for over one thousand years. The earliest records of the shower are replete with descriptions emphasizing the awe and horror with which the earliest of the Leonid meteor storms were received (cf. Hasegawa, 1993). More recently, observations from the 1833 Leonid storm in North America became the catalyst for the modern development of the subject of meteor astronomy.

Detailed observational histories of the shower have been published in many references (cf. Brown, 1999; Littman, 1998; Mason, 1995; Yeomans, 1981). As rich as the history of the observation of the stream has been, the history of the attempts to understand its origin, evolution and ultimately to make predictions about its possible future activity is equally rich. Proof of the complexity of the Leonid meteoroid stream lies in the fact that at the close of the 20th century, when yet another cycle of enhanced Leonid activity is at its peak, predictions regarding its activity are little more precise than a century ago.

Olmsted (1834) was the first to analyze the stream in detail. After witnessing the 1833 storm firsthand, he set about trying to understand the shower and was among the first to note that the stream appeared to radiate from one point in the sky, thus establishing the celestial

nature of the meteors involved. He also estimated the orbit for the stream and made an attempt to determine its periodicity. Olmsted's work was expanded upon by Olbers (1837) who was the first to estimate correctly the stream's period at 34 years and to predict that a return might be expected in 1867. Herrick (1841) was the first to analyze ancient Leonid returns and he arrived at a similar conclusion/estimate.

From the dates of the occurrence of the shower in older records, Newton (1863) suggested that the shower could have several possible periods. He was unable to distinguish between these on the basis of the ancient observations alone but suggested that computation of the rate of advance of the nodes for different orbits could be used in comparison with the nodal advance computed from the historical accounts to arrive at a solution. This was done by Adams (1867) and proved conclusively that the Leonids had an average 33.25 year period. This was the longest of the possible periods arrived at by Newton in his analysis and was identical to the period for the Leonids assumed by Le Verrier (1867) and Schiaparelli (1867) in their computations of the stream's orbit. Shortly after the determination of the Leonid meteor stream's orbit, it was recognized by several authors to be almost identical to that of 1866I thus leading to the second association between a comet and a meteor stream (the first having been the Perseids and comet Swift-Tuttle the year before).

The predictions made shortly after the 1833 shower were confirmed by major showers/storms in 1866 and 1867 as well as strong returns in 1865 and 1868, all heralding the major advances made in the understanding of the stream during the same years.

With the parent comet now known and the periodicity of the stream firmly established, confident predictions were made of a strong meteor shower in 1899. In the years immediately before the 1899 return, the shower did not produce particularly strong returns although there exists some evidence of increased activity in 1898. The first calculation of the perturbations by the outer planets on the segment of the stream encountered by the Earth in 1866 was made by Berberich (1898), who found that the Leonids had passed close to both Saturn and Jupiter in the few years before 1899 and as a result the meteoroids encountered in 1899 would be perturbed far inside the Earth's orbit. Similar calculations performed by Stoney and Downing (1899) indicated that the storm producing segment of the stream (which they termed the "ortho-Leonids") would be perturbed inwards by more than 0.01 A.U. These large nodal

perturbations were cautiously interpreted as being significant enough to perhaps lessen the display in 1899 but the authors of both works were hopeful that the stream was still wide enough to allow some member meteoroids to encounter Earth.

Murakami (1959, 1961a and 1961b) published a series of articles analyzing visual observations made in Japan from the 1930s through the late 1950s and showed that some enhanced activity was present in at least 1931 and 1932, though weak in comparison to the years around the 1833 and 1866 storms. He also investigated the formation of the stream from these observations and concluded that ejection velocities of order 10 m/s could account for the 1000 year lifetime of the observed shower.

Kazimirchak-Polonskaya *et al.* (1967) were the first to make use of computers to investigate perturbations on a collection of hypothetical Leonids starting in 1866 and integrated to the present epoch. They established that the orbit of the Leonids was stable over intervals of centuries and that Jupiter and Saturn were the primary planetary perturbers of the stream.

McIntosh (1973) used an analytical approach to study the effects of the cometary ejection process on the stream and was the first to recognize the importance of radiation pressure on Leonid meteoroids. His model suggested that the major showers occurring in different years close to the time of the comet's passage are from ejections at different perihelion passages. Comparison of the model's results with actual observations suggested that the observations could be best reproduced through dust emission at discrete points along the cometary orbit as opposed to near continuous emission.

A more detailed analytical model was proposed by Sekanina (1974). He included the effects of ejection velocities and radiation forces on individual meteoroids and accounted for planetary perturbations through the measurement of subsequent deviations of forward integrations of initial orbits differing slightly from Tempel-Tuttle. Using historical accounts of the stream in conjunction with this model, he suggested the past activity of the shower was the result of intermittent activity of Tempel-Tuttle, most notably ejections in 868, 1499 and 1767. He found that ejection velocities of order 10 - 100 m/s were needed to explain the observed storms.

The study of the relationship between Tempel-Tuttle and the Leonids was continued by Yeomans (1981). Using past observations of Tempel-Tuttle, he was able to construct an

historical ephemeris for the comet by solving for its non-gravitational parameters as well as numerically integrating the comet's equations of motion. Using this cometary ephemeris in conjunction with ancient Leonid observations, he developed an empirical model of the dust distribution around the comet. He found that most Leonid meteoroids lagged spatially outside and temporally behind the comet, in contrast to what would be expected based on the direction of the non-gravitational forces, which would tend to move meteoroids inside and ahead of the comet. Most notably, all past Leonid storms had occurred within 2500 days before or after the comet's perihelion passage and then only if the comet passed 0.025 A.U. inside or 0.01 A.U. outside the Earth's orbit. Based on these results, he concluded that both radiation forces and planetary perturbations were key evolutionary determinants while ejection velocities (which he suggested to be of the order 5-20 m/s) were less important to the development of the stream.

Kondrat'eva and Rezinikov (1985) independently developed an orbital ephemeris for Tempel-Tuttle. They studied the stream using the orbital elements of the comet near perihelion in conjunction with a numerical model where particles were ejected isotropically from the comet and acted upon by planetary perturbations. Through iterative adjustment of the initial orbit upon ejection, they determined the ejection velocities needed at each perihelion passage of the comet to produce the smallest encounter distance with the Earth at the time of the 1833, 1966 and 1999 Leonid returns. Their results suggested that the component of the ejection velocity perpendicular to the comet-sun direction is important in stream evolution, the ejection velocities needed were in the range 10-20 m/s and the ejection point along the cometary orbit is not significant to future development of the stream.

Williams *et al.* (1986) analytically constrain the ejection velocities by using the fact that some Leonid storms occur in two consecutive years and that the change in energy of the ejected particle is purely kinetic. They found that ejection at perihelion must be less than 1 m/s to account for storms occurring in two consecutive years and greater velocities were required for ejection further from perihelion.

A modern numerical model of the stream was presented by Wu and Williams (1991). They used the ephemeris of Yeomans (1981) and a model of meteoroid ejection from Tempel-Tuttle which was confined to the plane of the cometary orbit with steps of 30° in the direction of ejection and derived the resulting ejection speeds from the model of Whipple (1951). By

following the evolution of test particles ejected in this way under the influence of planetary perturbations and radiation pressure effects, they were able to confirm directly that the test meteoroids evolved to positions spatially outside and temporally behind the parent comet in support of Yeomans' (1981) empirical study.

Using a similar approach, Brown and Jones (1993) followed the evolution of several thousand test particles following Whipple's (1951) expression for the ejection velocities. They noted the possible importance of the 1:3 mean motion resonance with Jupiter on the stream's development and concluded that the stream's evolution is driven by planetary perturbations and modified by radiation pressure.

Kresak (1993) investigated the relationship between the IRAS dust-trails and meteor storms, which he viewed as the same phenomenon but observed from different perspectives. He explicitly noted the appearance of Leonid storms was controlled by close encounters of the stream with Jupiter which served to disperse the dense dust "trail" behind the comet and thus limit the stream's ability to produce meteor storms on Earth. He further suggested that the dispersion process responsible for meteor storms within a trail proceeded primarily through differences in radiation pressure between particles and to a lesser extent the initial ejection velocities of the particles involved. The correspondence between the IRAS dust trails and meteor storms suggested on the basis of observations of both, that the ejection velocities responsible for the formation of the trails were of order 5 m/s and the dominant particle population in the trails had $\beta=10^{-3}$.

Wu and Williams (1996) investigated the past evolutionary histories of ten photographically determined Leonid orbits and concluded that the semi-major axes and eccentricities of the observed Leonids were determined primarily by initial ejection velocities. Combining this fact with backward integrations of the observed Leonid meteoroids, they suggest that Leonids are ejected from Tempel-Tuttle with velocities of order 0.6 km/s. To simulate the formation of the stream, they utilized a mean ejection velocity at perihelion for 90 test particles from cometary passages in 1866, 1899 and 1932 which produce periods such that the meteoroids approach the Earth in 1966 (but were ejected with velocities less than 0.6 km/s) and then repeat this procedure for 1998-1999. They examined the number of meteoroids making close approaches to the Earth and concluded that only modest to weak showers may

be expected in 1998-1999.

Williams (1997) suggested that the lack of strong Leonid displays when the parent comet is far from perihelion might result from perturbations by Uranus. He noted that Tempel-Tuttle is close to a 5:2 mean motion resonance with Uranus and that the planet might be responsible for "sweeping" clean Leonid meteoroids from that portion of the orbital arc far from the parent comet, accounting for the lack of Leonid displays away from the comet's perihelion passage.

Asher (1999) investigated the likely ages of Leonid displays over the last 160 years. He showed that for short periods (up to a few orbital revolutions), most meteoroids released at perihelion on orbits sufficiently similar to Tempel-Tuttle experience deterministic evolution which can be used to map the specific perturbations from a given ejection epoch which producing Leonid meteors intersecting Earth's orbit at the time of witnessed showers/storms. Noting that differential planetary perturbations between daughter Leonids and Tempel-Tuttle is the dominant factor in the delivery of Leonids to Earth, he was able to estimate the separation distance at nodal crossing between previous ejections and the Earth's orbit at specific Leonid returns. On this basis he concluded that the storms of 1966 and 1833 were caused by ejections from Tempel-Tuttle in 1899 and 1799 respectively.

In this work, we attempt to simulate the formation of the Leonid stream using existing physical models, which describe the cometary-meteoroid ejection process. Using Monte Carlo techniques to produce a suite of initial meteoroid orbits, we then follow these test particles by applying numerical integration to epochs of documented Leonid activity over the last 160 years and compare the results to observations. We have previously applied a similar model to study of the Perseid stream (Brown and Jones, 1998).

In particular, we wish to compare the results of our integrations with observations to attempt to verify the general veracity of the initial conditions used and to determine what constraints can be placed on the initial conditions of the formation of the stream.

Notably we hope to address the following questions through simulation:

- What is the age and origin of the ejecta, which constitute documented Leonid storms/showers, particularly those of 1966/69, 1901/03, 1866/67 and 1832/33?
- What do the activity profiles from past Leonid storms, when compared to modelling results imply about initial ejection velocities from Tempel-Tuttle?
- What is the relationship between the orbital geometry of Earth and Tempel-Tuttle in the past relative to the delivery of Leonids at the present time?
- What is the dependence on initial velocities/conditions/densities/masses of meteoroids for delivery at Earth at the present epoch?
- What is the mean spread of the stream over time due to planetary perturbations (i.e. how does the relative density of the stream change over time)?
- What effect does each of the major planets have on the evolution of the stream?
- What are the dominant evolutionary processes affecting the structure of the stream (ejection velocities, radiation pressure or planetary perturbations) and over what time scales do they dominate the evolution of the stream?
- What is the best model representation of the ejection process?
- What causes the abrupt decrease in observed activity of the stream in years just before and after the return of Tempel-Tuttle?

6.2 Model for the Formation of the Leonids and Observational Considerations.

6.2.1 Overview of Model

To simulate the formation of the Leonid stream we proceed as previously for the Perseids (Brown and Jones, 1998). Briefly, the basic procedure consists of generating a suite of test particles close to each perihelion passage of Tempel-Tuttle and following each of these through to the epoch of interest. The "daughter" Leonids are created through random ejection on the sunward hemisphere of Tempel-Tuttle and are distributed at random in true anomaly inside 4 A.U. The osculating elements for Tempel-Tuttle are taken from Yeomans *et al.* (1996). A total of 10 000 test meteoroids are ejected in each decadal mass interval from 10 g - 10^{-5} g, for a total per perihelion passage of 70 000 test particles. This procedure is repeated for each of the last 15 perihelion passages of the comet so that each complete "run" consists of just over 1 million test particles.

After the initial conditions are specified in this way, each test particle is numerically integrated forward from ejection to the epoch of interest and followed until it reaches its descending node (the only point along its orbit at which it might possibly be observable from the Earth) and its Keplerian elements at the time of nodal passage are stored. The integration includes the direct and indirect perturbations of all planets from Venus to Neptune, radiation pressure and the Poynting-Robertson effect. The integrator used is a 4th order variable step-size Runge-Kutta (Jones, 1985).

This basic procedure is repeated for four different physical models of ejection and three different values of meteoroid bulk density for a total of 12 different runs. The four physical models are derived from the work of Crifo (1995) on distributed gas production within the cometary coma and the Jones (1995) model with variations in the heliocentric dependence on ejection velocity and a parabolic distribution in ejection probabilities. For each of these models we adopt bulk meteoroid densities of 0.1, 0.8 and 4.0 g/cm^{-3} in turn, due to uncertainties in the actual meteoroid bulk density and to investigate the role of differing assumed densities on the

evolution of the stream. These densities, along with the range in initial particle masses, translate into a range of β's from ~10^{-5} - 10^{-2}. Table 6.1 and its description provide more details for each of these physical model choices. Fig. 6.1 shows a typical range of ejection velocities from Tempel-Tuttle for these model choices. Note that we have used a mean radius of 2 km for 55P/Tempel-Tuttle of throughout in accordance with recent observations (Hainaut *et al.* 1998).

Our approach at this stage is to generate initial conditions which are "reasonable" within the constraints of our imperfect understanding of the cometary coma dust environment rather than to suggest any particular model as most appropriate. In particular, we recognize that there are large uncertainties in many of the physical quantities (i.e. density of meteoroids, relationship between meteoroid mass and luminosity etc.) and choose to instead explore the effects of widely different (but still "reasonable") ejection conditions (velocities, points of ejection and ejection directions) and meteoroid densities over a wide range of masses in this Monte Carlo fashion. This same approach has been used previously to study the formation and evolution of the Perseid stream (Brown and Jones, 1998) and more extensive details and discussion can be found in that work.

6.3 Observational Considerations

Leonid meteors are observable from the Earth only when their nodal distance from the sun is equal to the Earth's orbital distance and when the Earth is at the node at the same time. This automatically implies that only a very small percentage of all the meteoroids in the stream can actually be observed at Earth in any given year. However, this constraint is far too strict for the interpretation of modelling results; even with a total of 10^7 test particles only a handful would meet these conditions. As a result it becomes necessary to adopt some form of temporal and spatial sieving to make sensible, statistically meaningful results. The important consideration is what choice of temporal and spatial binning is still physically representative of the initial conditions without being so strict affords too few particles in the end to analyze. If our bins are too large we will "see" features in the final modelling which do not intersect the Earth; if too small we may miss features which now have too few particles representing them.

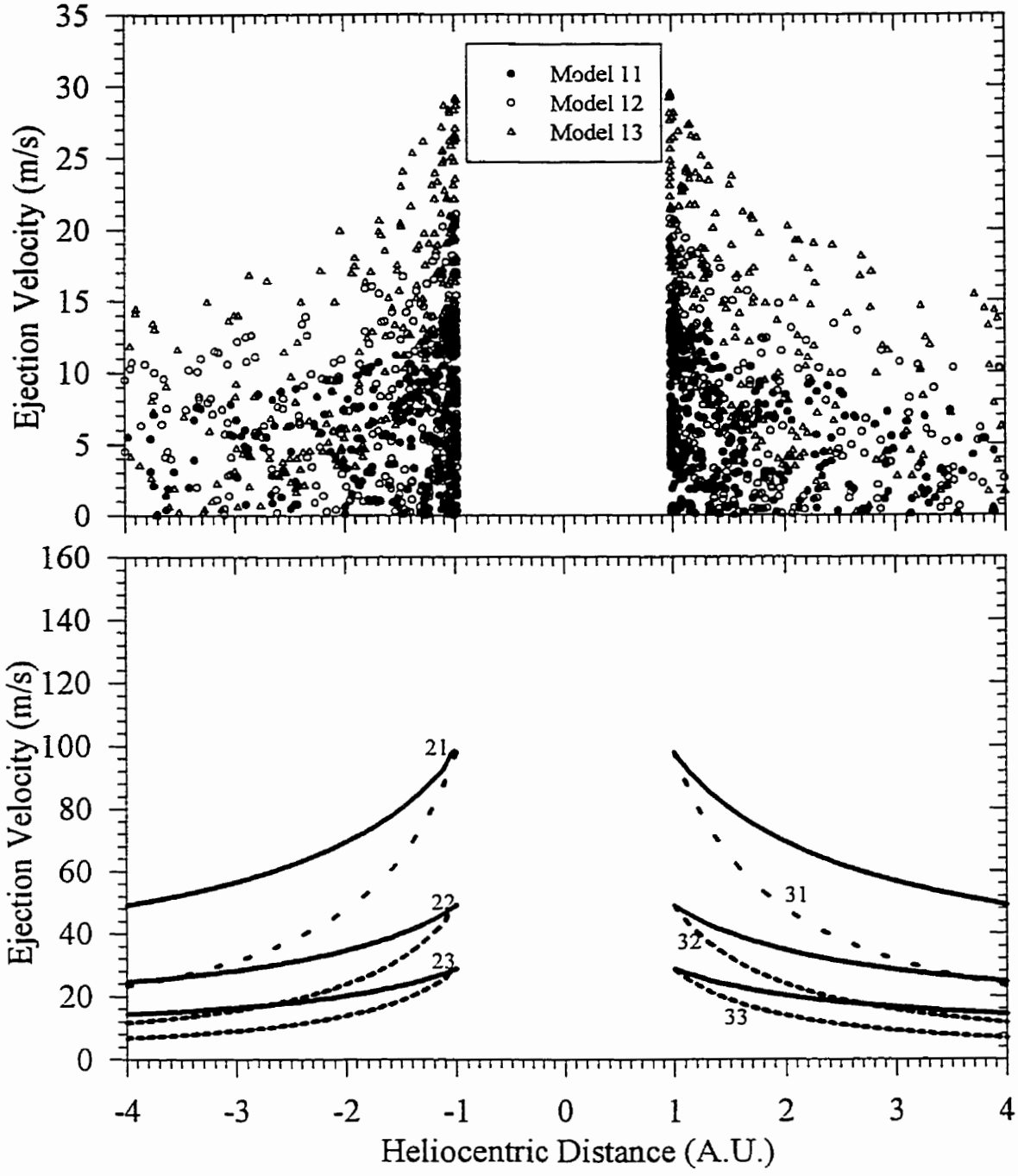

Fig 6.1: Ejection velocities for meteoroids of mass 10^{-3} g for Leonids for models 11,12 and 13 (top) and for 21-33 (bottom). Negative values in the abscissa are pre-perihelion.

Table 6.1: The model numbers, literature references for original material and ejection formulae used to simulate the formation of the Leonid meteoroid stream. Note that in addition to each model number a second number is also used to refer to the density as 1 (100 kg m^{-3}), 2 (800 kg m^{-3}) and 3 (4000 kg m^{-3}). Thus model 12 uses the Crifo distributed production model ejection velocity formula and assigns all meteoroids a bulk density of 800 kg m^{-3}.

Model #	Name	Ejection Formula
1	Crifo Distributed Production Crifo (1995)	$Log_{10}(V_{eject})=-2.143-0.605\,Log_{10}(radius)-0.5\,Log_{10}r$ $P(V-Veject)=\frac{1}{e^{3.7}}\exp\left[\frac{3.7-10.26(V-Veject)+4.12(V-Veject)^2}{1-1.03(V-Veject)+0.296(V-Veject)^2}\right.$
2	Jones Ejection Disiribution with Modified Heliocentric Velocity Dependence Jones (1995)	$V_{eject}=10.2r^{-0.5}\rho^{-\frac{1}{3}}R_c^{\frac{1}{2}}m^{-\frac{1}{6}}$ P(V-Veject) = 1 for V=Veject and 0 otherwise
3	Jones Ejection Distribution Jones (1995)	$V_{eject}=10.2r^{-1.038}\rho^{-\frac{1}{3}}R_c^{\frac{1}{2}}m^{-\frac{1}{6}}$ P(V-Veject) = 1 for V=Veject and 0 otherwise
4	Jones ejection distribution with parabolic probability distribution Jones (1995)	$V_{eject}=10.2r^{-1.038}\rho^{-\frac{1}{3}}R_c^{\frac{1}{2}}m^{-\frac{1}{6}}$ $P(V-Veject)=1-(\frac{V}{Veject}-1)^2$ for 0<V<2Veject and 0 outside this range

One approach is to use the inherent numerical limitations of the integrator in concert with the normal process of chaotic divergence of initially similar orbits. Together these produce a lower limit to the meaningful size of the spatial and temporal binning chosen over the time-scales of interest.

To investigate this, we use the initial osculating elements for Tempel-Tuttle in 1499 and integrate these forward to 1998, using the same numerical parameters used for particle integrations. By comparing these final results with those from the Yeomans *et al.* (1996) ephemeris we are able to define an effective lower limit for the useful binning intervals. In particular, since our integrations do not take into account the effects of non-gravitational forces for Tempel-Tuttle (which the Yeomans *et al.* (1996) results do) we expect that our results will be larger than the actual results; hence any choice for the binning intervals will be similarly conservative.

We have examined the differences between the osculating elements for Tempel-Tuttle from our integrations and those given from Yeomans *et al.* (1996) at the epoch of the comet's 1998 perihelion passage. On this basis, we have found that the difference in the times of perihelion passage and nodal distance after 500 years are, respectively, 0.025 years (roughly one week) and 7×10^{-4} A.U. (about 7 Earth diameters). This leads us to adopt a bin size of 0.02 years and 0.001 A.U. in nodal distance for the simulations. In a representative examination of both temporally and spatially larger bin sizes we noted that our final results became significantly different once bin sizes ~ 3 times larger than the above were used. The nodal distance was particularly sensitive to this.

As our purpose is (in part) to investigate the densest portions of the Leonid stream (these being associated with the "trails" from Tempel-Tuttle), we note that the above choice of bin sizes is compatible with the spatial size of IRAS dust trails, which are slightly smaller than 10^{-3} A.U. in width at 1 A.U (Kresak, 1993). Asher (1999) has also independently estimated the cross-section of the storm-producing portions of the Leonid stream as 10^{-3} A.U. in general accord with the foregoing.

An alternate approach is to adjust the bin sizing until the activity profiles for a particular year match those observed. Unfortunately, this requires some conversion between the number of accepted test particles and flux, which is not possible at this stage

(see next section). An approximate idea of usable bins can be generated, however, by examining the bin sizes at which "features" begin to appear that were (or were not) actually recorded. This technique was applied to the 1998 and 1966 shower/storm and confirmed our overall choice of bin widths in qualitative terms.

6.4 Simulation Results - Recent Epochs (1833-1965)

In what follows we describe in some detail the results of the simulations for different epochs and compare these to observations. Several important factors should be kept in mind. First, the simulations extend back only 500 years (except for the single long-term simulation referenced to the current (1998) epoch discussed in Sect. 6.5). Results showing a predominant population of meteoroids from this age may simply reflect the greater diffusion of older populations, leading to the acceptance of a small number of meteoroids under any conditions, and not the true population (which may be older still).

Secondly, the test particles accepted are counted and summed in each mass bin with no additional weighting. In reality, some initial mass distribution exists within the cometary coma and there should be many more small meteoroids than larger ones. However, the value for the mass distribution is very uncertain; there has only been one direct measurement of the mass distribution inside a cometary coma (McDonnell *et al.*, 1987) yielding a value of s=1.7 (from Halley's comet) and then only at masses smaller than those used here and made over a short interval of time. Ground-based observational attempts to determine this mass distribution exponent (cf. Fulle, 1996) have consistently suggested large changes in the exponent as a function of time as well as large inter-comet variations and pre/post perihelion asymmetries in the value of this exponent. Since the determination of a final "activity" here at Earth is heavily dependent on this power-law exponent, it becomes almost impossible a priori to make accurate flux estimates from model results without knowing the initial mass distribution exponent (if a single value even exists over the seven orders of magnitude mass investigated here). Limited experimentation with the present results using the Halley-determined value of the initial mass exponent (s=1.7) suggested that relative activities are somewhat unchanged (as

compared to a simple unweighted summation of all test particles), but this conclusion does not hold when significantly steep distributions (s=2 or higher) are used and where the presence of only 1-2 test particles of small mass can utterly distort the entire distribution.

As a result of this limitation, we are examining effectively the transfer efficiencies as a function of mass and are summing these values over discrete mass ranges in an attempt to cover a physically meaningful range in β. Fortunately, it is likely that for true Leonid meteoroids a range in bulk densities and shapes affords a modest range in β for any given mass making this approach a reasonable first approximation.

Variations in the accepted cone angle will likely modify the results, which follow. In an earlier study of the Perseid shower (Brown and Jones, 1998), we found only modest changes resulting from moderate shifts in the accepted cone angle and have chosen not to investigate this aspect further although it certainly warrants some attention. Given our very limited observation history of Tempel-Tuttle (cf. Yeomans *et al.*, 1996), it is unlikely we would be able to constrain cone angle solely on the basis of past observations. Re-examining all the results with cone angles as another variable is beyond the scope of this work.

6.4.1 The 1965 Epoch

Fig 6.2 shows a typical nodal footprint from the simulations using visual-class particles (mass>0.001 g) for the entire 1965 epoch for models 22 and 23 at three mass categories with 10 000 particles in each category ejected. Note the strongest concentration is just inside the Earth's orbit near the nodal point of Tempel-Tuttle. As expected, the spread in size of the nodal region increases as mass decreases. Fig 6.3a shows a similar distribution, with nodal distances plotted as a function of time for the ejection primarily responsible for the 1966 storm (1899). Note the monotonic increase in nodal distance as a function of nodal passage time for the densest region. This structure crosses the Earth's orbit at almost precisely the location of the 1966 Leonid storm and is almost certainly responsible for it. This pattern is the result of differential planetary perturbations on the material, primarily from Jupiter. Note that the removal of direct perturbations from Jupiter

leaves this material entirely inside the Earth's orbit (Fig 6.3b).

Using our adopted temporal and spatial sieving sizes, we have isolated the simulated activity from visual-sized Leonids for each year from 1961-1969. With these distributions, we have computed the locations of predicted maxima (defined in the simulations as simply the largest number of test particles in a particular bin) as a function of solar longitude for each of these years through weighting the results from each model by the number of test particles in the maximum bin. The locations of observed maximum from visual activity are from Chapter 5 and are given in Fig 6.4 along with the theoretical locations for the 1965 and previous epochs. Of note is the close correspondence between the observed locations of maximum and the weighted theoretical locations in 1966 and 1969. These years have the most complete observations and most certain times of maximum. The years before 1965 are poorly covered observationally and have few test particles.

In Table 6.2 we also list the ejection years which produce the largest number of test particles per model within our sieving constraints for each year. It is apparent that the displays in different years are from quite different sources. The outburst in 1961, for example, is due almost entirely to material ejected in 1499 or earlier, whilst the stronger outburst in 1969 is from ejecta released in 1932. Particularly interesting are the most probable sources of the displays from 1965 and 1966; the former is composed primarily of large meteoroids (see Fig 6.5) with ages >500 years, while the storm of 1966 is due to material ejected in 1899. These results lead to immediate explanations of why the 1965 display was long-lived and made up of many large meteoroids and why the 1969 display was so narrow and yet so far from the location of the 1966 display: the populations in the two years were of entirely different ages and hence had different perturbation histories.

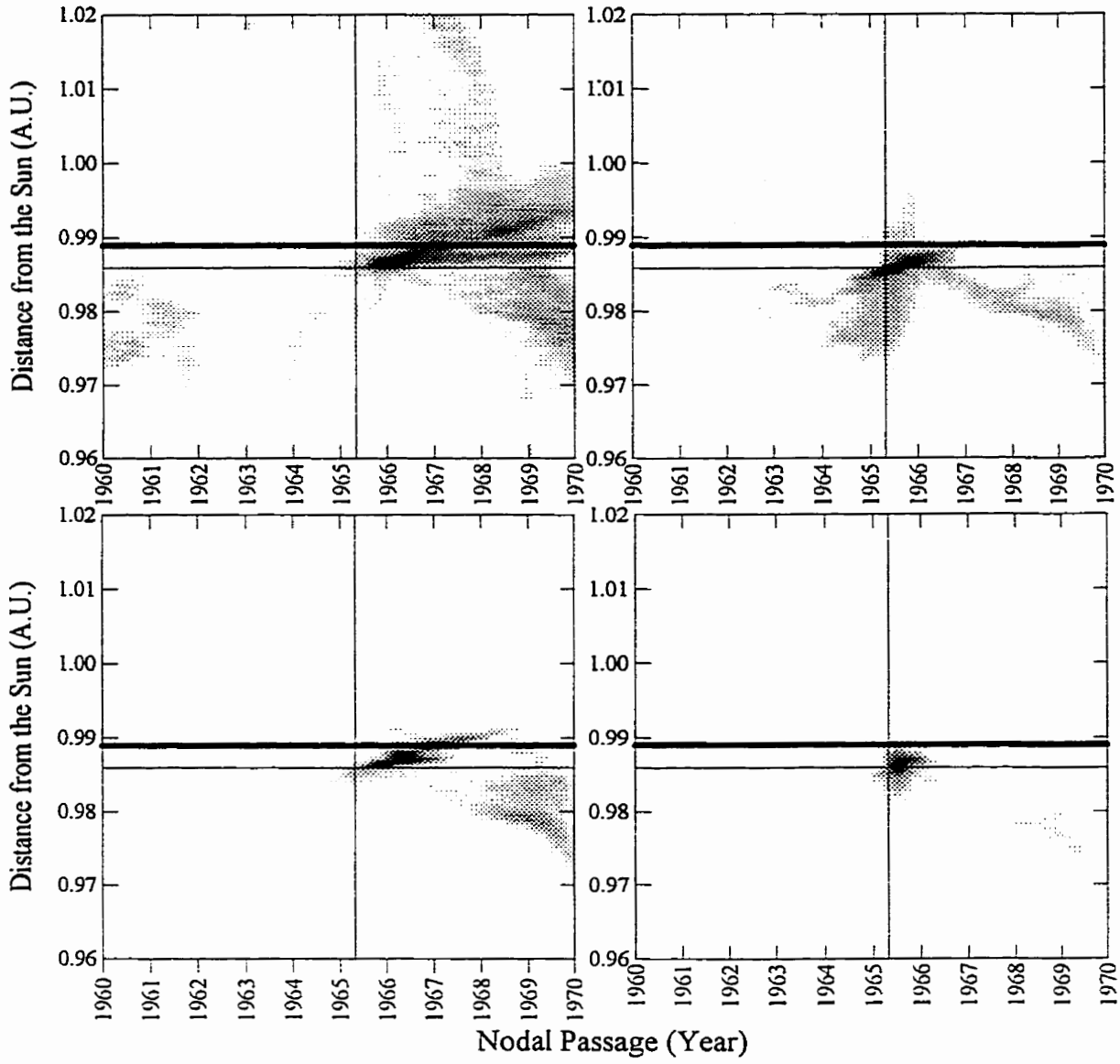

Fig 6.2: Test particle nodal distributions at the April 1965 epoch for model 31 meteoroids of mass 10^{-3} g ($\beta=4\times10^{-3}$) (top left), 10 g ($\beta=2\times10^{-4}$)(top right) and for model 12 meteoroids of mass 10^{-3} g ($\beta=10^{-3}$) (bottom left) and 10 g ($\beta=5\times10^{-5}$) (bottom right). The bold line is the distance of the Earth from the Sun on Nov 17 each year and the intersection of the thin lines marks the nodal crossing time and distance for 55P/Tempel-Tuttle during the 1965 epoch. The distributions represent the summation of all ejections from 1466 – 1932 A.D. for these particular mass categories.

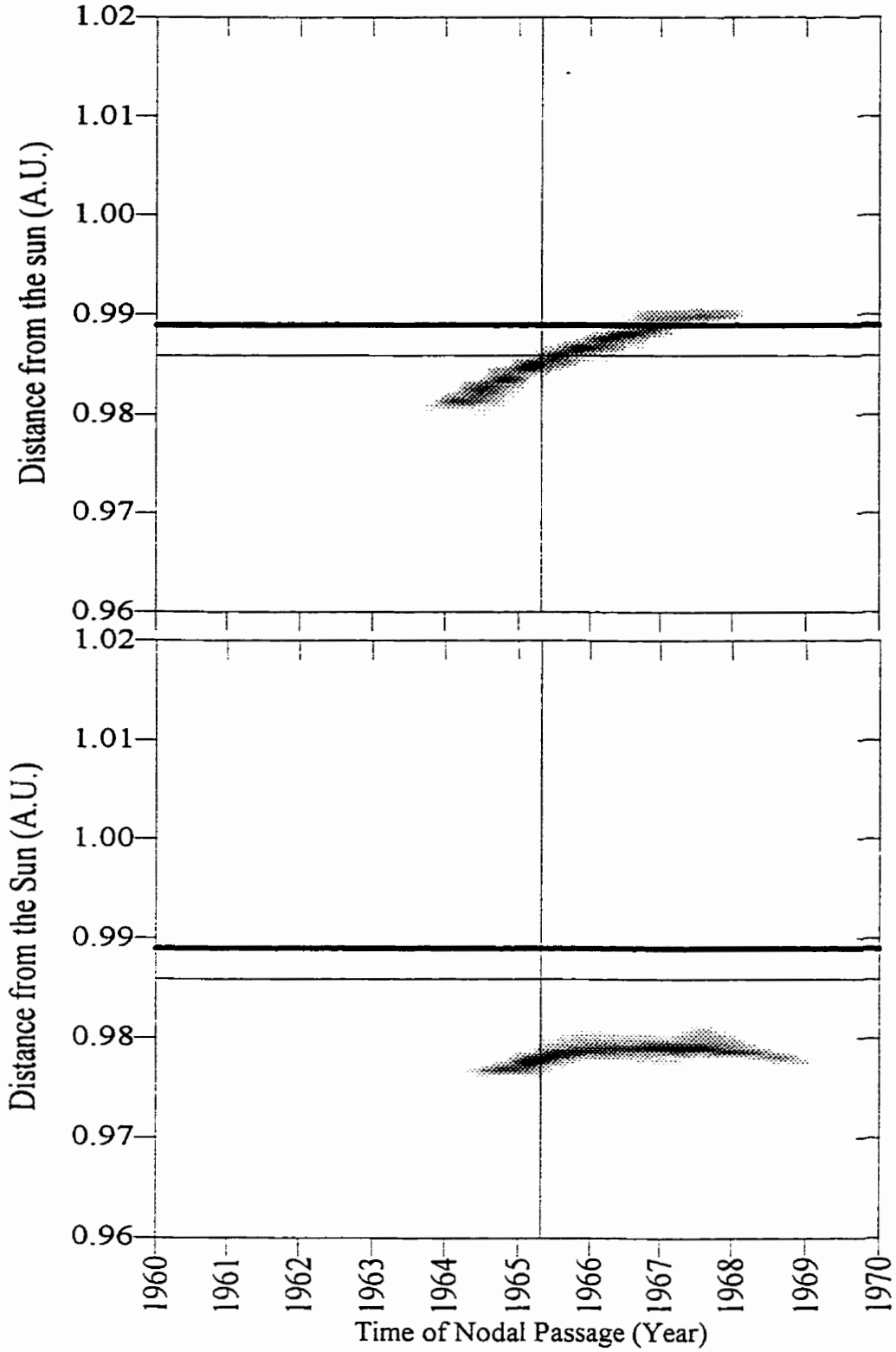

Fig 6.3: Nodal distribution for meteoroids ejected in 1899 of mass 0.1 g using model 42 at the 1965 epoch with all planetary perturbations (a) – (top) and without Jupiter (b) - (bottom).

Table 6.2. Age of Leonid showers for each given year as a function of the model. The first number in each box is the total number of test particles with nodal radaii within 0.001 A.U. of Earth and nodal passage within 1 week of the Earth's passage. Successive numbers give the primary ejection year contributing to activity from the model (in brackets) and the fraction of all particles in a particular year from the ejection.

Model/Year	1961	1964	1965	1966	1967	1968	1969
11	12 **1499(1.0)**	40 **1766(.93)** 1499(.05)	147 **1666(.41)** 1699(.22)	411 **1899(.70)** 1932(.27)	26 **1932(.88)** 1699(.12)	58 **1932(.97)** 1599(.03)	102 **1932(1.0)**
12	6 **1499(1.0)**	52 **1766(.81)** 1566(.08)	147 **1666(.35)** 1499(.20)	265 **1899(.94)** 1866(.03)	1 **1899(1.0)**	19 **1599(.47)** 1566(.32)	0
13	17 **1499(.94)** 1599(.06)	90 **1766(.51)** 1499(.17)	173 **1499(.42)** 1766(.19)	73 **1899(1.0)**	0	54 **1566(.61)** 1599(.39)	0
21	39 **1499(.79)** 1599(.08)	42 **1499(.24)** 1466(.19)	221 **1866(.21)** 1833(.15)	251 **1899(.74)** 1932(.20)	62 **1932(.53)** 1899(.47)	40 **1932(.58)** 1566(.15	34 **1932(1.0)**
22	44 **1499(.84)** 1599(.11)	74 **1766(.41)** 1499(.24)	207 **1466(.19)** 1499(.13)	219 **1899(.74)** 1932(.20)	16 **1932(.56)** 1899(.38)	30 **1599(.50)** 1566(.37)	0
23	33 **1499(.76)** 1599(.11)	124 **1766(.42)** 1499(.23)	210 **1466(.22)** 1499(.18)	123 **1899(.98)** 1932(.02)	0	46 **1566(.52)** 1599(.39)	0
31	18 **1499(1.0)**	38 **1766(.29)** 1499(.29)	198 **1666(.18)** 1866(.16)	313 **1899(.74)** 1932(.21)	57 **1932(.54)** 1899(.42)	42 **1932(.67)** 1599(.17)	37 **1932(1.0)**
32	32 **1499(.91)** 1599(.09)	101 **1766(.61)** 1499(.15)	225 **1466(.23)** 1499(.22)	221 **1899(.77)** 1932(.19)	17 **1899(.53)** 1932(.41)	36 **1599(.53)** 1566(.36)	0
33	28 **1499(.82)** 1599(.14)	129 **1766(.47)** 1499(.24)	209 **1499(.34)** 1466(.19)	97 **1899(.97)** 1866(.03)	0	55 **1566(.67)** 1599(.33)	0
41	24 **1499(.88)** 1599(.04)	39 **1766(.38)** 1466(.21)	168 **1666(.21)** 1699(.17)	248 **1899(.70)** 1932(.23)	53 **1932(.62)** 1899(.34)	41 **1932(.68)** 1599(.20)	34 **1932(1.0)**
42	22 **1499(.86)** 1566(.09)	79 **1766(.59)** 1499(.16)	201 **1499(.28)** 1699(.15)	238 **1899(.81)** 1932(.14)	16 **1932(.50)** 1899(.50)	32 **1599(.41)** 1566(.28)	4 **1932(1.0)**
43	25 **1499(.80)** 1599(.20)	104 **1766(.49)** 1499(.22)	181 **1499(.42)** 1466(.19)	122 **1899(.93)** 1866(.04)	2 **1899(1.0)**	43 **1566(.65)** 1599(.28)	0

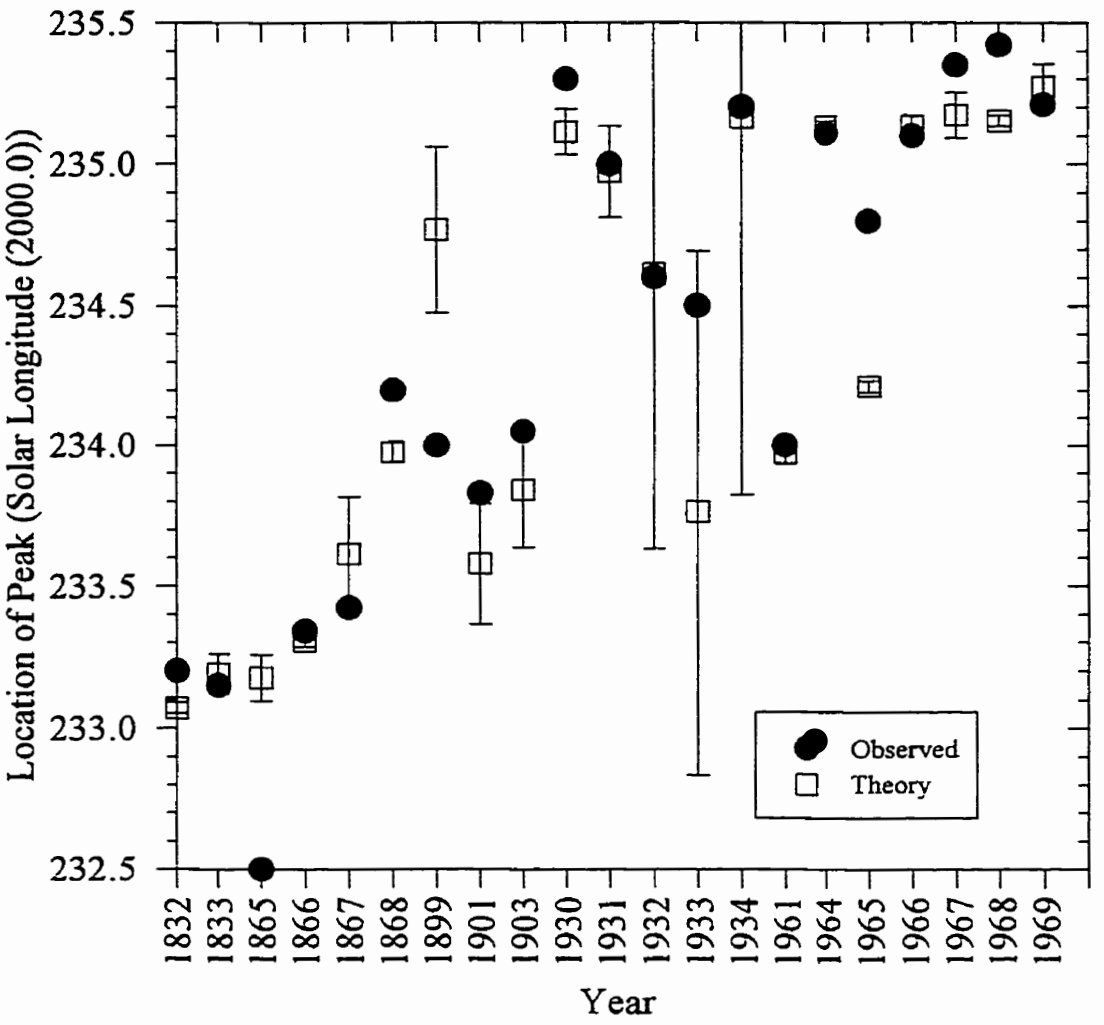

Fig 6.4: The observed locations for maxima (solid circles) for the Leonids from 1832 – 1969 (from Chapter 5) compared to the average weighted location from the modelling (open squares). The weighted location for each year is found by summing the peak locations found from each of the models (using a sieve of 0.001 A.U. and 1 week nodal passage time) and weighting by the number of test meteoroids in the solar longitude bin of the peak.

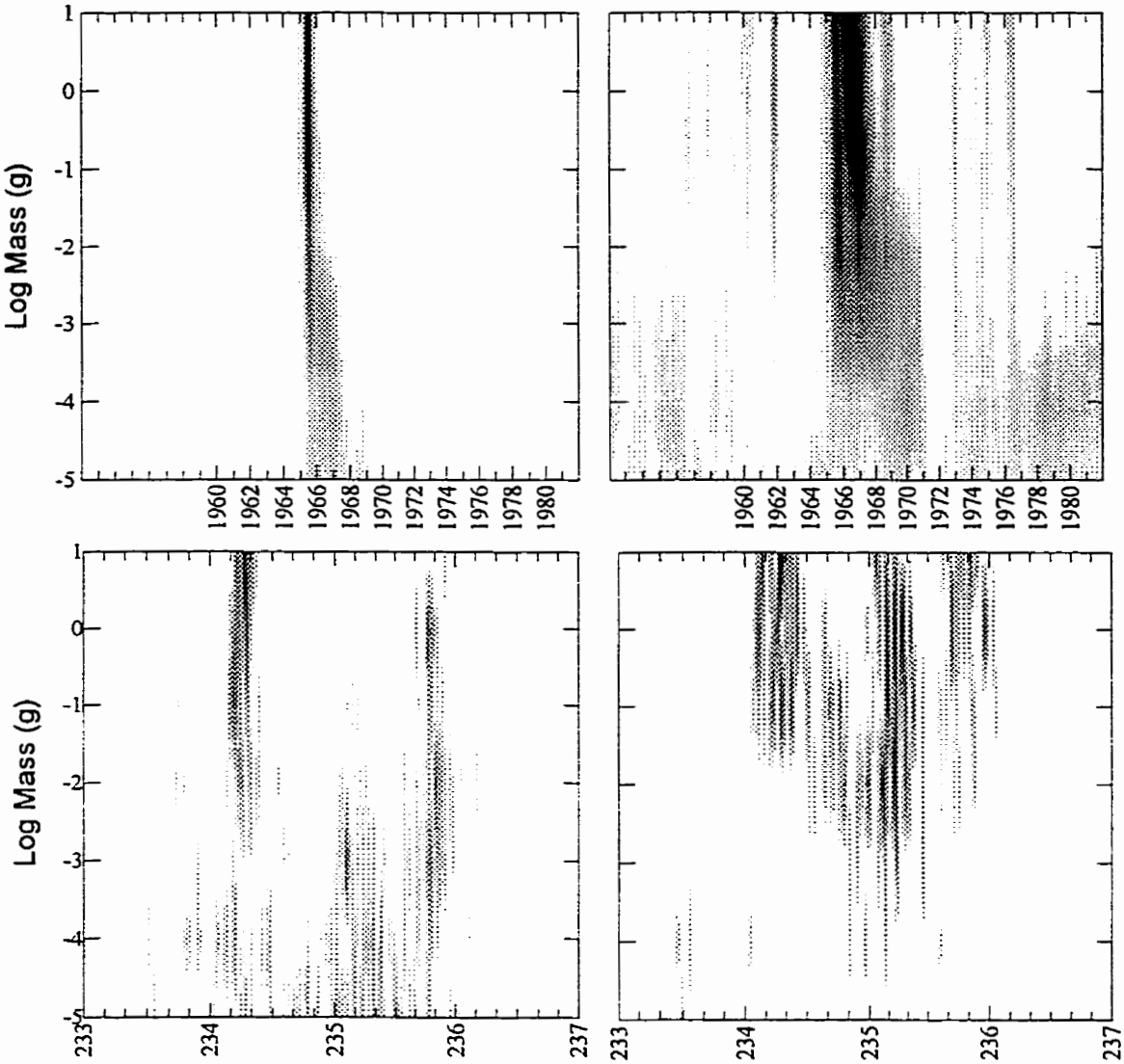

Fig 6.5: The distribution of Earth-intersecting meteoroids for model 13 (top left) and model 21 (top right) as a function of mass and time of nodal passage. The bottom plots show the distribution in solar longitude of Earth-intersecting Leonids during the 1965 Leonid shower for model 13 (lower left) and model 21 (lower right).

Of the displays in this epoch, the 1966 storm is the strongest and among the best documented. Fig 6.6a shows the distance between each of the "trails" ejected from Tempel-Tuttle from 1633-1932 at the time of the November, 1966 storm. Each point represents the average for a given model, the error margins representing the standard deviation of the individual points. It is clear that the 1899 trail passed extremely close to Earth in November, 1966 (independent of the ejection model or range of β used) while the trail from 1932 was several times more distant from Earth (and had wider spreads depending on the range of β and ejection model used). However the latter may still have contributed to activity.

Since it is only two revolutions old, its cross-sectional size provides a quasi-direct means of estimating initial ejection velocities since such young ejections should be relatively undisturbed by planetary perturbations. Fig 6.7 shows the gaussian width of the activity profile, for the two hours centred around the peak in November, 1966 from 1899 ejecta, for each model as a function of the normal component of the initial ejection velocity. Recalling that the gaussian width of the 1966 storm was of order 0.01°-0.015° (the former based on visual observations and the latter on radar observations (Brown *et al.*, 1997)), this implies normal components of ejection velocity of 2-3 m/s, corresponding (approximately) to total ejection velocities of order ~5 m/s based on our modelling.

To examine this question further, the initial velocities of material ejected in 1899 (which are accepted as within both our chosen binning intervals and the solar longitude interval from 235.1° - 235.2°) at the node in 1966 was investigated. Specifically, the radial, transverse and normal components of the ejection velocities as a function of ejection distance from the sun for each run and mass category were computed. It was found that some material at higher ejection velocities, possibly ejected as far as 4 A.U. from the sun in 1899, was accessible to the Earth at the time of the 1966 storm (though this does not necessarily mean Tempel-Tuttle was active at this distance to supply such material). However, the plots showed certain very narrow ranges in β (near 10^{-3}) at low ejection velocities that have an order of magnitude greater transfer efficiency than neighboring regions. Certainly the ejection models produce fewer high velocities (which also have larger degrees of freedom) but the sharpness of these transfer peaks cannot be

explained in this manner (and we can eliminate very high ejection velocities as incompatible with the observed cross-section of the storm from Fig 6.7). Examination of the masses involved and their ejection velocities suggests that, in the case of the 1966 storm, material with very low ejection velocities (3-5 m/s total) had much higher dynamical transfer efficiencies from 1899. In addition, these regions were confined to very small ranges in true anomaly as well as β. The implication is that the 1966 storm may have represented very specific as opposed to representative material ejected from Tempel-Tuttle in 1899, with other true anomalies not accessible to Earth.

Fig 6.6b shows these same trail distances for 1969 and demonstrates conclusively that the material in that year must have been from ejections in 1932 as no other trail was close to Earth. More interestingly, the 1969 display is notable only in those trails with an abundance of low density meteoroids and is confined to a very narrow range of possible beta's (β~0.005-0.01). This can be qualitatively understood as the dual requirements of having to increase the period of 1969-observable Leonids to allow them to trail the comet by some 4 years combined with the narrow profile implying a recent origin; only young, high-β particles meet both requirements. Fig 6.8 shows the relationship between the gaussian width of 1932 ejecta in 1969 versus the normal component of the initial ejection velocity for material within 2 hours of the measured peak. From the visually observed width of 0.02°, we arrive at normal components of the ejection velocity of order 5-7 m/s, implying total ejection velocities ~10 m/s.

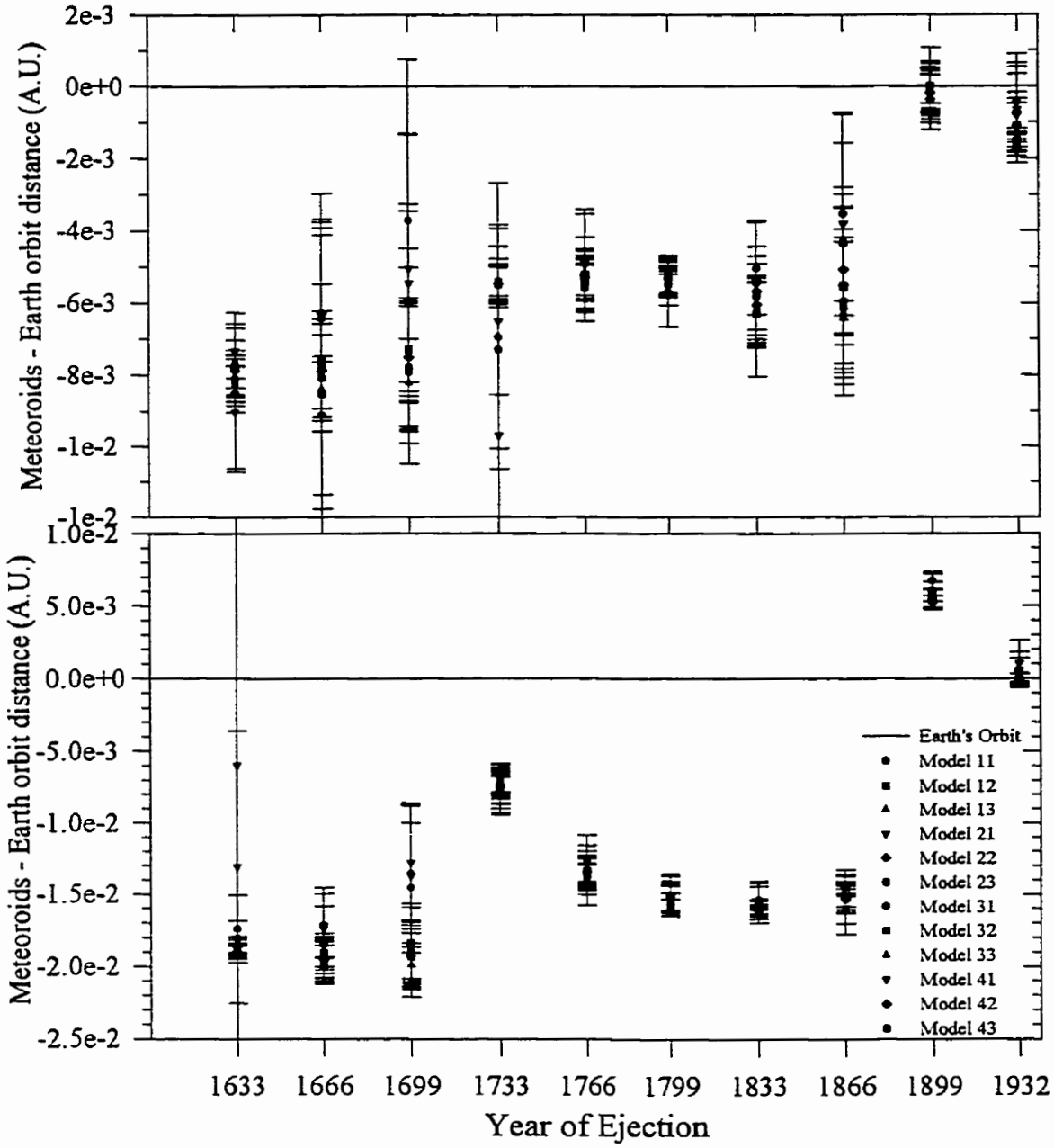

Fig 6.6: Average distance between ejected meteoroids in different years (abscissa) and the Earth at the time of the Leonid storm in 1966 (a) - (top) and the 1969 shower (b)- (bottom). Each model is represented by a different symbol – (see legend). Only test particles within 1 week of the peak of the shower in each year are included. The error margins are the standard deviations in the nodal distances from the sun for each model.

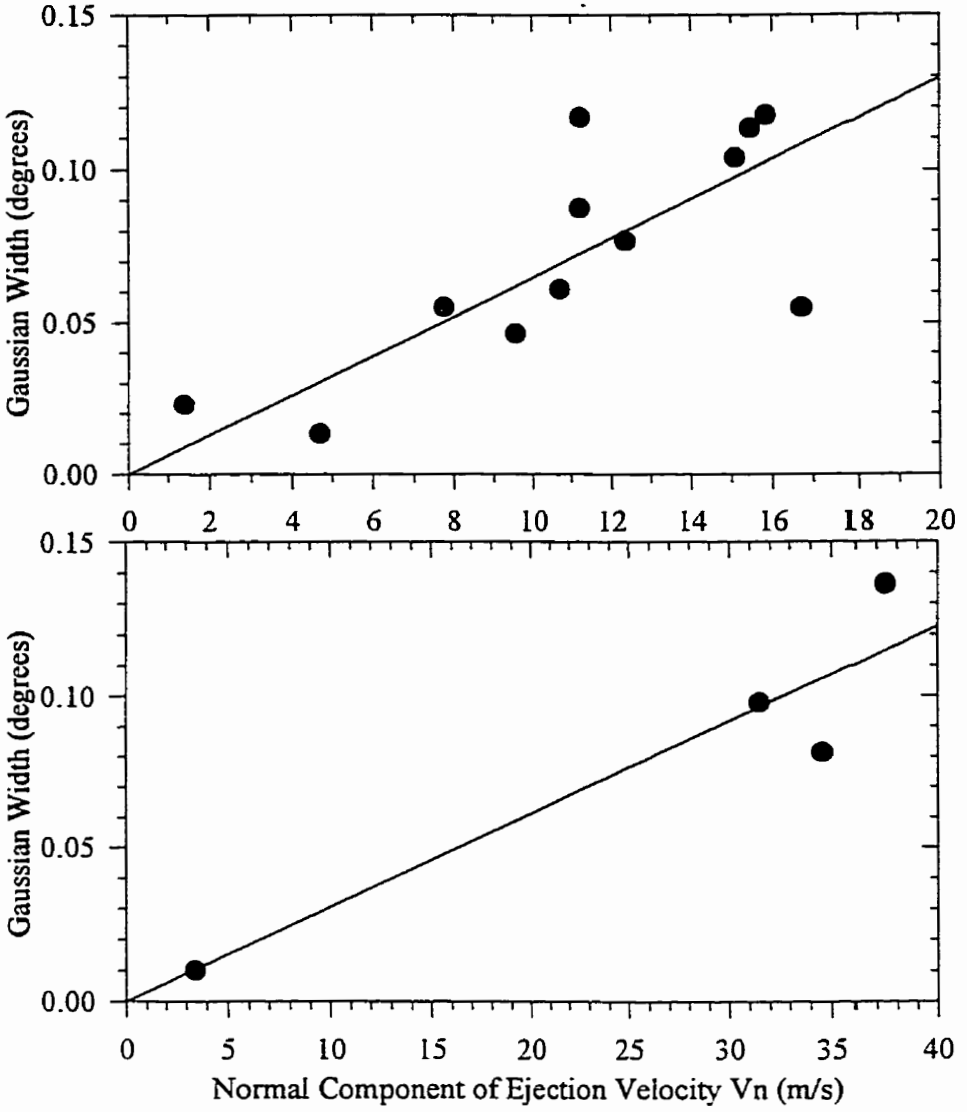

Fig 6.7 (top): The measured gaussian width from all models of the distribution of visual-sized Earth-intersecting meteoroids ejected in 1899 and encountered in 1966 between solar longitude 235.1°-235.2° as a function of the normal component V_n of the initial ejection velocity. Each model is represented by a single solid circle.

Fig 6.8 (bottom): The measured gaussian width from all models of the distribution of visual-sized Earth-intersecting meteoroids ejected in 1932 and encountered in 1969 between solar longitude 235.23°-235.33° as a function of the normal component V_n of the initial ejection velocity.

6.4.2 The 1932 Epoch

Fig 6.9 shows the cumulative number of test particles for models 11-21 as a function of nodal passage time during all Leonid returns from 1833-1998. The figure provides insight into the numbers of Leonid meteoroids passing through the node near the Earth as a function of time; of course the Earth samples only the stream once per year. The numbers of Earth-accessible test particles are significantly lower during the 1932 epoch than in 1965, a direct consequence of the larger comet-Earth orbital distance.

On many of the model outputs, a sharp increase in the number of test particles near the Earth occurs in 1932, near the time of the comet's passage. As well, in all models, this feature is short-lived, lasting only a few months and subsiding before the time of the 1932 shower. As a result, the lack of a major shower/storm during this cycle is unsurprising.

Indeed, from Table 6.3 it is apparent that all shower returns during this interval were dominated by old ejecta - typically 200-300 years in age and certainly not candidates for storms.

The locations of the observed shower maxima in Fig 6.4 for the 1932 epoch show good agreement between observed and theoretical values, particularly considering that the locations of the maxima result from ejections several centuries in age. The largest discrepancies (i.e. 1933) may well be the result of limited observational sampling, there being no observations available between 233.5°-234.5°.

The older activity throughout the 1930's is largely consistent with that expected from the simulations on the basis of the locations and magnitude of the maximum number of accepted test particles as compared to the observed peak ZHRs.

Table 6.3: Age of Leonid showers for a given year as a function of model. The first number in each box is the total number of test particles with nodal radaii within 0.001 A.U. of Earth and nodal passage within 1 week of the Earth's passage. Successive numbers give the primary ejection year contributing to the activity from the model and (in brackets) the fraction of all particles in a particular test year from this ejection.

Model/Year	1930	1931	1932	1933	1934
11	0	1 **1499(1.0)**	11 **1633(.45)** 1566(.27)	1 **1533(1.0)**	5 **1533(.60)** 1899(.40)
12	0	20 **1499(.50)** 1599(.20)	11 **1533(.36)** 1466(.27)	9 **1533(.67)** 1599(.33)	0
13	17 **1699(.94)** 1833(.06)	110 **1499(.35)** 1599(.12)	20 **1533(.40)** 1433(.30)	0	0
21	75 **1699(.49)** 1833(.31)	54 **1499(.28)** 1466(.22)	33 **1699(.33)** 1433(.12)	23 **1533(.57)**	18 **1899(.67)** 1433(.22)
22	74 **1699(.70)** 1833(.22)	122 **1499(.32)** 1466(.20)	26 **1699(.38)** 1433(.19)	11 **1533(.91)** 1599(.09)	1 **1599(1.0)**
23	69 **1699(.87)** 1833(.12)	194 **1499(.30)** 1466(.27)	29 **1433(.38)** 1533(.34)	12 **1533(1.0)**	0
31	31 **1699(.84)**	56 **1499(.27)** 1466(.21)	26 **1533(.54)** 1599(.12)	21 **1533(.81)** 1899(.19)	20 **1899(.75)** 1433(.25)
32	58 **1699(1.0)**	113 **1499(.27)** 1466(.23)	27 **1533(.67)** 1699(.15)	12 **1533(.92)** 1599(.08)	0
33	73 **1699(.99)** 1599(.01)	179 **1499(.39)** 1466(.16)	24 **1533(.71)** 1466(.25)	12 **1533(1.0)**	0
41	44 **1699(.50)** 1633(.20)	64 **1499(.39)** 1466(.16)	16 **1533(.50)** 1433(.19)	22 **1533(.73)** 1599(.05)	17 **1899(.76)** 1433(.18)
42	50 **1699(.80)** 1833(.14)	92 **1499(.35)** 1466(.25)	23 **1533(.57)** 1466(.17)	11 **1533(1.0)**	0
43	60 **1699(.90)** 1833(.07)	168 **1499(.26)** 1466(.24)	18 **1533(.72)** 1466(.17)	5 **1533(1.0)**	0

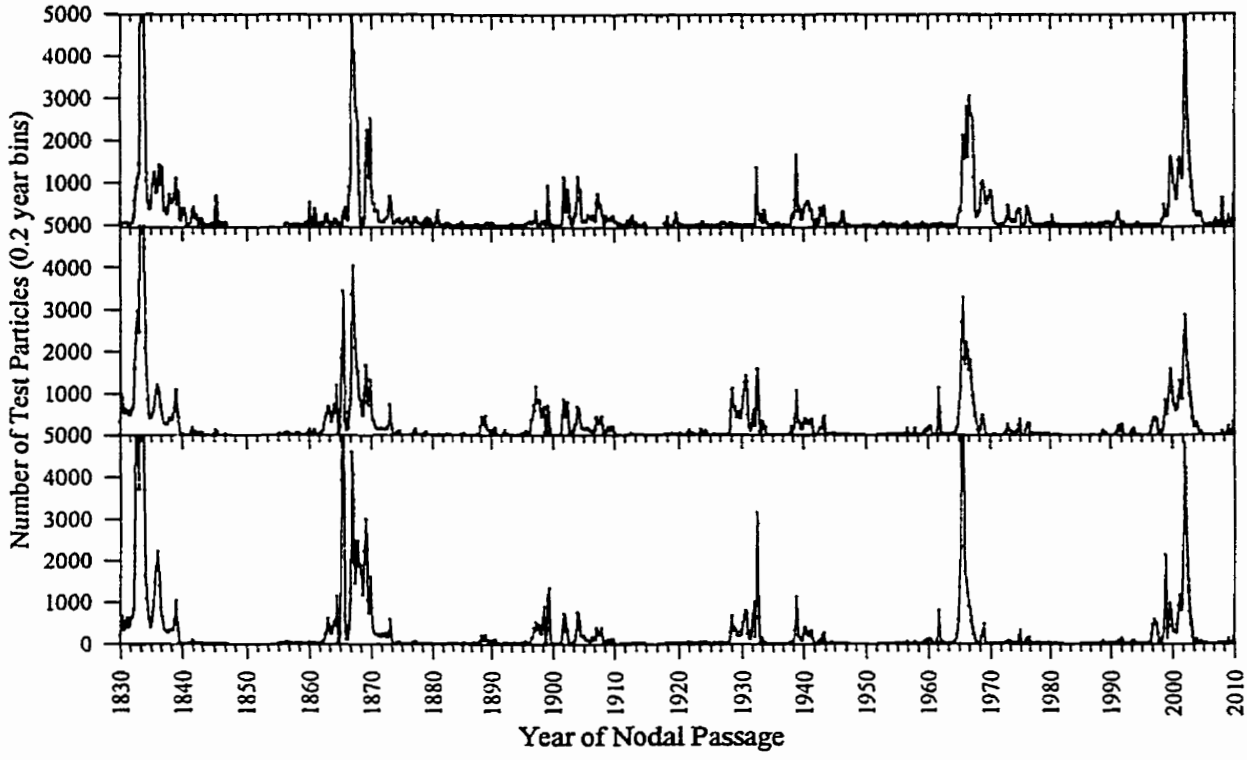

Fig 6.9: Total number of visual-sized test particles per 0.2 years for models 11 (top), 22 (middle) and 43 (bottom) that are within 0.001 A.U. of Earth's orbit.

6.4.3 The 1899 Epoch

As with the 1933 epoch, the 1899 epoch is most notable for its relatively weak activity and lack of any strong storms. However, the late occurrence of two modest showers in 1901 and 1903 did make the interval more active than in the 1930s. For the three years that had some observational determination of the location of peak activity (from Brown, 1999) and some test particles present, we plot these in Fig 6.5. Note that the 1898 display while observed to be relatively strong, had no test particles from any models "accepted" from the last 15 perihelion passages; it is probable that this return is older than 500 years.

The location of the peak in 1899 is uncertain for both the models (due to the small number of test particles involved) and also the observations due to the broad, flat level of

observed activity. The exact locations of the 1901 and 1903 shower peaks are somewhat uncertain observationally as a result of poor longitude coverage, but the agreement with the models is satisfactory.

Activity throughout this epoch is dominated by relatively strong perturbations from both Jupiter and Saturn in 1898 and 1895 respectively, an effect noted at the time (cf. Stoney and Downing, 1899). The net result of these two combined perturbations is to move most of the material nearest the nodal passage of the comet well inside the Earth's orbit. Fig 6.10 shows the distribution of nodal distances as a function of nodal passage times for meteoroids from models 11 and 32. This effect also shows up in the distribution of the total number of Earth-accessible meteoroids as a function of time of nodal passage as given in Fig 6.4. Note the gap from 1900-1901 and a smaller gap in early 1899 as well as the relatively small number of test particles involved compared to the 1966 and 1932 epochs.

Table 6.4 shows the breakdown of material and ages for each of these returns. None of the years had any significant contribution from recent passages; indeed, the 1901 display is likely the result of material ejected either in 1733 or 1566 while the 1903 display is most probably from material ejected in 1499-1533. For both these years, the material being of order 5-10 revolutions in age suggests lower fluxes (relative to storm years) and very modest activity at best (see section 4 for more details). Fig 6.11 shows the distance from Earth to past trails in 1901 and for the 1903 shower in Fig 6.12. Note that the location of the maximum in solar longitude is the only discriminant for the age of the ejection responsible for the 1901 display, with the 1566 ejection peaking some 0.2° later than both the observed peak and the peak associated with 1733 meteoroids. This highlights the uncertainty of using close approach distances between past ejections and current activity alone to judge the age of a given return.

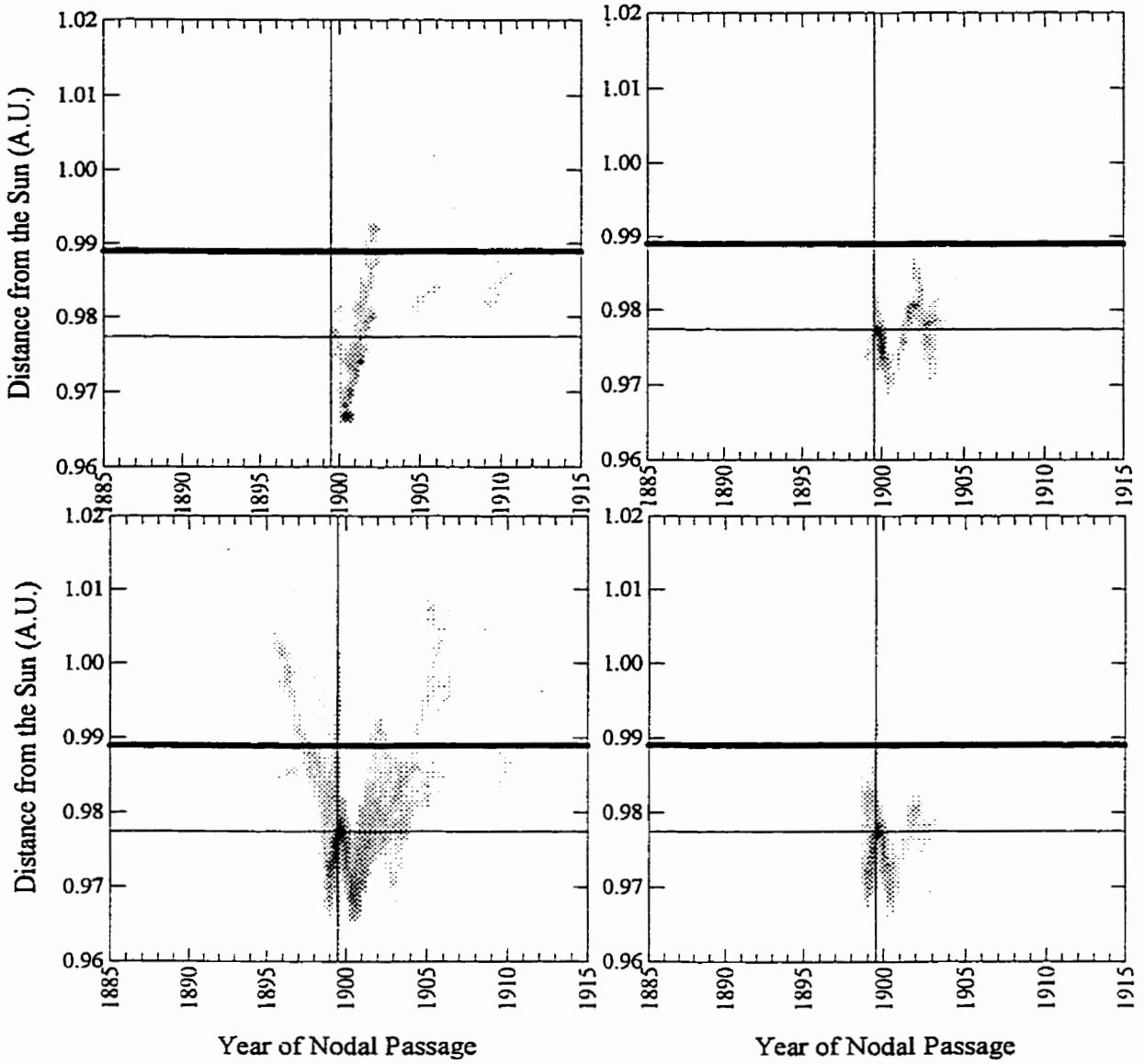

Fig 6.10: Test particle nodal distributions at the 1899 epoch for model 11 meteoroids of mass 10^{-1} g ($\beta=10^{-3}$) (top left), 10 g ($\beta=2\times10^{-4}$) (top right) and for model 32 meteoroids of mass 10^{-3} g ($\beta=10^{-3}$) (bottom left) and 10 g ($\beta=5\times10^{-5}$) (bottom right). The bold line is the distance of the Earth from the Sun on Nov 17 each year and the intersection of the thin lines marks the nodal crossing time and distance for 55P/Tempel-Tuttle during the 1899 epoch. The distributions represent the summation of all ejections from 1399 – 1866 A.D. for these particular mass categories.

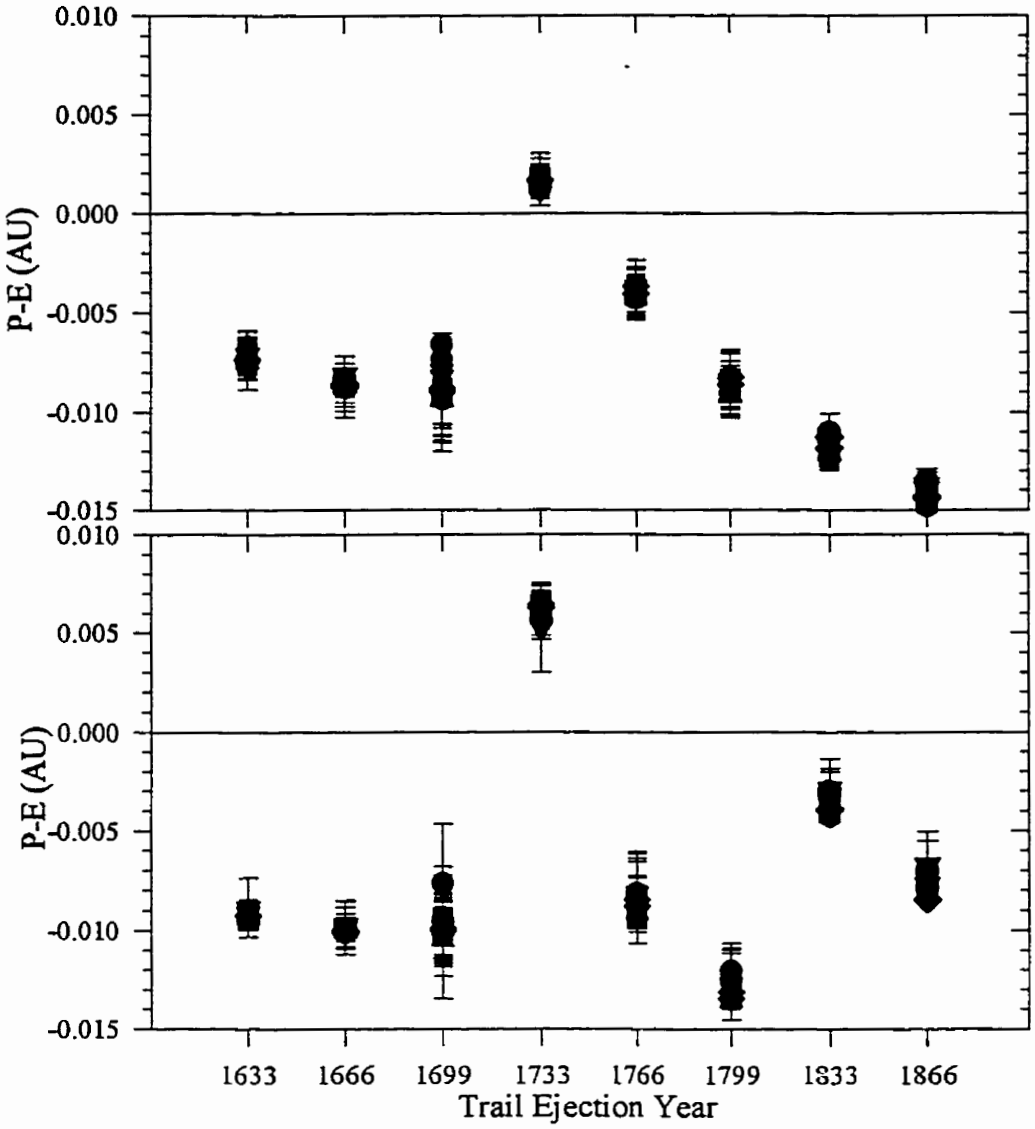

Fig 6.11 (top): Average distance between meteoroids ejected in different years (abscissa) and the Earth at the time of the Leonid shower in 1901. The model-symbol correspondence is the same as Fig 6.6. The error margins represent the standard deviations in the nodal distances from the sun for each model.

Fig 6.12 (bottom): Average distance between meteoroids ejected in different years (abscissa) and the Earth at the time of the Leonid shower in 1903. The model-symbol correspondence is the same as in Fig 6.6. The error margins represent the standard deviations in the nodal distances from the sun for each model.

Table 6.4: Age of Leonid showers for a given year as a function of model. The first number in each box is the total number of test particles with nodal radaii within 0.001 A.U. of Earth and nodal passage within 1 week of the Earth's passage. Successive numbers give the primary ejection year contributing to the activity from the model and (in brackets) the fraction of all particles in the year from this ejection.

Model/Year	1899	1901	1903
11	3 **1399(.67)** 1566(.33)	109 **1733(.39)** 1399(.17)	87 **1499(.23)** 1533(.22)
12	0	104 **1566(.55)** 1399(.17)	103 **1533(.50)** 1499(.17)
13	0	86 **1566(.55)** 1399(.24)	47 **1533(.49)** 1566(.19)
21	2 **1399(.50)**	58 **1733(.38)** 1766(.16)	49 **1533(.39)** 1499(.16)
22	0	68 **1399(.26)** 1566(.21)	65 **1533(.49)** 1499(.17)
23	2 **1566(.50)**	56 **1566(.36)** 1399(.32)	55 **1533(.56)** 1499(.11)
31	1 **1599(1.0)**	73 **1733(.40)** 1766(.16)	58 **1533(.45)** 1466(.14)
32	1 **1599(1.0)**	67 **1566(.36)** 1399(.22)	67 **1533(.63)** 1566(.12)
33	0	76 **1566(.50)** 1399(.22)	49 **1533(.47)** 1566(.24)
41	3 **1599(.33)** 1566(.33)	64 **1733(.38)** 1399(.19)	64 **1533(.31)** 1499(.22)
42	0	76 **1566(.32)** 1599(.20)	73 **1533(.55)** 1566(.14)
43	0	88 **1566(.61)** 1399(.17)	58 **1533(.50)** 1399(.17)

6.4.4 The 1866 Epoch

The 1866 epoch produced two Leonid meteor storms (1866, 1867) and at least one strong shower (1868). It also marked the first occasion when sufficient visual data were collected and recorded to produce activity profiles. Fig 6.13 plots the nodal radius as a function of nodal passage time for models 33 and 41 meteoroids with $10^{-5} < \beta < 4\times10^{-3}$. The densest portions are similar in shape to the previous epochs, namely a slight increase in nodal radius with time visible in all models and at all masses due to differential perturbations from Jupiter (principally) as well as Saturn. To demonstrate the significance of these perturbations on the observability of the stream at the 1866 epoch, Fig 6.14 a,b,c shows the nodal radius-time plot for material ejected in 1733 for model 22 meteoroids of mass 10^{-3}g ($\beta=10^{-3}$). The top plot is the actual distribution, the middle plot removes direct perturbations from Jupiter and the final plot eliminates both Jupiter and Saturn's influence. The accessibility of meteoroids from this ejection is entirely due to distant perturbations from Jupiter and Saturn, which moved nodes outward during the four revolutions since ejection, as was found for the 1966 storm. Other models and different β show very similar behaviour.

Table 6.5 shows the makeup of test particles as accepted from each model for the years 1865-1868. From Fig 6.4, only 1866 and 1867 have well-determined peak locations in agreement with the theoretical values; 1865 had very poor observer coverage (and was weak in the modelled activity) and 1868 shows a very broad maximum with poor longitude coverage, making its position uncertain by at least several hours.

The weak 1865 shower is likely caused by ejections in the time period 1533-1599 with no recent material evidently accessible in that year.

The storm of 1866 is almost certainly due to meteoroids ejected in any or all of 1733/1766/1799, with 1733 predominating when all solar longitudes are summed. A breakdown of the summation of the modelled meteoroids in a narrow window of three hours, centred on the measured position of the 1866 storm, shows a more even split among the three ejection years. It is probable that the 1866 storm was the result ofl material from at least two and possibly three ejections. Significantly, for the three hour

window nearest the peak, the sum of material from 1733-1766-1799 represented 95% or more of the total sum for all test particles from the last 500 years for all models.

The peak locations of the model activity profiles and the observed 1866 storm differ by approximately one hour (the model predictions being earlier near the node), more than the time difference found for the 1966 storm. This might be a significant effect, though it is close to the level of binning used.

The width of the storm profiles is assumed to be primarily the result of ejection velocities (cf. Kresak, 1992). In Fig 6.15 we show the final gaussian width of each modelled profile in 1866 for each particular ejection and the average normal component of the ejection velocity for the associated material in 1866. This is shown for each of the ejection epochs 1733, 1766 and 1799. It is clear that very low normal velocities are associated with very narrow peaks (as expected), but the spread at slightly larger widths for the 1733 ejection is more surprising. It is clear that the 1799 and 1766 ejections have small widths and exhibit the behaviour expected, with small increases in the average normal velocity component associated with similarly small increases in the final measured activity widths. For 1733 this pattern completely breaks down, with all models showing much larger widths at a given velocity than either of 1799 or 1766 and no correlation remaining between the initial ejection velocities and the nodal dispersions. Heuristically we expect some small increase in the width of the distribution over time due to planetary perturbations (though this is the opposite of what happens between the 1766 and 1799 ejections) but clearly this is an order of magnitude larger change than would be expected based on the observed differences between 1766 and 1799. In fact, planetary perturbations from Saturn and Jupiter acting solely on the 1733 ejecta near Tempel-Tuttle's 1733 and 1766 perihelion passages are entirely responsible for the rapid "dispersal" of this material normal to the stream's orbital plane. This is a prime example of a "trail" disconnection or dispersal caused by planetary perturbations (see Sect. 6.5) and underscores the possible pitfalls in using wider (weaker) Leonid showers to measure initial ejection velocities.

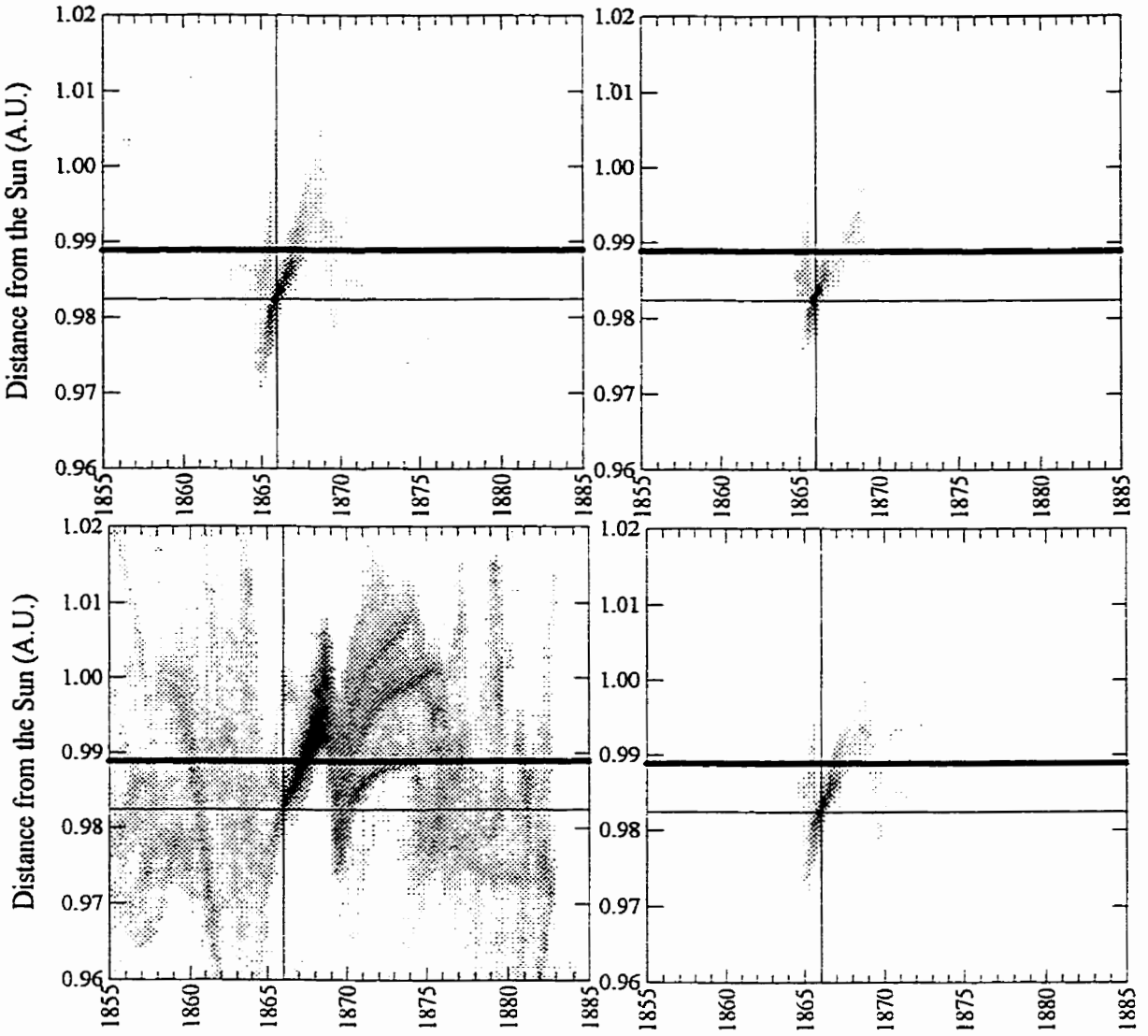

Fig 6.13: Test particle nodal distributions at the 1866 epoch for model 33 meteoroids of mass 10^{-3} g ($\beta=3\times10^{-4}$) (top left), 10 g ($\beta=2\times10^{-5}$) (top right) and for model 41 meteoroids of mass 10^{-3} g ($\beta=10^{-3}$) (bottom left) and 10 g ($\beta=2\times10^{-4}$) (bottom right). The bold line is the distance of the Earth from the Sun on Nov 17 each year and the intersection of the thin lines marks the nodal crossing time and distance for 55P/Tempel-Tuttle during the 1866 epoch. The distributions represent the summation of all ejections from 1366 – 1832 A.D. for these particular mass categories.

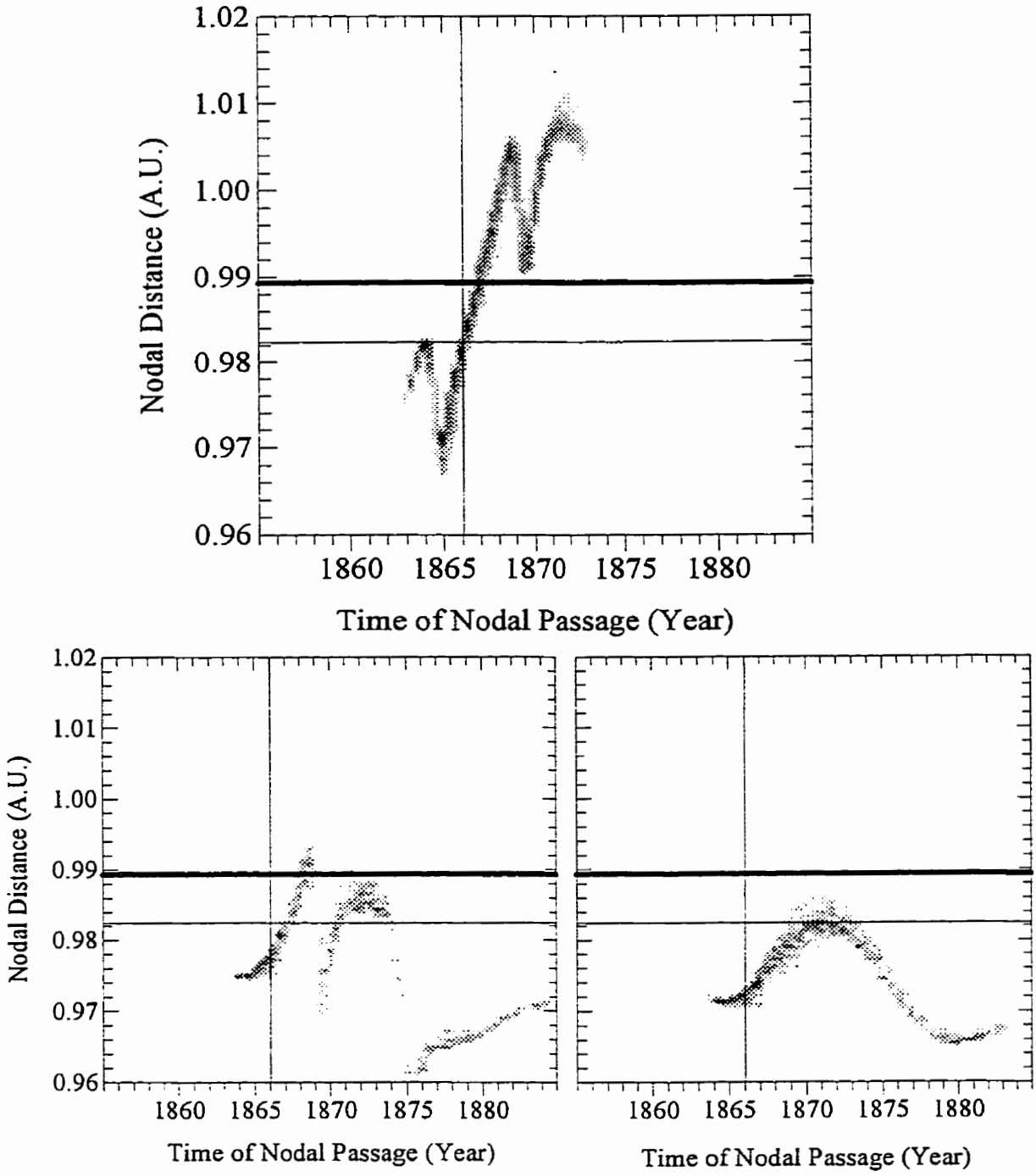

Fig 6.14: Nodal distribution for meteoroids ejected in 1733 using model 22 with a mass of 10^{-3} g at the 1866 epoch with all planetary perturbations (top), without Jupiter (bottom - left) and without Jupiter or Saturn (bottom – right).

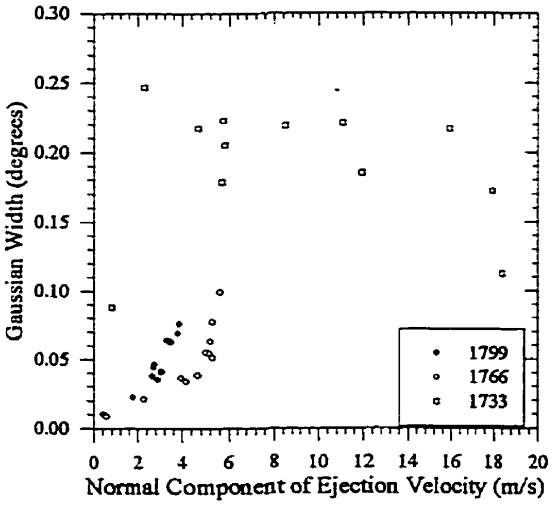

Fig 6.15 (top): The measured gaussian width, for all models of the distribution of visual-sized Earth-intersecting meteoroids ejected in 1733-1799 and encountered in 1866 between solar longitude 233.2°-233.4° as a function of the normal component V_n of the initial ejection velocity.

Fig 6.16 (below): The measured gaussian width, from all models of the distribution of visual-sized Earth-intersecting meteoroids ejected in 1832 and encountered in 1867 between solar longitude 233.3°-233.5° as a function of Vn.

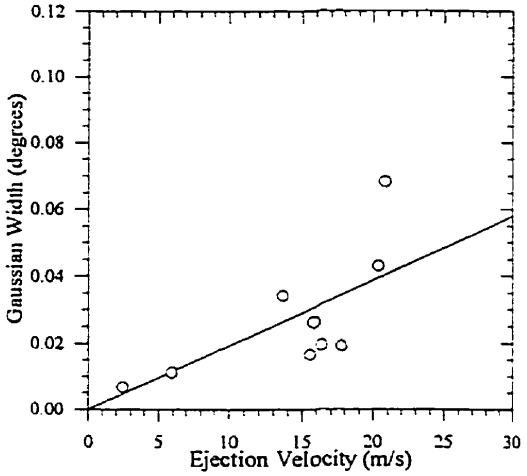

Table 6.5: Age of Leonid showers for a given year as a function of model. The first number in each box is the total number of test particles with nodal radaii within 0.001 A.U. of Earth and times of nodal passage within 1 week of the Earth's passage through the stream. The following numbers give the primary year contributing to the activity from the model and (in brackets) the fraction of all particles in a particular test year from this ejection.

Model/Year	1865	1866	1867	1868
11	63 **1599(.52)** 1566(.24)	816 **1733(.54)** 1766(.25)	268 **1833(.57)** 1699(.16)	68 **1833(.50)** 1566(.18)
12	59 **1599(.32)** 1566(.20)	1065 **1733(.64)** 1799(.16)	481 **1666(.38)** 1699(.25)	1095 **1466(.21)** 1499(.20)
13	39 **1599(.41)** 1533(.23)	854 **1733(.67)** 1766(.16)	533 **1666(.40)** 1699(.28)	997 **1533(.21)** 1599(.17)
21	23 **1599(.17)** 1533(.17)	407 **1733(.48)** 1766(.22)	252 **1833(.64)** 1666(.10)	180 **1833(.33)** 1533(.12)
22	22 **1566(.27)** 1533(.14)	780 **1733(.47)** 1766(.25)	269 **1833(.35)** 1666(.17)	255 **1833(.12)** 1533(.15)
23	31 **1566(.23)** 1533(.19)	1081 **1733(.61)** 1799(.19)	292 **1666(.30)** 1699(.25)	401 **1599(.15)** 1566(.15)
31	18 **1533(.33)** 1366(.28)	605 **1733(.41)** 1799(.32)	230 **1833(.55)** 1699(.10)	173 **1833(.36)** 1499(.12)
32	29 **1566(.24)** 1366(.17)	895 **1733(.53)** 1799(.22)	288 **1833(.29)** 1666(.23)	292 **1533(.17)** 1599(.14)
33	26 **1599(.27)** 1366(.23)	1055 **1733(.65)** 1799(.16)	384 **1666(.39)** 1699(.24)	448 **1533(.17)** 1599(.15)
41	24 **1599(.29)** 1566(.29)	564 **1733(.43)** 1799(.26)	228 **1833(.60)** 1666(.11)	179 **1833(.32)** 1599(.03)
42	32 **1599(.22)** 1466(.25)	924 **1733(.53)** 1799(.21)	336 **1833(.25)** 1666(.24)	354 **1533(.15)** 1599(.12)
43	27 **1533(.33)** 1599(.26)	953 **1733(.65)** 1766(.17)	457 **1666(.41)** 1699(.23)	579 **1533(.19)** 1599(.16)

Based on these results, the storm of 1866 is most probably due to material from 1766 and/or 1799, the 1733 material being much less concentrated than that of the other two returns. Its predominance in the overall breakdown of the dominant ejection years from 1866 is understandable given that we are integrating its activity over the entire range of solar longitudes in 1866; in the smaller intervals associated with the 1866 storm, 1799 and 1766 ejections prevail.

Assuming the ejections in 1799/1766 caused the 1866 storm, the observed width in 1866 near 0.02° would imply average normal components of ejection velocity of at most 1-3 m/s at most based on our modelling results. This finding is consistent with total average ejection velocities of order 5 m/s, very similar to that found for the 1966 storm.

The range of β from 1799 and 1766, from our initial ejection models which "compose" the 1866 storm are relatively limited, (though the distribution is wider than for the 1966 storm), with a strong peak near 2×10^{-4} and an overall range from $8\times10^{-5} < \beta < 4\times10^{-4}$. Examination of the orbital locations of ejection in these peak β intervals shows no concentration in true anomaly analogous to the 1966 storm ejecta from 1899.

The 1867 storm is interesting as it appears to be from younger material than 1866 (i.e. only one revolution old). As this storm lagged behind the comet by almost two full years, it is unsurprising (and indeed required) that the β are all higher than in 1866, with a peak near 10^{-3} and a range from 4×10^{-4} to 2×10^{-3}.

Fig 6.16 shows the equivalent gaussian widths of the 1833 ejecta in 1867 versus the normal component of the ejection velocity, to be, on average, higher than 1866 for a given solar longitude width (as expected for younger ejecta). The relation between width of the final distribution and ejection velocity is not as precise as for the material making up the 1866 return, in large part due to the smaller number of test particles available (a factor of 2-5 less than in 1866 depending on the model). As well, the sharp peaks for such young ejecta are nearer in width to the bin size used (0.005 degs in solar longitude). The observed width of the 1867 storm (0.022°) corresponds to material which has normal components of ejection of ~10 m/s and total ejection velocities of 15-20 m/s.

The 1868 shower shows no distinct peak or maximum in the observations, though typical model results (Fig 6.17) suggest a broad peak in activity should have occurred. The

observed broad maximum for the short sampling time of the observations (~5 hours) does not contradict this result and suggests that this material may have been quite old, though no single ejection era is particularly dominant in 1868 (see Table 6.6).

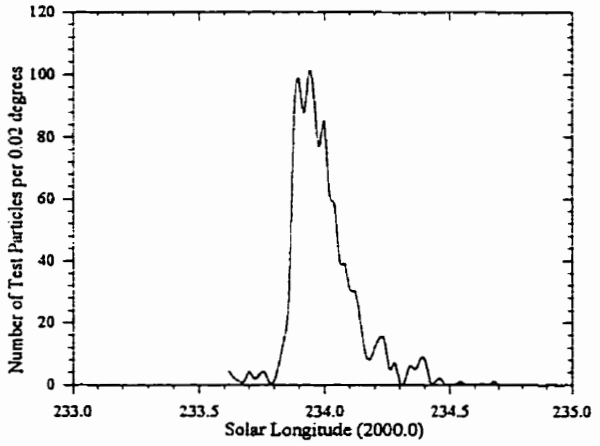

Fig 6.17: Number of visual-sized Earth-intersecting test particles as a function of solar longitude in 1868 for model 12.

6.4.5 The 1833 Epoch

The storms of 1832 and 1833 were not well documented. Other than an approximate time of maximum for both (see Brown, 1999), no clear activity profile is available.

From the computed nodal distribution it is determined that the densest portion of the stream passes very close to Earth's orbit in 1833. The characteristic upward sloping nodal distance (due to distant direct perturbations from Jupiter) is visible as in the previous epochs studied.

From Fig 6.9, it is notable that the maximum numbers reached in this interval for all models is a factor of several above most previous epochs, attesting to the high delivery efficiency in this era. The peak in test particle flux is reached in 1833 between the times of

the 1832 and 1833 storms.

The 1832 storm appears to have been long-lived (Brown, 1999) and the particle makeup in this year supports an origin of at least four or five revolutions in age for the shower/storm of 1832. Table 6.6 lists the years contributing to the integrated flux over all solar longitudes in 1832. It is clear that older material (particularly from 1666) dominates the fluence. Fig 6.18a shows the location of the last six ejection "trails" in 1832 relative to the Earth's orbit. The 1699 and 1666 trails are clearly closest to Earth in 1832, explaining the results in Table 6.7. Fig 6.19a shows the stream activity profile for model 12 on November 12/13, 1832. The activity lasts almost twelve hours in general accord with observations. The discrepancy between the relative youth of the trails and the large spread in nodal longitudes is, in part, a consequence of inbound perturbations by Jupiter on the section of these trails in 1732. Note that all models have significant numbers of test particles in 1832 only for values of $\beta<5\times10^{-4}$.

The 1833 storm is most likely the result of the 1799 ejection. Table 6.6 shows clearly the dominance of this population near the Earth on Nov 13, 1833. Fig 6.18b shows the trail locations in 1833 for ejections back to 1633. Note that while 1799 is marginally closer than the previous three trails, the increased diffusion for the older trails lessens their relative contributions compared to 1799. The distribution of test particle masses in 1833 is shown in Fig 6.19b. It is clear from the figure that the majority of the test particles are encountered near 233.17°, less than 0.5 hours from the estimated time of maximum (cf. Brown, 1999). A broader distribution covering all masses is also apparent in this and other models and may explain the reports of heightened activity for several hours on either side of the main maximum.

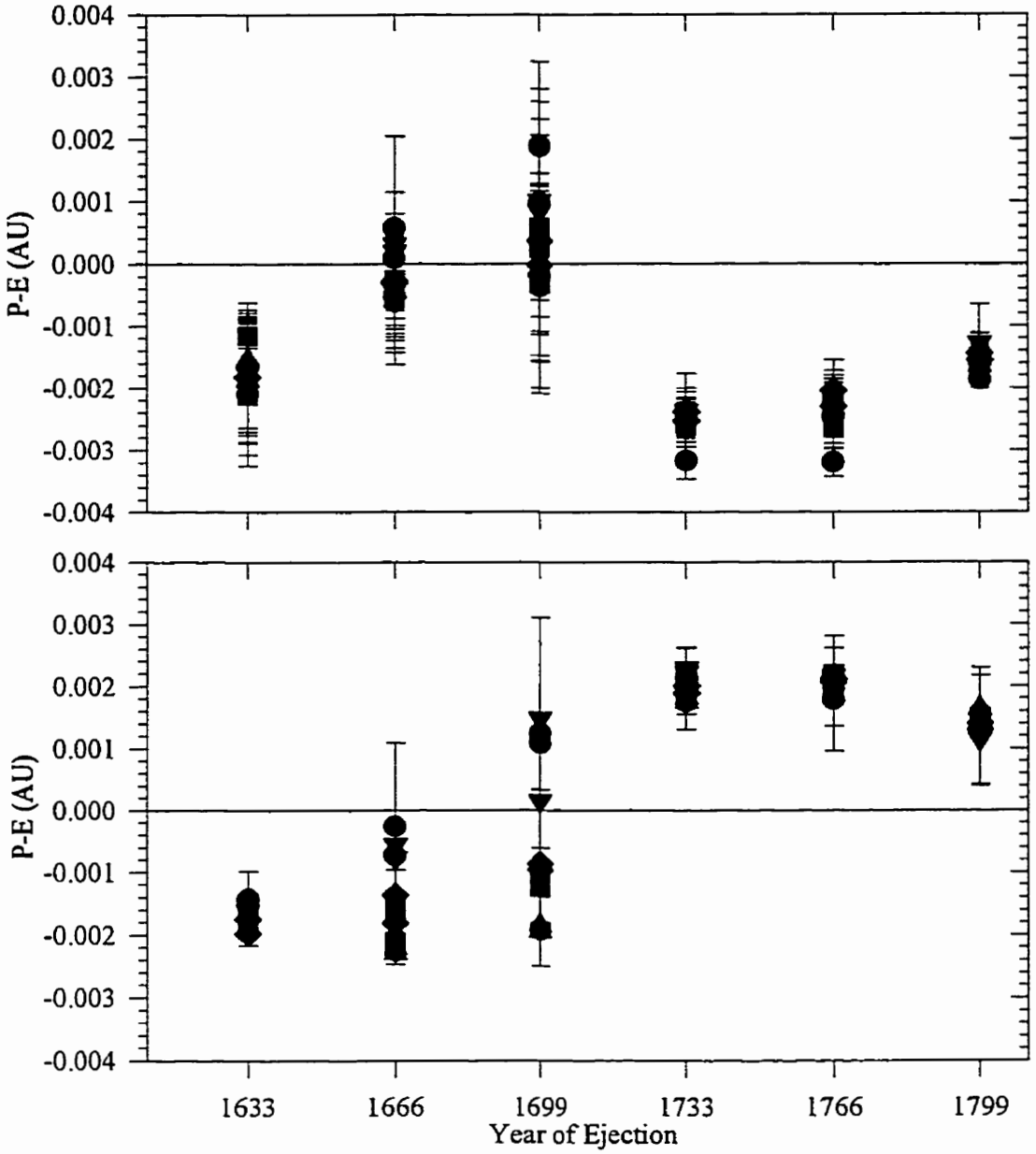

Fig 6.18: Average distance between ejected meteoroids in different years (abscissa) and the Earth at the time of the Leonid storm in 1832 (a) - (top) and the 1833 shower (b)- (bottom). Symbol-model correspondence is the same as in Fig 6.6. Only test particles within 1 week of the peak of the shower in each year are included. The error margins represent the standard deviations in the nodal distances from the sun for each model.

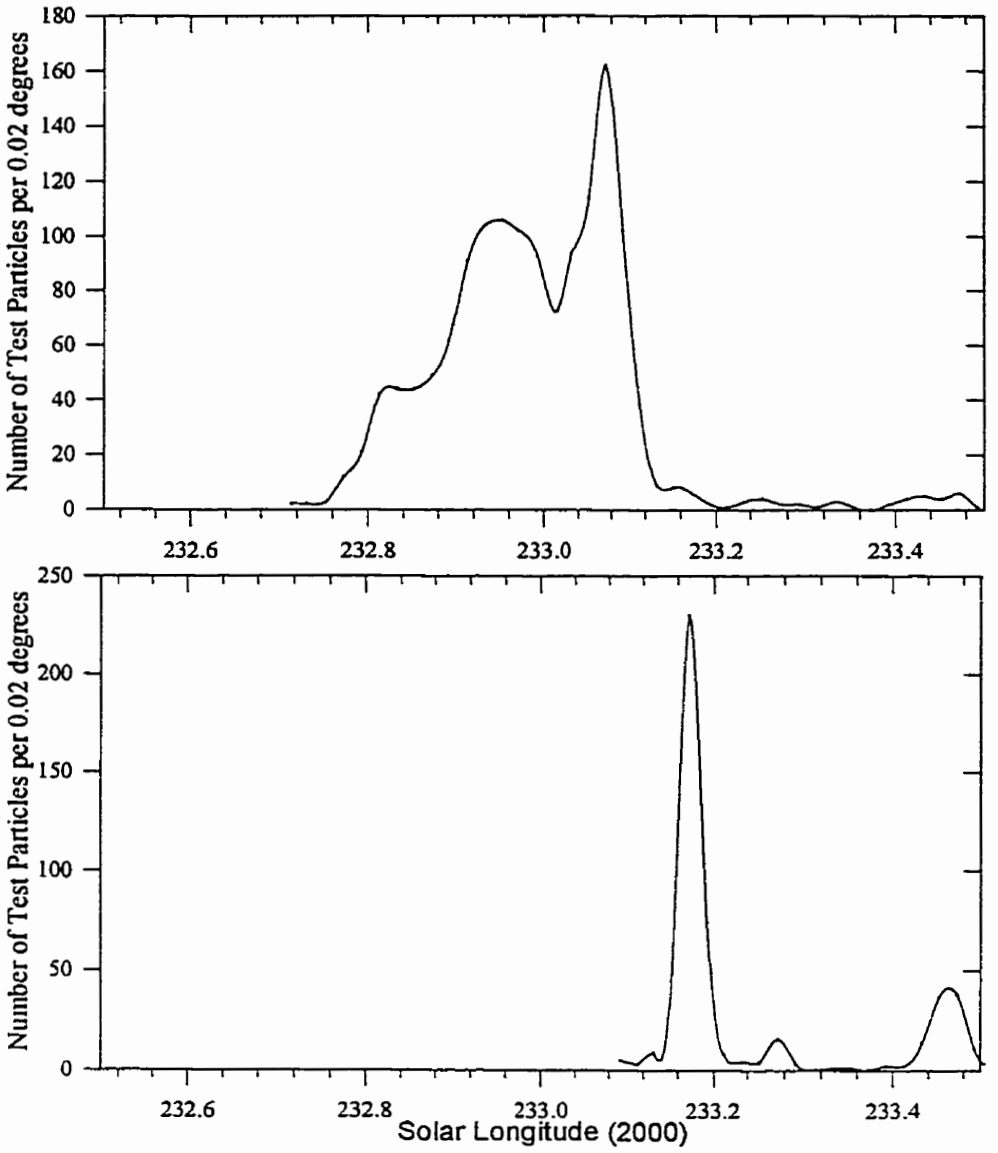

Fig 6.19: Number of Earth-intersecting test particles as a function of solar longitude in 1832 (a – top) and in 1833 (b- bottom) for model 12 meteoroids.

Table 6.6: Age of Leonid showers for a given year as a function of model. The first number in each box is the total number of test particles with nodal radaii within 0.001 A.U. of Earth and times of nodal passage within 1 week of the Earth's passage through the stream. The following numbers give the primary year contributing to the activity from the model and (in brackets) the fraction of all particles in a particular test year from this ejection. Columns for 1832a and 1833a refer to only those meteoroids between 233-233.3°.

Model/Year	1832	1833	1832a	1833a
11	278 **1666(.85)** 1399(.06)	832 **1799(.67)** 1766(.12)	31 **1399(.52)** 1333(.23)	672 **1799(.83)** 1766(.15)
12	1439 **1666(.37)** 1699(.27)	609 **1799(.56)** 1733(.13)	343 **1366(.18)** 1333(.17)	402 **1799(.85)** 1766(.10)
13	1871 **1666(.28)** 1699(.23)	390 **1799(.33)** 1733(.32)	686 **1399(.22)** 1333(.16)	150 **1799(.85)** 1766(.07)
21	417 **1799(.25)** 1666(.21)	572 **1799(.70)** 1766(.12)	168 **1799(.35)** 1333(.14)	394 **1799(.85)** 1766(.12)
22	583 **1666(.32)** 1633(.13)	548 **1799(.64)** 1733(.11)	207 **1799(.20)** 1333(.16)	363 **1799(.87)** 1766(.10)
23	815 **1666(.26)** 1699(.15)	434 **1799(.54)** 1733(.17)	321 **1399(.25)** 1333(.17)	269 **1799(.88)** 1766(.09)
31	397 **1666(.39)** 1799(.15)	519 **1799(.71)** 1766(.08)	141 **1799(.36)** 1399(.12)	349 **1799(.87)** 1766(.09)
32	665 **1666(.35)** 1699(.14)	541 **1799(.65)** 1733(.12)	233 **1799(.15)** 1333(.17)	373 **1799(.90)** 1766(.06)
33	862 **1666(.31)** 1699(.21)	396 **1799(.44)** 1733(.28)	291 **1399(.24)** 1433(.16)	191 **1799(.92)** 1766(.06)
41	460 **1666(.35)** 1699(.16)	499 **1799(.70)** 1766(.09)	154 **1799(.29)** 1399(.15)	344 **1799(.88)** 1766(.10)
42	796 **1666(.34)** 1699(.15)	537 **1799(.59)** 1733(.10)	270 **1399(.19)** 1433(.16)	345 **1799(.88)** 1766(.10)
43	1126 **1666(.31)** 1699(.20)	423 **1799(.42)** 1733(.28)	396 **1399(.22)** 1433(.16)	210 **1799(.84)** 1766(.09)

6.5 Long-term Integrations

In an effort to understand the longer term dynamics of the stream over an interval comparable to the full duration of its observed activity (first recorded in 902 A.D.), we have used the ephemeris of Tempel-Tuttle back to 82 A.D. and generated test particles for each perihelion passage for model 22. This represents a total of 57 perihelion passages of the comet. Each passage had 10 000 particles ejected at each of the seven decadal masses as in all other integrations. The integrations were stopped and information on each test particle stored at the nodal passage closest to the current epoch (1998). We have chosen model 22 as this was found to be the model most successful in reproducing Perseid activity in Brown and Jones (1998), without knowing *a priori* if the model will also be representative of the Leonids.

Fig 6.20 shows the fraction of all Leonids from each past ejection accessible to Earth (i.e. having nodes within 0.001 A.U.) at the present epoch (as a fraction of the total), along with the distance between the Earth's and the comet's orbit.

Two distinct temporal regimes are apparent: ejections since 1100 A.D. and those before. Through a combination of the longer time available for diffusion for old ejecta and (for ejections prior to 850 A.D.) larger distances from Earth's orbit, the older ejecta contribute significantly less on an ejection-by-ejection basis than does more recent material (as would be expected). The very small number of particles accessible prior to ~1100 A.D. suggests that the "annual" activity from the stream is due to material with an effective age of this order (roughly 1 millenium).

Interestingly, for most ejections since 1100 A.D. there is only a weak correlation between the total number of particles visible at the present epoch and the distance between the Earth's and comet's orbit. While the largest numbers are from ejections where the comet's orbit is inside the Earth's, the difference is marginal compared to slightly older ejecta where the comet's orbit is outside the Earth's. Much of the material in the 1100-1500 A.D. range which ends up at Earth, has small β (i.e. large meteoroids).

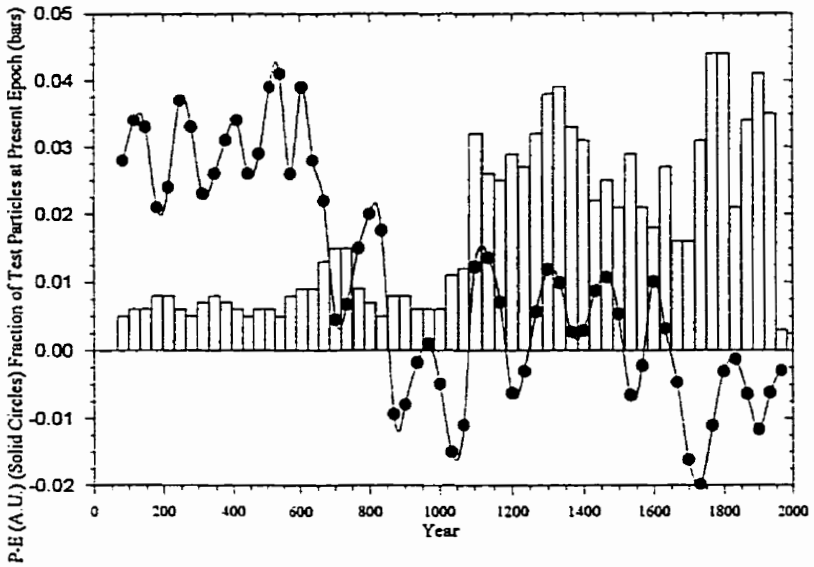

Fig 6.20 (above): The fraction of all visual-sized Leonid meteoroids within 0.001 A.U. of the Earth (at the 1998 epoch) as a function of the epoch of their ejection (bars). The solid line and circle represent the distance between the cometary node and the Earth referenced to the time of perihelion at each epoch.

Fig 6.21 (below): The fraction of visual-sized Leonid meteoroids within 0.001 A.U. of the Earth at the 1998 epoch for three different models over the last 500 years.

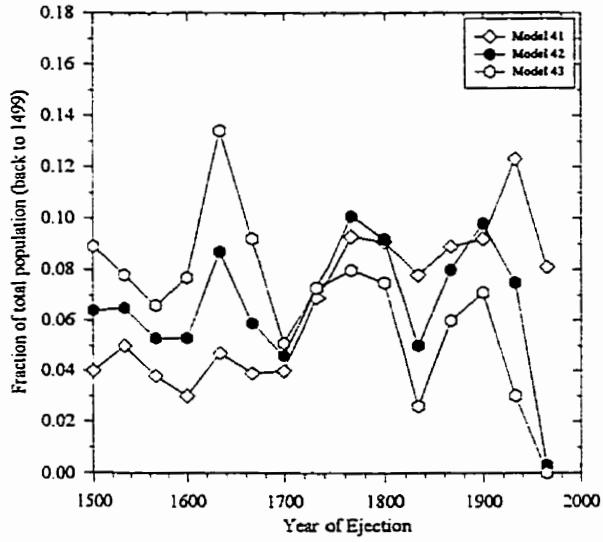

For ejection times from 300-500 years before the present, a distinct trend is visible in all models, such that higher densities (lower β's) are associated with larger numbers of particles currently visible at Earth. For ejections less than 300 years in age, no clear density-dependent sorting is in evidence as shown in Fig 6.21. This may be an effect of faster diffusion for higher β driven by differential planetary perturbations.

Thus, in terms of the total number of particles accessible at present to the Earth presently, the comet-Earth distance is only of secondary importance. This is likely a direct result of the fact that, throughout almost all of this interval, the comet orbit-Earth distance has been very small and so nodal diffusion (due to planetary perturbations), on time-scales from < tens of revolutions dominate the slight changes in comet-Earth distance (except potentially for the oldest ejecta where the distances become large and for the very concentrated young material which Earth can only intersect if it is sufficiently close to the comet's orbit).

It is important to note that the total number of test particles currently "intersecting" the Earth's orbit from a given ejection as we have measured it is not directly correlated with the magnitude of the resulting peak activity, but rather is a crude measure of the integrated flux along the orbit (i.e. integrated in mean anomaly) and across it (i.e. integrated in solar longitude). To determine the probable peak flux and significance of recent ejections, it is necessary to quantify the average decrease in flux at the node for the stream as a whole - that is, measure the dilution along the orbit (due to spreading caused by differing periods), across it (due to diffusion in the nodal longitude) and perpendicular to the stream orbit in a radial direction (spread in nodal distances).

To examine the question of diffusion in more detail, we have computed the average standard deviation, σ, of ascending node, nodal distance from the sun and mean anomaly in the elements for all visual-sized Leonid meteoroids (referenced to their nodal passages). The resulting distributions over the last 2000 years for model 22 are shown in Figs 6.22, 6.23 and 6.24 respectively. These are the standard deviations in the plotted quantities for individual (not cumulative) ejections for the years specified.

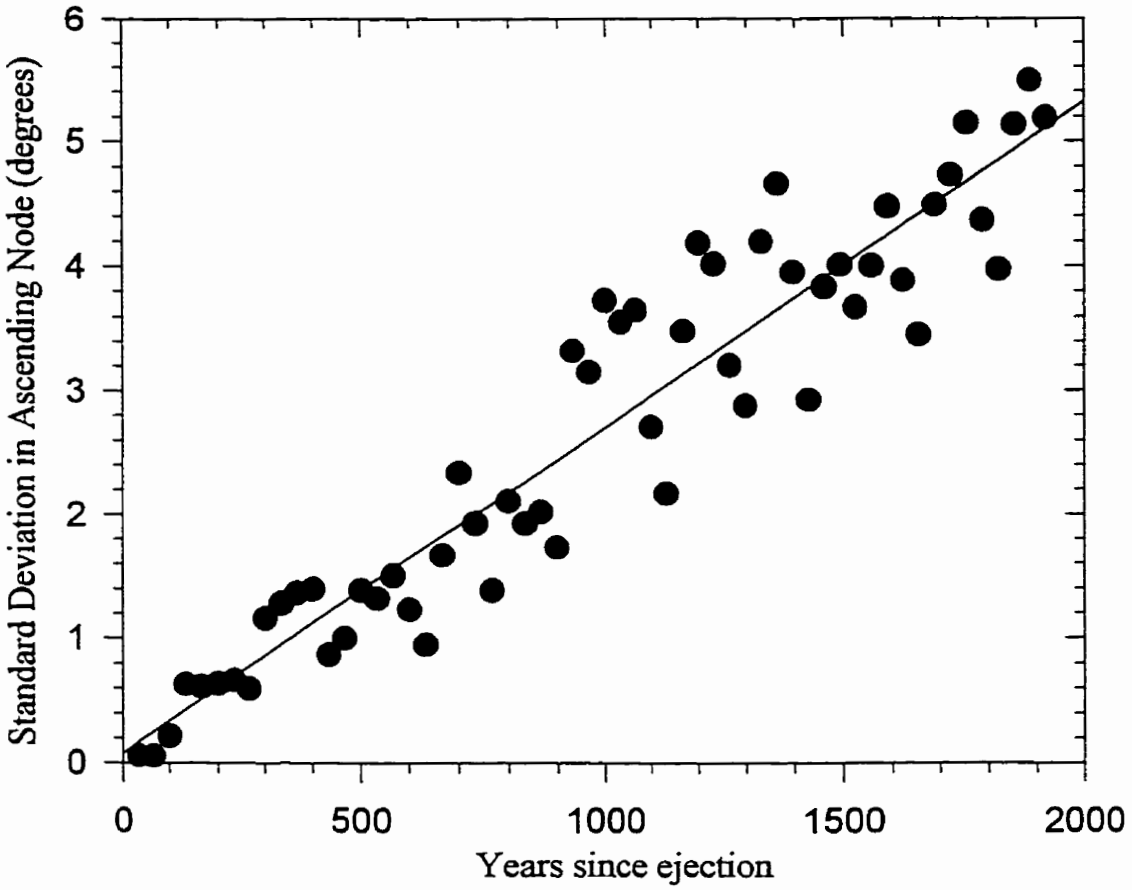

Fig 6.22: The standard deviation in the value of the ascending node for all visual-class meteoroids from model 22 for the last 2000 years. The solid line is the regression fit corresponding to Eq 6.1.

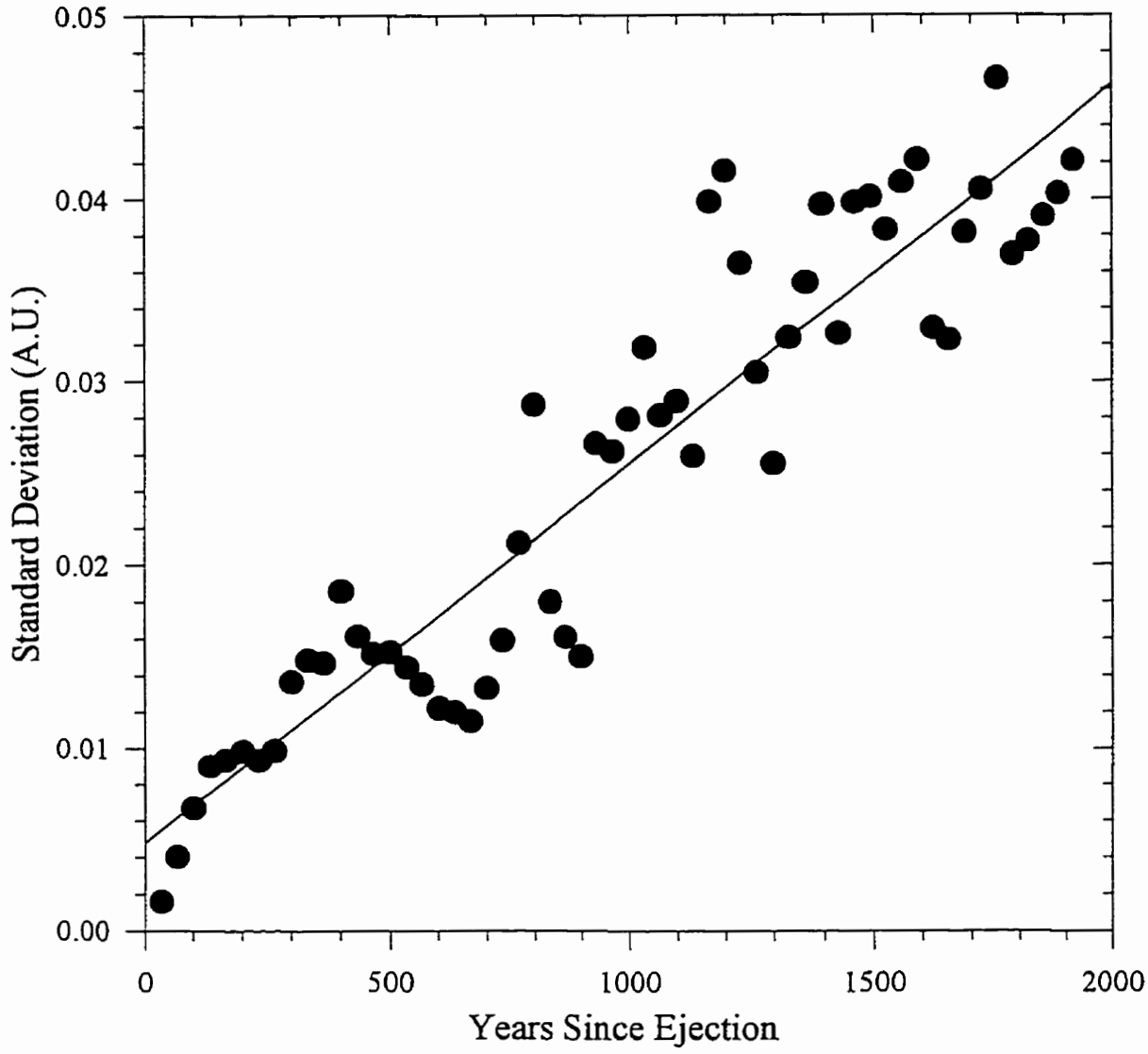

Fig 6.23: The standard deviation in the nodal radius for each ejection from 89 – 1965 using model 22 and visual-sized meteoroids. The solid line represents the regression fit as found in Eq. 6.2.

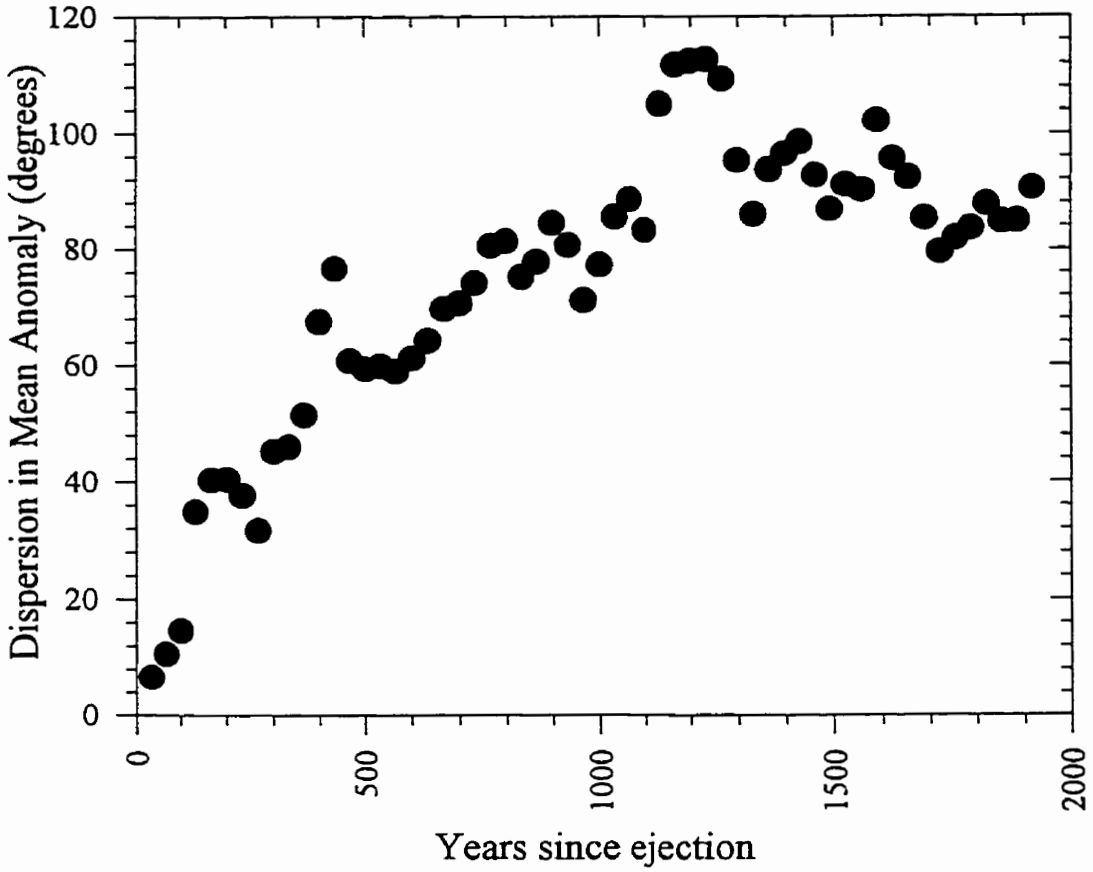

Fig 6.24: The standard deviation in the mean anomaly for all visual-class Leonid meteoroids ejected using model 22 over the last 2000 years.

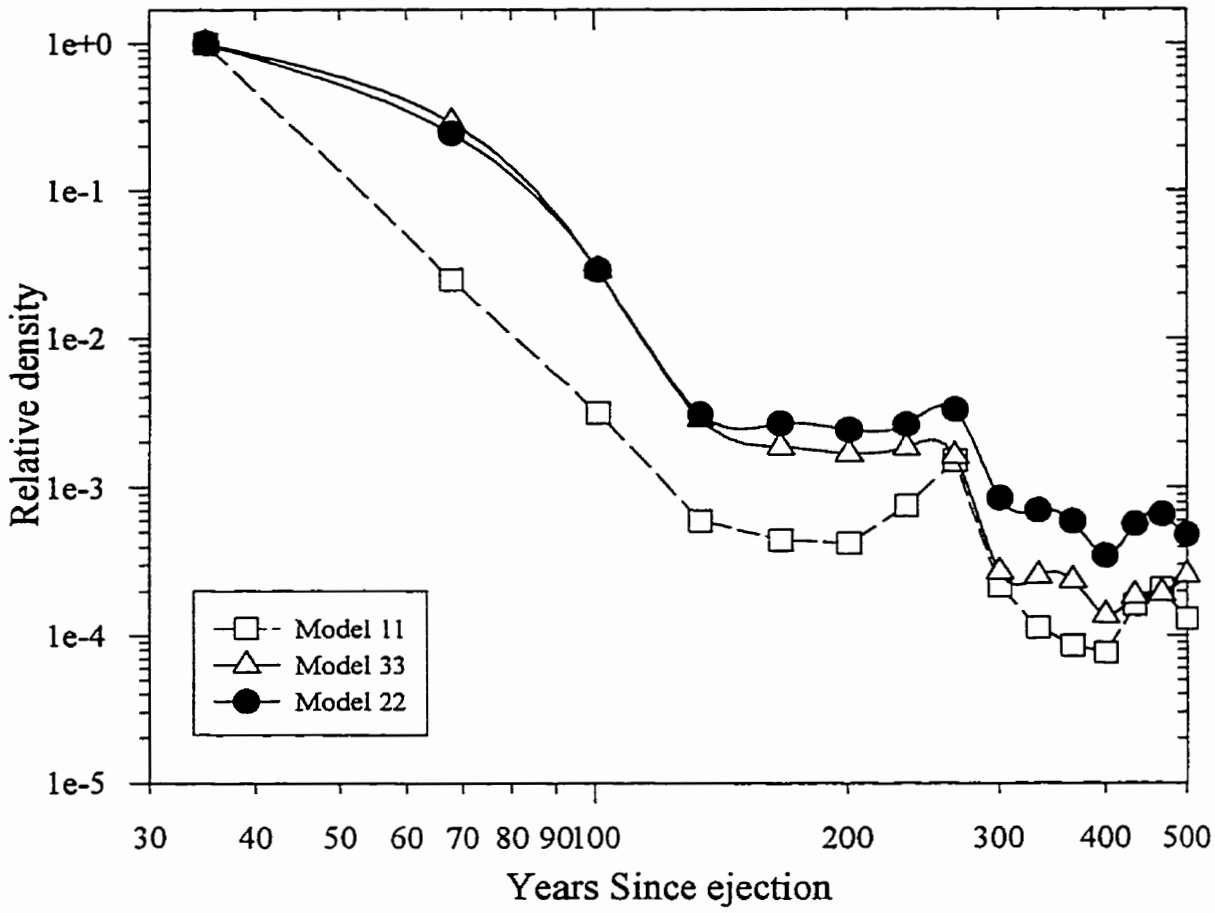

Fig 6.25: The evolution of the average relative particle density for visual-class meteoroids within the Leonid meteoroid stream, measured at the node, for models 11, 22 and 33 (see legend).

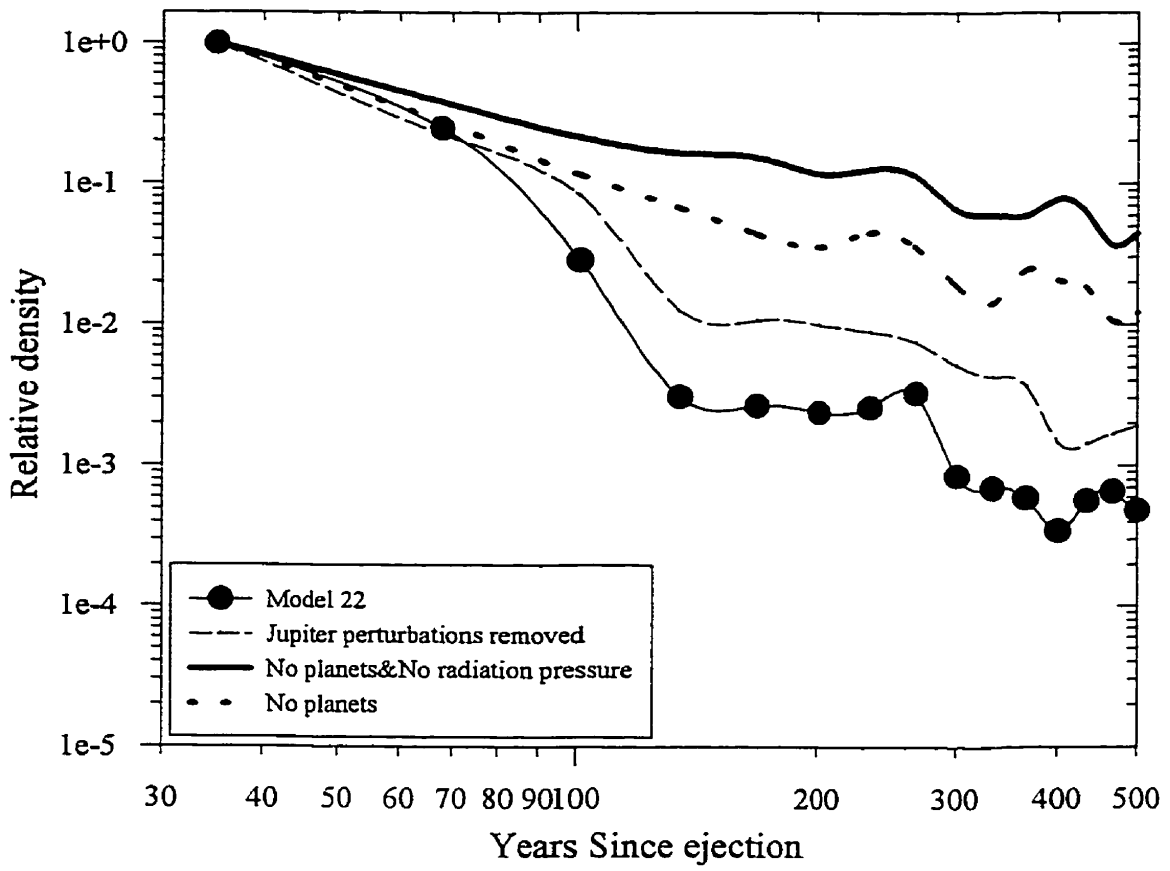

Fig 6.26: Comparison of the evolution of the average relative density change in the Leonid stream as a function of time: using model 22 initial ejection conditions for visual-sized meteoroids with Jupiter removed; all planetary perturbations removed and finally with all planetary perturbations and radiation pressure forces removed (see legend).

It is apparent that significant fluctuations in these values occur as a result of planetary perturbations, mainly from Jupiter (see later). However, the general trend of increasing dispersion with age is present in all distributions.

For model 22 meteoroids, averaged over the visual-sized mass classes (10^{-3} g - 10 g or $5\times10^{-5} < \beta < 10^{-3}$), a linear relationship in the dispersion of the nodal longitude (in degrees, J2000), λ, holds over the full 2000 years and is of the form

$$\sigma_{\lambda} = (0.08 \pm 0.1) + (2.6 \pm 0.1) \times 10^{-3}\, T \qquad (6.1)$$

where T is in years from Jan 1, 2000 A.D. measured positive backwards. Similarly, the dispersion in the nodal radius, r, in A.U. can be represented as

$$\sigma_{r} = (4.8 \pm 1.2) \times 10^{-3} + (2.1 \pm 0.1) \times 10^{-5} T \qquad (6.2)$$

Taken together, these two distributions provide a time-dependent measure of the mean spread in the cross-section of the stream on the ecliptic plane and also demonstrate that the rate of nodal longitude spread is roughly twice that due to the spread in nodal radius for model 22.

The relative rate of spreading along the orbital arc is measured through the dispersion in mean anomaly within the stream. However, after less than ~10 revolutions (depending on the values of β involved), a significant fraction of meteoroids will have made n-1 revolutions relative to the comet and the mean anomaly spread and its average become less meaningful measures.

In particular, for model 22 meteoroids, we have found that some particles begin lapping after ~200 years. For ejections less than 200 years in age, the spread in mean anomaly, M, for model 22 meteoroids can be represented by

$$\sigma_{M} = (0.7 \pm 5.8) + (0.19 \pm 0.04) T \qquad (6.3)$$

Taken together, these three equations can provide an idealized measure for the average relative rate of change of particle density and hence flux within the stream as measured at

the node. They also provide an approximate indication of the average length of time dense structures such as the storm-producing portions of the stream can endure.

Using the actual measured dispersions in the ascending nodes, nodal distance and mean anomaly, we can calculate the modelled average relative change in density compared to the density after only one revolution (the youngest material which we can sample at Earth). This is shown graphically in Fig 6.25 for model 22 and for three other models for comparison.

From Fig 6.25, the decrease in density of the stream as measured at the node after formation is such that it falls by ~2-3 orders of magnitude between its first revolution and a century later, almost independent of the starting model and range of β's involved. This offers a potential explanation as to why Leonid showers a significant distance away from the comet's perihelion passage are far less noteworthy in their maxima (due to the large decrease in flux for older material, which lies further from the comet's nodal passage). It also implies that Leonid returns more than 3-4 passages old are likely to result in only modest peak activities; the storm-producing segment of the shower is certainly only a few revolutions old at most based on this result. Note that the behaviour in Fig 6.25 is relative to the average peak concentration measured at the point of the average mean anomaly and so represents the smallest decrease in density expected - locations further from the peak concentration will have even smaller fluxes relative to the initial values; the values in Fig 6.25 are average upper limits. Note that the intermodel differences in the average absolute level of relative density is deceptive as each model obviously has a slightly different "initial" density after one revolution, depending on the range of ejection velocities and β represented.

The steep decrease in density over the first three to four revolutions, followed by a leveling off, suggests that different dispersive mechanisms dominate evolution over differing time-scales.

To examine this question, in Fig 6.26 we have plotted the results of model 22 integrations again. As well, the same integration has been performed removing the direct perturbations from Jupiter (dashed line), all direct planetary perturbations (dotted line) and finally all planetary perturbations as well as radiation pressure effects (solid line). Here the

solid line represents the diffusional effects of initial ejection velocities alone, which for model 22 averages several tens of meters per second near perihelion. At these ejection velocities, the initial dense stream would take nearly ten revolutions to fall to 10% of its first revolution density for the range of ejection velocities adopted. Radiation pressure effects produce nearly another order of magnitude decrease in density over the same time interval and planetary perturbations decrease the density yet another order of magnitude with Jupiter being the primary agent in the decrease after the first ten revolutions.

For the first few revolutions (which are relevant to the question of meteor storms), the effects of radiation pressure and ejection velocity dominate until after approximately the third revolution when the effects of planetary perturbations begin to determine the stream's subsequent density evolution.

In addition to the large variation in flux, the location in solar longitude of the maximum of the Leonid shower does show a significant variation from year-to-year (cf. Brown, 1999). It is typically assumed that any significant showers/storms will occur at or near the node of the comet (cf. Yeomans, 1981), an entirely reasonable assumption predicated on the youth of the material involved and thus the expected similarity in the orbital evolution of the parent comet and daughter meteoroids. Fig 6.27 shows the solar longitude location of the maximum concentration of meteoroids delivered to the present epoch for each of the last 57 perihelion passages of the comet for model 22 meteoroids. Each point represents the present location of the maximum number of test particles in 0.02° degree bins, with the error margins corresponding to the positions where this number has fallen to one-sigma less than the peak value from ejection during the time of the comet's passage along the abscissa.

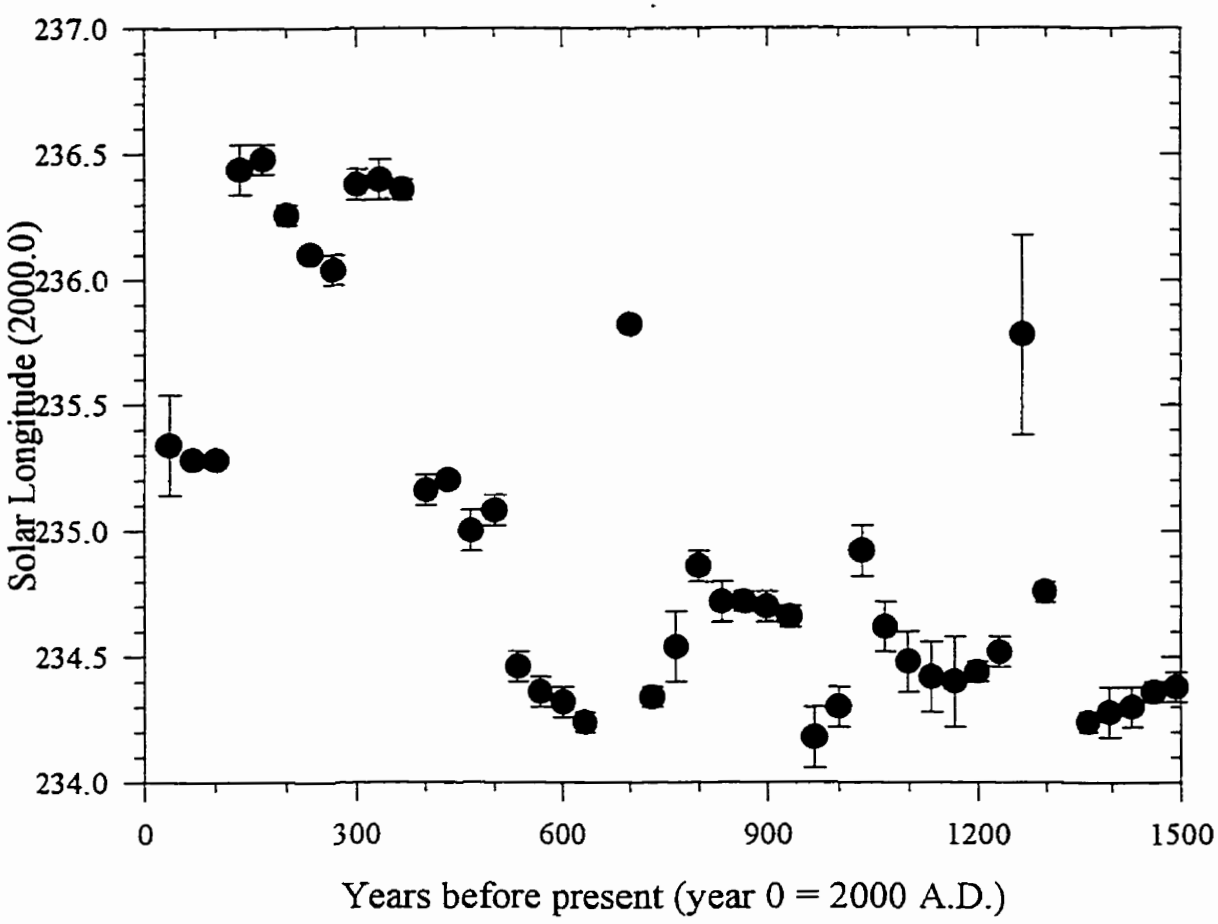

Fig 6.27: The locations of maximum particle concentration as a function of solar longitude for ejections over the last 1500 years referenced to the 1998 epoch. Each dot represents the most populated solar longitude bin at the present epoch for model 22 ejections at the era given in the abscissa of visual-class meteoroids. Only meteoroids within 0.001 A.U. of Earth's orbit are counted.

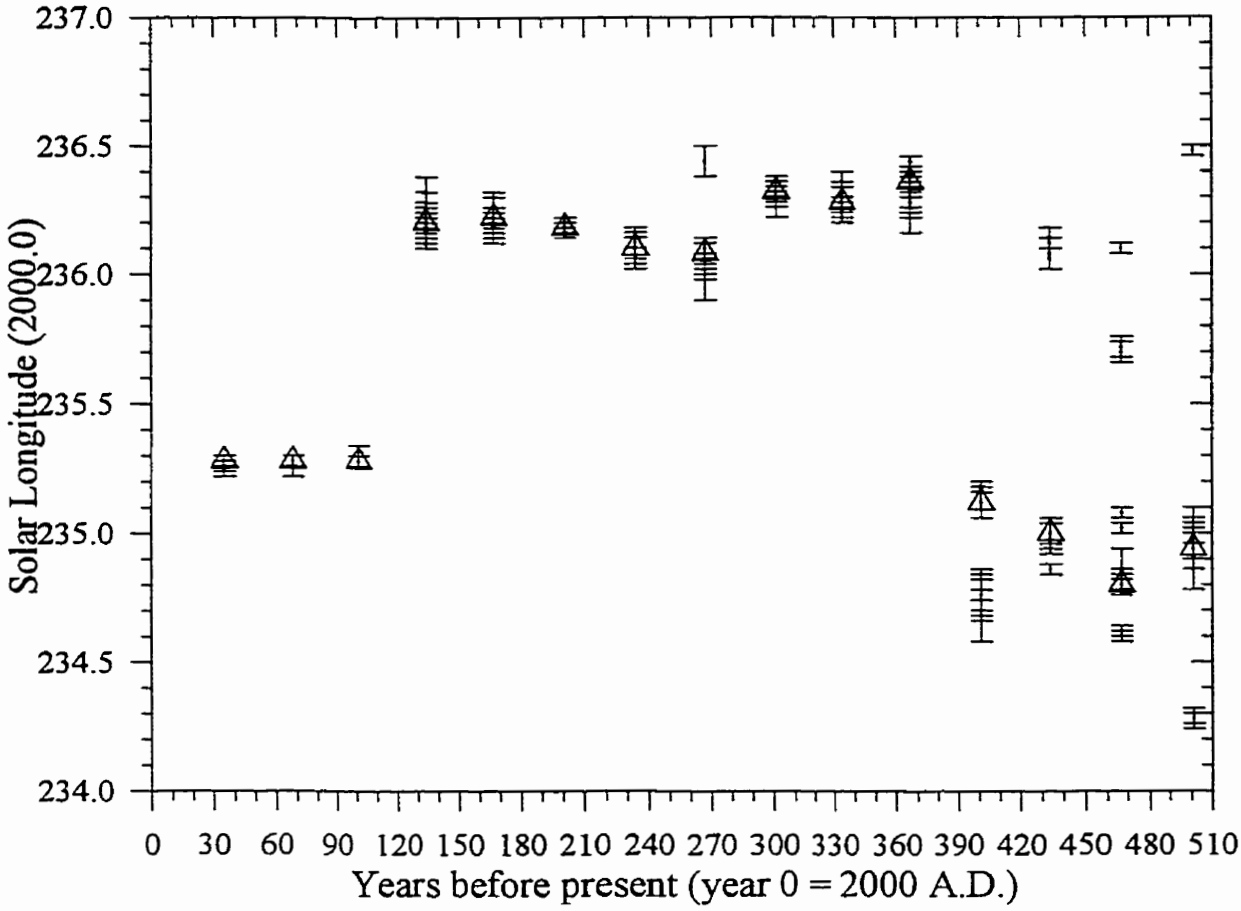

Fig 6.28: The locations of maximum particle concentration as a function of solar longitude for ejections over the last 500 years referenced to the 1998 epoch. Each open triangle represents the most populated solar longitude bin at the present epoch for model 22 ejections of visual-class meteoroids at the era given in the abscissa (same as Fig 6.27). Locations and error ranges for other peaks for all other models are also given as error bars.

It is immediately apparent that the positions of the maximum are correlated with their ejection times; specifically, groups of "maxima" are clustered at or near the same positions for several revolutions and then move some distance. The abrupt changes in peak locations are entirely caused by the perturbing effects of Jupiter, which acts to shift the locations relative to the comet through perturbations perpendicular to the orbital plane of the stream.

That ejecta from different years are so tightly correlated in peak solar longitude implies that the locations of maximum in years showing heightened activity at the present epoch can be used as an approximate measure of the likely age of material involved. That this effect is not strongly model nor density dependent, we show in Fig 6.28, the same plot as in Fig 6.27 but with all models given (the open triangles refer to the same plot as Fig 6.27, namely model 22). It is apparent that over the last 500 years at least, the shifts are fairly model and density independent.

6.6 Discussion

6.6.1 Role of Planetary Perturbations

The Leonids are a high inclination stream and do not pass close to any planet other than Earth. The closest distances between the present orbit of Tempel-Tuttle and each of the three major outer planets are shown in Fig 6.29. Based on this geometry it would seem that all three planets might affect the stream to varying degrees.

As discussed in connection with the Perseids (see Chapter 4), streams of high eccentricity can be significantly affected for Earth-intersection from distant direct perturbations by the Jovian planets. These distant encounters on the stream were shown to produce small perturbations on Perseid meteoroids which lead to intersection with the Earth.

Unlike the relatively straightforward planetary impulse pattern with the Perseids, the Leonids may experience significant perturbations both before and after perihelion from both Saturn and Jupiter. To further complicate the situation, the orbital period of the

stream is such that the section of the stream which experiences perturbations from Jupiter pre-perihelion also experiences more distant direct perturbations from Jupiter on the post-perihelion leg, the interval being three years between the encounters. Additionally, since Jupiter makes approximately 2.5 revolutions for each complete revolution of Saturn (and the encounter longitudes between the stream and Jupiter or Saturn are nearly the same), the Jupiter-Saturn pre-perihelion impulses tend to come in pairs (within 1-2 years of each other). From Fig 6.29 it is also apparent that the stream can have close encounters with Uranus near aphelion, an effect that has been suggested to be of pre-eminent importance in the stream's development (Williams, 1997).

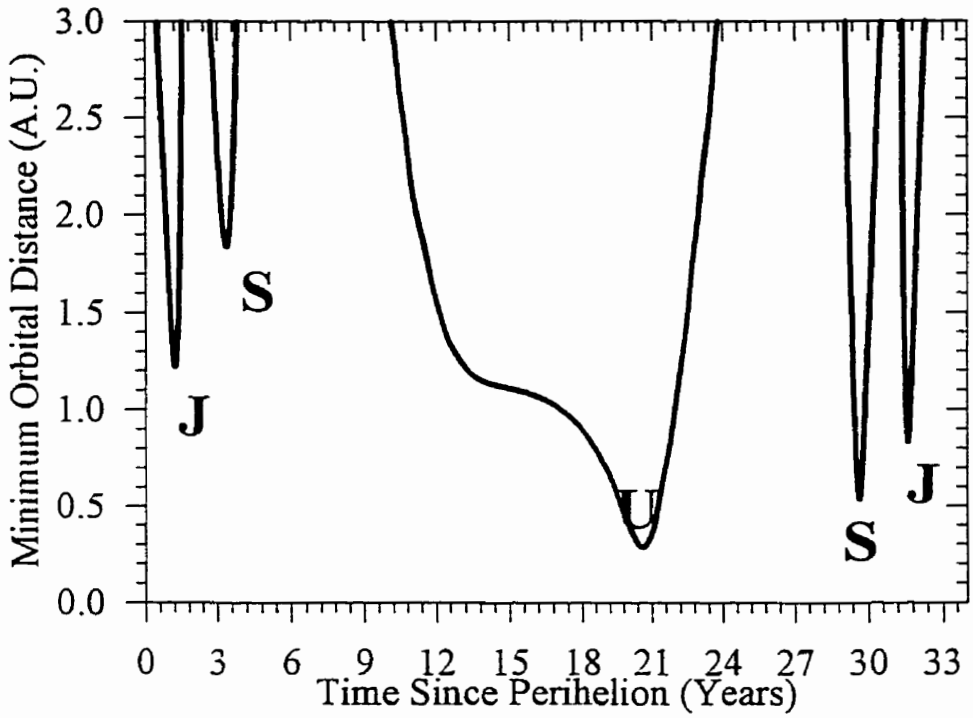

Fig 6.29: The minimum distance of 55P/Tempel-Tuttle's current osculating orbit (referenced to the 1998 epoch of perihelion) from the orbit of each of the major planets as a function of the time since perihelion for hypothetical test particles making the minimal approach distance to each planet's orbit.

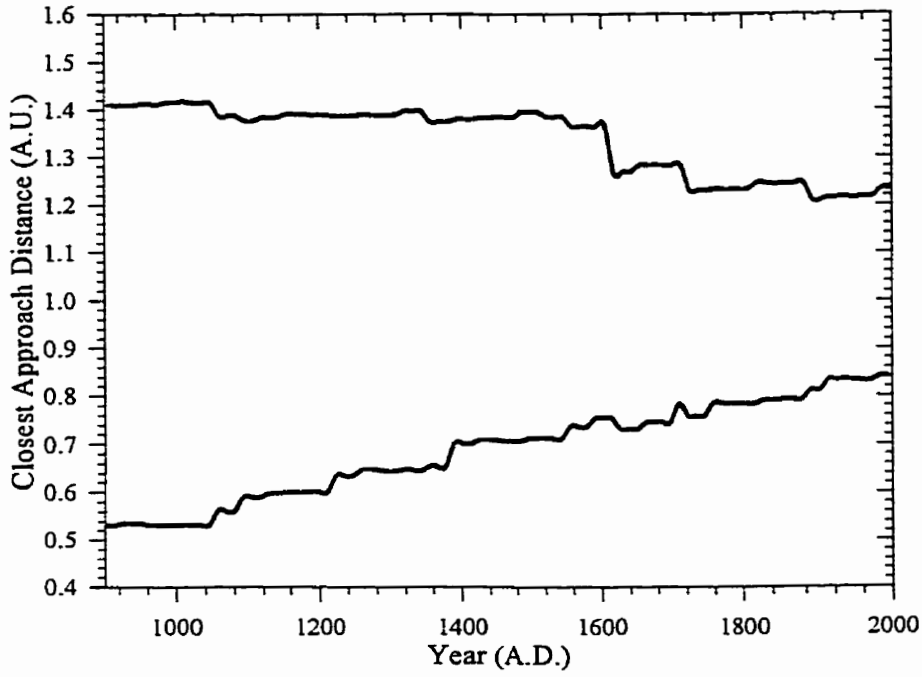

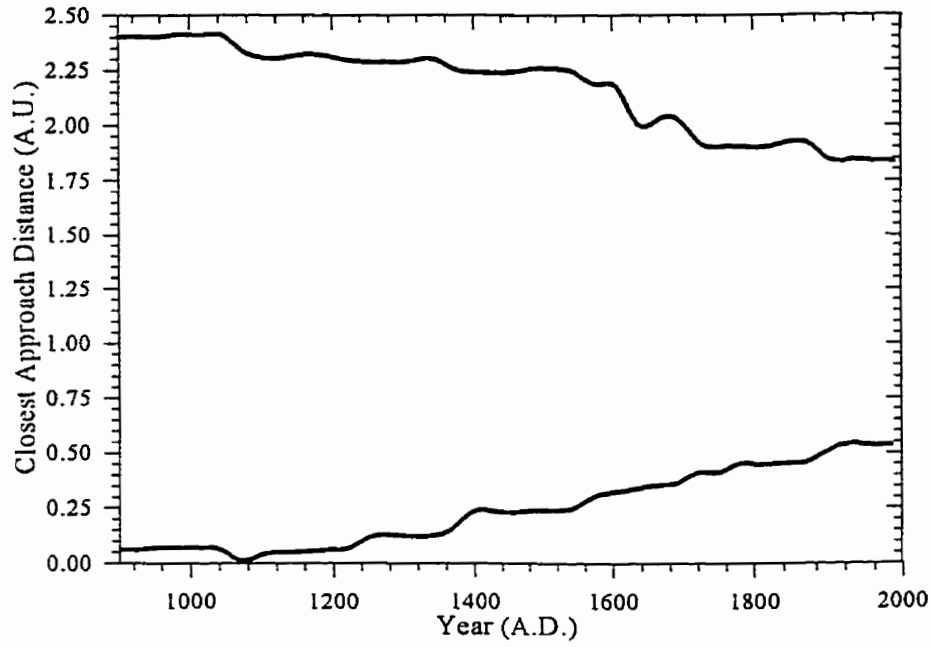

Fig 6.30 (top): Minimal approach distance between 55P/Tempel-Tuttle's osculating orbit at perihelion and Jupiter's orbit. The upper curve is for outbound (post-perihelion) passages and the lower curve is for inbound (pre-perihelion) passages.

Fig 6.31 (bottom): Same as Fig 6.30 but for Saturn's orbit.

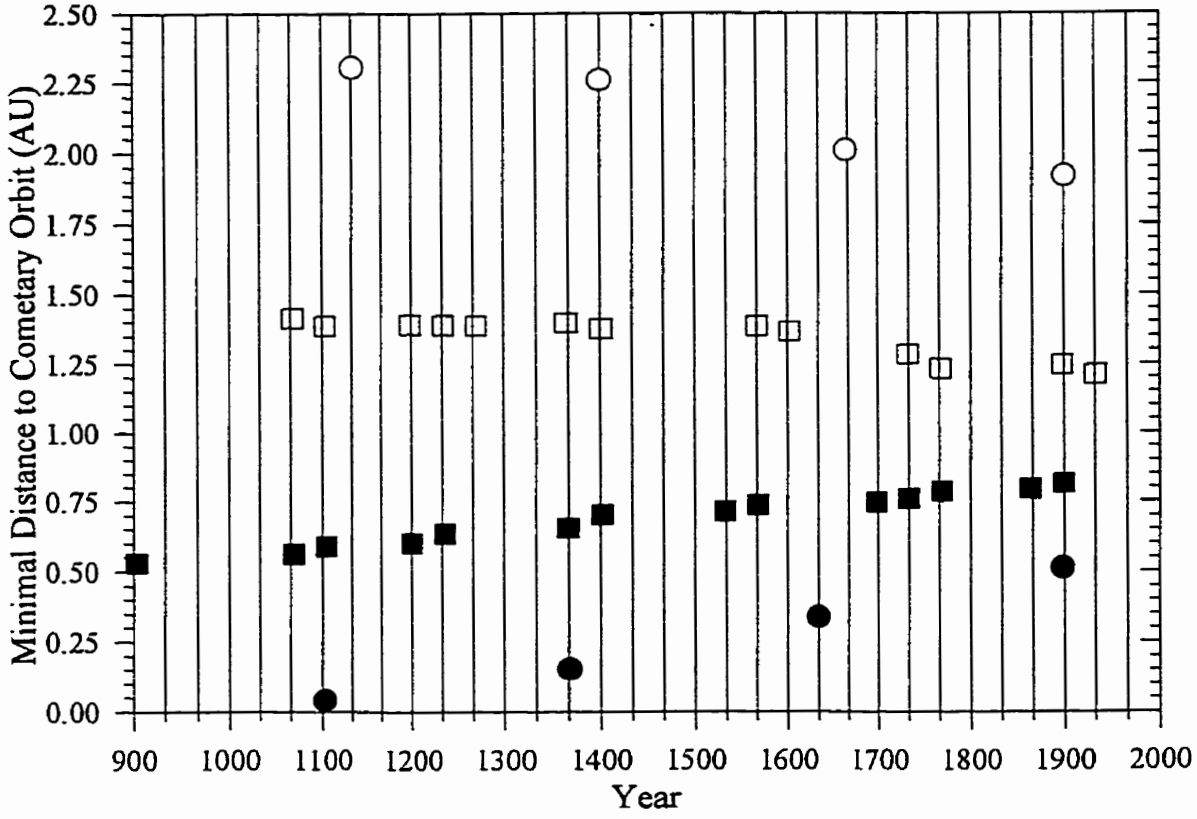

Fig 6.32: Actual close approaches of Jupiter (squares) and Saturn (circle) to 55P/Tempel-Tuttle at the epoch of its (nearest) perihelion passages to these encounters. Only approaches to the orbit of Tempel-Tuttle that are within 20° of the mean anomaly of the comet are shown. The solid symbols are for inbound (pre-perihelion) perturbations on the stream and the open symbols are for outbound (post-perihelion) encounters with the Leonids. The symbols are placed at the instant when the maximally perturbed portion of the stream reaches the descending node.

Our approach to investigating the effects of perturbations on the stream numerically is to remove each planet in turn and note the effects on the stream's development as a whole as opposed to attempting any analytic treatment for such a complex system.

To first order, the pre-perihelion effects of Jupiter and Saturn may be expected to dominate as they have the closest planetary encounters of major planets with the stream. We recall that the stream is a nearly continuous ribbon of material and that some Leonid meteoroids will always experience the maximum perturbations due to close approaches by the planets.

However, as the parent comet orbit varies with time, so too will the encounter conditions of the stream over the last 1000 years. In Figs 6.30 and 6.31 we show the varying minimum approach distance between Tempel-Tuttle and Jupiter and Saturn respectively.

From Fig 6.30 it is clear that the pre-perihelion Jovian perturbations have become significantly lessened over the last thousand years while the post-perihelion effects have increased slightly. Fig 6.31 paints a more interesting picture. While the post-perihelion distance between the comet's orbit and Tempel-Tuttle has increased slightly, the pre-perihelion effects have become much smaller, though the encounter distance is still less than is the case for Jupiter. Intriguingly, the minimum approach distance between Saturn and the stream reached a broad minimum for the pre-perihelion encounter between 900-1200 AD when the distance averaged ~0.05 A.U. The extreme minimum distance reached in 1070 AD was of order 0.02 A.U., which is inside the Saturnian satellite system. This suggests that Leonid showers were visible on Saturn (and Titan) some 900 years ago. It is unlikely that Leonid storms comparable to those seen on Earth occurred at Saturn, as the stream is significantly wider at Saturn's distance and the encounter velocities lower. Indeed, the only time Saturn reached its minimum distance to the Leonid orbit and passed within 10° of mean anomaly of Tempel-Tuttle during this time period was in mid-1099 when the two bodies were separated by approximately 0.6 A.U. (Yeomans *et al.*, 1996) (though Saturn passed less than 0.05 A.U. from Tempel-Tuttle's orbit a few months later).

Fig 6.32 shows the years (referenced to the time the affected material passed

through the descending node) in which encounters with either Jupiter or Saturn occurred along the stream orbit within ±20° of the mean anomaly of the parent comet. It is these encounters that have the largest effect on the storm producing segment of the stream and that would be expected a priori to cause a significant change in the densest portion of the stream (without necessarily affecting the parent comet as greatly).

The encounter pattern with Jupiter is such that every five orbits of Tempel-Tuttle, two successive close approaches to the stream are made by the planet on both the inbound and outbound leg of the stream orbit. These tend to have their maximum perturbations in front of and behind the comet in opposite pairs (i.e. the inbound perturbation maximizes behind the comet and then on the next orbit of Tempel-Tuttle the outbound perturbations maximizes behind the comet and vice-versa for perturbations in front of the comet).

The impulsive perturbation cycle with Saturn is such that every eight to nine revolutions of the comet, a similar pattern occurs with a perturbation (typically) first on the inbound leg of the stream and then on the next orbit of the comet on the outbound leg. The encounters after perihelion tend to move the nodal points of the affected meteoroids away from the sun, while the pre-perihelion passages tend to move meteoroid nodal points inward. Thus, depending on the geometry between the comet and the Earth, these perturbations (in the short-term) may serve to move the material to intersect the Earth (as was the case with the 1899 material perturbed in 1901 and again in 1932 moving the nodal point out far enough to be encountered in November, 1966) or to not intersect it (as was the case for material released in the previous eight revolutions prior to 1899 which was already largely interior to Earth's orbit at the node and was perturbed further inward due to pre-perihelion perturbations from both Saturn in 1895 and Jupiter in 1898).

These encounters also serve to disrupt and diffuse the dense cometary trail of material developed over the previous five passages of the comet. When strong perturbations occur they serve to move some material away from the comet and may be the limiting factor in the development of the dense Leonid storm producing segments of the trail. Kresak (1992; 1993) was among the first to recognize that encounters between Jupiter and the Leonids could disrupt the dense trail behind Tempel-Tuttle. In the present work, it is clear that the stream decreases in density quickly (Sect 6.5) and such

disruptions (or more gradual perturbations) can easily move the trail away from the comet, but the material may still intersect the Earth and cause a storm (as occurred in 1966). It is the magnitude of the disruption (compared to gradual perturbations) and what its effect on the trail relative to the comet-Earth geometry which affects the appearance or not of a storm as seen at Earth.

To investigate the effects from each of the planets on stream development as a whole, we plot the dispersion in mean anomaly, nodal radius and ascending nodal longitude as a function of time for each planet removed in turn over the last 500 years for model 22 meteoroids in Figs. 6.33, 6.34 and 6.35 respectively (compare to Figs 6.22, 6.23 and 6.24).

From Fig 6.33 it is apparent that while the abrupt changes in dispersion in mean anomaly are due to planetary perturbations (mainly Jupiter), the overall effects are small and the dispersion is not controlled primarily by planetary perturbations, but rather by radiation pressure effects and ejection velocities. Note the complete lack of observable effect due to removal of Uranus.

Fig 6.34 clearly demonstrates that Jupiter is the primary mechanism in the diffusion of the nodal radius, with increasingly lesser effects from Saturn and Uranus. Perturbations perpendicular to the orbital plane, which directly affect the nodal longitude, are completely dominated by Jupiter (an observation previously made also by Kresak (1992)). Fig 6.35 shows that there is nearly an order of magnitude difference in nodal longitude dispersion with Jupiter present as with it removed; far lesser effects are due to Saturn and there are almost no measurable effects from Uranus.

In terms of the final activity profiles visible at Earth, the net effect of the removal of each of the planets on the number of particles visible as a function of time at Earth follows the same pattern, with the largest changes involving removal of Jupiter or Saturn and much smaller effects from the removal of Uranus.

The clear trend (as might be expected a priori) is for the planetary perturbations to be dominated by Jupiter with small effects from Saturn (with the possible exception of close approaches to the stream orbit some 900 years ago) and lesser still from Uranus.

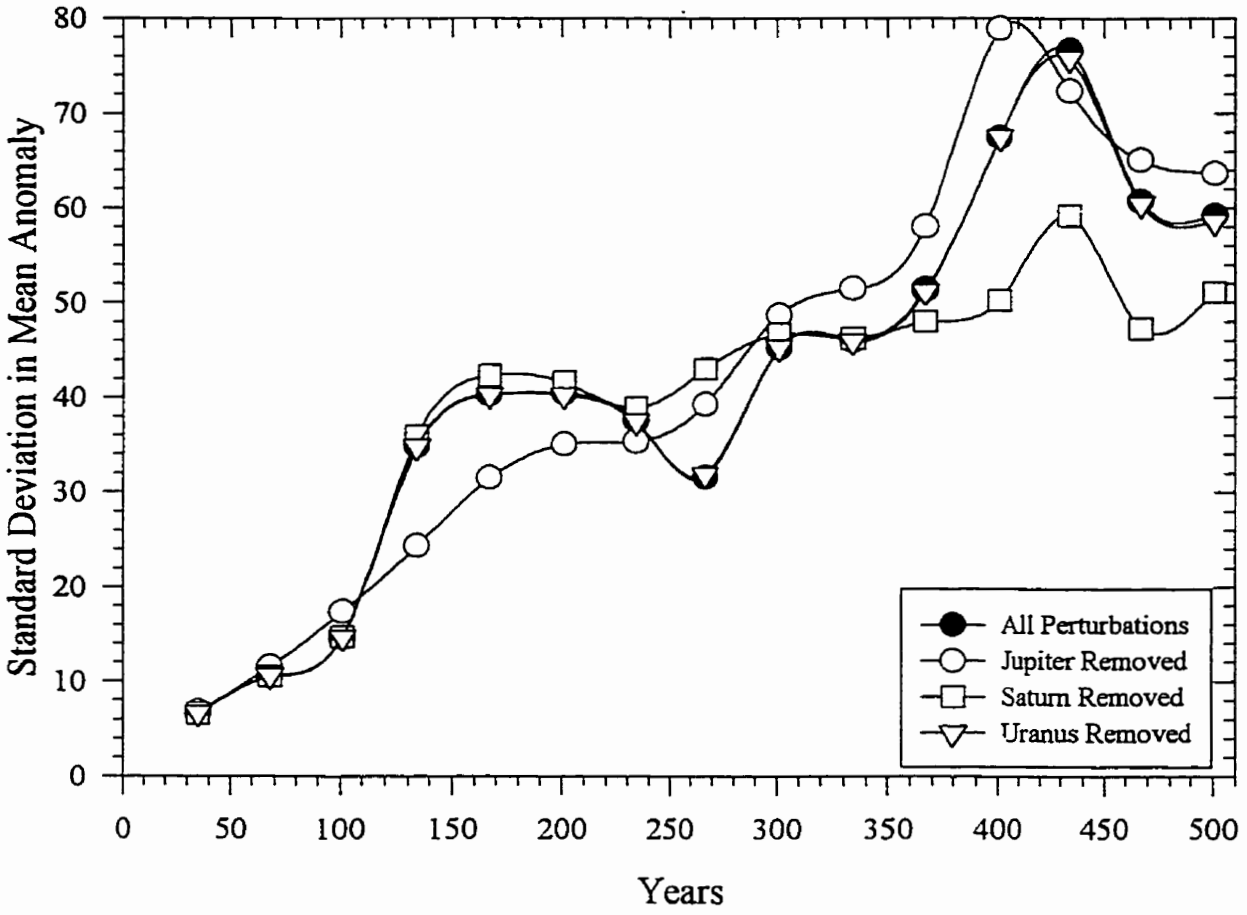

Fig 6.33: The standard deviation in the mean anomaly for all visual-class Leonid meteoroids ejected using model 22 over the last 500 years (solid circles). Also shown are the same initial conditions with the direct perturbations from Jupiter, Saturn and Uranus removed (see legend).

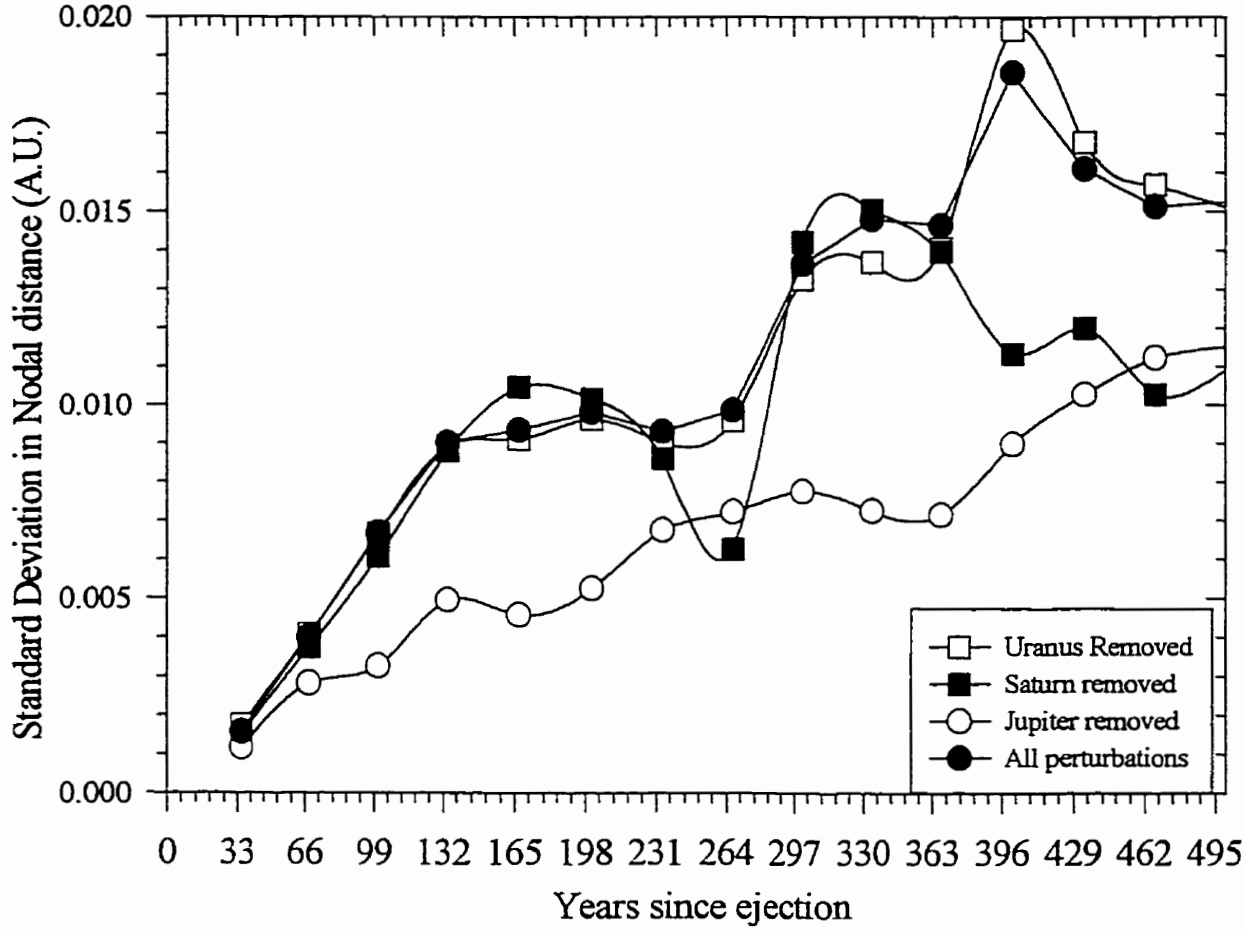

Fig 6.34: The standard deviation in the nodal radius for each ejection over the last 500 years using model 22 visual-sized meteoroids (solid circles). This is compared to the standard deviation in the nodal radius with Jupiter removed (open circles), Saturn removed (solid squares) and Uranus removed (open squares). Note the large effect of removing Jupiter.

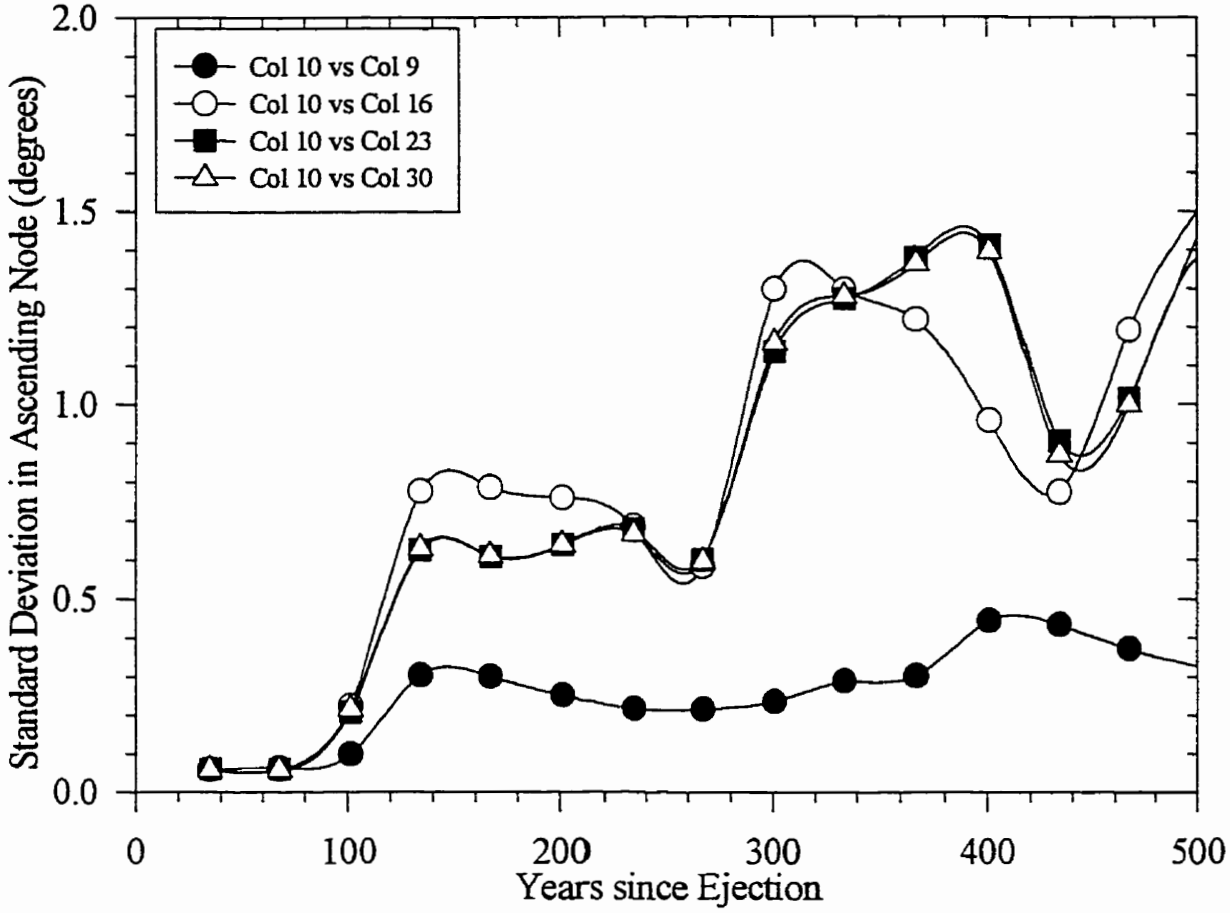

Fig 6.35: The standard deviation in the ascending nodal longitude for model 22 visual-class meteoroids ejected over the last 500 years at the present epoch with all perturbations included (solid squares), with Jupiter removed (solid circles), Saturn removed (open circles) and Uranus removed (open triangles) for comparison. Note the dominant effect of Jupiter and the negligible effect of Uranus.

Perturbations from Uranus appear to have greatest effect upon the delivery of meteoroids near the time of the nodal passage of Tempel-Tuttle, a result not in contradiction with the concept of the 5:2 near-resonance "protecting" meteoroids nearest the comet from perturbations (Williams, 1997). Without Uranus far fewer meteoroids reach Earth in the one to five years after the comet's passage as shown in Fig 6.36. Note, however, that Uranus increases the number of meteoroids for years well away from the comet's passage, in contradiction to the role for the planet proposed by Williams (1997).

6.6.2 The Role of Resonances

That the major outer planets dominate the evolution of the stream after time intervals >100 years with radiation pressure and ejection velocities playing significant roles in the first few revolutions was established in the previous section. The precise mechanism of the interaction, however, is still to be defined.

Stoney and Downing (1898) were the first to note the near commensurabilities in the period of the stream with Jupiter (5:14), Saturn (8:9) and Uranus (5:2). Emel'yanenko (1984) noted the possible role the 5:14 resonance with Jupiter might have on the density of material in the stream and Williams (1997) has suggested a major role for the 5:2 resonance with Uranus in removing meteoroids from Earth-intersection.

We expect a resonance to be manifested in an oscillation in the value of the semi-major axis. Fig 6.37 shows this value for Tempel-Tuttle over the last 2000 years. The value does oscillate with a period near 166 years (five revolutions of the comet). This suggests either Jupiter or Uranus may play a role in the evolution of the parent comet (and by implication much of the youngest portions of the Leonid stream). However, the amplitude of the oscillation is not constant, nor does the period hold strictly over this full 2000 year interval and the location of the resonance (the mean value of semi-major axis) does not remain fixed.

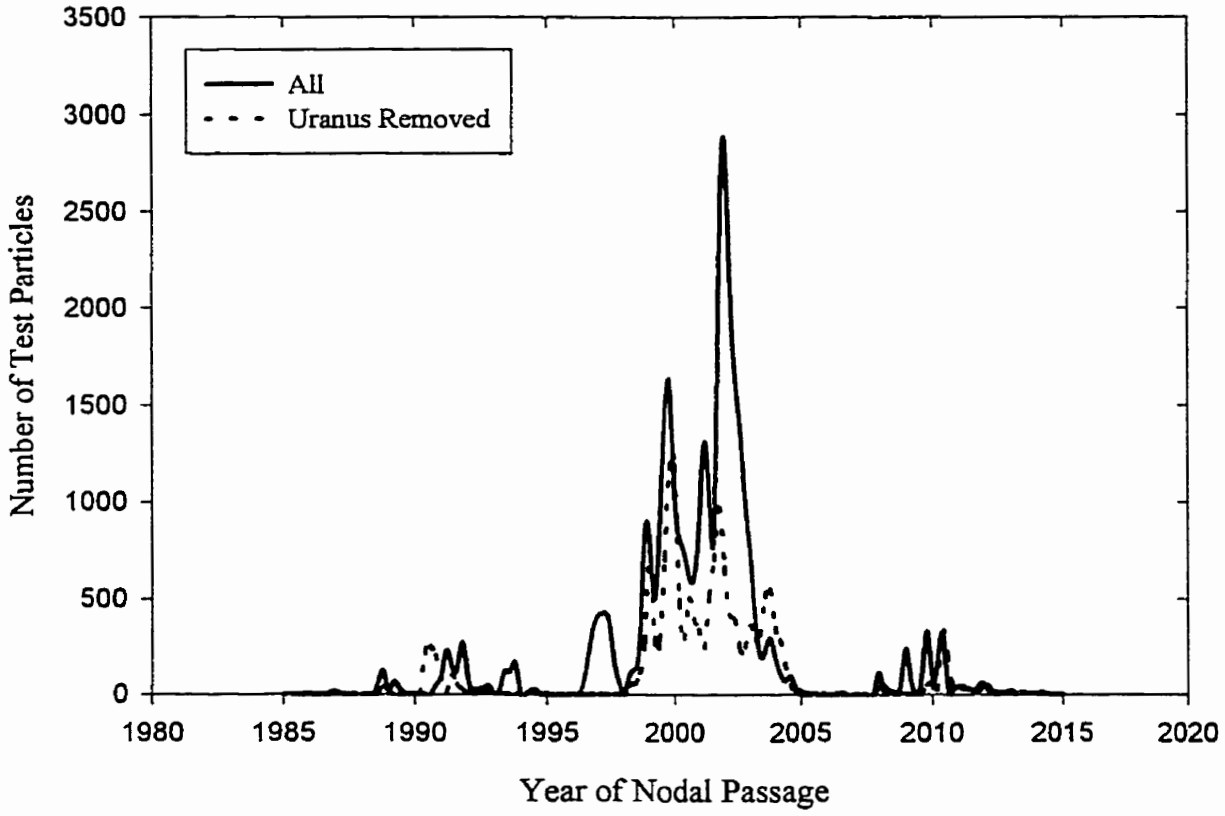

Fig 6.36: The effect of Uranus on delivery of Leonid test particles to Earth. The solid curve represents visual-sized Leonid meteoroids which have nodal points within 0.001 A.U. of Earth (binned in units of 0.2 years) from all ejections over the last 500 years using model 22 for initial ejection velocity conditions. The dotted line shows the same, but with the direct perturbations of Uranus removed. Much larger changes in the numbers of Earth-intersecting Leonids are found by removal of Jupiter and/or Saturn.

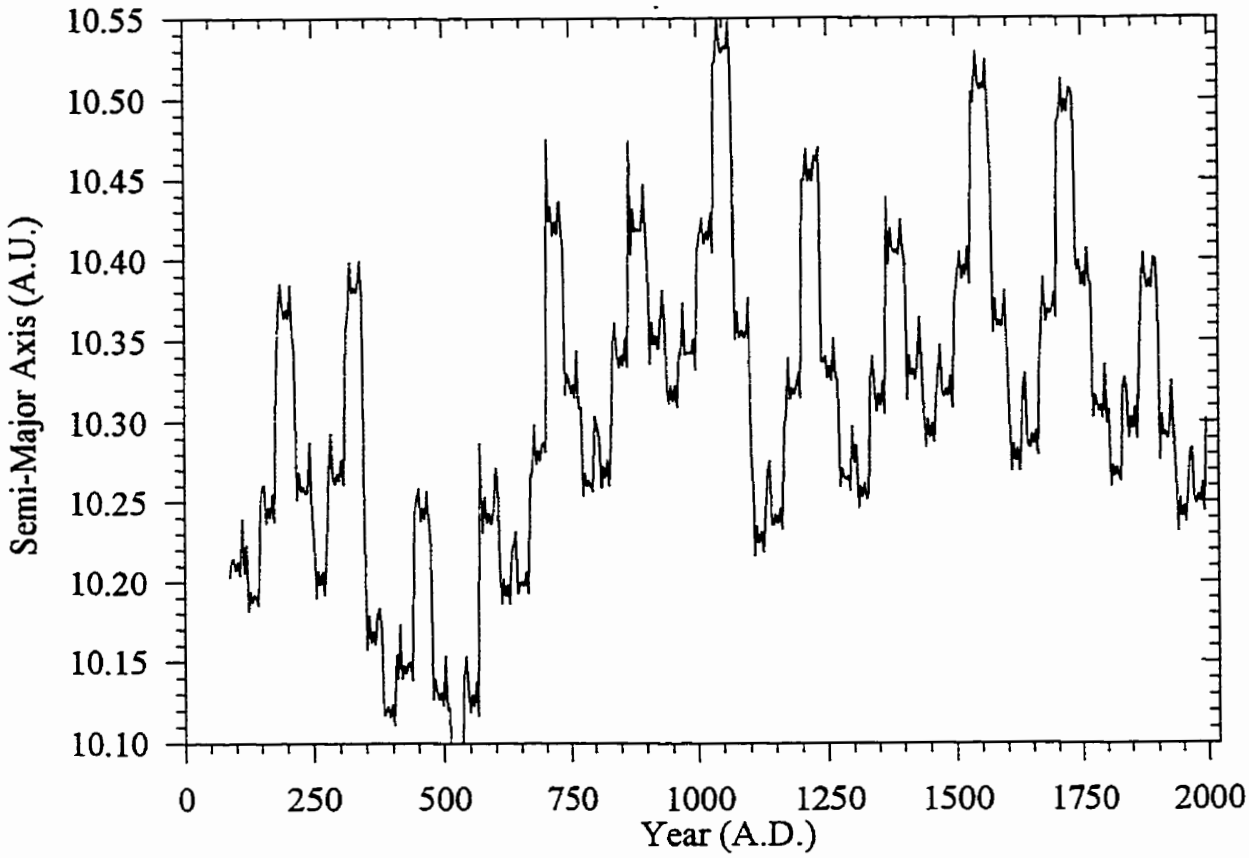

Fig 6.37: The semi-major axis of 55P/Tempel-Tuttle over the last 2000 years.

This result implies that any resonance which affects Tempel-Tuttle is unstable and that the comet may be continually slipping into and out of resonances (possibly with both Jupiter and Saturn which have resonances centred at 10.33 A.U. and 10.31 A.U. respectively).

To determine if any of these mean motion commensurabilites are the actual sites of resonances with Tempel-Tuttle, we examine the critical resonance argument (σ) which is of the form (Schubart, 1968; Chambers, 1995):

$$\sigma = i\lambda_p - j\lambda + (j-i)\varpi \qquad (6.4)$$

where λ_p is the mean longitude of the major body (planet) involved, λ is the mean longitude of the minor body and ϖ is the longitude of perihelion of the minor body for a resonance of the form *i:j* where *i* is the integer period of the minor body and *j* the integer period of the major body. This critical argument will show regular librations about a fixed value of σ over time if the bodies are in a stable *i:j* resonance.

Fig 6.38a, b, and c show the value for the critical argument for Jupiter (5:14), Saturn (8:9) and Uranus (5:2). From Fig 6.38c it is clear that Tempel-Tuttle has not been in the 5:2 resonance with Uranus at any period over the last 2000 years. From Fig 6.38a there does appear to be some aperiodic librations in the 5:14 critical argument beginning ~600 AD. These are not the regular oscillations indicative of a stable libration for a Halley-type comet (cf. Chambers, 1995), but suggest more complex behaviour such as a continuous movement into and out of the resonance over this period, chaotic motion or the simultaneous effect of more than one resonance. Unfortunately, the period of the oscillations is of order 400 - 500 years and shows only a few periods of this oscillation for the time interval in which we have an accurate ephemeris for Tempel-Tuttle. Indeed, it is possible that the sudden shift completely out of the resonance at 600 AD may be the simple result of the larger errors in computing Tempel-Tuttle's elements back this far (Yeomans, 1998, pers comm).

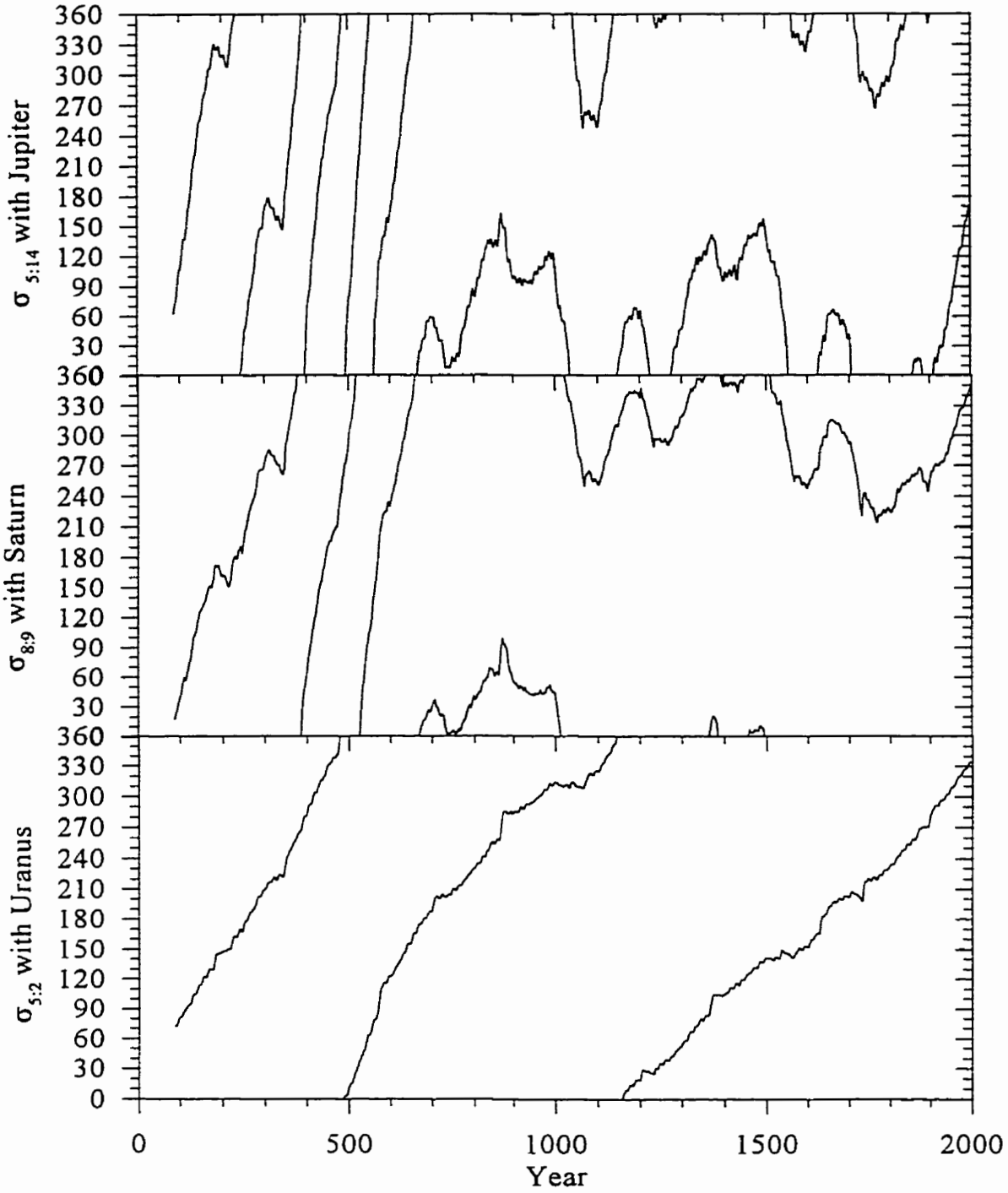

Fig 6.38: Evolution of the critical argument for Tempel-Tuttle with respect to the 5:14 resonance with Jupiter (a – top); the 8:9 resonance with Saturn (b – middle); and the 5:2 resonance with Uranus (c – bottom).

The librations are about the comet's perihelion (centred for convenience at 180° in Fig 6.38a). Fig 6.38b shows the 8:9 critical argument with Saturn which displays similar coherent behaviour. However, the librations in Fig 6.38b are not fixed about one value for σ and drift significantly over just a single period (~600 years). In fact, this may be entirely due to the near commensurability between the periods of Jupiter and Saturn (which are nearly in the ratio of 5:2), as the closeness in the semi-major axis of the 8:9 with Saturn (at 10.31 A.U.) and the 5:14 with Jupiter (at 10.33 A.U.) implies that a drift in mean anomalies between the two planets at conjunction is approximately 1° per decade, entirely accounting for the ~60° shift over 600 years for similar features in the aperiodic oscillation in Fig 6.38b. Alternatively, this may reflect a more complex three-body resonance (eg. Murray *et al.*, 1999). It therefore appears most probable that the primary resonance, which influences Tempel-Tuttle and the Leonids, is the 5:14 with Jupiter.

Interestingly, the low semi-major axis values prior to 600 AD may be associated with the 4:11 resonance with Jupiter, the critical argument of which shows librations similar to the 5:14 from 0-600 AD (though over only one cycle and therefore not entirely convincing).

The apparent lack of a stable resonance at these high resonance orders is not wholly unexpected; indeed for high eccentricity orbits the strongest (first-order) resonances are of the type *1:k* (Chambers, 1995), where *k* is an integer. Thus we expect the resonances discussed here to be weak. As a result, even if Tempel-Tuttle enters one of these high order resonances, slight changes in orbital energy from planetary perturbations may easily exceed the energy in a high-order resonance and quickly shift the body out of the resonance regime once again, as was noted by Carusi et al (1987). The resonance behaviour in 6.38a may best be described as chaotic, based on its alteration from rotation to oscillation as defined by Murray *et al.* (1999).

Carusi *et al.* (1987) also showed that many Halley-family comets (those with Tisserand<2, as is the case for Tempel-Tuttle where T=-0.6) show regular librations about integer multiples of Jupiter's revolution period. They found that typical cycles were of order five to six cometary revolution periods for this behaviour, very similar to what we

find here for the 5:14 with Jupiter for Tempel-Tuttle. Carusi *et al.* (1987) have also shown that most Halley-family comets are under the influence of Jupiter (essentially what is found in the present investigation for Tempel-Tuttle).

Despite the weak nature of many of the Jovian resonances, Jupiter's influence on the distribution of semi-major axis of Leonid meteoroids in our simulations is significant. Examining the distribution of test particle semi-major axis as a function of time with Jupiter present and with it absent (Fig 6.39a,b) demonstrates that one of the primary effects of Jupiter is to increase/decrease the concentration of particle semi-major axes near several resonances. Of particular note is the role Jupiter plays in accelerating the movement of Leonid meteoroids to large semi-major axis values and concentrations close to 10.8 A.U., which is near the location of the 1:3 resonance with Jupiter, previously noted as important for the Leonids (Brown and Jones, 1993). This might be a partial reason for strong showers in the two to three years after the parent comet. An example is the cluster of meteoroids ejected in 1866 near 10.9 A.U. (most likely shepherded by the 1:3) which might, for example, encounter Earth in November, 2000.

While it is clear that resonances do have a major effect on the stream, the magnitude of the role for any one resonance depends to a great degree on the spreading in the semi-major axis due to radiation pressure forces and initial ejection velocities. The most probable resonances affecting the stream, based on these examined distributions are the 5:14, 4:11 and 1:3 resonances with Jupiter and the 8:9 with Saturn.

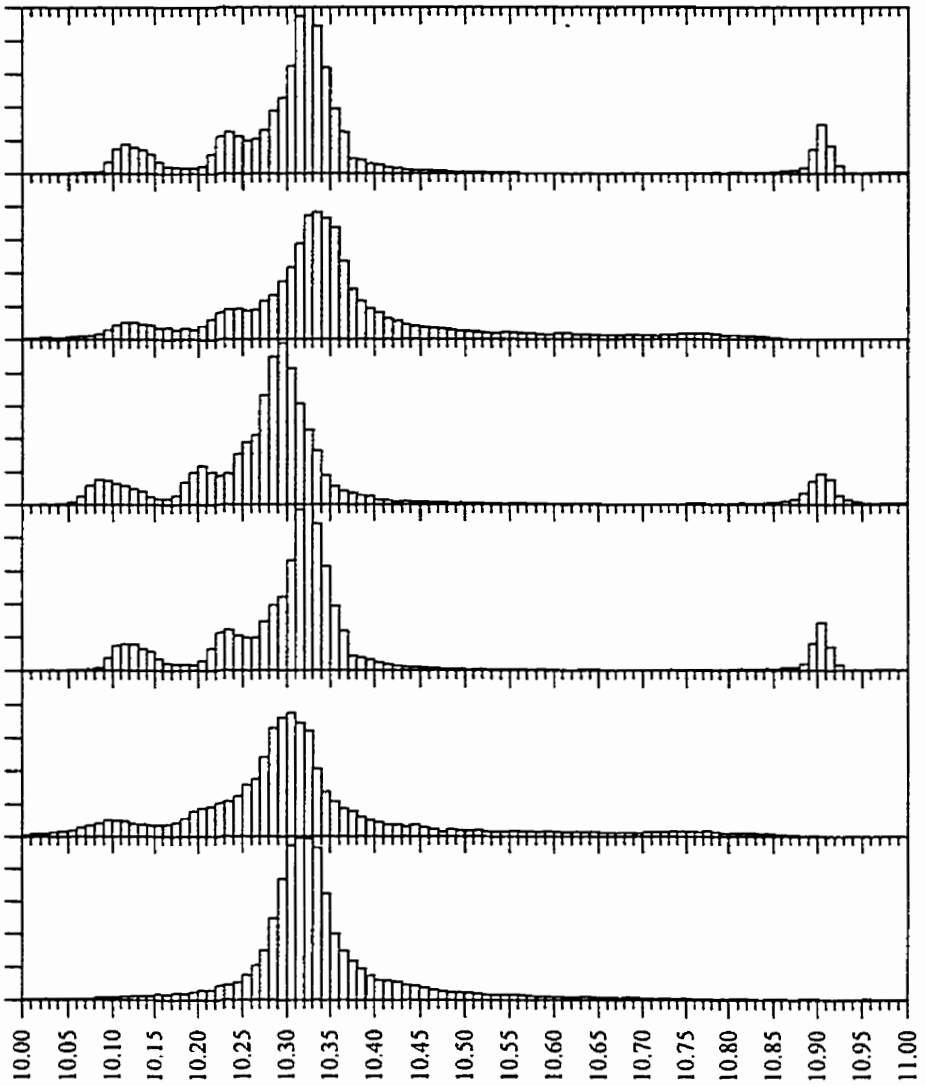

Fig 6.39a: The distribution of model 22 visual-class Leonid test particle semi-major axis ejected in 1899 using model 22 and followed to the present epoch. First (top) plot shows the distribution with all planets and forces included. Second plot shows distribution with Jupiter removed, third with Saturn removed and the fourth with Uranus removed; the fifth plot is with all planets removed; the last is with all planets and radiation pressure removed. Ordinate is the number of test particles per 0.01 A.U. bin in semi-major axis (abscissa), each major tick being 1000 test particles.

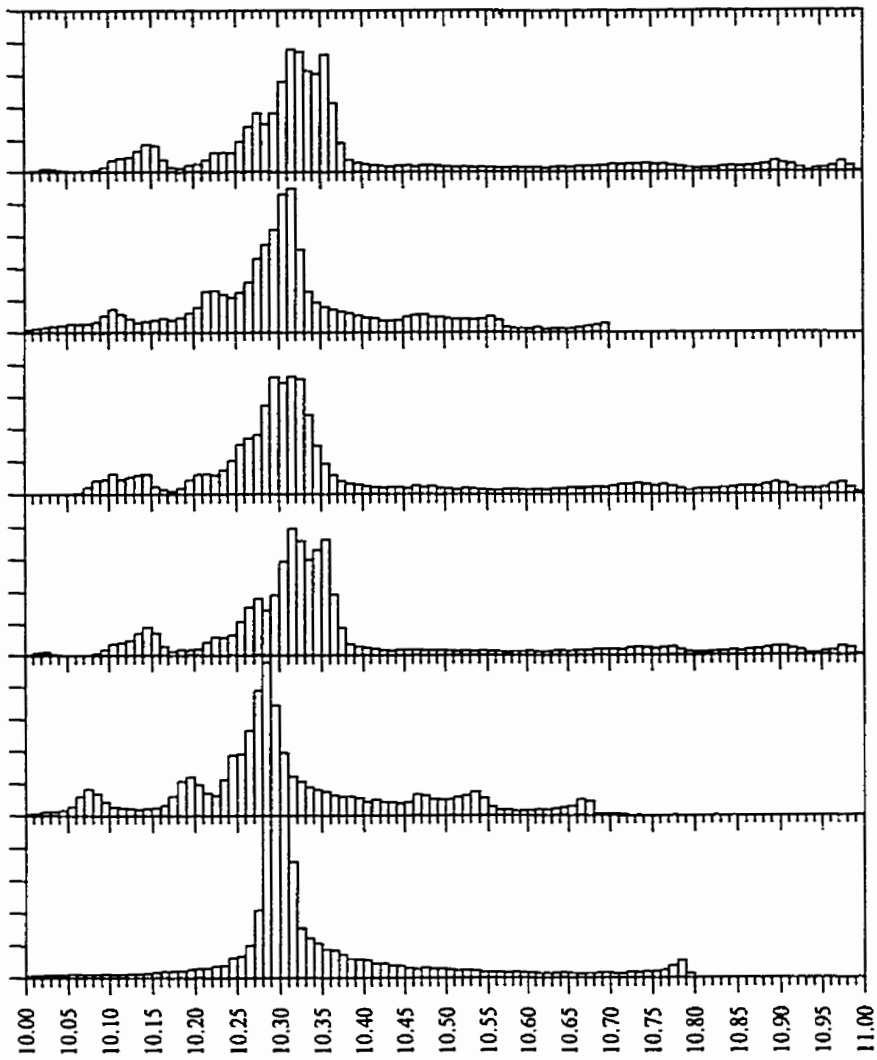

Fig 6.39b: The distribution of visual-class Leonid test particle semi-major axes ejected in 1799 using model 22 and followed to the present epoch. First (top) plot shows the distribution with all planets and forces included. Second plot shows distribution with Jupiter removed; third with Saturn removed; and the fourth with Uranus removed. The fifth plot is the distribution with all planets removed and the last is with all planets and radiation pressure removed. Ordinate is the number of test particles per 0.01 A.U. bin in semi-major axis (abscissa), each major tick being 1000 test particles.

6.7 Current Leonid Cycle (1998 Epoch)

6.7.1 Model Comparison and Interpretation of Leonid showers 1994-1998

Of all the recent Leonid epochs, the current one has been the most studied and has the most precise activity curves available.

Fig 6.9 shows the number of particles with nodal passages as a function of time for several models with our adopted binning. The peak circa 2002 is due to very old material and while many test particles are involved, they are very spread out in solar longitude and unlikely to be associated with storms.

For each year with sufficient test particles, Table 6.7 lists the breakdown in terms of the most significant ejections summed over all solar longitudes. As the table reveals, only a few of the years nearest the passage of the comet have significant amounts of recent ejecta; all other years are from much older passages of the comet.

To investigate more fully the change in age composition for the oldest material of the stream from year-to-year, beginning with the first observed activity in 1994, we make use of the integrations carried out in Sect 6.5 for model 22. Fig 6.40 shows the number of test particles per perihelion passage accepted in the given year to a sieve distance of 0.001 A.U.

Activity in 1994 is primarily from ejections 600-700 years old, while the 1995 return is a century older still. Observations of these returns (see Chapter 5) were characterized by broad activity with an abundance of larger meteoroids, which would be expected given the large amount of time available for planetary perturbations to cause significant spreads in the nodal longitudes and for the increased loss of smaller particles (both trends are directly confirmed through these integrations whereby the largest particles in these years have the highest transfer efficiencies).

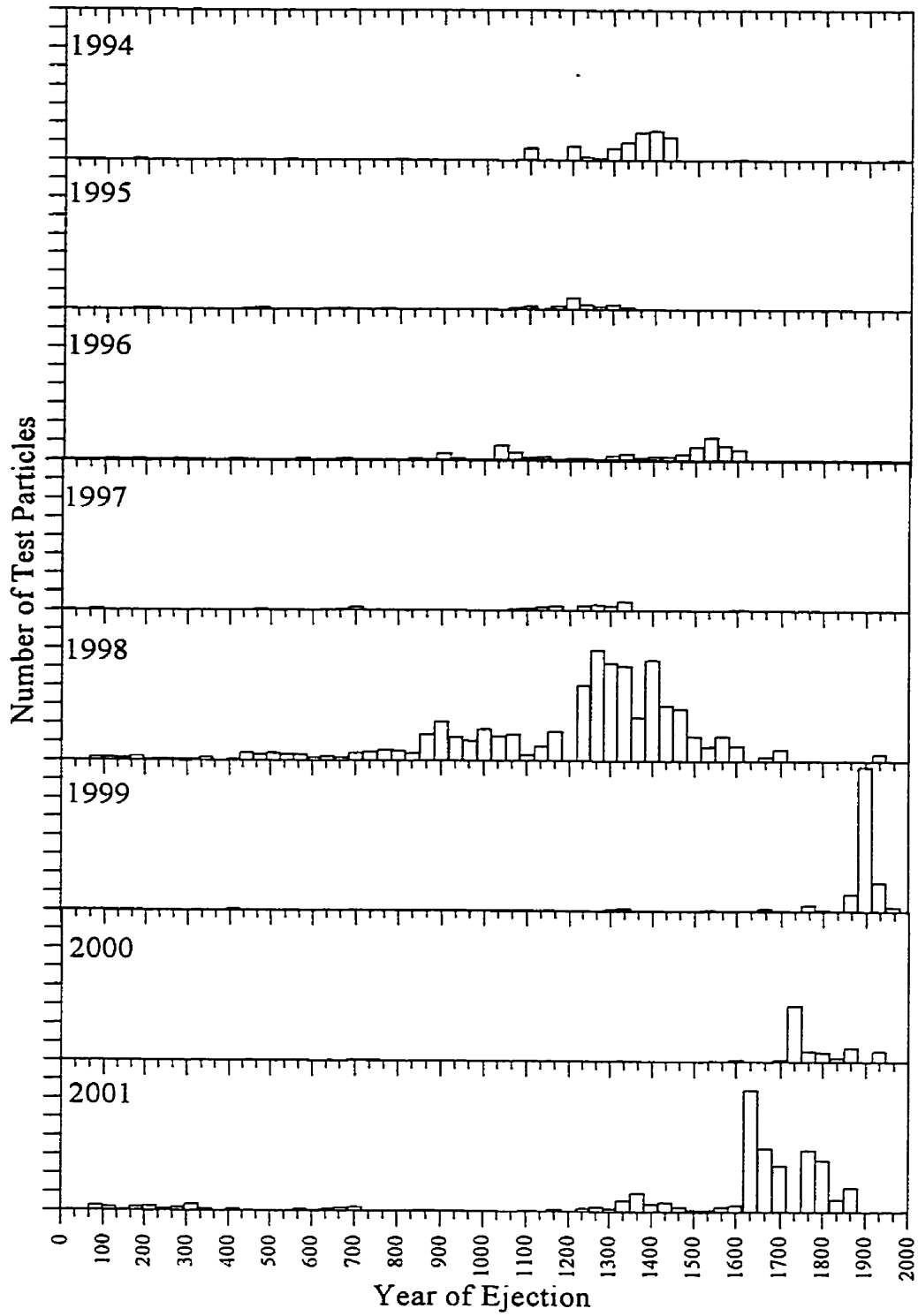

Fig 6.40: The total number of Earth-intersecting meteoroids from model 22 from all ejections over the last 2000 years for Leonid returns from 1994-2001. The ordinate is the same for all plots and runs from 0 to 170.

The 1996 return is the first that shows significant contributions less than 500 years old (and hence is the first year listed in Table 6.8). All models suggest that the activity in this year was primarily from one or a combination of meteoroids ejected during the passages from 1533-1599. Observations from 1996 (Langbroeck, 1999; Brown *et al.*, 1998) show clear evidence of a narrow enhancement of activity near 235.17° in addition to a broad background component similar to that observed in 1994 and 1995. Using the long-term model 22 integrations, the material accepted in the solar longitude range 235.1°-235.2° is composed mainly of material from 1499, but with smaller additional contributions for 100 years on either side of this epoch. It is not possible to narrow the likely ejection era further, but based on these results we can say that a more recent origin for this structure is unlikely. Examination of broader acceptance sieves, both spatial and temporal, failed to yield any material less than 400 years in age in these solar longitude ranges from any models. The location of this peak is unsurprising in light of the results shown in Sect 6.5 (Figs 6.27 and 6.28); material 400-500 years old has peak activity locations in solar longitude in the region from 235°-235.2°, very similar, coincidentally, to peak locations from recent ejections.

The narrow width of this feature (approximately two to three hours full width), however, is more consistent with dispersions in ascending nodes for ejections of order three to four revolutions at most (see Eq. 6.1) and not 10-15 revolutions old as suggested by the previous considerations alone. One possibility is that the material is much younger than the modelling suggests; in this case the material may represent particles outside the range of β and ejection velocities studied. Alternatively, the population may be as old as suggested here but have extremely small β and have experienced very similar planetary perturbations (a "clump"). As the narrow filament was rich in smaller meteoroids, a final possibility is a combination of the two; namely very young material with very small β ($<10^{-5}$) which falls outside our range of adopted β and corresponding ejection velocities. For this material to precede the comet by 1.5 years suggests that small β's are likely and leads to the probable hypothesis that the material associated with this narrow structure was of higher bulk density than the average in the stream.

Modelling for 1997 suggests a return to older meteoroids, namely 600 - 800 years

in age. Observations in 1997 (Arlt and Brown, 1998) were hampered by a full moon but confirm a broad background, rich in bright meteors, as expected for such old material. A narrower faint component may have been recorded somewhat later than 1996, but its presence is uncertain. The fainter population of Leonids shows no evidence of significant fragmentation (Hawkes *et al,* 1998), a further indication of an older population as the modelling suggests.

The modelling results for 1998 are dominated by large meteoroids occurring significantly before the nodal passage of the comet. From Fig 6.40, the age of material composing the 1998 return is primarily between 500 - 800 years, but significant amounts of even older material are also present. Notable is a possible small contribution only of more recent material (from 1932) and little else younger than 1700, a result consistent across all models (see Table 6.7). Fig 6.41 shows the distribution in mass of accepted test particles and a significant component of larger meteoroids.

Fig 6.41 (bottom): The distribution in Log mass as a function of solar longitude in 1998 for model 22 Earth-intersecting Leonids summed for all ejections from 89-1965 A.D.

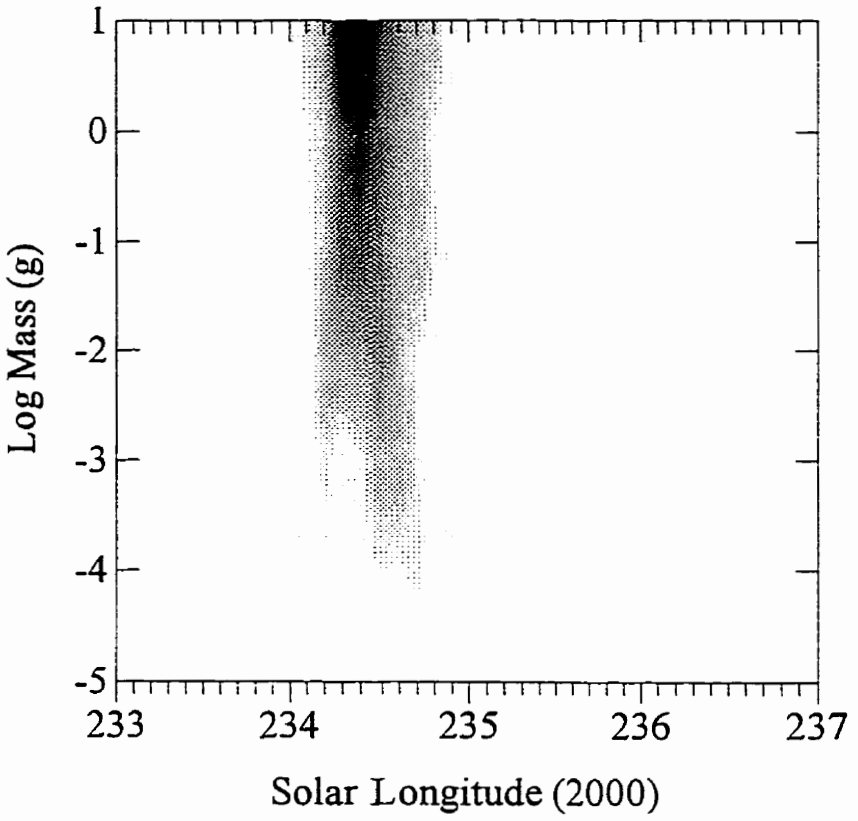

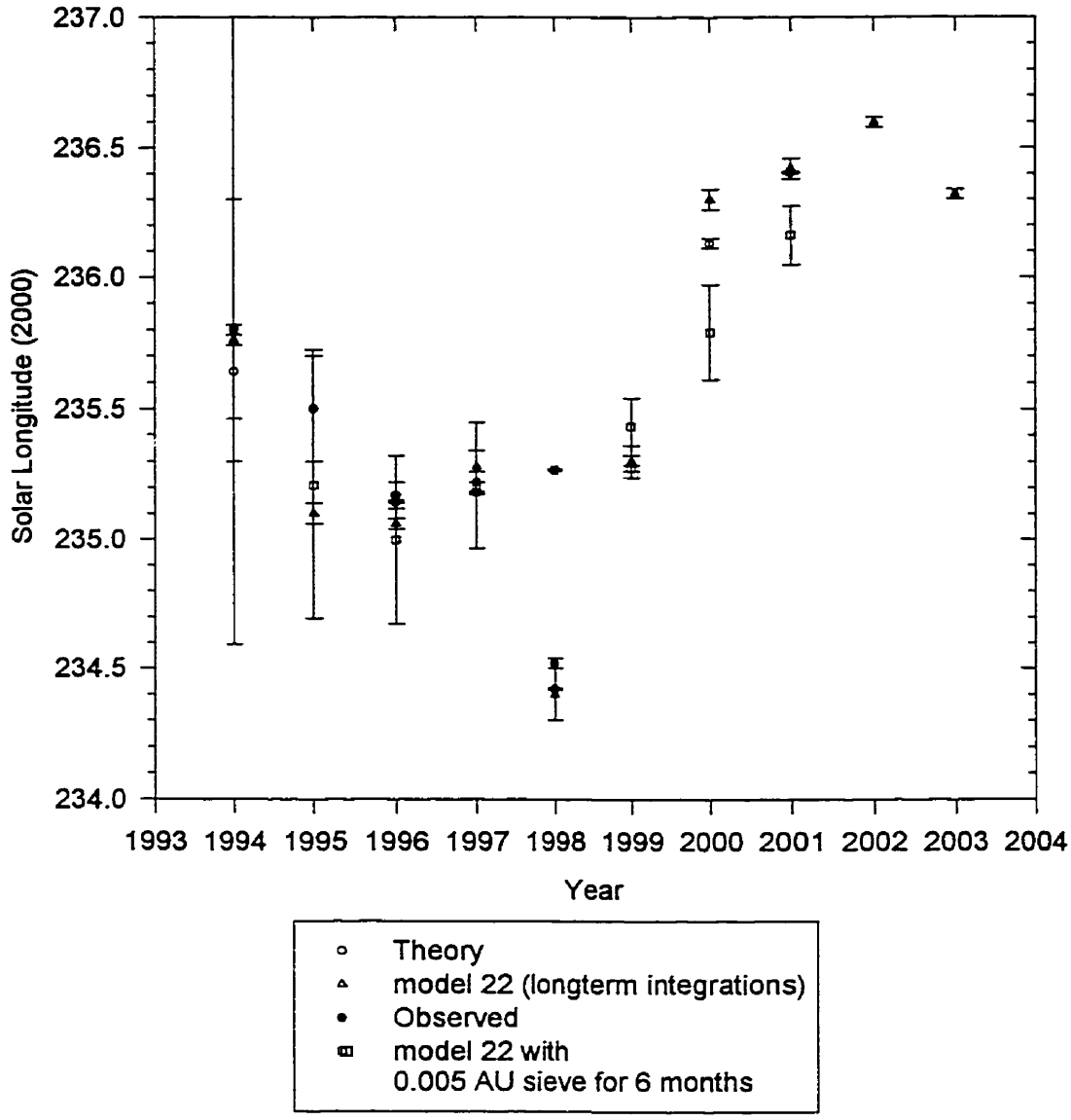

Fig 6.42: Locations of peak ZHR's for the 1998 Leonid epoch. The observed locations (for 1998 and earlier) as well as several model predictions are given as shown in the legend.

6.7.2. Leonid returns 1999-2002 : Predictions based on the modelling

Based on all results to this point, using the best combinations of acceptable models, sieve sizes and temporal nodal acceptance widths we may estimate the expected behaviour of the shower over the next four years.

Fig 6.42 shows the measured position of the peak ZHR for the Leonids from 1994-1998. Also shown in the figure are the theoretical locations based on a weighted average of all models using a 0.001 A.U. sieve with two week nodal time bins. For comparison the peak locations which are derived with a 0.005 A.U. bin and six month nodal time bins are also shown. For completeness, we have also noted the locations of maxima based on the long-term model 22 integrations, the only reliable measure of peak locations for those years with significant material older than 500 years.

The agreement between observations and the modelling is encouraging. A major discrepancy occurs in 1998 when the wide binning (0.005 A.U.) places the maximum near the node, while the true ZHR maximum (and the maximum chosen with narrower acceptance criteria) is nearly 20 hours earlier. In 1998, this was the result of inclusion of large quantities of material which were still significantly inside the Earth's orbit but which we believe are more likely to be visible at Earth in 1999. The distance to the most recent trails in 1998 is shown in Fig 6.43.

Also shown in Fig 6.43 is the trail distribution in 1999. In 1999 we expect (using all methods) the peak to be near the node of the comet, while later returns are anticipated significantly later. This trend is a direct result of slightly older material dominating the influx from 2000 onwards, with these ejections having maximum locations nearer 236° (see Figs. 6.27 and 6.28).

A similar trend has been observed (and predicted - see Chapter 4) for the Perseid shower for similar reasons. As Table 6.7 and Fig 6.43 indicate, in 1999 we will intersect the youngest material during the current cycle, namely ejecta from 1899.

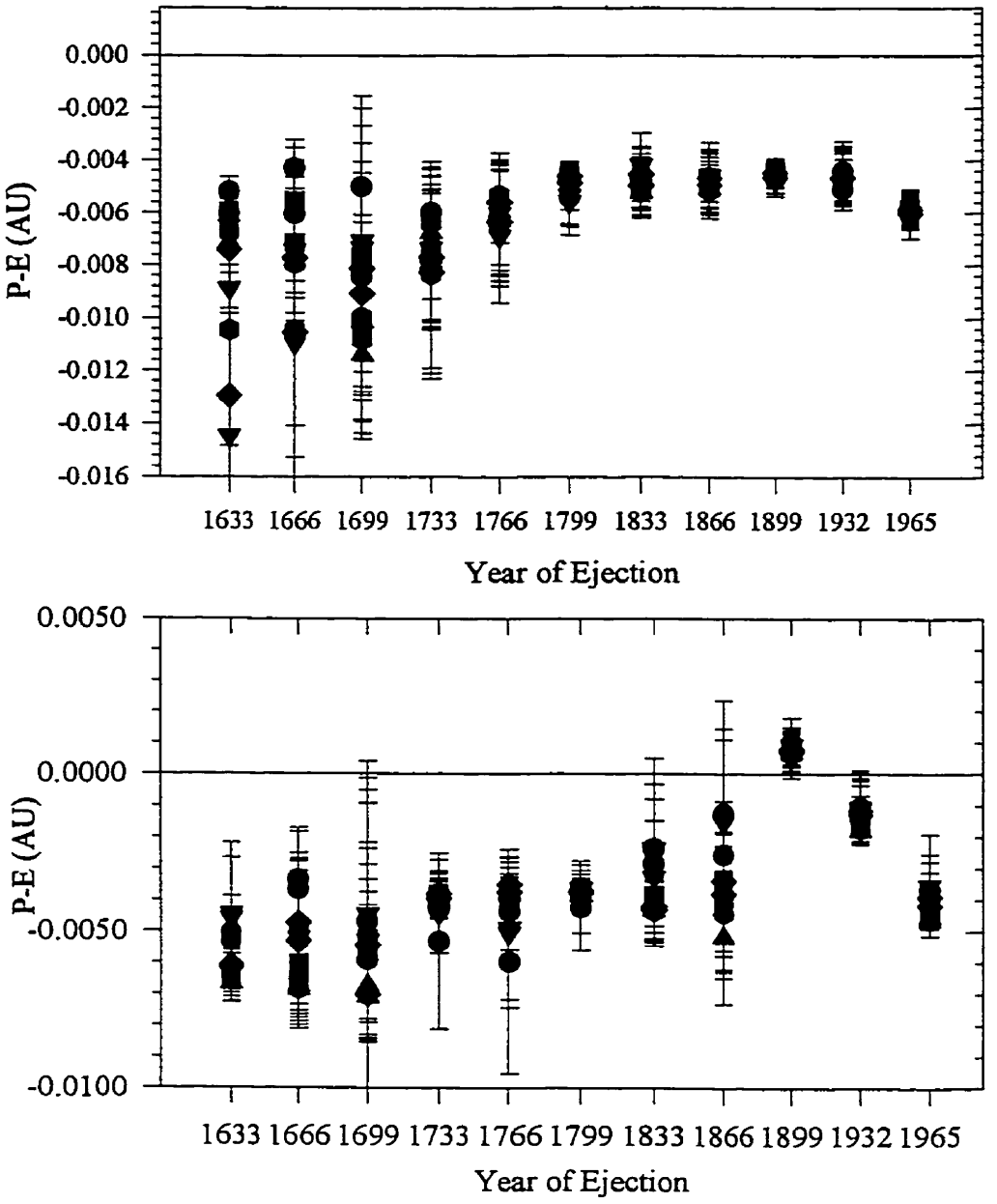

Fig 6.43: The distance from the Earth of various "trails" ejected by Tempel-Tuttle in the years listed on the abscissa. The symbols correspond to the same models as Fig 6.6. Top plot shows trail distances to Earth for test particles within 1 week of the time of the shower in 1998. The bottom plot shows the same for 1999.

This same cometary trail most probably caused the 1966 storm (see Sect 6.4.1). Fig 6.43 shows the distance between the center of each of the last eleven cometary trails and the Earth's orbit at the time of the 1999 return. Note the spread in mean distances and the large region covered by the error margins (which represent the standard deviation of the nodal radii for the particular model). While 1899 is closest to the Earth's orbit (the models having means from $6\text{-}8\times10^{-4}$ A.U. from Earth's orbit), the 1932 ejection is likewise close and might be expected to contribute also to any storm. Both 1866 and 1833 overlap with Earth's orbit within the limits of their error margins, but the spreads in their nodal radii are large both between models and for any individual model. This is a direct consequence of the planetary perturbations these meteoroids experienced circa 1899-1901. As a result, should a storm occur, it is most likely to be produced by material from 1899 or (less likely) from 1932. Both trails are still compact based on our modelling, have not suffered severe planetary perturbations and pass reasonably close to the Earth. While the numbers are small, the modelling does suggest we may just skirt the outer portions of either (or both) of these trails producing quite possibly a very strong shower or small storm at Earth.

Comparison with 1966 and the same trail shows that we are approximately three times further away from the 1899 trail than in 1966; thus a 1966 class storm is unlikely. Using the modelled decrease in density for the stream as a function of time from Sect 6.5, we expect diffusion to have decreased the trail spatial density by approximately 5-10 times since 1966. Additionally, as we pass three times further from the trail center than in 1966, and assuming a r^{-2} drop-off in density from the centre of the trail, we may tentatively estimate any storm occurring in 1999 to be ~two orders of magnitude lower in flux than in 1966. Assuming a similar mass index holds in 1999 as was observed for the 1966 storm, we tentatively estimate a peak ZHR value of order 1000 - 2000 with a peak slightly after the nodal longitude of Tempel-Tuttle in 1999. From the modelling, the 1999 display is likely to display a broader particle population and to be richer in small meteoroids relative to 1998, with the modelling suggestive of a peak in the neighborhood of β=0.001.

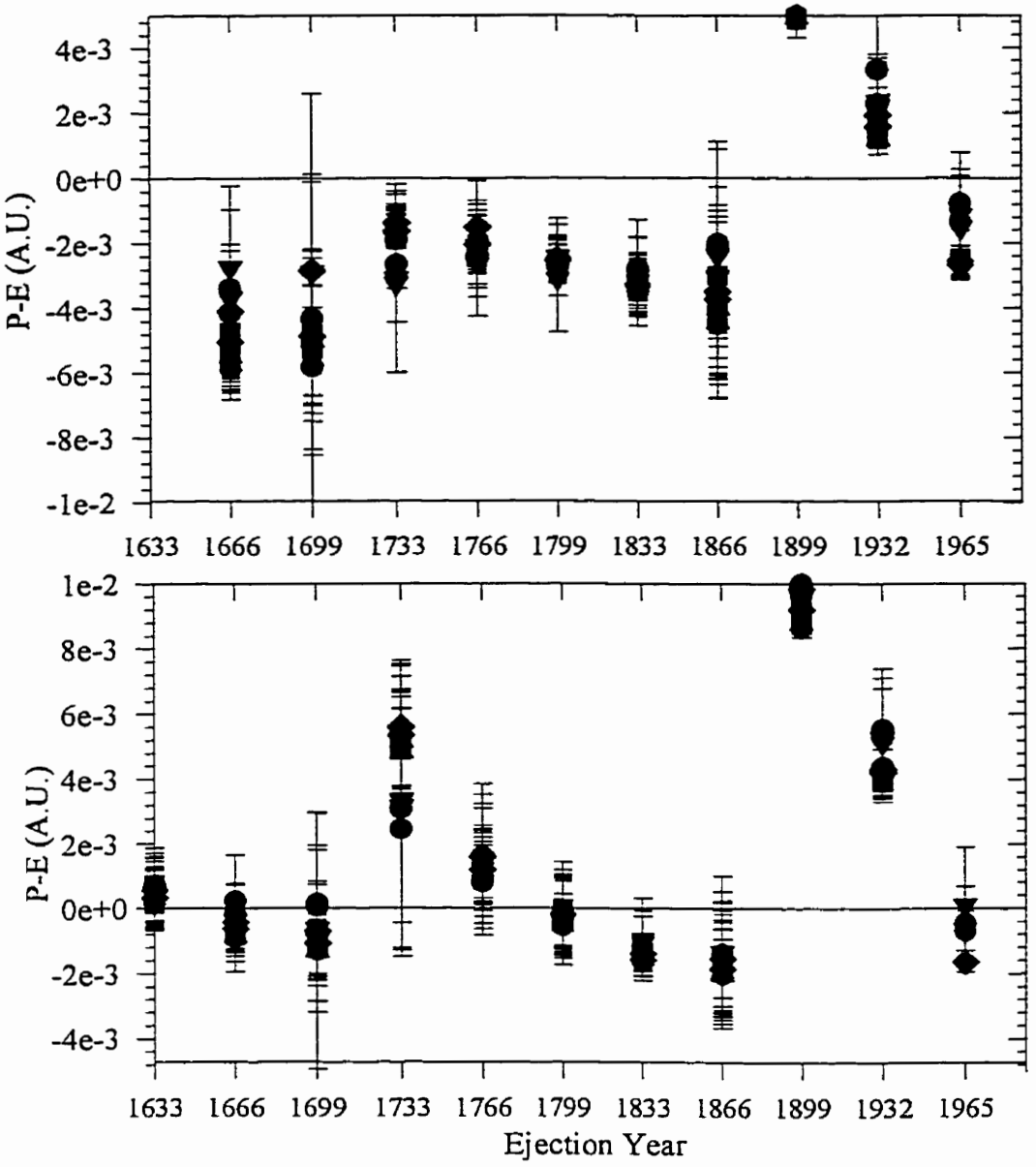

Fig 6.44: The distance from the Earth of various "trails" ejected by Tempel-Tuttle in the years listed on the abscissa. The symbols correspond to the same models as Fig 6.6. Top plot shows trail distances to Earth for test particles within 1 week of the time of the shower in 2000. The bottom plot shows the same for 2001.

Table 6.7. Age of Leonid showers for a given year as a function of modelling. The first number in each box is the total number of test particles with nodal radaii within 0.001 A.U. of Earth and times of nodal passage within 1 week of the Earth's passage through the stream. The following numbers give the primary year contributing to the integrated activity from the model and (in brackets) the fraction of all particles in a particular test year from this ejection. This summation is for all particles at all solar longitudes in the given year.

Model/Year	1996	1998	1999	2000	2001
11	0	32 **1600(.94)** 1533(.03)	191 **1899(.59)** 1932(.15)	198 **1733(.65)** 1965(.10)	613 **1699(.24)** 1633(.23)
12	2 **1533(.50)**	134 **1499(.49)** 1599(.20)	197 **1899(.70)** 1932(.14)	103 **1733(.52)** 1866(.19)	991 **1666(.35)** 1633(.34)
13	57 **1533(.47)** 1566(.21)	273 **1499(.48)** 1599(.21)	71 **1899(.80)** 1932(.08)	99 **1733(.76)** 1866(.06)	910 **1666(.39)** 1633(.34)
21	35 **1533(.43)** 1566(.29)	77 **1499(.22)** 1599(.17)	224 **1899(.58)** 1932(.23)	109 **1932(.28)** 1965(.19)	286 **1633(.21)** 1766(.20)
22	63 **1533(.38)** 1566(.24)	106 **1499(.25)** 1599(.15)	216 **1899(.71)** 1932(.14)	116 **1733(.52)** 1866(.13)	423 **1633(.31)** 1666(.16)
23	120 **1533(.33)** 1566(.25)	169 **1533(.28)** 1566(.24)	167 **1899(.77)** 1932(.11)	100 **1733(.64)** 1766(.18)	597 **1633(.34)** 1666(.25)
31	39 **1533(.31)** 1599(.26)	115 **1566(.25)** 1599(.22)	241 **1899(.58)** 1932(.22)	95 **1932(.22)** 1733(.19)	297 **1633(.28)** 1766(.20)
32	73 **1533(.30)** 1599(.27)	207 **1499(.24)** 1599(.23)	232 **1899(.75)** 1932(.18)	87 **1733(.54)** 1866(.14)	468 **1633(.29)** 1666(.20)
33	90 **1599(.28)** 1566(.27)	303 **1566(.26)** 1599(.25)	110 **1899(.89)** 1866(.05)	107 **1733(.70)** 1766(.08)	695 **1633(.34)** 1666(.33)
41	29 **1533(.45)** 1566(.17)	100 **1499(.26)** 1699(.23)	240 **1899(.60)** 1932(.19)	116 **1733(.31)** 1932(.14)	343 **1633(.27)** 1766(.16)
42	55 **1566(.29)** 1533(.25)	189 **1499(.28)** 1566(.23)	186 **1899(.76)** 1932(.15)	96 **1733(.42)** 1866(.18)	583 **1633(.34)** 1666(.26)
43	85 **1533(.41)** 1599(.21)	273 **1499(.29)** 1599(.27)	107 **1899(.84)** 1932(.08)	77 **1733(.68)** 1866(.14)	733 **1633(.35)** 1666(.33)

Fig 6.44 shows the proximity of the recent trails to the Earth at the time of the 2000 Leonid shower. Both the 1965 and 1932 trails may be modestly close to the Earth depending on the physical properties of the particles; however, in both cases it is probable that the centre of these recent trails will be much more than 10^{-3} A.U. from Earth, a likely requirement for the production of storms. Indeed, the bulk of the particles encountered from the modelling in 2000 is largely from the 1733 ejection (the same trail which produced the 1866 Leonid storm) and possibly the 1866/1932/1965. It is probable that a strong shower, and possibly a small storm, may occur in 2000, but it would likely be smaller than the 1999 shower. Peak ZHRs in this year are more likely in the range of a few hundred and if the older material from 1733 dominates it is probable the maximum will occur near 236.3° (while a dominant population of newer material would peak shortly after the nodal longitude of the comet).

The 2001 modelled shower marks a return to older material, and is proportionately richer in larger meteoroids than the 2000 modelled display (though showing a wider range in accepted masses than 1998). In terms of dense recent trails, Fig 6.43 shows that only the 1965 or the 1866 (or older) trails might be significant. All the material from 1965 that is accessible in 2001 has very high β ($\sim 5\times10^{-3}$), reminiscent of the 1969 shower geometry. Peak ZHRs are likely in the range of a few hundred, and a short-lived shower similar to 1901/1903 peaking at 236.4° is suggested by the modelling, assuming that older material dominates. This older material (from 1633-1699) shows a peak transfer efficiency near $\beta \sim 10^{-4}$.

The 2002 shower shows potential for material from several trails to interact with Earth. The Earth's proximity to each of these trails in 2002 suggests that if significant numbers of relatively small β particles are present a strong shower (comparable to the 1969 Leonid outburst) might occur. Of course the main concentrations in these trails passed through the descending node several years earlier and thus only modest particle numbers would be expected (relative to storm years). Notable is the confinement of this outburst to a narrow range of β from 5×10^{-4} - 10^{-3}.

6.8 Summary and Conclusions

Based on the foregoing numerical modelling of the Leonid stream we may directly summarize the most probable answers to the questions posed in Sect 6.1.

1. The age and origin of the ejecta which constitute the primary Leonid storms (outlined in Chapter 5) all have recent (less than two or at most three passages old) ejection origins. The only possible exception is the return in 1832 that may consist of meteoroids released ~150 years earlier, but the actual character of the 1832 display (whether a storm or a long enduring shower consisting of bright meteors) is in doubt. All storms in these years were caused by cometary trails averaging (summed over all models and visual masses) $(8\pm6)\times10^{-4}$ A.U. from Earth's orbit at the time of the storms. The trails associated with the strongest storms were less than 7×10^{-4} A.U. in width and one to three times (on average) this amount in radial spread for our chosen range of βs. The trails may best be described as "thick" sheets or elongated tubes. The dense trails are moved to Earth-intersection through perturbations by Jupiter and Saturn, in the above cases in particular by distant, primarily post-perihelion perturbations which move the trails outward as a function of nodal return time and thus allow trails to reach Earth.

That storms occur outside Tempel-Tuttle's orbit and after its nodal passage has been previously noted (cf. Yeomans 1981). However, the mechanism most identified as causing this behaviour has been the direct effects of radiation pressure (Yeomans 1981; Wu and Williams 1991). From Fig 2.6 and Figs 6.3, 6.14 we see that radiation pressure changes to the nodal radii for the majority of Leonid meteoroids (released near perihelion) are negligible in comparison to the effects of planetary perturbations for meteoroids of the sizes considered here, a conclusion also reached by Sekanina (1974). Radiation pressure does cause meteoroids to lag the comet as demonstrated extensively in our simulations, but this alone is not a sufficient condition for causing storms. The distant perturbations from Jupiter affect a significant portion of the stream on most passages of Tempel-Tuttle; it is the effect of these on the future nodal distances of Leonid meteoroids that allows material which progressively lags the comet to move outward from the sun at the node

and intersect the Earth.

2. The most complete information concerning the initial ejection velocities comes from comparison of the activity curves for the 1866, 1867, 1966 and 1969 storms/showers with the modelled results. Comparing the observed profiles of these showers with the final activity widths from test particles released during the perihelion passage causing the storms and the relating these back to the normal components of the ejection velocities, we find that a range of probable ejection velocities has been established. In particular, the best fits to the observed profile were found for meteoroids with total ejection velocities of ~5 m/s for the 1866 storm, 15-20 m/s for 1867, 3-4 m/s for the 1966 storm and 10-15 m/s for the 1969 outburst. These values represent the average expected ejection velocities for material encountering the Earth at the time of these storms and do not necessarily represent the actual distribution of ejection velocities at the comet. These results simply suggest that significant numbers of meteoroids must be ejected from Tempel-Tuttle with velocities <20 m/s. Meteoroid populations ejected at higher velocities and which can be detected at Earth have final activity widths inconsistent with the observed widths. Note that the best fit velocities vary from storm to storm due to differences in the favorability of Earth-intersection based on initial ejection geometry, subsequent perturbations etc. and do not reflect changes in the mean ejection velocities between perihelion passages (which are the same in our modelling).

3. and 4. The comet-Earth distance for past ejections plays a minor role only in determining the future (~centuries) delivery of Leonid meteoroids to Earth. This results directly from the fact that the magnitude of the change in nodal distance due to planetary perturbations is much larger than the average comet-Earth distance over the last millenium. Strong perturbations from Jupiter, for example, may move the nodal points of Leonid meteoroids en masse by up to 0.01 A.U. every ~150 years, with the average comet-Earth separation being smaller than this value. Meteoroids with smaller β arrive in Earth-intersecting orbits more frequently after 300 years, independent of initial ejection conditions, possibly due to lesser overall differential planetary perturbations (and thus diffusion) compared to higher-β populations.

5. Numerical computation of the average relative change in stream density, as measured at the descending node, shows that the average flux within the stream for the models and masses studied decreases by between two and three orders of magnitude 100-150 years after ejection, with different models showing similar behaviour. Fig 6.25 summarizes the typical model results for the average relative changes in density.

6. Jupiter dominates the evolution of the Leonid stream. It is the main perturbing force on the Leonids, and its perturbations "peak" every five revolutions of 55P/Tempel-Tuttle. Mean motion resonances, particularly the 5:14, 4:11 and 1:3, affect the development of the stream by removing and/or concentrating Leonid meteoroids in semi-major axis intervals determined by these resonances. Saturn affects the stream to a smaller degree, but acts in concert with Jupiter to affect noticeably the delivery of Leonids to Earth, potentially through the 8:9 mean motion resonance. Uranus has a much lesser effect on the stream and its 5:2 mean motion resonance shows no effects on the semi-major axis distribution of Leonids, nor has Tempel-Tuttle been located in this resonance over the last 2000 years. Uranus does appear to modify the delivery to Earth of some Leonid meteoroids shortly after nodal passage of Tempel-Tuttle, in partial agreement with the conclusions of Williams (1997). That Uranus dominates many of the evolutionary aspects of the stream, however, as suggested by Williams (1997) is not confirmed by our work.

7. From Fig. 6.26, the combined effects of initial ejection velocity and radiation pressure limit the flux of the stream over intervals <100 years. Over longer time intervals, the flux is limited by planetary perturbations, primarily from Jupiter. For the lower ejection velocities suggested from **2** (which are several times lower than utilized in Fig 6.26), the effects of radiation pressure may be expected to dominate the first century of density decrease in the stream for smaller meteoroids.

8. From **1** the most representative models would appear to be those with the lowest ejection velocities, namely Crifo's extended production model 1. Of the three densities

chosen for model 1, the lowest density (corresponding to the largest cross-sectional areas for a given mass) also has the lowest ejection velocities. To confirm this, we have computed the residuals between the observed activity profiles of the four Leonid returns for which we have the greatest confidence in ejection origin and sufficient observations (1866, 1867, 1966 and 1969) and the complete model profile. These normalized residuals are given in Table 6.9. As expected, model 11 is the best fit overall. That the ejection velocities from Tempel-Tuttle are low has been repeatedly emphasized in previous work (see Sect 1.1), with values very similar to those we find most probable. Whipple-sized ejection velocities appear to be too high by a factor of several for Tempel-Tuttle. Given the various uncertainties in the physical properties of the meteoroids and the great simplifications of the Whipple approach (compared to modern coma-dust models such as Crifo and Rodinov 1999), it is hardly surprising that the model is not a precise analog to reality for every comet.

The disagreement between the predicted Whipple ejection velocities and our most probable velocities is not outrageous. Use of smaller average cross-sections or the existence of specific active areas producing jets with more sunward average velocity components (and hence smaller normal velocities) than our uniform hemispherical production could all account for the discrepancies within the uncertainties. Indeed, Wu and Williams (1996) have proposed ejection velocities up to an order of magnitude higher than those predicted by the Whipple formalism, underlining the range of inherent uncertainty.

Table 6.8: Normalized residuals of fit between the total scaled model activity profiles and gaussian fits to ZHR curves in each of the given years. For each model distribution, the largest peak number of test particles per 0.005° solar longitude bins was scaled to match peak ZHRs in the solar longitude interval about the observed storm peak and other model bins were then scaled by this factor. The resulting theoretical ZHR profiles for all models were subtracted from the observed gaussian fits over the same number of bins and the sum of the squares of these differences computed. These final residual values were then scaled such that the smallest residual was given the value of unity. As a consequence of the large differences in absolute numbers, the values of the normalized residuals between years has little meaning – only the relative values of fit within a given year are meaningful. Model residuals omitted for a given year are due to no test particles being accepted near the observed ZHR maximum.

Model\Year	1969	1966	1867	1866
11	1	1	2.975	1
12	-	15.845	3.087	1.561
13	-	8.799	-	1.512
21	1.213	4.299	1	1.087
22	-	22.293	1.624	1.309
23	-	4.041	-	1.264
31	1.25	9.468	1.986	1.098
32	-	5.23	1.564	1.196
33	-	2.897	-	1.685
41	2.662	13.396	1.429	1.115
42	-	4.595	2.288	1.668
43	-	8.579	1.824	1.563

9. The sudden large increases in Leonid flux near the time of comet's passage and the equally sudden decrease three to four years after its perihelion passage are a natural consequence of the rapid diffusion of older material within the stream and Earth's sampling farther from the maximum density within the stream (which is typically <20° mean anomaly after the comet). From Fig 6.40, for example, Leonid returns only one to two years after perihelion passage of the comet are the only years which have significant populations of meteoroids with ejection ages of less than a century (see also a similar trend in Tables 6.3-6.7). Based on **1**, these are also the only returns where material is dense enough to cause a storm or strong shower. In years when material even a few revolutions older is encountered, the flux has fallen greatly. This is in part a consequence of diffusion of older material (Fig 6.25) and of the Earth's sampling temporally further from the densest portions of the trail(s) within the stream. The age of the annual component of the Leonids is of order ~1000 years based on the results of Sect 6.5, with ejections older than this contributing little at the present time to the stream fluence. This age is consistent with the first recorded observations of the Leonid storms in 902 A.D. and with the ~10 day total duration of the shower (from Chapter 5), producing an age estimate of <2000 years using the results of Fig 6.22. A contributing factor limiting the lifetime of the broader, annual component of the stream, may be the closer inbound encounter distances to Jupiter and Saturn 900 – 1000 years ago (see Figs 6.30 and 6.31). This may also account for the drop in the number of test meteoroids in the present epoch at Earth from ejections prior to 1100 A.D.

References

Adams, J.C. 1867. On the Orbit of the November meteors, *Mon. Not. R. Astron. Soc.*, **27**, 247-252.

Arlt, R. and P. Brown. 1998. Bulletin 12 of the International Leonid Watch: Final results of the 1997 Leonids and prospects for 1998. *WGN J. Int. Met. Org.* **26(4)**, 161-165.

Asher, D.J. 1999. On the Leonid Storms of 1833 and 1966, *MNRAS*, in press.

Berberich, A. 1898. On the orbit-perturbations of the Leonid meteor-stream since 1890. *Astron. Nachr.* **147**, 359.

Brown, P. 1999. The Leonid Meteor Shower: Historical Visual Observations, *Icarus*, in press.

Brown, P. and J. Jones. 1993. Evolution of the Leonid meteor stream. In *Meteoroids and Their Parent Bodies* (J. Stohan and I. P. Williams, Eds.) pp. 57-61. Astronomical Inst. Slovak Acad. Sci., Bratislava.

Brown, P. and J. Jones. 1998. Simulation of the formation and evolution of the Perseid meteoroid stream. *Icarus* **133**, 36-68.

Brown, P., M. Simek, and J. Jones. 1997. Radar Observations of the Leonids: 1964-1995, *A&A*, **322**, 687-695.

Carusi, A., L. Kresak, E. Perozzi and G. B. Valsecchi. 1987. High-order librations of Halley-type comets. *Astron. Astrophys.* **187**, 899.

Chambers, J. E. 1995. The long term dynamical evolution of comet Swift-Tuttle. *Icarus* **114**, 372-386.

Crifo, J. F. 1995. A general physicochemical model of the inner coma of active comets. I-Implications of spatially distributed gas and dust production. *Astrophys. J.* **445**, 470-488.

Crifo, J.F. and A.V. Rodionov 1999. Modelling the Surface Activity of Cometary Nuclei, IAU Symposium 168, in press.

Emel'yanenko, V. V. 1984. Meteor-stream density evolution by planetary perturbations. *Sov. Astron. Letters* **10**, 131.

Fulle, M. 1996. Dust environment and nucleus spin axis of comet P/Tempel 2 from models of the infrared dust tail observed by IRAS. *Astron. Astrophys.* **311**, 333-339.

Greenberg, R. 1977. Orbit-orbit resonances in the solar system - Varieties and similarities. *Vistas Astron.* **21(3)**, 209-239.

Hainaut, O.R., K.J. Meech, H. Boehnhardt and R.M. West, 1998. Early Recovery of Comet 55P/Tempel-Tuttle, *A&A*, 333, 746-752.

Hasegawa, I. 1993. Historical records of meteor showers. In *Meteoroids and Their Parent Bodies* (J. Stohl and I. P. Williams, Eds.), pp.209-227. Astronomical Inst. Slovak Acad. Sci., Bratislava.

Hawkes, R. L., M. Campbell, D. Babcock and P. Brown. 1998. The physical structure of Leonid meteoroids: evidence from optical observations. In *Proceedings of the Leonid Meteoroid Storm and Satellite Threat Conference, Manhattan Beach, California, April 27-28, 1998* (D. Lynch, Ed.). American Institute of Aeronautics and Astronautics, Los Angeles.

Herrick, E. C. 1841. Contributions towards a history of the star-showers of former times. *Amer. J. Sci. Arts*. **40**, 349.

Jones, J. 1985. The structure of the Geminid meteor stream. I – The effect of planetary perturbations. *Mon. Not. R. Astron. Soc.* **217**, 523-532.

Jones, J. 1995. The ejection of meteoroids from comets. *Mon. Not. R. Astron. Soc.* **275**, 773-780.

Kazimirchak-Polonskaja, E.I., Belijaev, N.A., Astapovic, I.S., and A.K. Terentjeva. 1968. Investigation of the perturbed motion of the Leonid meteor stream. In *Physics and Dynamics of Meteors Proceedings of IAU Symp No. 33*, (L. Kresak, and P.M. Millman, Eds.),pp. 449-475, D. Reidel, Dordrecht-Holland.

Kondrat'eva, E. D. and E. A. Reznikov. 1985. Comet Tempel-Tuttle and the Leonid meteor swarm. *Astron. Vest.* **19**, 96.

Kresak, L. 1992. On the ejection and dispersion velocities of meteor particles. *Contr. Skalnate. Pleso* **22**, 123-130.

Kresak, L. 1993. Cometary dust trails and meteor storms. *Astron. Astrophys.* **279**, 646-660.

Langbroek, M. 1999. Leonid outburst activity 1996: A broad structure and a first occurrence of a narrow peak in fainter meteors, *MAPS*, **34**, 137-147.

Le Verrier, U-J-J. 1867. Sur les Etoiles filantes de 13 Novembre et du 10 Aout, *Comptes Rendus*, **64**, 94-99.

Littman, M. 1998. *The Heavens on Fire*. Cambridge University Press, Cambridge.

Mason, J. W. 1995. The Leonid meteors and comet 55P/Tempel-Tuttle. *J. Brit. Astron. Assoc.* **105 (5)**, 219-235.

McDonnell, J. A. M., and 9 colleagues. 1987. The dust distribution within the inner coma of comet P/Halley 1982i—Encounter by Giotto's impact detectors. *Astron. Astrophys.* **187**, 719-741.

McIntosh, B. A. 1973. Origin and evolution of recent Leonid meteor shower. In *Evolutionary and Physical Properties of Meteoroids (NASA SP-319)* (C. G. Hemenway, P. M. Millman, and A. F. Cook, Eds.), pp. 193-199. NASA, Washington, DC.

Murakami, T. 1959. On the structure of the Leonid stream. *Pub. Astron. Soc. Japan.* **11**, 171.

Murakami. T. 1961. On the structure of the Leonid stream, II. Magnitude-distribution of meteoric particles in the Leonid stream. *Pub. Astron. Soc. Japan*. **13**, 51.

Murakami, T. 1961. On the structure of the Leonid stream, III. The formation and development of the Leonid stream. *Pub. Astron. Soc. Japan*. **13**, 212.

Murray, N. Holman, M. and M. Potter, 1999. On the origin of chaos in the asteroid belt, *AJ*, **116**, 2583-2589.

Newton, H. A. 1863. Evidence of the cosmical origin of shooting stars derived from the dates of early star-showers. *Amer. J. Sci. Arts (2nd Series)*. **37**, 145.

Olbers, H. W. M. 1837. Die Sternschnuppen. In *Schumacher's Jahrbuch fur 1837*, pp. 36.

Olmsted, D. 1834. Observations of the meteors of November 13, 1833. *Am. J. Sci.* **25**, 354-411; 26, 132-174.

Schiaparelli, G. V. 1867. Sur les Etoiles Filantes, et specialement sur l'identification des

Orbites des Essaims d'Aout et de Novembre avec celles des Cometes de 1862 et de 1866. *Comptes Rendus* **64**, 598-599.

Schubart, J. 1968. Long-period effects in the motion of Hilda-type planets. *Astron. J.* **73**, 99-103

Sekanina, Z. 1974. Meteoric storms and the formation of meteor streams. In *Asteroids, Comets and Meteoric Matter* (C. Cristescu, W. J. Klepczynski, and B. Milet, Eds.), pp. 239-267. Scholium Int., New York.

Stoney, G.J. and A. M. Downing. 1899. Perturbations of the Leonids. *Proc. Roy. Soc. London.* **64**, 403.

Whipple, F. L. 1951. A comet model II. Physical relations for comets and meteors. *Ap. J.* **113**, 464.

Williams, I. P. 1997. The Leonid meteor shower - Why are there storms but no regular annual activity? *Mon. Not. R. Astron. Soc.* **292**, L37-L40.

Williams, I. P., C. Johnson, and K. Fox. 1986. Meteor storms. In *Asteroids, Comets, Meteors II;Proceedings of the International Meeting, Uppsala, Sweden, June 3-6, 1985* (C.-I. Lagerkvist, B. A. Lindblad, H. Lundstadt, and H. Rickman, Eds.) pp. 559-563. Astronomiska Observatoriet, Uppsala, Sweden.

Wu, Z. and I. P. Williams. 1991. Formation of the Leonid meteor stream and storm. In *Asteroids, comets, meteors 1991; Proceedings of the International Conference, Flagstaff, Arizona, June 24-28, 1991* (A. W. Harris and E. Bowell, Eds.) pp. 661-665. The Lunar and Planetary Institute, Houston, Texas.

Wu, Z. and I. P. Williams. 1996. Leonid meteor storms. *Mon. Not. R. Astron. Soc.* **280**, 1210-1218.

Yeomans, D. 1981. Comet Tempel-Tuttle and the Leonid meteors. *Icarus* **47**, 492-499.

Yeomans, D., K. K. Yau and P. R. Weissman. 1996. The impending appearance of comet Tempel-Tuttle and the Leonid meteors. *Icarus* **124**, 407-413.

Chapter 7: Conclusions, Summary and Future Work

7.1 Summary and Conclusions

In this thesis I have developed and applied a numerical model for the formation and subsequent evolution of two meteoroid streams, the Perseids and Leonids. The numerical results have been compared to available observations of the streams and the best physical representations of the cometary decay processes involved derived as a result.

The two streams, while periodic in nature, are very different. Two key reasons for these differences may be identified. First, the parent comet of the Perseids (Swift-Tuttle) is larger, probably older and is certainly more active than Tempel-Tuttle; with the relative mass difference of the comets being more than two orders of magnitude. Secondly, the encounter distance/geometries of the two comets with the Earth and their orbital energies are very different. Swift-Tuttle has a nodal point which has always been outside the Earth's orbit in the recent past and almost an order of magnitude further than Tempel-Tuttle's nodal point, while at the same time having less than 1/2 the specific energy of Tempel-Tuttle's orbit.

One manifestation of the first difference is in the best fit ejection velocities from each comet which are most able to reproduce observed stream activity at Earth: for Swift-Tuttle this yields best-fit ejection velocities of order 10 - 100 m/s for visual class ($<10^{-3}$ g) meteoroids, while for Tempel-Tuttle the fits are most consistent with average ejection velocities of a few m/s and certainly <20 m/s. The age of the Perseids, of order ~25 000 years for the core component of the stream, is an order of magnitude greater than for the Leonids, implying a far greater distribution of material perpendicular to the Perseid orbit and thus a much longer period of activity (as is observed).

The difference in encounter geometries is critical. From our simulations, we find the delivery of Perseid meteoroids to Earth is tightly correlated with the distance to the comet at the time of ejection; no similarly strong correlation exists for the Leonids. The

greater distance for Perseids implies that we only skirt the outer portions of the densest portions of the stream; this effect is further enhanced by radiation pressure which is slightly more significant for the larger orbit of the Perseids than for the Leonids. The youngest Leonids may have nodal points so close to the Earth as to be accessible to it after only one or a few revolutions; as a result Earth may access the very densest portions of the Leonid stream and strong storms may result. No similar geometry exists for the Perseids and this effect, combined with higher Perseid ejection velocities, greater relative radiation pressure effects and lower orbital energy (and longer period) for the stream implies much faster diffusion of the densest portions of that stream, relative to the Leonids. Such distinctions provide a probable explanation for the difference in magnitude between the observed relative strengths of the periodic and annual components of the two streams. It also suggests that storms comparable to the Leonids from the Perseid stream are unlikely.

Similarities, however, do exist between the two showers. Planetary perturbations, most notably from Jupiter, dominate the evolution of both streams. These planetary perturbations also move nodal points into Earth-crossing orbits and directly result in the "periodic" component of the showers. For the Perseids, it is pre-perihelion perturbations from Jupiter and Saturn which move meteoroid nodal distances in the present epoch inward enough to intersect the Earth; for the Leonids, more distant direct perturbations cause much smaller but systematic differential perturbations which move the nodal distances outward. The effects of terrestrial perturbations are small to negligible for both showers, despite Earth being the planet, which passes closest to the mean stream orbits.

As well, the time-scale (in terms of stream revolution periods) over which various evolutionary forces rule is similar. For the Perseids, the initial ejection velocities are important over the first ~5 revolutions post-ejection after which radiation pressure and planetary perturbations control subsequent evolution. The ejection velocities and radiation pressure effects for the Leonids are the key mechanisms in stream development for the first three or four revolutions after which planetary perturbations take over. The makeup of the "outbursts" and (for the Leonids) "storms" are also comparable in age for the two streams - typically less than five or six revolutions old. The systematic shifts in the positions of maximum from year to year for both streams are clearly linked to the

differing age of the primary meteoroid populations represented in both cases.

For the first time, we have investigated through simulation, a number of characteristics associated with both the Perseids and Leonids. The probable age for the various outbursts of the Perseid stream observed over the last decade and the location of these outburst maxima have been identified and correctly predicted (and post-dicted). Using observed radiant dispersion and average location as well as shower duration and width we have also estimated the age for the core population of the Perseids (~25 000 years), its ultimate age (>100 000 years) and shown that the outbursts we are currently experiencing from the stream are young (typically less than five revolutions of the comet in age). We have also identified the most probable ejection origin(s) for each outburst and their physical cause (impulsive perturbations from Jupiter and Saturn). As well, we have also directly associated sungrazing and hyperbolic ejection of test meteoroids from the Perseids as probable sinks for the stream over periods comparable to the age of the core and diffuse population as well as clarifying the role of the Earth in the evolution of the Perseid stream as minor.

The age and origin of the storms from the Leonids observed over the last 200 years have been established and found to be in general agreement with previous determinations made by Kondra'teva and Reznikov (1985), Kondra'teva et al., (1997) and Asher (1999). The distances from each of the dense cometary "trails" causing these storms was found to agree well with the independent determinations of Asher (1999). We have found that material evolving outside the orbit of comet Tempel-Tuttle does so primarily through previous distant direct perturbations from Jupiter, often on the outbound leg of the Leonid orbit. Radiation pressure does not directly increase noticeably the nodal distances for the masses examined, though it does cause meteoroids to lag the comet. It is these differential perturbations, due to distant, direct, often outbound Jovian effects, which cause stream meteoroids to move significantly outward relative to the cometary nodal position; a similar effect has been mentioned by Asher (1999). We have compared the observed widths of several Leonid storms with those suggested through modelling and determined that the most probable normal component of ejection velocities for Leonids for the largest storms is 1-5 m/s, in agreement with previous investigators using other methods (eg. Kresak 1993). The overall ejection velocities are

of order ~10 m/s for the population causing storms. The density diffusion has been quantitatively examined and found to decrease by two to three orders of magnitude in approximately 100 years for the densest portion of the stream; the temporal regimes in which various forces likely dominate evolution have also been identified. The possible role of several mean motion resonances and Tempel-Tuttle has been examined as has the effect these resonances may have on the distribution of semi-major axes within the Leonid stream.

7.2 Future Work

Numerical modelling of meteor streams has developed in concert with the availability of fast computers. Only in the last decade have computers fast enough to efficiently follow the orbital evolution of significant numbers of test particles been available.

Interestingly, though the speed of computers has increased significantly, most workers have not exploted this to investigate the effects changes in the many free parameters have on the final distribution of meteoroids through computation of many additional test particles. For example, Wu and Williams (1996) recently studied the Leonids, but they used only a few hundred test particles to investigate it. The reason has become apparent in undertaking this work: with 10^7 or more test particles to follow, the limiting factor is not the computation time, but rather the daunting task of analyzing and interpreting (as well as storing) this amount of information. Yet many of the results in this thesis would not have been apparent had only a few hundred (or even a few thousand) test particles been examined. For many of the tasks in interpretation it is only the very small sub-population near the Earth at the time of past (or future) shower apparitions which are important; from this perspective most of the particles are a "waste" of integration time (though not in the case of macro-features of the streams such as diffusion). Wu and Williams (1996), for example, have attempted to overcome this by recognizing that only specific values of mean anomaly at a single point of ejection will produce near intersection with Earth at some future date. However, even modestly small ejection speeds, (in many directions, at varying positions along the orbital arc of the comet and covering differing values of radiation pressure) quickly complicate this simple

situation and make its applicability limited.

In its ideal form, the simulation of the evolution of the stream could be entirely divorced from the need to adopt any physical model for the stream formation. Instead a grid of ejection velocity and radiation pressure combinations could be formulated at each step along the orbital arc for each past apparition of the comet and then the evolution of each particle followed to Earth-intersection. In this way the most "efficient" ejection conditions could be established and then compared to physical models.

The other limiting factor in our understanding of meteor stream evolution is a paucity of observations. While activity curves for showers are regularly produced from observations each year, many more precise radiant determinations would provide a more complete testbed for studying the evolution of streams.

Perhaps the most promising technique, however, for studying the ejection conditions and evolution of (young) meteoroid streams is hyperprecise velocity/trajectory information. The backward integration of very precise individual meteor observations offers the greatest hope of unlocking the secret of the magnitude/direction of meteoroid ejection as well as location. Gustafson (1989) has attempted such a technique for some precisely observed Geminids with modest success. Potentially the most powerful technique in this regard is down-the-beam radar observations of head-echoes (Taylor et al. 1995) which would permit velocity determinations to of order a few m/s as well as trajectory information comparable in precision to photographic observations.

References

Asher, D. 1999. The Leonid Meteor storms of 1833 and 1966, *MNRAS*, in press.

Gustafson, B. 1989. Geminid meteoroids traced to cometary activity on Phaethon, *A&A*, **225**, 533.

Kondrat'eva, E.D. and E.A. Reznikov. 1985. Comet Tempel-Tuttle and the Leonid meteor swarm, *Sol. Sys. Res.*, **19**, 96.

Kondrat'eva, E. D., I.N. Murav'eva,and E.A. Reznikov, 1997. On the Forthcoming Return of the Leonid Meteoric Swarm, *AVest*, **31**, 489.

Kresak, L. 1993. Cometary Dust Trails and Meteor Storms, A&A, **279**, 646.

Taylor, A.D. M.A. Cervera, W.G. Elford and D.I. Steel, 1995. A new Technique for Radar Meteor Speed Determination: Inter-pulse Phase Changes from head echoes, in *Physics, Chemistry and Dynamics of Interplanetary Dust*, eds. B. Gustafson and M. Hanner, p. 75, Astronomical Society of the Pacific.

Wu, Z. and I.P. Williams, 1996. Leonid Meteor Storms. *MNRAS*, **280**, 1210.

Appendix A : Orbital Element definitions and the Orbital elements of 55P/Tempel-Tuttle and 109P/Swift-Tuttle

To completely define the shape and orientation of an orbit in space, it is necessary to specify five elements. Fig A.1 describes the elliptic orbit in space and defines these quantities.

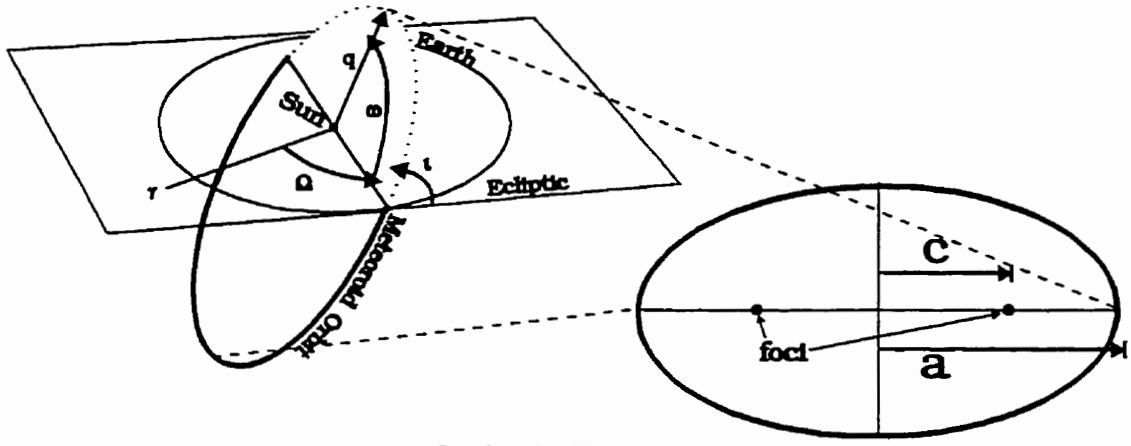

e=eccentricity of orbital ellipse (c/a)
i=inclination (angle between ecliptic and plane of orbit)
q=perihelion distance
ω=argument of perihelion (angle in orbit between ascending node and point of perihelion)
Ω=longitude of ascending node (angle from vernal equinox to point orbit crosses from under to above ecliptic plane)

Fig A.1 General elements of an orbit. Five elements are needed to specify the orientation of an orbit in the solar system and one additional element to specify the precise position of the meteoroid.

Table A1: Osculating orbital elements for 55P/Tempel-Tuttle and 109P/Swift-Tuttle during their most recent periehlion passages. a is the semi-major axis of the orbit in Astronomical Units, e is the eccentricity, i is the inclination of the orbit from the ecliptic plane in degrees, Ω is the longitude of the ascneding node in degrees, ω is the argument of perihelion in degrees, q is the perihelion distance in A.U., rnode is the radius of the decending node in A.U. and T is the time of the most recent perihelion. Fig A1 describes the meaning of these orbital elements in more detail. All angular measures are referenced to J2000.0.

Comet	a	e	i	Ω	ω	q	rnode	T
55P/Tempel-Tuttle	10.33	.9055	162.5	235.26	172.5	0.976598	0.9806	02/28/98
109P/Swift-Tuttle	26.32	.9636	113.4	139.44	153.0	0.95822	1.031	12/12/92

Appendix B

Copyright Releases and Declarations of co-author contributions